Exploring the Thermal and Mechanochemical Reactivity of 1,2-Oxazine Hetero-Diels–Alder Adducts for Stimuli-Responsive Polymers

Derek C. Church

A dissertation

submitted in partial fulfillment of the

requirements for the degree of

Doctor of Philosophy

University of Washington

2017

Reading Committee:

Prof. Andrew J. Boydston, Chair

Prof. Dustin J. Maly

Prof. Alshakim Nelson

Program Authorized to Offer Degree:

Department of Chemistry

University of Washington

Abstract

Exploring the Thermal and Mechanochemical Reactivity of 1,2-Oxazine Hetero-Diels–Alder Adducts for Stimuli-Responsive Polymers

Derek C. Church

Chair of the Supervisory Committee:
Professor Andrew J. Boydston
Department of Chemistry

Stimuli-responsive materials is an area of significant research with a broad scope of applications in fields such as drug delivery, self-healing materials, and lithography. The ideal stimuli-responsive polymer construct is engineered in such a way that the desired activation occurs only when the proper stimuli is spatially and temporally applied. Light-, pH-, redox-, thermal-, mechanical- and enzymatic-stimuli have successfully been harnessed to trigger various responses in polymeric materials. The continued growth of this field relies upon the development of new stimuli-responsive chemical motifs. To this end, my research has focused on the potential of 1,2-oxazines as a new stimuli-responsive moiety within the context of polymer systems. These compounds have been demonstrated to undergo a thermally induced [4 + 2] cycloreversion to release a diene and nitrosocarbonyl dienophile. My research has sought to study and harness the

thermal reversibility of this adduct and the subsequent breakdown of the dienophile component to trigger processes such as depolymerization of a polymer chain as well as releasing the therapeutically relevant gaseous small molecule, nitroxyl (HNO). Collectively, these constructs can achieve slow, sustained activation at physiologically relevant temperatures or rapid activation at higher temperatures by exogenous means such as the use of photothermal dyes. I have also looked at the propensity of 1,2-oxazines to undergo mechanochemical activation in solution under strong elongational fields. A fundamental understanding of not only how polymer topology may affect mechanophore activation in general but also the regiochemical application of force across the oxazine itself was explored.

TABLE OF CONTENTS

LIST OF FIGURES

LIST OF SCHEMES

List of Tables

ACKNOWLEDGEMENTS

First and foremost, I need to thank my advisor. Through a combination of tough love and patience, A.J. has made me not only a stronger scientist but a stronger person as well, and for that I am forever indebted to him. A.J. has allowed me to pursue various projects, providing extraordinary support and enthusiasm. I wish all the best for his research program and hope to continue seeing exciting science from his lab in the future.

I need to thank the members of my first-year cohort, Dr. Kelli Ogawa, Dr. Greg Peterson and Dr. Mike Larsen. They were tremendous scientists and hard-workers that have provided me a constant source of motivation and inspiration to excel in the lab.

The lab has expanded considerably since the first group of grad students and the second generation of lab members have also been amazing. In particular, I want to thank Dr. Adam Goetz, Laura Murphy, Tori Kensy, Johanna Schwartz and Carl Thrasher for making the end of my time in the lab really enjoyable.

I would be remiss to not acknowledge the awesome people I've met here in Seattle. I can't list all of you but thank you for giving reprieve and solace from the grad school grind. I'm glad I met all of you and wish you nothing but the best.

Finally, I need to thank my parents for all of their love and support that have gotten me to this point.

DEDICATION

To my parents

Chapter 1. STIMULI-RESPONSIVE MATERIALS BASED ON DIELS–ALDER CHEMISTRY

1.1 INTRODUCTION

Stimuli-responsive materials represent a broad area of research in which the goal is to engineer polymers that undergo controlled responses to specific stimuli. Ideally, activation only occurs when the engendered stimuli is applied. While considerable research into stimuli-responsive materials are geared towards biomedical applications,[1-4] diverse fields such as dynamic covalent materials,[5] shape memory polymers[6] and lithographic materials[7] would not be possible without the continued development of stimuli-specific responses in polymer-based systems. A key component to the development of these stimuli-sensitive functional materials is the use of chemical moieties that respond to specific stimuli, such as pH, photo, thermal, mechanical or enzymatic inputs.

One such moiety that has attracted increasing attention is the Diels–Alder (DA) adduct. The DA reaction is an atom-economical [4 + 2] cycloaddition that proceeds between a 1,3-diene and a dienophile. Researchers have used this adduct to construct polymers via step-growth polymerizations[8] as well as a means of polymer conjugation to synthesize complex topologies such as linear multi-block copolymers, graft copolymers, star polymers, dendrimers and networks.[8,9] However, researchers have also harnessed the ability of certain DA adducts to readily undergo a retro Diels–Alder (rDA) reaction under moderate thermal impetus and catalyst-free conditions to create stimuli-responsive materials (Figure 1.1).[10] Researchers have taken advantage of this thermoreversibility and incorporated the DA adduct into polymer scaffolds or networks towards applications such as self-healing materials,[11] shape memory polymers,[12] and

nanoimprinting[13]. Additionally, DA adducts have been explored in the biomedical arena towards drug delivery and tissue engineering applications.[14]

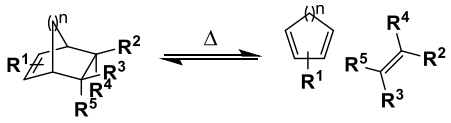

DA adduct	Diene and Dienophile	Temperature of DA/rDA
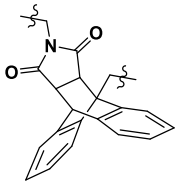	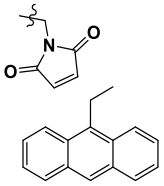	~ 100 °C/ ~ 200 °C[26,27]
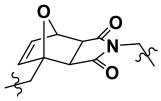	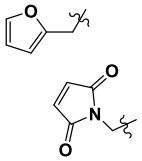	~ 65 °C/ ~ 110 °C[8]
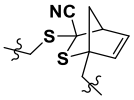	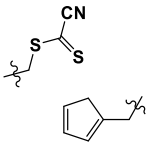	~ 40 °C/ ~ 100 °C[33]
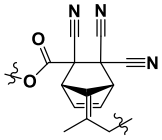	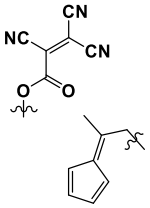	~ -10 °/ ~ 50 °C[28,29]

Commonly the DA adduct is constructed using an electron rich diene and an electron deficient dienophile (normal electron demand), however it can also be constructed such that the diene is electron deficient and the dienophile is electron rich (inverse electron demand).[15,16] Dienes or dienophiles that incorporate heteroatoms into their structure can also undergo a hetero Diels–Alder (HDA) reaction.[17] Collectively, the ability to tune the thermal equilibrium between adduct formation and the rDA reaction by altering the diene and dienophile components is very attractive for obtaining stimuli-responsive materials in the desired temperature window.

While the reversibility of the DA adduct under thermal stimuli is generally well understood, growing research demonstrates that the use of mechanical energy input is also capable of driving the cycloreversion process.[18] The subsequent sections will further explore the use of thermal and mechanical stimuli to modulate the DA/rDA equilibrium in the context of stimuli-responsive materials.

1.2 THERMAL-STIMULI

The work of Kuramoto et al. is the first to report the thermoreversibility of DA adducts within polymer constructs.[19] A linear polymer was constructed from the DA adduct addition polymerization of difurfuryladipate and N,N'-bismaleimido-4-4'-diphenylmethane at 60 °C. At 90 °C, the rDA reaction dominated resulting in 85% adduct decomposition and depolymerization. Subsequent polymerization and depolymerization cycles were conducted, clearly demonstrating the thermoreversibility of these adducts and the fidelity at which these reactions occur in the context of macromolecular systems.

Pioneering research from the Wudl group demonstrated that networks produced with the furan-maleimide adduct have favorable mechanical properties on par with commercial

crosslinked epoxy resins and unsaturated polyesters (Scheme 1.1).[20] However, damaged materials containing the dynamic adducts were capable of autonomous healing by heating the material above 150 °C to cause retro-cycloaddition of the adduct. Upon cooling, adduct formation became favored and new covalent bonds across the damaged area could be formed, healing the material. This report set the tone for the potential of DA adducts for self-healing and recyclable thermosets/thermoplastics and has inspired many subsequent reports.[21]

Scheme 1.1. Multi-topic furan and maleimide components for DA network.

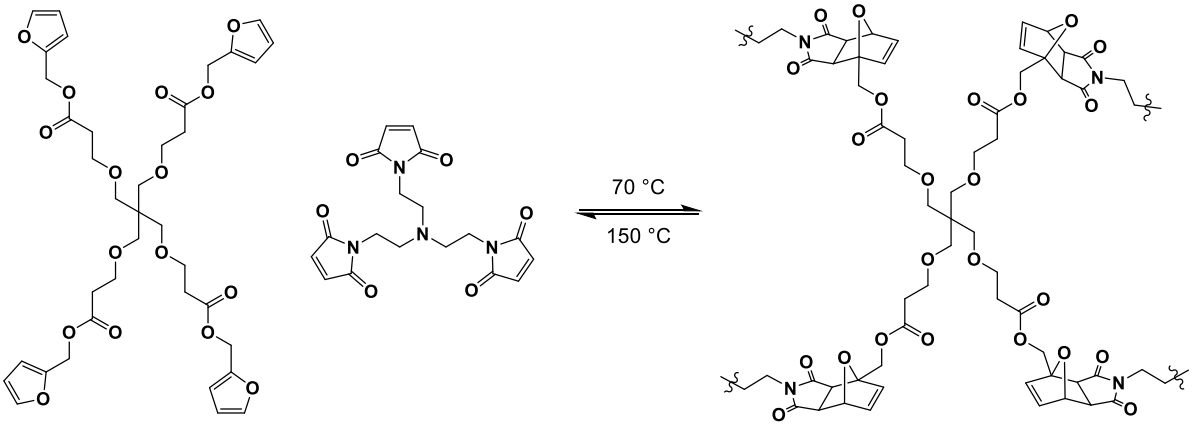

Fewer examples have reported on the potential of DA adducts for drug delivery from polymer scaffolds. Notable examples include the release of maleimide-modified lipoic acid as a model drug from a dendrimder[22] as well as furan-labeled RGDS peptide from a hydrogel for tissue engineering applications.[23] Interestingly, in both cases therapeutic release was attributed to rDA under physiological conditions, despite noticeable rDA of the furan-maleimide adduct typically occurring at temperatures in excess of 110 °C. This can be rationalized however as the removal of maleimide via hydrolysis from the DA/rDA equilibrium. Thus, the equilibrium is driven towards adduct dissociation without the need for increasing temperatures.[24,25]

The more obvious means of changing the thermal DA/rDA equilibrium is changing the diene and dienophile pair (Figure 1.1). The widely used furan-maleimide adduct is readily formed at temperatures around 65 °C while temperatures in excess of 110 °C are required for the rDA reaction to dominate.[8] By changing the diene component to anthracene, a more thermally stable adduct is formed in which rDA does not occur until temperatures above 200 °C are reached, at which point deleterious thermal decomposition is also prevalent.[26,27]

Recent work in the field has sought for new moieties that can provide the same dynamic behavior but under milder conditions and shorter reaction times. Towards this end, reactions between fulvene-dicyanofumarate DA coupling partners[28,29] and the use of HDA adducts appear to be promising routes.[30-34] For example, Inglis et al. have developed dynamic covalent polymers and networks based on the HDA adduct between dithioesters and cyclopentadiene (Scheme 1.2).[31-34] Dithioester-based adducts containing pyridine or phosphonate electron-withdrawing groups (EWG) undergo rapid rDA in less than 5 minutes at 80 °C, while adduct formation and self-healing of the polymer network occurs at room temperature albeit in the presence of small amounts of catalyst. When a cyano moiety is used as the EWG, catalyst-free adduct formation is achieved, however at slightly higher temperatures (~40 °C). Continued exploration of novel DA adducts will further broaden the scope of thermally-responsive DA dynamic materials.

Scheme 1.2. Use of dithioester and cyclopentadiene coupling partners for dynamic materials.

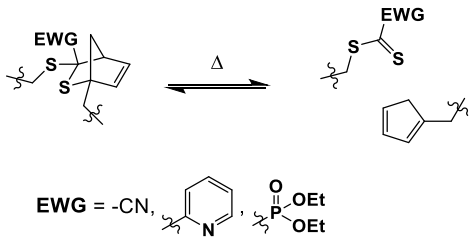

1.3 MECHANICAL-STIMULI

Before exploring the mechanical response of DA adducts in macromolecular systems, a broader understanding of the effect of force along a polymer backbone must be mentioned. In the 1930s, the effects of mechanical force on a polymer backbone were first observed in both the solid state and in solution as a decrease in molecular weight of the polymer.[35] Radical trapping experiments[36] and electron paramagnetic resonance (EPR) spectroscopy[37] demonstrated that this decrease in molecular weight was due to homolytic covalent bond scission along the polymer backbone. These results implied that mechanical force could be used to break covalent bonds within a polymer chain, albeit in an irreversible, degradative process of the material. Recently, researchers have harnessed mechanical force towards productive chemical transformations and stimuli-responsive polymeric materials. The advent of mechano-sensitive moieties termed "mechanophores" has allowed the examination of force on the atomic and molecular levels to further expand the scope of mechano-responsive materials.[38]

Various methods have been developed to study polymer mechanochemistry. These include extensional flow techniques, solid-state elongation or compression as well as single molecule force spectroscopy, each of which are capable of accessing various strain rates and maximum achievable forces.[39,40] Regardless of the technique used, the respective mechanophore of study must be centrally located within a polymer chain, where the elongational forces are greatest, to be mechanochemically active.[41] This agrees with the early theoretical work[42] and experimental observations[43] in which elongation of a linear polymer chain resulted in midpoint chain scission where the forces are greatest.

Mechanophores can undergo diverse transformations such as homolytic and heterolytic cleavage, dative bond scission, electrocyclic ring opening and cycloreversion reactions (Figure

1.2A).[38] The simplest means of rationalizing these scissile covalent processes come from the Bell model in which a linear relationship exists between the application of force and lowering of the transition state energy (Figure 1.2B).[44] Further modifications to this theory account for the shifting of reactant and transition state structures along the reaction coordinate diagram under mechanical force.[45]

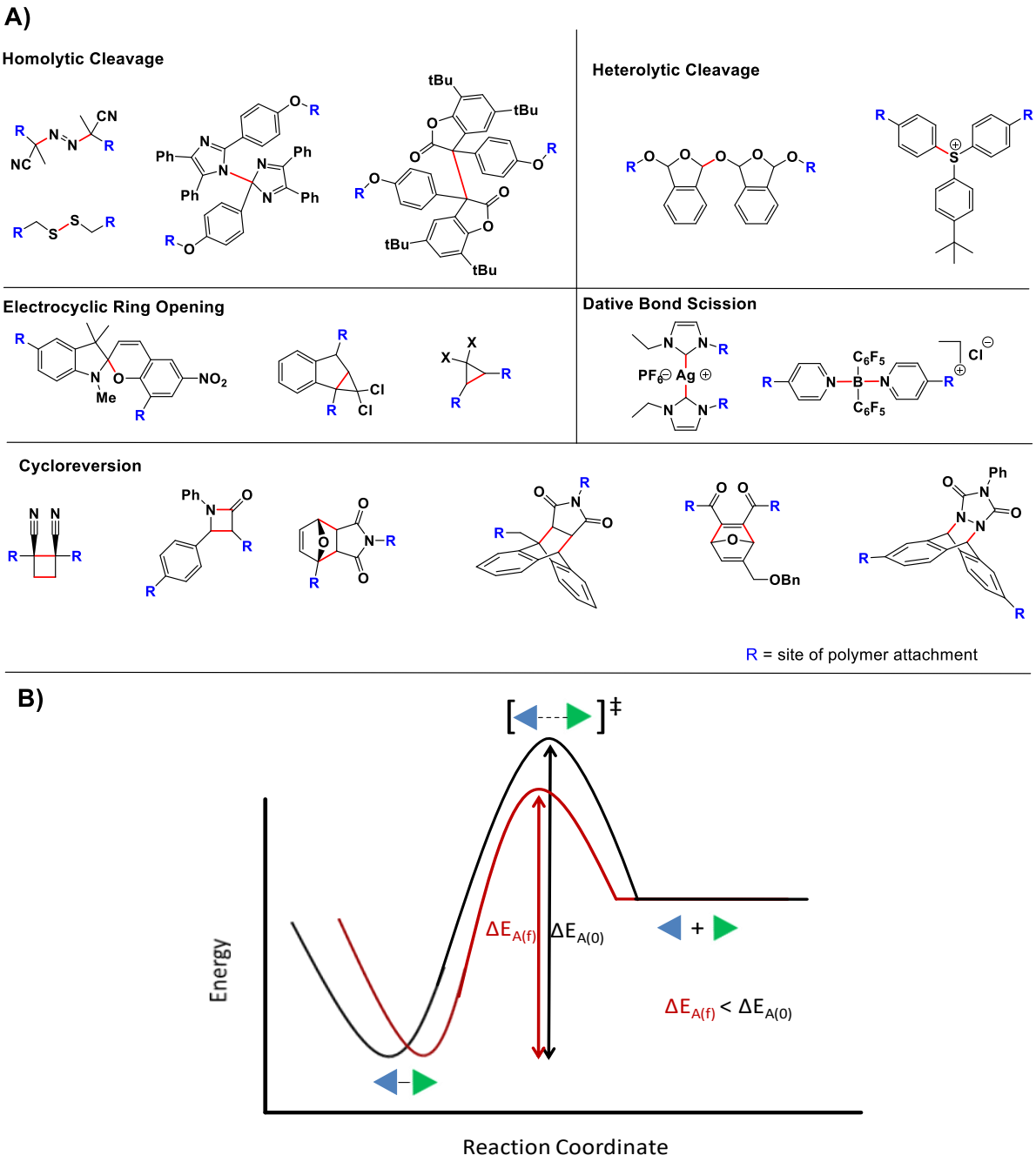

Figure 1.2. A) Examples of known mechanophores. Bonds in red indicate scissile bonds. B) Depiction of change in potential energy surface (PES) and activation energy (ΔE_A) along reaction coordinate diagram due to mechanical force. PES and $\Delta E_{A(0)}$ of a reaction under no external force (black) compared to the change in PES and $\Delta E_{A(f)}$ when a reaction is coupled to mechanical force (red).

These theoretical investigations can partially explain some of the experimentally observed distinctions between the use of mechanical force and purely thermal reaction pathways. For example, the anthracene-maleimide adduct is readily activated by mechanical force. This has been demonstrated in both solution using high extensional flow fields[18,46-48] as well in the solid state.[49] Thermally, however, this adduct requires high temperatures (250 – 300 °C) for the rDA reaction to occur which can also lead to simultaneous thermal decomposition of the resulting components.[26,27] Additionally, mechanochemical activation of a mechanophore is affected by the regiochemical points of polymer attachment, a phenomenon that is absent using purely thermal impetus.[50-52] For example, by attaching polymer at the 9-position of the anthracene component of the anthracene-maleimide adduct leads to cycloreversion while polymer attachment at the 2-position actually leads to suppression of mechanochemical reactivity.[53]

The work from the research group of Bielawski is commonly attributed to the first detailed demonstration of the use of mechanical force to initiate cycloreversion of a DA adduct (Figure 1.3A).[18] Importantly, only chain-centered DA adducts, where the forces along the polymer chain are at a maximum, underwent cycloreversion and subsequent trapping by UV active moieties. Sijbesma later adapted the anthracene-maleimide mechanophore adduct as initially demonstrated by Bielawski to include an extended π network upon mechanochemical activation (Figure 1.3B).[49] By incorporation of these adducts into cross-linked polymer networks, very sensitive probes for mechanical stress were obtained.

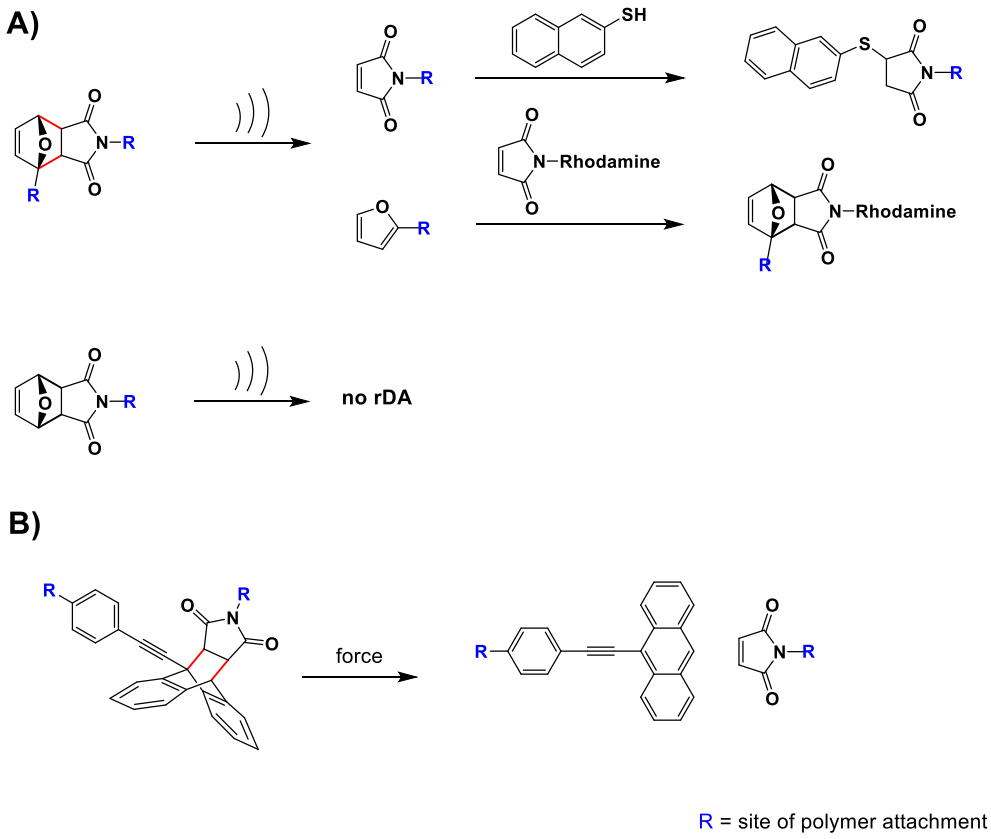

Figure 1.3. A) Probing mechanochemical reactivity of furan-maleimide Diels–Alder adduct in a linear polymer chain via ultrasound. B) Incorporation of extended π network at the 9-position of anthracene leads to very sensitive mechanical force probes. Bonds in red indicate scissile bonds.

Subsequent work from the Boydston and Craig groups demonstrated that [4 + 2] cycloreversion can also occur orthogonal to the applied polymer elongation via bond bending activation (Figure 1.4). By incorporating oxanorbornadiene[54] or triazolinedione-anthracene based DA adducts[55] into elastomeric scaffolds, repeatable mechanophore activation was achieved without scissile degradation of the polymer network. These contributions are an important advance towards pulsatile mechanochemical activation.

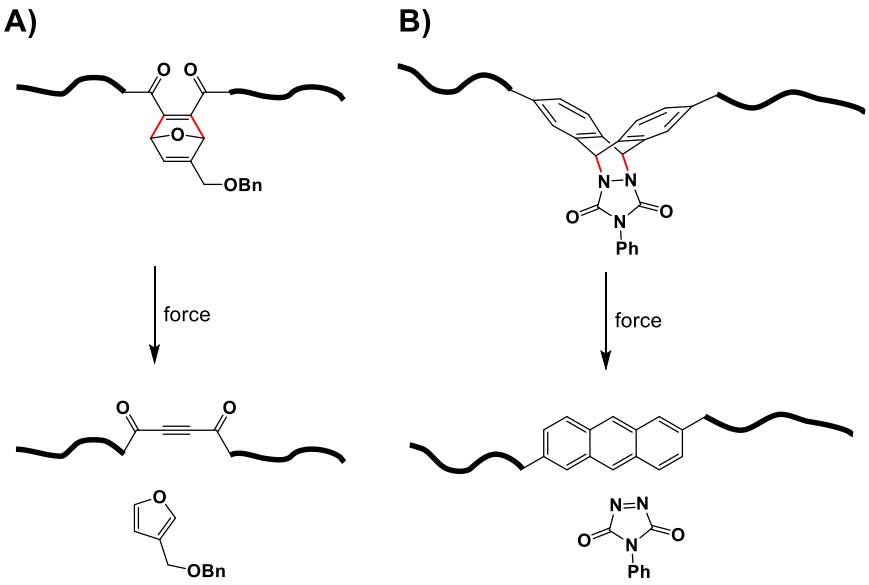

Figure 1.4. A) Oxanorbornadiene and B) triazolinedione-anthracene adducts for "flex" activation [4 + 2] cycloreversion. Bonds in red indicate scissile bonds.

It must be noted that as early as 2002 Wudl (see section 1.2) surmised that "…the retro-DA reaction should be the major cause for crack propagation" in his furan-maleimide adduct network as it contains the weakest bonds throughout the cross-linked network.[20] Additionally in 2011, Yoshie et al. incorporated the anthracene-maleimide adduct into poly(ethylene adipate) networks and demonstrated that mechanically-induced crack propagation manifested as scission at the DA adduct, evidenced by an increase in the anthracene fluorescence signal.[56] Subsequent re-mending at 100 °C displayed a loss of the anthracene signal and partial recovery of the mechanical properties, suggesting adduct re-formation had occurred. While it was only until the methodical studies conducted by Bielawski proved the reversibility of DA adducts under mechanical force, the substantial existing literature utilizing DA adducts in self-healing materials clearly demonstrate the potential for these moieties in mechanoresponsive materials.[57-61]

1.4 CONCLUSIONS

The Diels–Alder reaction has been a powerful tool towards the synthesis of complex macromolecular architectures. Certain constructs of these DA adducts, typically when a strong electron withdrawing dienophile and a cyclic diene are used, are readily reversible at moderate temperatures. Recent results have demonstrated that the application of mechanical force to polymers containing these adducts is also capable of mediating the cyloreversion process. These discoveries have inspired the development of DA adduct-containing macromolecular systems that are responsive to thermal or mechanical stimuli for various applications ranging from self-healing materials to drug delivery. For this field, it is of paramount interest to continue exploring the bounds of thermal and mechanical-sensitive DA adducts such that the exact properties can be met for the desired application.

1.5 REFERENCES

1) Kamaly, N.; Yameen, B.; Wu, J.; Farokhzad, O. C. *Chem. Rev.* **2016**, *116*, 2602.
2) Blum, A. P.; Kammeyer, J. K.; Rush, A. M.; Callmann, C. E.; Hahn, M. E.; Gianneschi, N. C. *J. Am. Chem. Soc.* **2015**, *137*, 2140.
3) Mura, S.; Nicolas, J.; Couvreur, P. *Nat. Mater.* **2013**, *12*, 991.
4) Karimi, M.; Ghasemi, A.; Sahandi Zangabad, P.; Rahighi, R.; Moosavi Basri, S. M.; Mirshekari, H.; Amiri, M.; Shafaei Pishabad, Z.; Aslani, A.; Bozorgomid, M.; Ghosh, D.; Beyzavi, A.; Vaseghi, A.; Aref, A. R.; Haghani, L.; Bahrami, S.; Hamblin, M. R. *Chem. Soc. Rev.* **2016**, *45*, 1457.
5) García, F.; Smulders, M. M. J. *J. Polym. Sci. Part A Polym. Chem.* **2016**, *54*, 3551.

6) Pilate, F.; Toncheva, A.; Dubois, P.; Raquez, J. M. *Eur. Polym. J.* **2016**, *80*, 268.

7) Kaitz, J. A.; Lee, O. P.; Moore, J. S. *MRS Commun.* **2015**, *5*, 191.

8) Gandini, A. *Prog. Polym. Sci.* **2013**, *38*, 1.

9) Tasdelen, M. A. *Polym. Chem.* **2011**, *2*, 2133.

10) Kwart, H.; King, K. *Chem. Rev.* **1968**, *68*, 415.

11) Liu, Y.-L.; Chuo, T.-W. *Polym. Chem.* **2013**, *4*, 2194.

12) Lewis, C. L.; Dell, E. M. *J. Polym. Sci. Part B Polym. Phys.* **2016**, 1340.

13) Thongsomboon, W.; Sherwood, M.; Arellano, N.; Nelson, A. *ACS Macro Lett.* **2013**, *2*, 19.

14) Gregoritza, M.; Brandl, F. P. *Eur. J. Pharm. Biopharm.* **2015**, *97*, 438.

15) Diels, O.; Alder, K. *Justus Leibigs Ann. Chem.* **1928**, *460*, 98.

16) Knall, A.-C.; Slugovc, C. *Chem. Soc. Rev.* **2013**, *42*, 5131.

17) Heravi, M. M.; Ahmadi, T.; Ghavidel, M.; Heidari, B.; Hamidi, H. *RSC Adv.*, **2015**, *5*, 101999.

18) Wiggins, K. M.; Syrett, J. a; Haddleton, D. M.; Bielawski, C. W. *J. Am. Chem. Soc.* **2011**, *133*, 7180.

19) Kuramoto, N.; Hayashi, K.; Nagai, K. *J. Polym. Sci. Part A, Polym. Chem.* **1994**, *32*, 2501.

20) Chen, X.; Dam, M. A.; Ono, K.; Mal, A.; Shen, H.; Nutt, S. R.; Sheran, K.; Wudl, F. *Science* **2002**, *295*, 1698.

21) Roy, N.; Bruchmann, B.; Lehn, J. M. *Chem. Soc. Rev.* **2015**, *44*, 3786.

22) Castonguay, A.; Wilson, E.; Al-Hajaj, N.; Petitjean, L.; Paoletti, J.; Maysinger, D.; Kakkar, A. *Chem. Commun.* **2011**, *47*, 12146.

23) Koehler, K. C.; Anseth, K. S.; Bowman, C. N. *Biomacromolecules* **2013**, *14*, 538.

24) Kirchhof, S.; Brandl, F. P.; Hammer, N.; Goepferich, A. M. *J. Mater. Chem. B* **2013**, *1*, 4855.

25) Kirchhof, S.; Strasser, A.; Wittmann, H.-J.; Messmann, V.; Hammer, N.; Goepferich, A. M.; Brandl, F. P. *J. Mater. Chem. B* **2015**, *3*, 449.

26) Syrett, J. A.; Mantovani, G.; Barton, W. R. S.; Price, D.; Haddleton, D. M. *Polym. Chem.* **2010**, *1*, 102.

27) Jones, J. R.; Liotta, C. L.; Collard, D. M.; Schiraldi, D. A. *Macromolecules* **1999**, *32*, 5786.

28) Boul, P. J.; Reutenauer, P.; Lehn, J. M. *Org. Lett.* **2005**, *7*, 15.

29) Reutenauer, P.; Buhler, E.; Boul, P. J.; Candau, S. J.; Lehn, J. M. *Chem. - A Eur. J.* **2009**, *15*, 1893.

30) Samoshin, A. V; Hawker, C. J.; Alaniz, J. R. De. *ACS Macro Lett.* **2014**, *3*, 753.

31) Inglis, A. J.; Sinnwell, S.; Stenzel, M. H.; Barner-Kowollik, C. *Angew. Chemie* **2009**, *48* (13), 2411.

32) Inglis, A. J.; Nebhani, L.; Altintas, O.; Schmidt, F. G.; Barner-Kowollik, C. *Macromolecules* **2010**, *43*, 5515.

33) Oehlenschlaeger, K. K.; Mueller, J. O.; Brandt, J.; Hilf, S.; Lederer, A.; Wilhelm, M.; Graf, R.; Coote, M. L.; Schmidt, F. G.; Barner-Kowollik, C. *Adv. Mater.* **2014**, *26*, 3561.

34) Schenzel, A. M.; Klein, C.; Rist, K.; Moszner, N.; Barner-Kowollik, C. *Adv. Sci.* **2016**, *3*, DOI: 10.1002/advs.201500361.

35) Staudinger, H.; Heuer, W. *Ber. Dtsch. Chem. Ges.* **1934**, *67*, 1159.

36) Bawn, C. E. H.; Mellish, S. F. *J. Chem. Soc. Faraday Trans.* **1951**, *47*, 1216.

37) Tabata, M.; Sohma, J. *Eur. Polym. J.* **1980**, *16*, 589.

38) Li, J.; Nagamani, C.; Moore, J. S. *Acc. Chem. Res.* **2015**, *48*, 2181.

39) Caruso, M. M.; Davis, D. A.; Shen, Q.; Odom, S. A.; Sottos, N. R.; White, S. R.; Moore, J. S. *Chem. Rev.* **2009**, *109*, 5755.

40) Wiggins, K. M.; Brantley, J. N.; Bielawski, C. W. *Chem. Soc. Rev.* **2013**, *42*, 7130.

41) Carrington, S. P.; Odell, J. A. *J. Nonnewton. Fluid Mech.* **1996**, *67*, 269.

42) Harrington, R. E.; Zimm, B. H. *J. Phys. Chem.* **1965**, *69*, 161.

43) Odell, J. A.; Muller, A. J.; Narh, K. A.; Keller, A. *Macromolecules* **1990**, *23*, 3092.

44) Bell, G. I. *Science* **1978**, *200*, 618.

45) Konda, S. S. M.; Brantley, J. N.; Bielawski, C. W.; Makarov, D. E. *J. Chem. Phys.* **2011**, *135*, 164103-1.

46) Church, D. C.; Peterson, G. I.; Boydston, A. J. *ACS Macro Lett.* **2014**, *3*, 648.

47) Li, J.; Hu, B.; Yang, K.; Zhao, B.; Moore, J. S. *ACS Macro Lett.* **2016**, *5*, 819.

48) Li, H.; Göstl, R.; Delgove, M.; Sweeck, J.; Zhang, Q.; Sijbesma, R. P.; Heuts, J. P. A. *ACS Macro Lett.* **2016**, *5*, 995.

49) Göstl, R.; Sijbesma, R. P. *Chem. Sci.* **2016**, *7*, 370.

50) Groote, R.; Szyja, B. M.; Leibfarth, F. A.; Hawker, C. J.; Doltsinis, N. L.; Sijbesma, R. P. *Macromolecules* **2014**, *47*, 1187.

51) Gossweiler, G. R.; Kouznetsova, T. B.; Craig, S. L. *J. Am. Chem. Soc.* **2015**, *137*, 6148.

52) Robb, M. J.; Kim, T. A.; Halmes, A. J.; White, S. R.; Sottos, N. R.; Moore, J. S. *J. Am. Chem. Soc.* **2016**, *138*, 12328.

53) Konda, S. S. M.; Brantley, J. N.; Varghese, B. T.; Wiggins, K. M.; Bielawski, C. W.; Makarov, D. E. *J. Am. Chem. Soc.* **2013**, *135*, 12722.

54) Larsen, M. B.; Boydston, A. J. *J. Am. Chem. Soc.* **2014**, *136*, 1276.

55) Gossweiler, G. R.; Hewage, G. B.; Soriano, G.; Wang, Q.; Welshofer, G. W.; Zhao, X.; Craig, S. L. *ACS Macro Lett.* **2014**, *3*, 216.

56) Yoshie, N.; Saito, S.; Oya, N. *Polymer* **2011**, *52*, 6074.

57) Peterson, G. I.; Larsen, M. B.; Ganter, M. A.; Storti, D. W.; Boydston, A. J. *ACS Appl. Mater. Interfaces* **2015**, *7*, 577.

58) Imato, K.; Kanehara, T.; Ohishi, T.; Nishihara, M.; Yajima, H.; Ito, M.; Takahara, A.; Otsuka, H. *ACS Macro Lett.* **2015**, *4*, 1307.

59) Klukovich, H. M.; Kean, Z. S.; Iacono, S. T.; Craig, S. L. *J. Am. Chem. Soc.* **2011**, *133*, 17882.

60) Diesendruck, C. E.; Peterson, G. I.; Kulik, H. J.; Kaitz, J. a; Mar, B. D.; May, P. a; White, S. R.; Martínez, T. J.; Boydston, A. J.; Moore, J. S. *Nat. Chem.* **2014**, *6*, 623.

61) Peterson, G. I.; Boydston, A. J. *Macromol Rapid Commun* **2014**, *35*, 1611.

Chapter 2. THE DYNAMIC NATURE OF 1,2-OXAZINES DERIVED FROM PERALKYLCYCLOPENTADIENE AND NITROSOCARBONYL SPECIES

2.1 INTRODUCTION

For decades, the hetero-Diels–Alder (HDA) reaction of nitrosocarbonyl species has been utilized as a versatile synthetic transformation for production of 1,2-oxazines (Scheme 2.1).[1-7] Attractive aspects include the potential for regio- and stereocontrolled introduction of nitrogen and oxygen into carbon frameworks, and ample opportunities for downstream manipulation of the *N*-substituted oxazine. In a subset of examples of 1,2-oxazine applications, the ready reversibility of the HDA reaction was targeted as a means to control *in situ* generation of highly reactive nitrosocarbonyl moieties. For example, King, Miyata, and Toscano have highlighted the potential to use this cycloreversion for generation of HNO, a purported therapeutic, presumably following hydrolysis of the nitrosocarbonyl intermediate.[8-14]

Scheme 2.1. Generalized depiction of the reversible HDA reaction of nitrosocarbonyls.

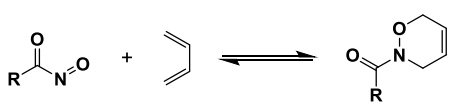

More recently, the dynamic HDA reaction of nitrosocarbonyls has been applied in the design of advanced polymeric architectures and functional materials. A key example from

Read de Alaniz and coworkers demonstrated application of nitrosocarbonyl HDA reactions to prepare block copolymers via highly efficient polymer chain end coupling.[15] In their report, reactive nitrosocarbonyl dienophiles were generated *in situ* at polymer chain ends either by oxidation of hydroxamic acids or cycloreversion of 9,10-dimethylanthracene-based adducts. In the presence of a complementary cyclopentadiene-terminated polymer, efficient chain end coupling was accomplished.

Inspired by this movement toward applications in the polymer field, we considered integration of polymer chain end coupling and nitrosocarbonyl hydrolysis to enable controlled *deconstruction* of block copolymers.[16] For this purpose, the 1,2-oxazine moiety was employed as a thermally labile trigger. Upon thermolysis, subsequent hydrolysis of the nitrosocarbonyl intermediate initiated a controlled depolymerization sequence leading to deconstruction of a self-immolative polymer block. Clearly, the "click-like" nature of the HDA reaction, tunable cycloreversion of oxazines, diverse reactivity of nitrosocarbonyl species, and overall structural modularity provide a powerful combination for advances in polymer and materials designs.

We became interested in the potential applications of polymers and network materials bearing high densities of oxazine moieties. One may envision, for example, taking advantage of robust dynamic covalency to access covalent adaptable networks as has been demonstrated for Diels–Alder and HDA adducts.[17-21] Such systems display broad tunability with regard to stimuli-responsiveness and overall materials properties, stemming largely from the modularity of the diene and dienophile building blocks. On the other hand, controlled breakdown of oxazine-rich materials could enable controlled release of HNO. HNO generation has received a lot of attention in recent years due to its

purported use as a treatment of cardiovascular diseases and as an anticancer agent.[22-26] Notably, the breadth of potential applications place disparate demands on the reactivity of the oxazine and constituent nitrosocarbonyl species (high fidelity cycloaddition/ cycloreversion versus hydrolytic instability) while maintaining a need for retro-HDA reactions to take place at moderate temperatures. To further explore the chemical space and potential applications of oxazine-based systems, we have investigated the reversibility and robustness of a series of oxazines relevant to polymer-oriented applications. Herein, we describe our investigations of the reactivity of oxazines derived from a series of nitrosocarbonyl dienophiles and a peralkylated cyclopentadiene. Particular focus is placed upon comparative analysis of the reversibility of the HDA reaction as a function of nitrosocarbonyl structure, and overall fidelity of the cycloaddition/cycloreversion equilibrium versus deleterious side reactions.

2.2 Results and Discussion

Motivated by potential downstream applications in the development of functional polymeric materials, we targeted oxazines that were based upon readily polymerizable norbornene frameworks.[27] Additionally, we centered upon cyclopentadiene-based oxazines to provide an attractive starting point for balance between stability and reversibility of the HDA adducts. Toward this end, coupling of carboxylic acid **1** and alcohol **2** in the presence of carbonyldiimidazole provided ester **3** in 70% isolated yield (Figure 2.1). This pivotal intermediate was then used to prepare a series of oxazines via HDA reaction with nitrosocarbonyl species generated *in situ*. [1,28-30]

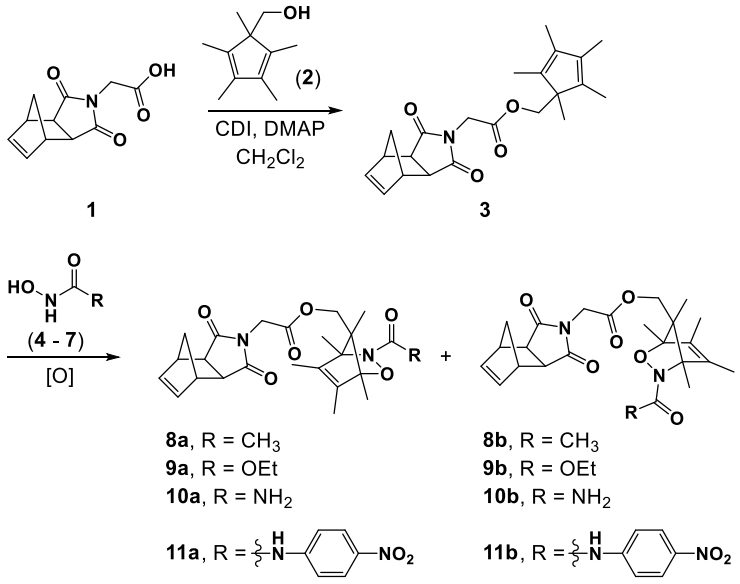

Oxidation Conditions

Oxazine	**Oxidant**	**Time (h)**	**Isolated Yield**
8	TBAP	2	64%
9	TBAP	2.5	97%
10	TBAP	3	88%
11	CuCl, pyridine	18	70%

Figure 2.1. Synthesis of norbornene-tethered oxazine isomers. In each case, reactions proceeded to 100% conversion as judged by TLC.

We initially evaluated the use of CuCl/pyridine to catalyze the nitrosocarbonyl formation. Although good yields of **11** were achieved via oxidation of **7** in the presence of **3**, analogous reactions with coupling partners **4** - **6** were met with limited success. Turning instead to tetrabutylammonium periodate as a stoichiometric oxidant remedied the situation, providing the corresponding oxazines **8** - **10** in good to excellent yields. Notably, each oxazine was isolated as a mixture of what appeared to be a roughly 3:1 ratio of two diastereomers (each racemic).

Separation of the isomers by standard chromatographic techniques was unsuccessful. However, we found that slow vapour diffusion of diethyl ether into solutions of **10** in CH_2Cl_2 produced single crystals suitable for X-ray analysis. We were able to separate crystals that were ultimately found to be individual diastereomers **10a** and **10b** (Figure 2.2), which can be viewed as *anti* and *syn* isomers, respectively. With small quantities of each diastereomer of **10** at hand, we were able to obtain a discrete ^{1}H NMR spectrum for each. From these, we identified **10a** as the major diastereomer produced in the initial mixture of products. The C*H*$_3$ groups indicated in Figure 3 proved to be useful diagnostic handles for ^{1}H NMR analyses and tracking of *anti* and *syn* isomers for oxazines **8**, **9**, and **11** by analogy to **10**.

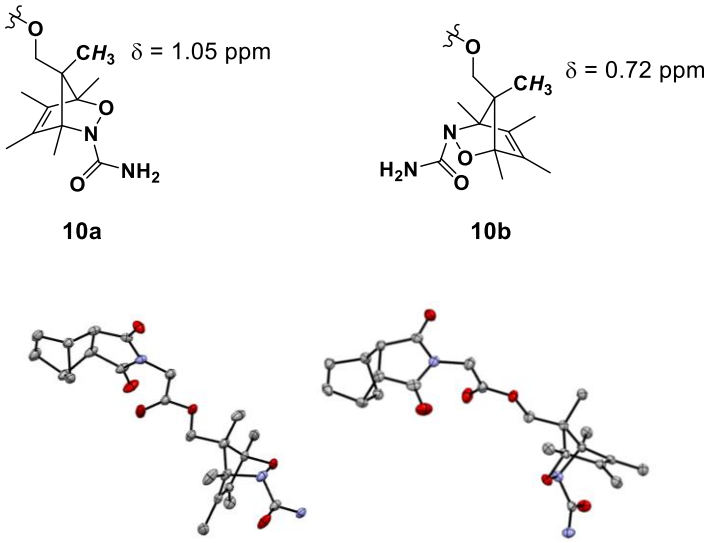

Figure 2.2. Molecular structures obtained via single crystal X-ray analysis of (left) **10a**, and (right) **10b**. Ellipsoids drawn at the 50% probability level, protons removed for clarity.

We next turned toward probing the dynamic nature of each oxazine. Specifically, each set of isomers was heated in DMSO-d_6 (15 mM) and monitored by ^{1}H NMR spectroscopy. In each case, the initial mixture contained a roughly 3:1 ratio of diastereomers, which equilibrated to a roughly 1:1 ratio over time. At ambient temperature, no observable isomerization took place for any of the oxazines over the course of several hours. When heated at 37 °C (Figure 2.3, top), we observed gradual equilibration of the diastereomers with strong dependence upon the nature of the nitrosocarbonyl component. For example, oxazine **8** did not appear to reach equilibrium even within 12 d at 37 °C, indicating much slower isomerization than oxazines bearing more electron donating substituents (cf. **9** - **11**). Oxazine **9** appeared to isomerize more rapidly than **8**, but also continued to show gradual change in the ratio of isomers up to 12 d. The hydroxyurea-derived systems (**10** and **11**) were found to approach equilibrium at the highest relative rates. The facile isomerization, particularly of **10** and **11**, at 37 °C suggests to us that these platforms may be suitable for incorporation into dynamic covalent networks or related materials that become active under biological conditions.

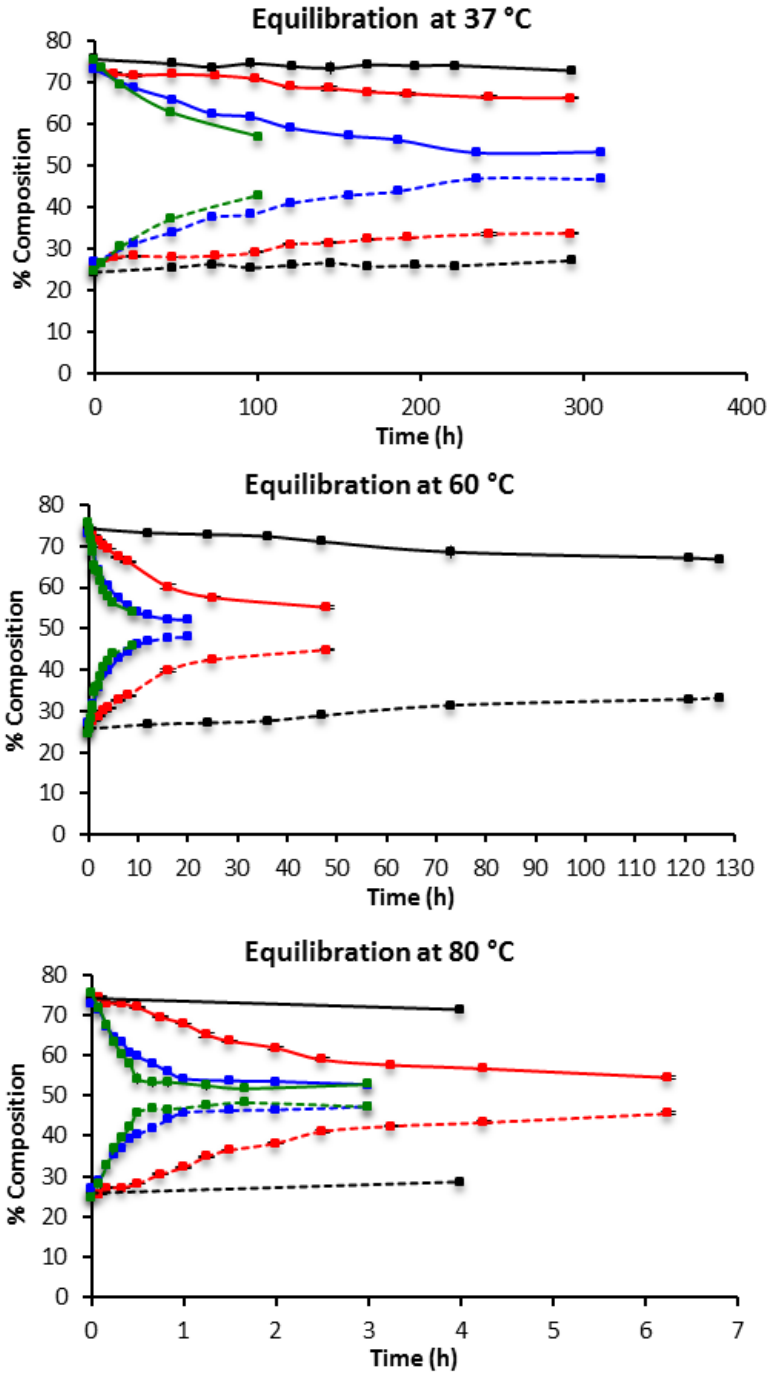

Figure 2.3. Equilibration of oxazines in DMSO-d_6. Solid line = isomer A, dashed line = isomer B. Black = **8**, red = **9**, blue = **10**, green = **11**. Data points are an average of three runs, errors bars = one standard deviation, lines are for visual aid only.[31] Percent composition refers to the ratio of isomers A and B.

The general trend in isomerization rate (**8** < **9** < **10** < **11**) was preserved at the higher temperatures as well (Figure 2.3). At 60 °C (Figure 2.3, middle), the least reactive oxazine (**8**) displayed discernible isomerization over the course of several days, whereas changes in the diastereomeric ratios for **10** and **11** appeared to have ceased after a few hours. Further increase in the temperature to 80 °C (Figure 2.3, bottom) resulted in full equilibration within minutes for **10** and **11** (50 and 25 min, respectively), whereas the composition of **8** continued to show gradual change over the course of several hours (see Supporting Information for extended plots).

As stated previously, the oxazine retro-HDA reaction releases nitrosocarbonyl species, which have the potential to undergo hydrolysis, dimerization, or ene reactions.[3232)] These deleterious reactions were not observed to any appreciable extent in the experiments represented in Figure 4 despite prolonged reaction times and no special precautions being taken to dry the DMSO solvent. To explore the oxazine reactivity in aqueous environment, we examined each of the oxazines at 60 °C in a 30% D_2O/DMSO-d_6 mixture, which was the maximum D_2O content at which each of the oxazines remained soluble at room temperature. Each oxazine mixture was monitored by ^{1}H NMR spectroscopy for 156 h. Oxazines **8** and **9** showed no loss of oxazine content and isomerization rates similar to those observed in DMSO-d_6. In contrast, examination of oxazine **10** revealed a small amount of cyclopentadiene **3** (4.5%) developing over the course of the experiment (Figure 2.4, top). Presumably, the formation of **3** can be ascribed to hydrolysis of the intermediate nitrosocarbonyl species. When oxazine **11** was examined under the aqueous reaction conditions, we found nearly complete loss of both oxazine isomers and concomitant formation of **3** (Figure 2.4, bottom). Collectively, these results

confirm that the oxazine moiety can be structurally tuned toward either robust dynamic behaviour or controlled degradation.

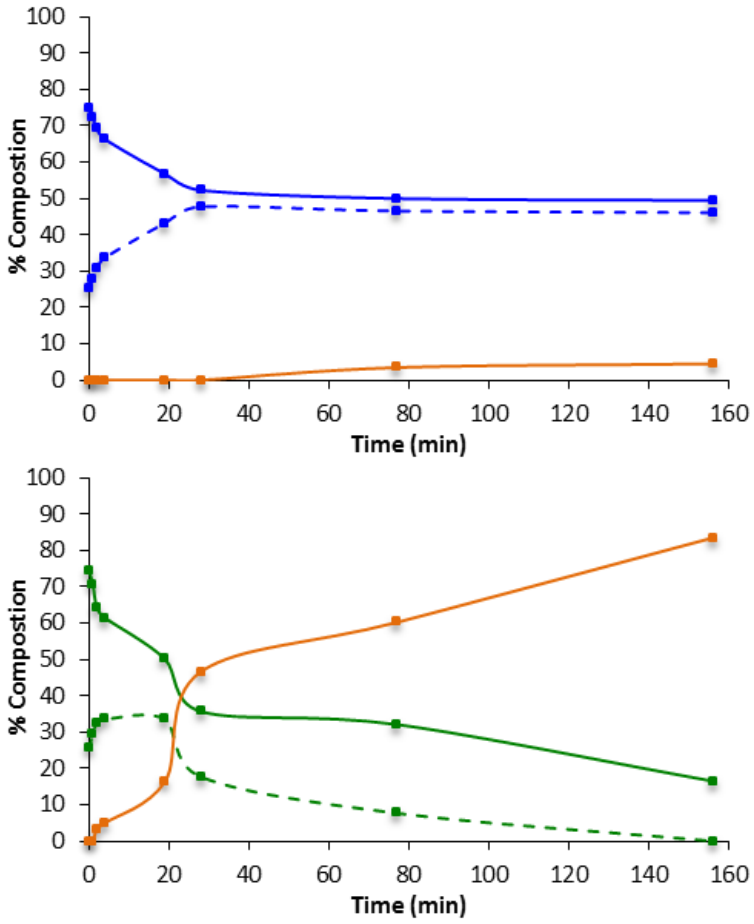

Figure 2.4. Equilibration and hydrolysis of oxazines in D_2O/DMSO-d_6 at 60 °C.[31] Solid line = isomer A, dashed line = isomer B. (top) Oxazine **10** in blue, cyclopentadiene **3** in orange. (bottom) Oxazine **11** in green, cyclopentadiene **3** in orange. Data points are an average of two runs, lines are for visual aid only. Percent composition refers to the fraction of each species relative to the total sum of isomer A, isomer B, and **3**.

Encouraged by the results from the small molecule oxazine studies, we next explored whether the dynamic nature would remain consistent within related polymeric systems. Toward this end, we synthesized **poly(11)** via ring-opening metathesis polymerization (ROMP) using a third-generation Grubbs catalyst (Scheme 2.2).[33] Specifically, monomer **11** was reacted with the Ru-based initiator (35:1 initial monomer to initiator ratio) in CH_2Cl_2 at 0 °C for 3 h, at which point full consumption of monomer was confirmed by ^{1}H NMR analysis. Following termination of the polymerization with ethyl vinyl ether, filtration through alumina/Celite, and isolation by precipitation of the polymer into methanol, we obtained **poly(11)** in 20% isolated yield. Analysis of **poly(11)** by ^{1}H NMR spectroscopy and gel-permeation chromatography (GPC) indicated intact oxazines (3:1 ratio of isomers), a weight-average molecular weight (M_w) of 30.0 kDa, and a molecular weight dispersity ($Đ$) of 1.05.

Scheme 2.2. ROMP of **11** to produce **poly(11)**.

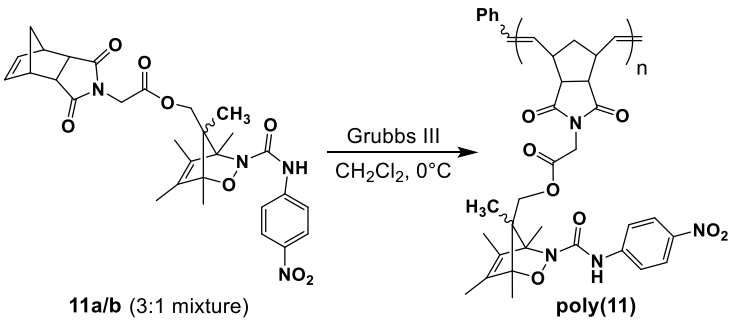

Oxazines are a mixture of *anti* and *syn* isomers.

With **poly(11)** in hand, we then monitored the isomerization of the oxazine units using a solution of the polymer in DMSO-d_6 at 60 °C and variable-temperature ^{1}H NMR spectroscopy (VT-NMR). The alkene proton resonances within the polymer backbone

were compared with the diagnostic methyl signals of the oxazine isomers over the course of the experiment. Under these conditions, **poly(11)** showed no signs of degradation of the oxazine units and complete isomerization within 5 h, consistent with the equilibration time of monomer **11** (Figure 2.5).

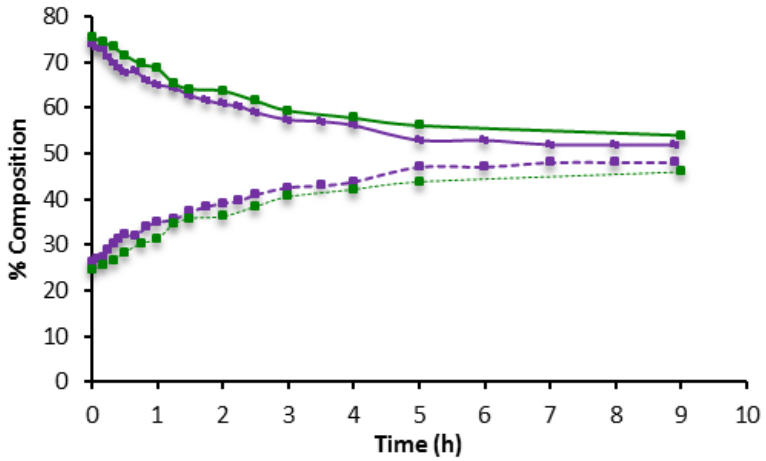

Figure 2.5. Equilibration of oxazine **11** (green) and **poly(11)** (purple) in DMSO-d_6 at 60 °C. Solid line = *anti* isomer, dashed line = *syn* isomer. Percent composition refers to the ratio of *anti* and *syn* isomers

To investigate the potential for dynamic nitrosocarbonyl exchange from the polymeric system, **poly(11)** was heated at 60 °C in the presence of either oxazine **9** or **10**, each in a 2:1 ratio relative to oxazine repeat units in **poly(11)** (Scheme 2.3). After heating each mixture, the solution was added dropwise into an excess of cold methanol, causing selective precipitation of the polymeric species. In each case, ^{1}H NMR analysis of the final polymers revealed signals consistent with successful conversion of oxazine units, giving rise to **poly(9-*co*-11)** and **poly(10-*co*-11)** from the corresponding small molecule oxazines. Each copolymer was found to have a ca. 2:1 ratio of oxazine units consistent

with the initial feed ratios. These experiments confirm the ability to successfully crossover oxazine functionality with a polymeric system, and may provide opportunities for post-polymerization modifications and reversible crosslinking strategies.

Scheme 2.3. Dynamic oxazine crossover between **poly(11)** and small molecule oxazines **9** and **10**.

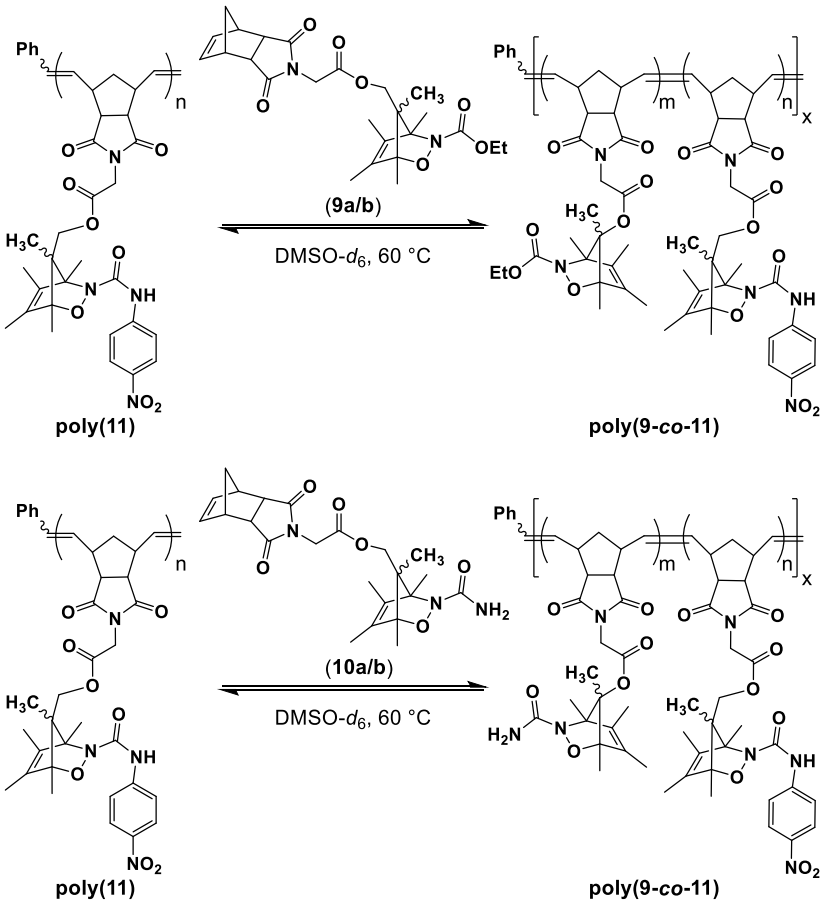

Oxazines are a mixture of *anti* and *syn* isomers.

2.3 Conclusion

We have investigated a series of *N*-carbonyl-substituted oxazines that display readily reversible HDA reactivity. Coincidental production of a diastereomeric mixture of each oxazine provided a convenient method for comparative analysis of their dynamic nature as a function of structure and temperature. The systems appeared to be relatively well behaved, with dynamic equilibration and preservation of oxazine content persisting for several hours at elevated temperatures. Moreover, we found encouraging results toward incorporation of these oxazines into dynamic covalent networks and release platforms based upon polymer-oriented and hydrolysis studies. Collectively, this short series of compounds displays a broad range of (retro)HDA rates and general robustness that may help to guide the design of adaptable network materials and functional polymers.

2.4 References

1) Bodner, B. S.; Miller, M. J. *Angew. Chem. Int. Ed.* **2011**, *50*, 5630.

2) Palmer, L. I.; Frazier, C. P.; Read de Alaniz, J. *Synthesis* **2014**, *46*, 269.

3) Kirby, G. W. *Chem. Soc. Rev.* **1977**, *6*, 1.

4) Kirby, G. W.; Sweeny, J. G. *J. Chem. Soc. Perkin Trans. 1* **1981**, 3250.

5) Kirby, G. W.; Mcguigan, H.; Mackinnon, J. W. M.; McLean, D.; Sharm, R. P. *J. Chem. Soc. Perkin Trans.* **1985**, *1*, 1437.

6) Corrie, J. E. T.; Kirby, G. W.; Mackinnon, J. W. M. *J. Chem. Soc. Perkin Trans.* **1985**, *1*, 883.

7) Christie, C. C.; Kirby, G. W.; McGuigan, H.; Mackinnon, J. W. M. *Chem. Soc. Perkin Trans.* **1985**, *1*, 2469.

8) Xu, Y.; Alavanja, M.; Johnson, V. L.; Yasaki, G.; King, S. B. *Tetrahedron Lett.* **2000**, *41*, 4265.

9) Zeng, B.; Huang, J.; Wright, M. W.; King, S. B. *Bioorg. Med. Chem. Lett.* **2004**, *14*, 5565.

10) Atkinson, R. N.; Shorey, B. M.; King, S. B. *Tetrahedron Lett.* **1996**, *37*, 9287.

11) Adachi, Y.; Nakagawa, H.; Matsuo, K.; Suzuki, T.; Miyata, N. *Chem. Commun.* **2008**, 5149.

12) Matsuo, K.; Nakagawa, H.; Adachi, Y.; Kameda, E.; Aizawa, K.; Tsumoto, H.; Suzuki, T.; Miyata, N. *Chem. Pharm. Bull. 60*, 1055.

13) Evans, A.S.; Cohen, A. D.; Gurard-Levin, Z. A.; Kebede, N.; Celius, T. C.; Miceli, A. P.; Toscano, J. P. *Can. J. Chem.* **2011**, *89*, 130.

14) King, S. B. *Curr. Top. Med. Chem.* **2005**, *5*, 665.

15) Samoshin, A. V.; Hawker, C. J.; Read de Alaniz, J. *ACS Macro Lett.* **2014**, *3*, 753.

16) Peterson, G. I.; Church, D. C.; Yakelis, N. A.; Boydston, A. J. *Polymer* **2014**, *55*, 5980.

17) Oehlenschlaeger, K. K.; Guimard, N. K.; Brandt, J.; Mueller, J. O.; Lin, C. Y.; Hilf, S.; Lederer, A.; Coote, M. L.; Schmidt, F. G.; Barner-Kowollik, C. *Polym. Chem.* **2013**, *4*, 4348.

18) Kloxin, C. J.; Scott, T. F.; Adzima, B. J.; Bowman, C. N. *Macromolecules*, **2010**, *43*, 2643.

19) Jin, Y.; Yu, C.; Denman, R. J.; Zhang, W. *Chem. Soc. Rev.* **2013**, *42*, 6634.

20) Rowan, S. J.; Cantrill, S. J.; Cousins, G. R. L.; Sander, J. K. M.; Stoddart, J. F. *Angew. Chem. Int. Ed.* **2002**, *41*, 898.

21) Gandini, A. *Prog. Polym. Sci.* **2013**, *38*, 1.

22) Miranda, K. M.; Nagasawa, H. T.; Toscano, J. P. *Curr. Top. Med. Chem.* **2005**, *5*, 649.

23) Guthrie, D. A.; Ho, A.; Takahashi, C. G.; Collins, A.; Morris, M.; Toscano, J. P. *J. Org. Chem.* **2015**, *80*, 1338.

24) Guthrie, D. A.; Nourian, S.; Takahashi, C. G.; Toscano, J. P. *J. Org. Chem.* **2015**, *80*, 1349.

25) Sutton, A. D.; Williamson, M.; Weismiller, H.; Toscano, J. P. *Org. Lett.* **2012**, *14*, 472.

26) Guthrie, D. A.; Kim, N. Y.; Siegler, M. A.; Moore, C. D.; Toscano, J. P. *J. Am. Chem. Soc.* **2012**, *134*, 1962.

27) Conrad, R. M.; Grubbs, R. H. *Angew. Chem. Int. Ed.* **2009**, *48*, 8328.

28) Frazier, C. P.; Bugarin, A.; Engelking, J. R.; Read de Alaniz, J. *Org. Lett.* **2012**, *14*, 3620.

29) Chaiyaveij, D.; Cleary, L.; Batsanov, A. S.; Marder, T. B.; Shea, K. J.; Whiting, A. *Org. Lett.* **2011**, *13*, 3442.

30) Frazier, C. P.; Palmer, L. I.; Samoshin, A. V.; Read de Alaniz, J. *Tetrahedron Lett.* **2015**, *56*, 3353.

31) 1,4 Dicyanobenzene was used as an internal NMR standard in the trials.

32) Keck, G. E.; Webb, R. R.; Yates, J. B. *Tetrahedron* **1981**, *37*, 4007.

33) Love, J. A.; Morgan, J. P.; Trnka, T. M.; Grubbs, R. H. *Angew. Chem. Int. Ed.* **2002**, *41*, 4035.

2.5 EXPERIMENTAL

2.5.1 *General Considerations*

Dry THF, pyridine, DMSO, and CH_2Cl_2 were obtained from a Glass Contour solvent purification system. All other reagents and solvents were used as obtained from commercial sources. Grubbs 3rd generation catalyst, $(iMesH_2)(C_5H_5N)_2(Cl)_2Ru{=}CHPH$, was synthesized according to literature procedure.[1)] ^1H and ^{13}C NMR spectra were recorded on a Bruker AVance 300 or 500 MHz spectrometer. Chemical shifts are reported in delta (δ) units, expressed in parts per million (ppm) downfield from tetramethylsilane using the residual protio-solvent as an internal standard ($CDCl_3$, ^1H: 7.26 ppm and ^{13}C: 77.16 ppm and DMSO-d_6, ^1H: 2.50 ppm). HRMS was performed on a Thermo LTQ Orbitrap with a resolution setting of 30,000. Gel permeation chromatography (GPC) was performed using a GPC setup consisting of: a Shimadzu pump, 3 in-line columns, and Wyatt light scattering and refractive index detectors THF as the mobile phase.

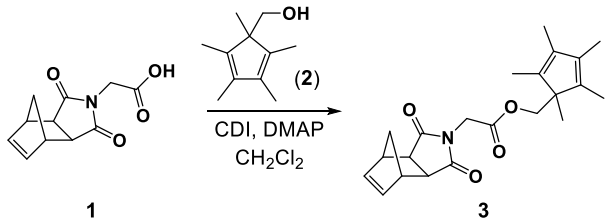

2.5.2 *Synthesis of **3***

Compounds **1** and **2** were synthesized according to the literature.[2,3] Into a flame-dried, N2-purged round bottom flask, N,N-carbonyldiimidazole (1.4 g, 8.7 mmol, 1.3 eq.), a stir bar, and 15 mL of CH2Cl2 were added. To this solution, **1** (1.9 g, 8.7 mmol, 1.3 eq.) was added portion-wise. The reaction mixture was then stirred at room temperature for 45 minutes. After this time,

DMAP (81.8 mg, 0.7 mmol, 0.1 eq.) and **2** (1.1 g, 6.7 mmol, 1.0 eq.) in 15 mL of CH_2Cl_2 were added to the reaction mixture. The reaction mixture was then stirred at room temperature for 18 hours. The solution was then washed successively with 1 M HCl (2 × 30 mL), sat. NaHCO3 (2 × 30 mL), and brine (2 × 30 mL). The organic layer was dried over Na2SO4 and then concentrated under reduced pressure. The resulting residue was purified by flash chromatography (10% EtOAc/Hex) on silica gel and the product was isolated as a white solid (70% yield). ^{1}H NMR (300 MHz, $CDCl_3$) δ 6.20 (t, J= 1.7 Hz, 2H), 4.03 (s, 2H), 3.91 (s, 2H), 3.19 (s, 2H), 2.62 (s, 2H), 1.65 (d, J = 9.0 Hz, 12H), 1.56 (d, J = 9.9 Hz, 1H), 1.41 (d, J = 9.6 Hz, 1H), 0.84 (s, 3H). ^{13}C NMR (125 MHz, $CDCl_3$) δ 176.7, 166.6, 138.0, 137.8, 135.1, 66.8, 55.2, 47.8, 45.2, 42.7, 39.1, 16.7, 10.9, 10.0. HRMS: [M+H]+ calcd for $C_{22}H_{28}NO_4$, 370.2018; found, 370.20247.

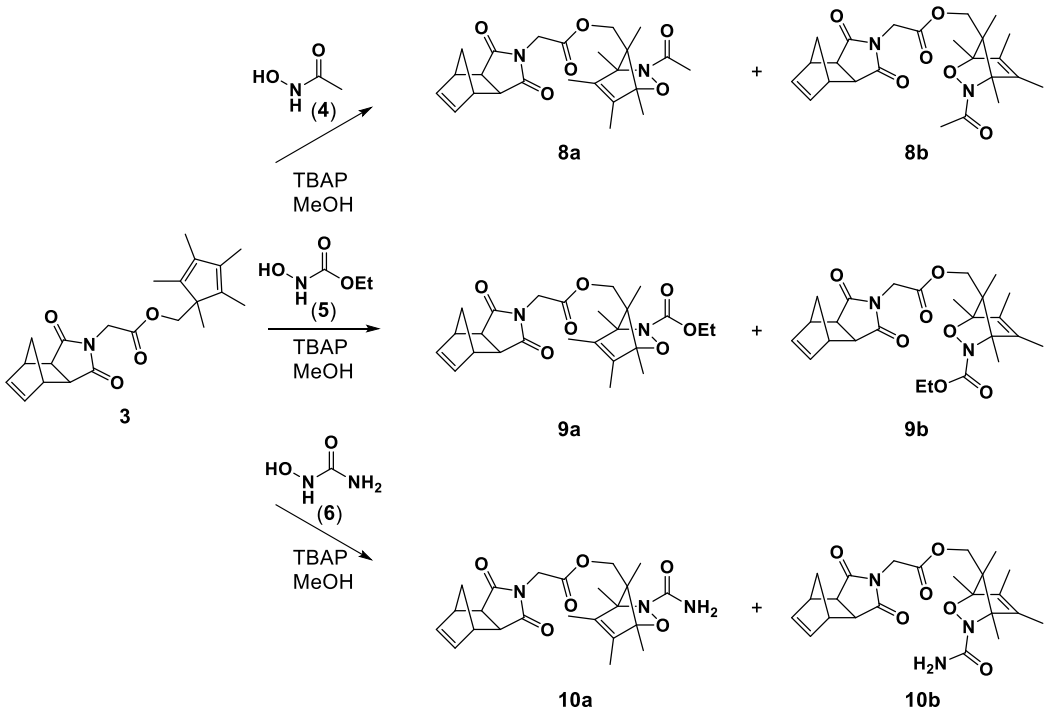

2.5.3 *General Procedure for Synthesis of **8 – 10***

A N_2-purged round bottom flask was charged with **3** (0.586 g, 1.6 mmol, 1.0 eq.), tetrabutylammonium periodate (0.8371 g, 1.9 mmol, 1.2 eq.), a stir bar, and MeOH (50 mL). To

this solution, hydroxyurea (1.9 mmol, 1.2 eq.) in 30 mL of MeOH was added dropwise. The reaction mixture was stirred vigorously and monitored by TLC. Upon consumption of **3**, the organic layer was concentrated under reduced pressure and then taken up in EtOAc. The organic solutin was then washed successively with sat. aq. Na_2SO_3 (2 × 30 mL) and sat. aq. $NaHCO_3$ (2 × 30 mL). The organic layer was dried over Na_2SO_4 and then concentrated under reduced pressure. The crude material was purified by flash chromatography (50% EtOAc/Hex) on silica gel and the products were isolated as white solids.

8: Isolated yield = 64%. ^{1}H NMR (300 MHz, $CDCl_3$) δ 6.30 (t, *J*= 1.7 Hz, 2H), 4.30–4.12 (m, 2.5H), 3.90–3.81 (m, 1.5H), 3.31 (t, *J*= 1.6 Hz, 2H), 2.75 (s, 2H), 1.87–1.86 (m, 3H), 1.77–1.74 (m, 3H), 1.67–1.63 (m, 7H), 1.54–1.51 (m, 1H), 1.37 (s, .75H), 1.33 (s, 2.25H), 1.02 (s, 2.25H), 0.73 (s, 0.75H). ^{13}C NMR (125 MHz, $CDCl_3$) δ 178.2, 177.1, 166.9, 139.8, 138.1, 132.5, 94.6, 79.7, 68.2, 66.8, 61.4, 48.1, 45.5, 42.9, 39.3, 24.0, 12.4, 12.1, 10.9, 9.4, 1.1. HRMS: $[M+H]^+$ calcd for $C_{24}H_{31}N_2O_6$, 443.2182; found, 443.21971.

9: Isolated yield = 97%. ^{1}H NMR (300 MHz, $CDCl_3$) δ 6.30 (s, 2H), 4.31–4.20 (m, 2.5H), 4.13 (q, *J*= 7.08 Hz, 2H), 3.85 (s, 1.5H), 2.75 (s, 2H), 1.73 (m, 3H), 1.67–1.65 (m, 3H), 1.60–1.51 (m, 5H), 1.38–1.35 (m, 3H), 1.24 (t, *J*= 7.0 Hz, 3H), 1.04 (s, 2.25H), 0.73 (s, 0.75H). ^{13}C NMR (125 MHz, $CDCl_3$) δ 177.09, 177.07, 166.9, 160.2, 138.0, 133.8, 94.2, 80.1, 77.3, 77.1, 76.8, 68.4, 66.6, 62.0, 61.5, 48.1, 45.4, 42.9, 39.3, 14.5, 13.0, 12.4, 12.0, 11.6, 10.8, 9.5, 1.0. HRMS: $[M+H]^+$ calcd for $C_{25}H_{33}N_2O_7$, 473.2288; found, 473.23041.

10: Isolated yield = 88%. ^{1}H NMR (300 MHz, $CDCl_3$) δ 6.31 (t, *J*= 1.6 Hz, 2H), 4.36–4.14 (m, 2.5H), 3.89–3.81 (m, 1.5H), 3.31 (t, *J*= 1.6 Hz, 2H), 2.75 (s, 2H), 1.76–1.74 (m, 3H), 1.69–1.63 (m, 7H), 1.57–1.51 (m, 2H), 1.37 (s, .75H), 1.33 (s, 2.25H), 1.05 (s, 2.25H), 0.72 (s, 0.75H). ^{13}C NMR (125 MHz, $CDCl_3$) δ 177.2, 167.0, 164.7, 138.1, 132.2, 100.1, 95.0, 80.7, 68.6, 66.8, 61.7,

60.4, 48.2, 45.5, 43.0, 39.4, 12.7, 11.1, 9.3, 1.1 . HRMS: $[M+H]^+$ calcd for $C_{23}H_{30}N_3O_6$, 444.2135; found, 444.21479.

10a: ^{1}H NMR (300 MHz, $CDCl_3$) δ 6.31 (t, *J*= 1.7 Hz, 2H), 4.24 (d, *J*= 17.1 Hz, 1H), 4.17 (d, *J*=17.0 Hz, 1H), 3.87 (d, *J*= 10.9 Hz, 1H), 3.83 (d, *J*= 10.9 Hz, 1H), 3.32 (t, *J*= 1.7 Hz, 2H), 2.76 (s, 2H), 1.76 (d, *J*= 1.3 Hz, 3H), 1.69 (d, *J*= 1.3 Hz, 3H), 1.66–1.63 (m, 4H), 1.54 (d, *J*= 10.3 Hz, 1H) 1.33 (s, 3H), 1.05, (s, 3H).

10b: ^{1}H NMR (300 MHz, $CDCl_3$) δ 6.31 (t, *J*= 2.0 Hz, 2H), 4.35 (d, *J*= 11.8 Hz, 1H), 4.21 (d, *J*= 11.8 Hz, 1H), 3.32 (t, *J*= 1.6 Hz, 2H), 2.75 (s, 2H), 1.74 (d, *J*= 1.5 Hz, 3H), 1.66 (d, *J*= 1.1 Hz, 1H), 1.65–1.61 (m, 4H), 1.54 (d, 10.1 Hz, 1H), 1.37 (s, 3H), 0.73 (s, 3H).

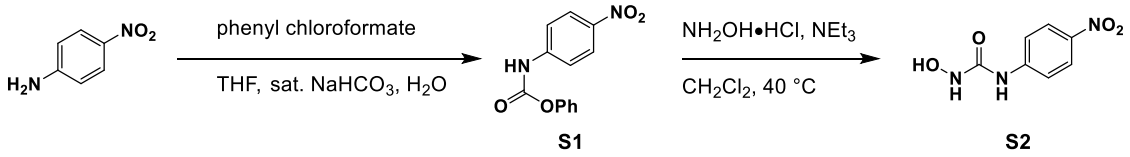

2.5.4 *Synthesis of **S1***

Preparation of **S1** by an alternative method was previously reported. A round bottom flask was charged with 4-nitroaniline (0.7001 g, 5.0 mmol, 1.0 eq.), a stir bar, 2 mL of THF, 0.6 mL of sat. $NaHCO_3$, and 0.4 mL of H_2O. Phenyl chloroformate (0.64 mL, 5.1 mmol, 1.02 eq.) was then added drop-wise via an addition funnel. The resulting mixture was stirred at room temperature for 3 hours. The reaction mixture was then diluted with EtOAc and then washed with sat. $NaHCO_3$ (2 × 10mL) followed by brine (1 × 10 mL). The organic layer was dried over Na_2SO_4 and then concentrated under reduced pressure. The resulting carbamate was used without further purification (97% crude yield). ^{1}H NMR (500 MHz, $CDCl_3$) δ 8.21 (d, J = 9.0 Hz, 2H), 7.60 (d, J = 9.0 Hz, 2H), 7.49 – 7.35 (m, 3H), 7.30 – 7.24 (m, 1H), 7.19 (d, J = 7.8 Hz, 2H). ^{13}C NMR (125 MHz, $CDCl_3$) δ 151.3, 150.2, 143.6, 143.5, 129.7, 126.4, 125.4, 121.6, 118.2.

2.5.5 *Synthesis of **S2***

Preparation of **S2** by an alternative method was previously reported.[5)] Into a flame-dried, N_2-purged round bottom flask was added carbamate **S1** (0.6 g, 2.32 mmol, 1.0 eq.), NEt_3 (0.32 mL, 2.32 mmol, 1.0 eq.), CH_2Cl_2 (2.32 mL) and a stir bar. Separately, hydroxylamine (0.559 g, 8 mmol) and potassium carbonate (2.222 g, 16 mmol) was free-based in dry DMSO (4 mL) for 12 hours. A solution of free-based hydroxylamine (2.32 mL in DMSO, 4.64 mmol, 2.0 eq.) was then added into the solution containing **S1**. The resulting mixture was then heated at 40 °C and stirred for 3 hours. After being removed from heat and returning to room temperature, the reaction mixture was added into 30 mL of H_2O and extracted with EtOAc (2 × 10 mL). The combined organic layers were dried over Na_2SO_4 and then concentrated under reduced pressure. The desired product was obtained as a yellow solid (83% yield). ^{1}H NMR (500 MHz, DMSO) δ 9.49 (s, 1H), 9.27 (s, 1H), 9.15 (s, 1H), 8.14 (d, J = 9.0 Hz, 2H), 7.92 (d, J = 8.9 Hz, 2H). ^{13}C NMR (125 MHz, DMSO-d_6) δ 157.8, 146.4, 141.4, 124.8, 118.5.

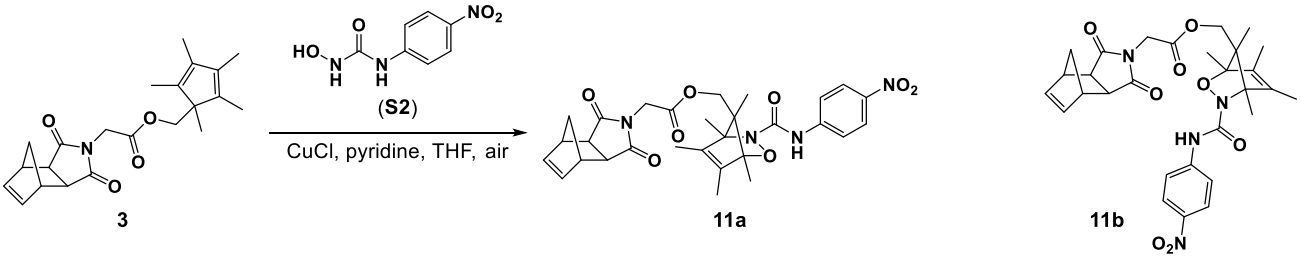

2.5.6 *Synthesis of **11***

A round bottom flask was charged with **3** (0.336 g, 0.9 mmol, 1.0 eq.), **S2** (0.359 g, 1.8 mmol, 1.2 eq.), a stir bar, and THF (10 mL). CuCl (0.037 g, 0.36 mmol, 0.4 eq.) and pyridine (7.3 µL, 0.09 mmol, 0.1 eq.) were then added. The reaction mixture was vigorously stirred under

ambient conditions for 18 hours. EtOAc (10 mL) and sat. aq. EDTA (10 mL) were then added to the reaction mixture. The organic layer was separated and then washed successively with sat. EDTA (2 × 10 mL) and brine (2 × 10 mL). The organic layer was dried over Na_2SO_4 and then concentrated under reduced pressure. The crude material was purified by flash chromatography (20% EtOAc/Hex) on silica gel and the product was isolated as a yellow solid (70% yield). ^{1}H NMR (300 MHz, $CDCl_3$) δ 8.10 (d, J= 8.9 Hz, 2H), 7.75 (s, 1H), 7.56 (d, *J*= 9.3 Hz, 2H), 6.27 (s, 2H), 4.39–4.16 (m, 2.5H), 3.92–3.84 (m, 1.5H), 3.32 (s, 2H), 2.77 (s, 2H), 1.77–1.75 (m, 3H), 1.71–1.65 (m, 6.5H), 1.56–1.53 (m, 1.5H), 1.46–1.43 (m, 3H), 1.10 (s, 2.25H), 0.78 (s, 0.75H). ^{13}C NMR (126 MHz, $CDCl_3$) δ 177.11, 177.07, 166.8, 159.7, 143.7, 143.1, 139.2, 138.01, 137.98, 132.5, 125.1, 118.5, 100.0, 96.8, 96.3, 81.3, 68.1, 65.9, 62.1, 60.8, 48.1, 45.5, 42.9, 39.2, 15.3, 13.0, 12.7, 12.6, 12.5, 12.0, 11.1, 10.9, 9.3. HRMS (ESI): $[M+H]^+$ calcd for $C_{29}H_{33}N_4O_8$, 565.2298; found, 565.23191.

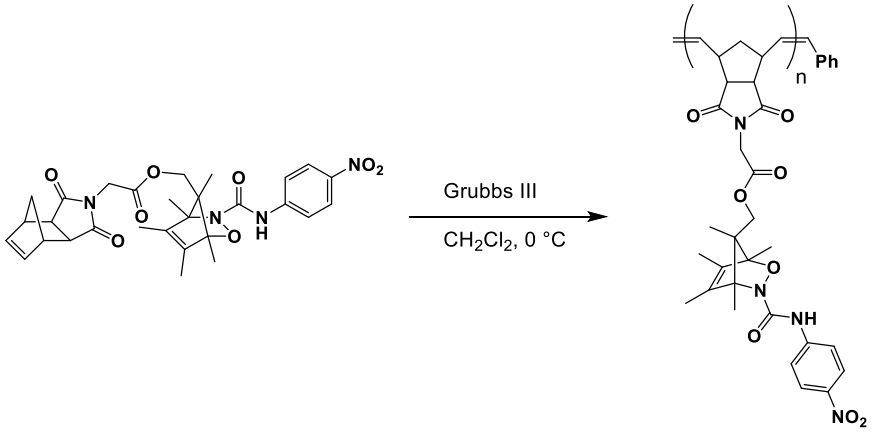

poly(11)

2.5.7 *Synthesis of* ***poly(11)***

Into a flame-dried, N_2-purged round bottom flask, monomer **11** (733 mg, 1.3 mmol, 35 eq.), a stir bar, and 2.6 mL of CH_2Cl_2 were added. Once homogeneous, the solution was cooled in an ice bath at 0 °C and Grubbs 3rd generation catalyst (26.6 mg, 0.04 mmol, 1.0 eq.) in 4.6 mL of

CH_2Cl_2 was quickly added. The reaction solution was stirred for 3 hours, during which time the ice bath expired. Ethyl vinyl ether (4.0 mL) was then added to the reaction mixture and the solution was stirred for an additional 10 minutes. The reaction mixture was then concentrated under reduced pressure and dissolved in a minimal amount of CH_2Cl_2. The polymer solution was then filtered through an alumina/Celite plug using CH_2Cl_2 as eluent. The solution volume was reduced under reduced pressure and then added dropwise into an excess of methanol, causing the polymer to precipitate from solution. The polymer was then collected by vacuum filtration, washed with additional methanol, and then dried under vacuum to provide a light yellow powder (147 mg, 20% yield). M_w = 30.0 kDa, M_n = 25.7 kDa, Đ = 1.05.

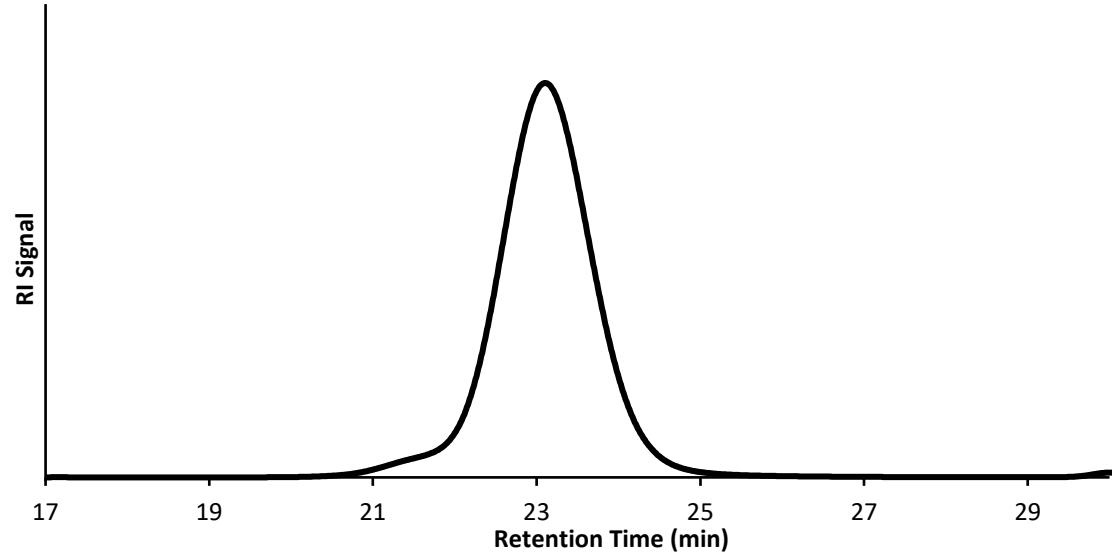

Figure 2.6. GPC trace of **poly(11)**.

2.5.8 *General Method for Monitoring Small-Molecule Isomerization*

Into a 20 mL flame-dried, N_2-purged scintillation vial sealed with a rubber septum, oxazine (0.0298 g, 0.067 mmol, 1.0 eq.), 1,4-dicyanobenzene (0.0085 g, 0.066 mmol, 0.99 eq.), 4.5 mL DMSO-d_6, and a stir bar were added. The vials were then submerged into a pre-heated oil bath

maintained at the designated temperature. At designated time points, 0.3 mL aliquots were removed by syringe and transferred into NMR tubes and then frozen in an ice bath until the NMR spectra were collected. Runs were done in triplicate.

2.5.9 *General Method for Monitoring **poly(11)** Isomerization*

In an N_2-purged NMR tube, **poly(11)** (0.0051 g, 0.0002 mmol) was dissolved in anhydrous DMSO-d_6 (0.5 mL). The isomerization was monitored using a Bruker AVance 499 MHz spectrometer equipped with a variable temperature probe set to 60 °C, taking 8 scans every five minutes.

2.5.10 *General Procedure for Nitrosocarbonyl Exchange between **poly(11)** and Small molecules **9** and **10***

Into a 7 mL flame-dried, N_2-purged vial was charged with **poly(11)** (0.031 g, 0.0012 mmol, 1 eq.), 3.67 mL DMSO, and a stir bar. To this solution was also added either **9** (0.052 g, 0.110 mmol, 92 eq.) or **10** (0.050 g, 0.110 mmol, 92 eq.). The vial was then sealed with a rubber septum and submerged into an oil bath preheated to 60 °C where it was maintained for 27 hours in the case of **9** or 7 hours in the case of **10**. Each solution was added dropwise into an excess of cold methanol, causing precipitation of polymeric species [**poly(9-*co*-11)** and **poly(10-*co*-11)**]. The resulting mixtures were then centrifuged, decanted, and the resulting solids washed with methanol, and centrifuged twice more. The polymer residues were then collected and dried under vacuum.

2.5.11 *General Method for Monitoring the Small-Molecule Hydrolysis*

Into a 20 mL scintillation vial sealed with a rubber septum, oxazine (0.0418 g, 0.074 mmol, 1.0 eq.), 1,4-dicyanobenzene (0.0101 g, 0.078 mmol, 1.05 eq.), 4.96 mL DMSO-d_6, 1.97 mL D_2O and a stir bar were added. The vials were then submerged into a pre-heated oil 60°C bath. At designated time points, 0.3 mL aliquots were removed by syringe into NMR tubes and frozen in an ice bath until the NMR spectra were collected. Runs were done in duplicate.

2.5.12 *Extended Time Plots for Isomerization of **8**.*

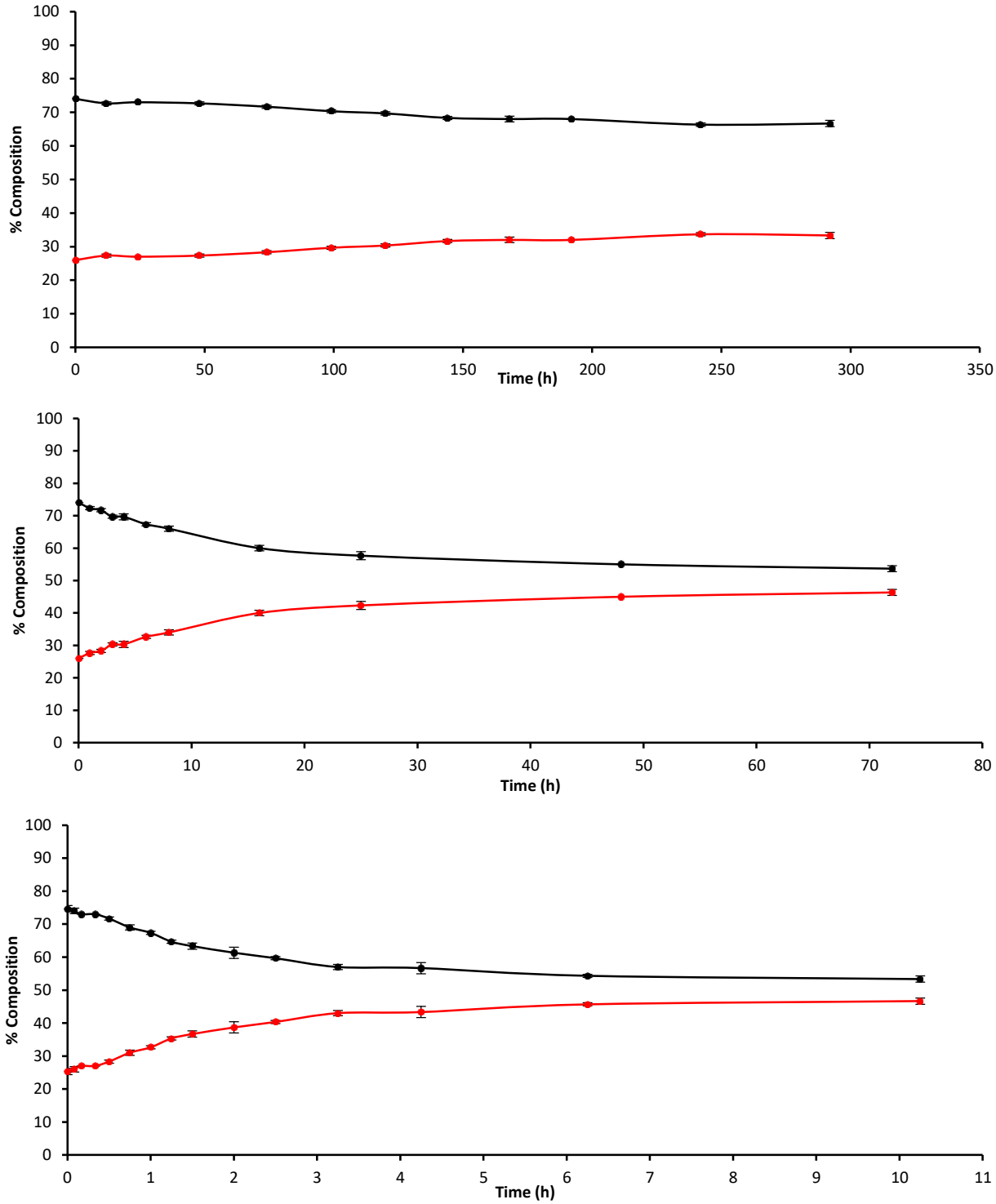

Figure 2.7. Black = **8a**, red = **8b**. Top = 37 °C, middle = 60 °C, bottom = 80 °C. Average of three runs, error bars = one standard deviation, lines are visual aid.

2.5.13 *NMR Spectra*

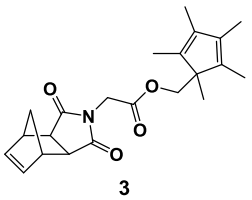

3

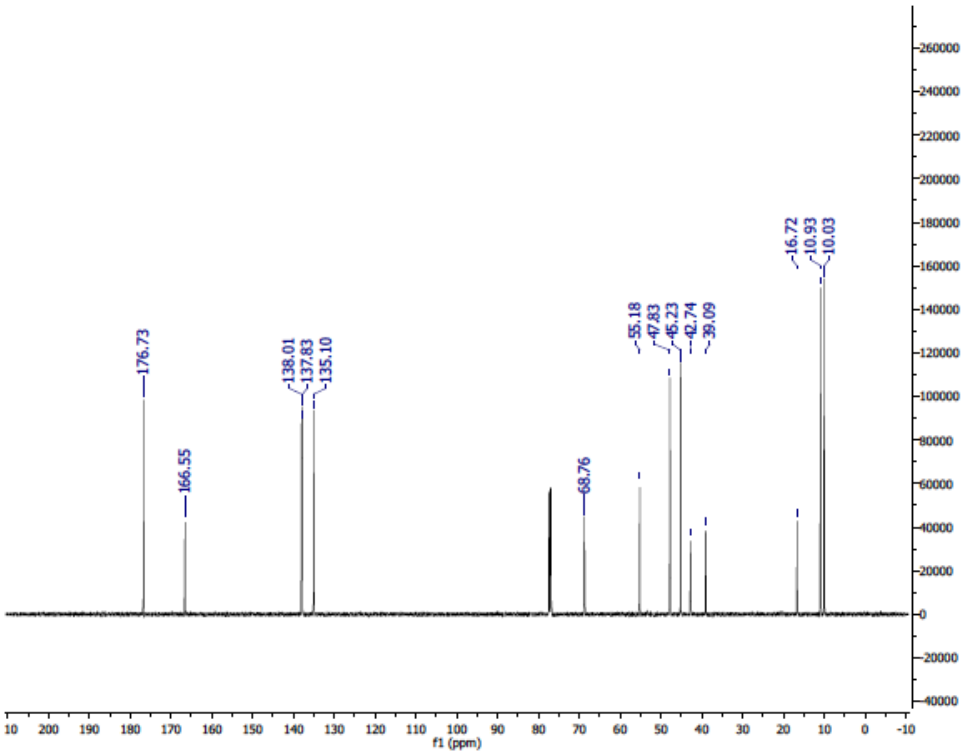

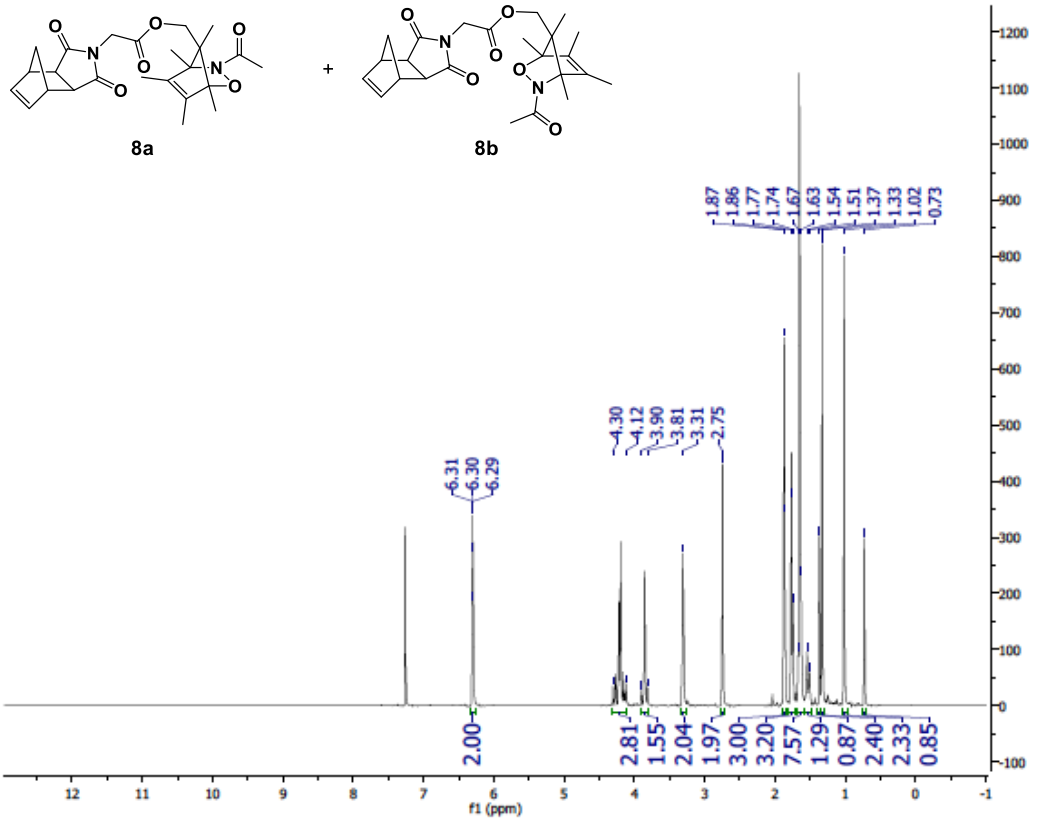
8a
+
8b
6.31
6.30
6.29
4.30
4.12
3.90
3.81
3.31
2.75
1.87
1.86
1.77
1.74
1.67
1.63
1.54
1.51
1.37
1.33
1.02
0.73
2.00
2.81
1.55
2.04
1.97
3.00
3.20
7.57
1.29
0.87
2.40
2.33
0.85
f1 (ppm)

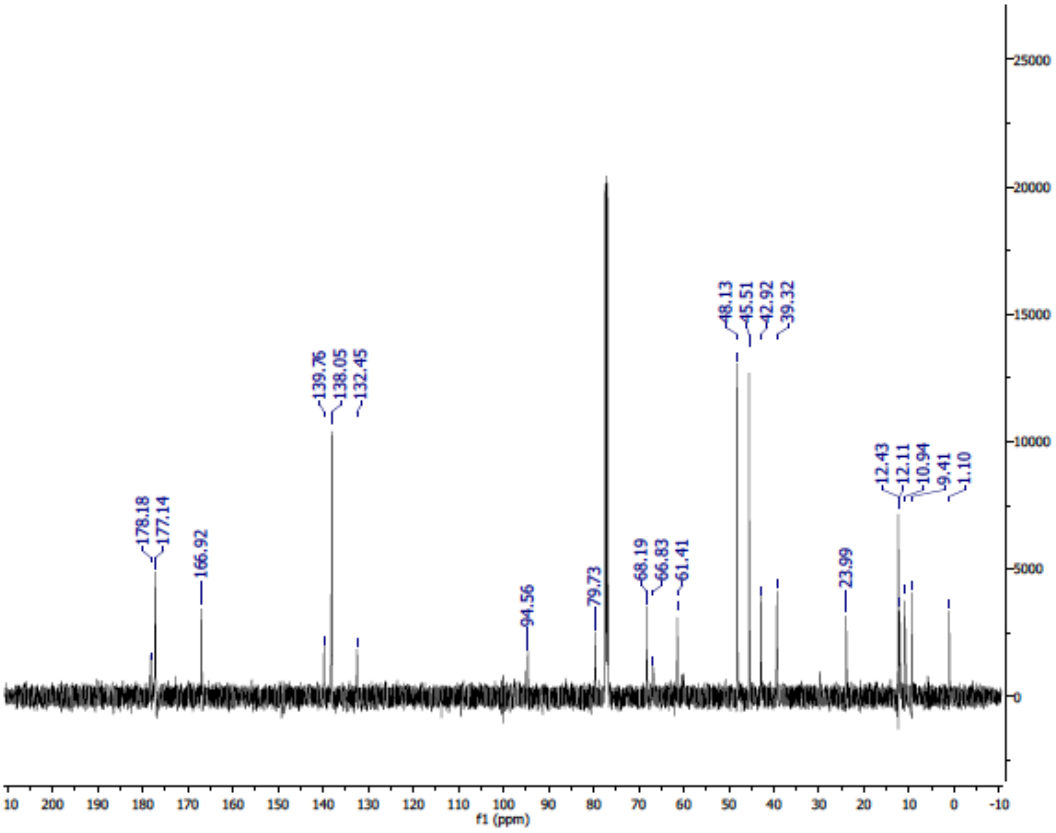
178.18
177.14
166.92
139.76
138.05
132.45
94.56
79.73
68.19
66.83
61.41
48.13
45.51
42.92
39.32
23.99
12.43
12.11
10.94
9.41
1.10
f1 (ppm)

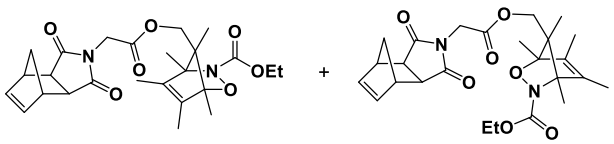

9a + 9b

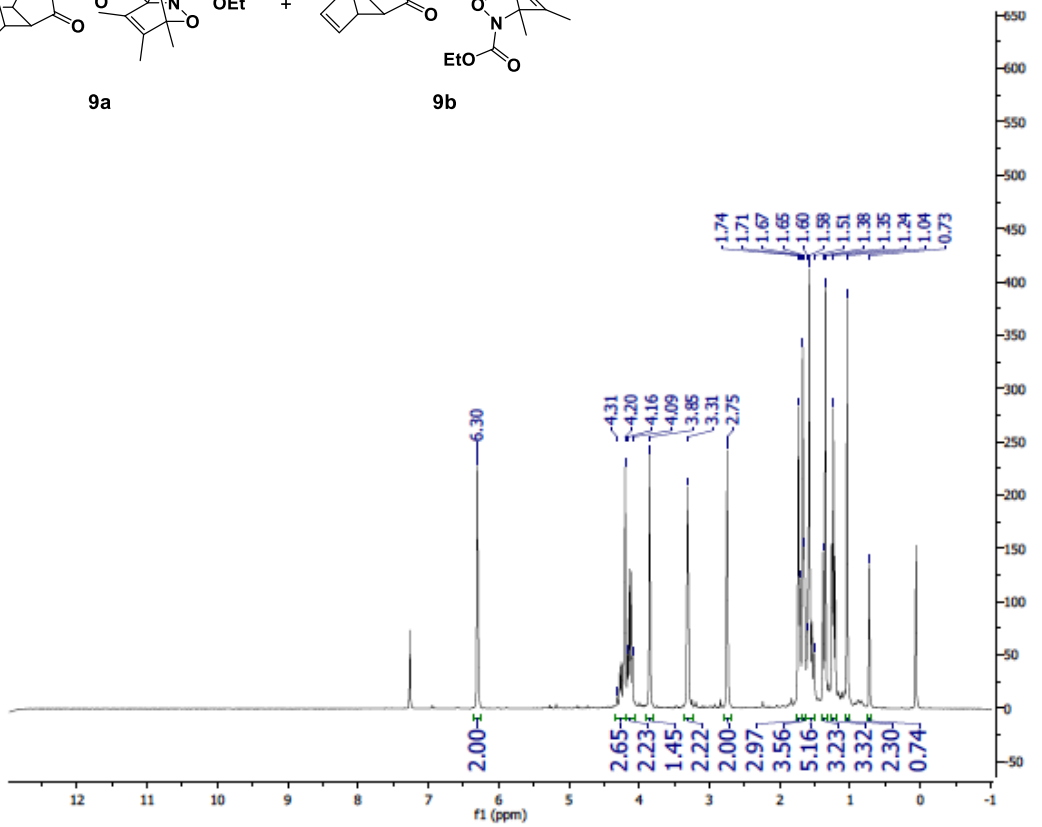
6.30
4.31
4.20
4.16
4.09
3.85
3.31
2.75
1.74
1.71
1.67
1.65
1.60
1.58
1.51
1.38
1.35
1.24
1.04
0.73
2.00
2.65
2.23
1.45
2.22
2.00
2.97
3.56
5.16
3.23
3.32
2.30
0.74
f1 (ppm)

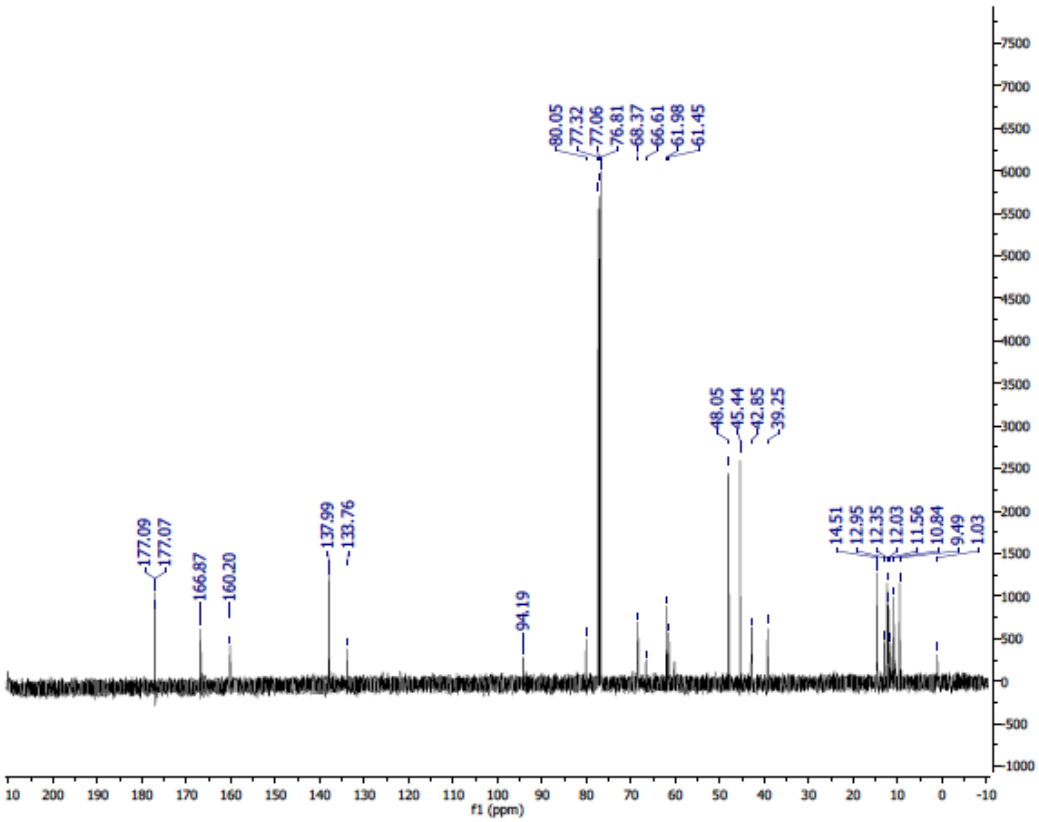
177.09
177.07
166.87
160.20
137.99
133.76
94.19
80.05
77.32
77.06
76.81
68.37
66.61
61.98
61.45
48.05
45.44
42.85
39.25
14.51
12.95
12.35
12.03
11.56
10.84
9.49
1.03
f1 (ppm)

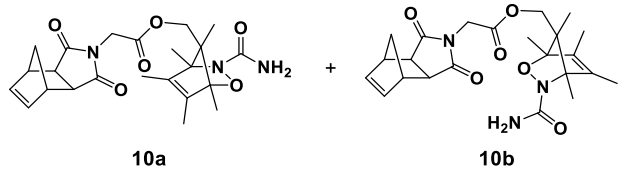

10a + 10b

6.31
4.36
4.14
3.89
3.81
3.31
2.75
1.76
1.74
1.69
1.63
1.57
1.51
1.37
1.33
1.05
0.72
2.00
2.80
1.57
2.04
1.95
3.01
7.57
1.80
0.87
2.42
2.30
0.87
f1 (ppm)

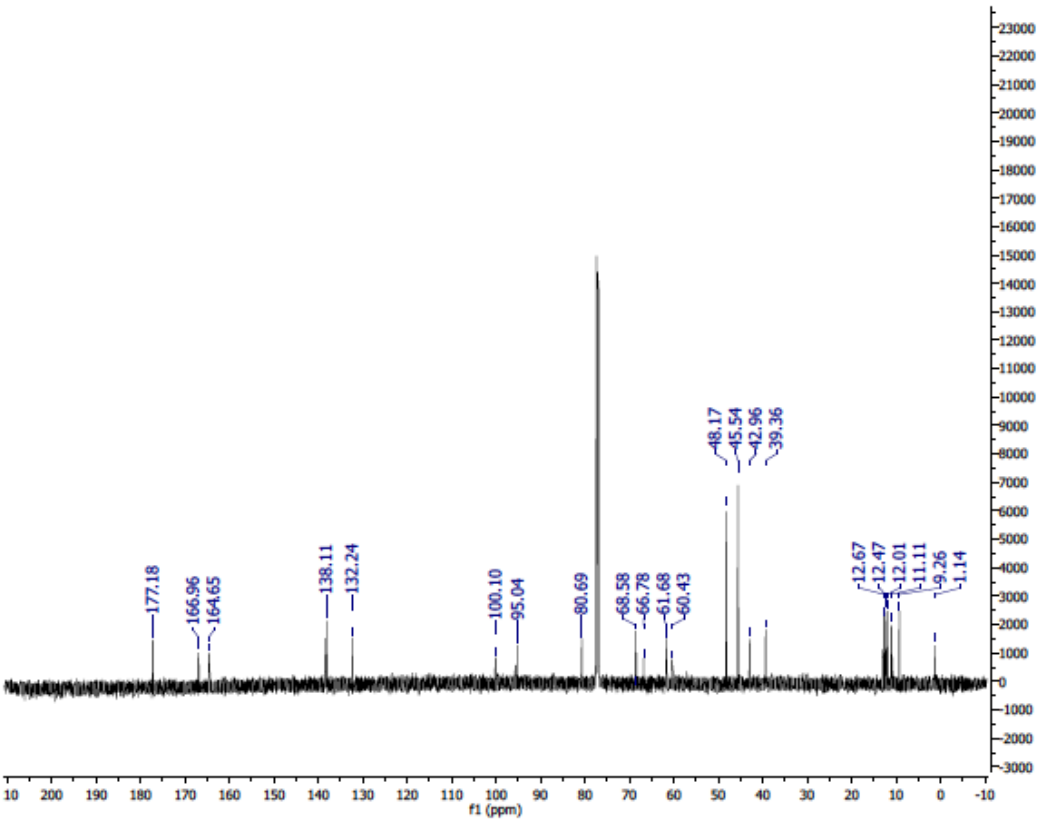
177.18
166.96
164.65
138.11
132.24
100.10
95.04
80.69
68.58
66.78
61.68
60.43
48.17
45.54
42.96
39.36
12.67
12.47
12.01
11.11
9.26
1.14
f1 (ppm)

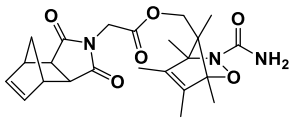

10a

1.76
1.76
1.69
1.68
1.64
1.63
1.55
1.52
1.33
1.05
6.31
4.27
4.21
4.20
4.14
3.89
3.85
3.84
3.81
3.32
2.76
2.00
1.15
0.93
1.05
0.94
2.07
2.00
2.97
3.05
3.86
1.15
3.29
3.02
f1 (ppm)

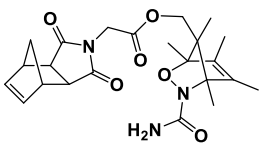

10b

1.74
1.74
1.66
1.66
1.64
1.56
1.52
1.37
0.73
4.36
4.33
4.22
4.19
6.31
3.32
2.75
2.00
1.03
3.20
2.08
2.01
2.92
3.89
4.24
1.41
3.12
3.04
f1 (ppm)

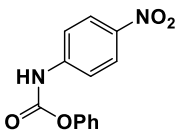
NO2
HN
O
OPh

S1

8.22
8.20
7.61
7.59
7.44
7.42
7.40
7.30
7.28
7.27
7.20
7.19
2.00
2.12
3.07
1.00
1.85

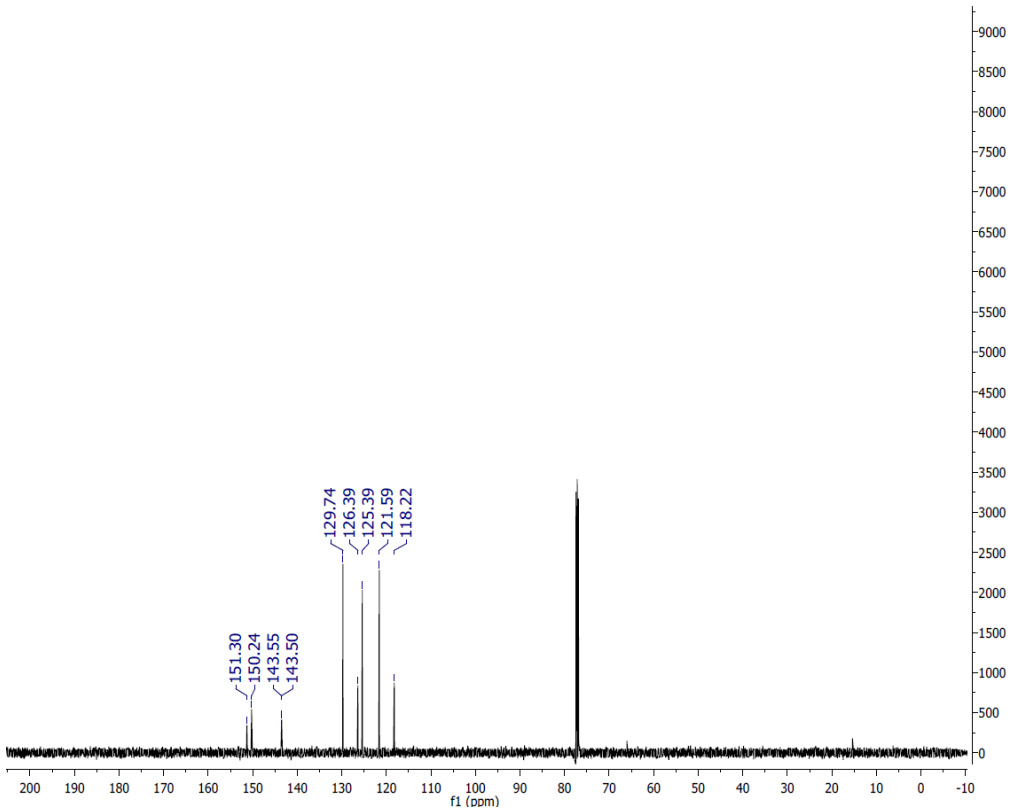
129.74
126.39
125.39
121.59
118.22
151.30
150.24
143.55
143.50
f1 (ppm)

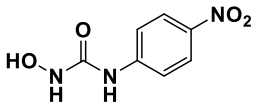
HO
N
H
O
N
H
NO2

S2

9.49
9.27
9.15
8.15
8.14
7.93
7.91
1.20
1.17
1.16
1.74
2.00
f1 (ppm)

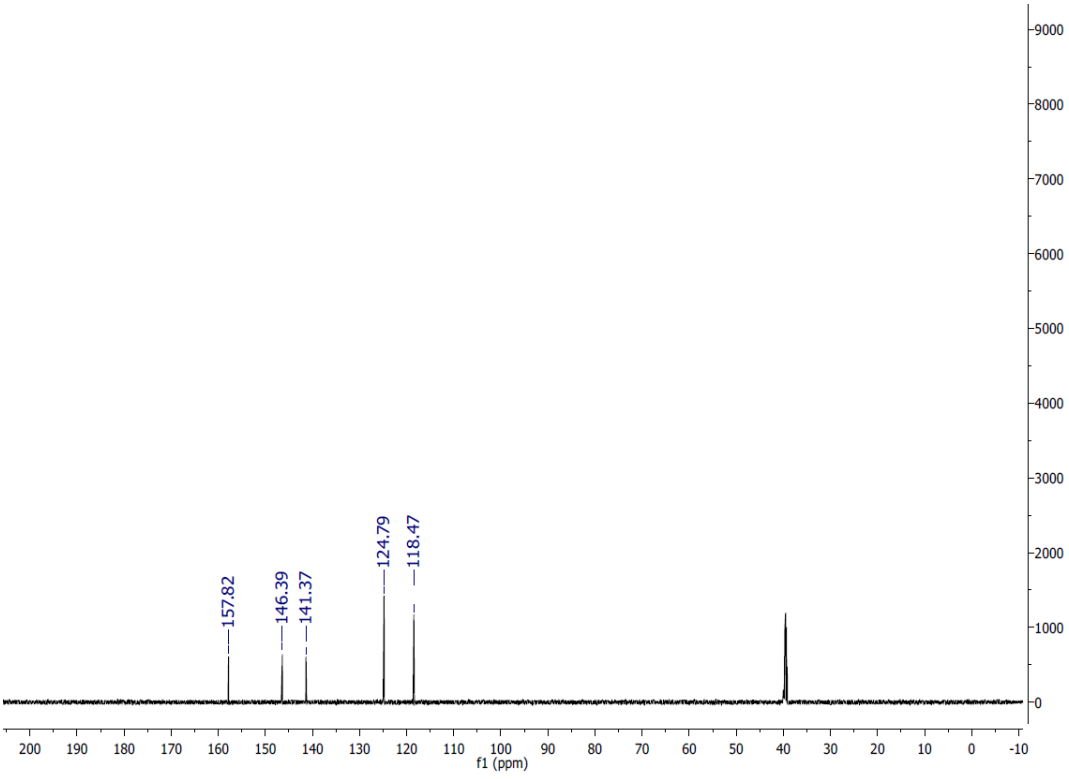
157.82
146.39
141.37
124.79
118.47
f1 (ppm)

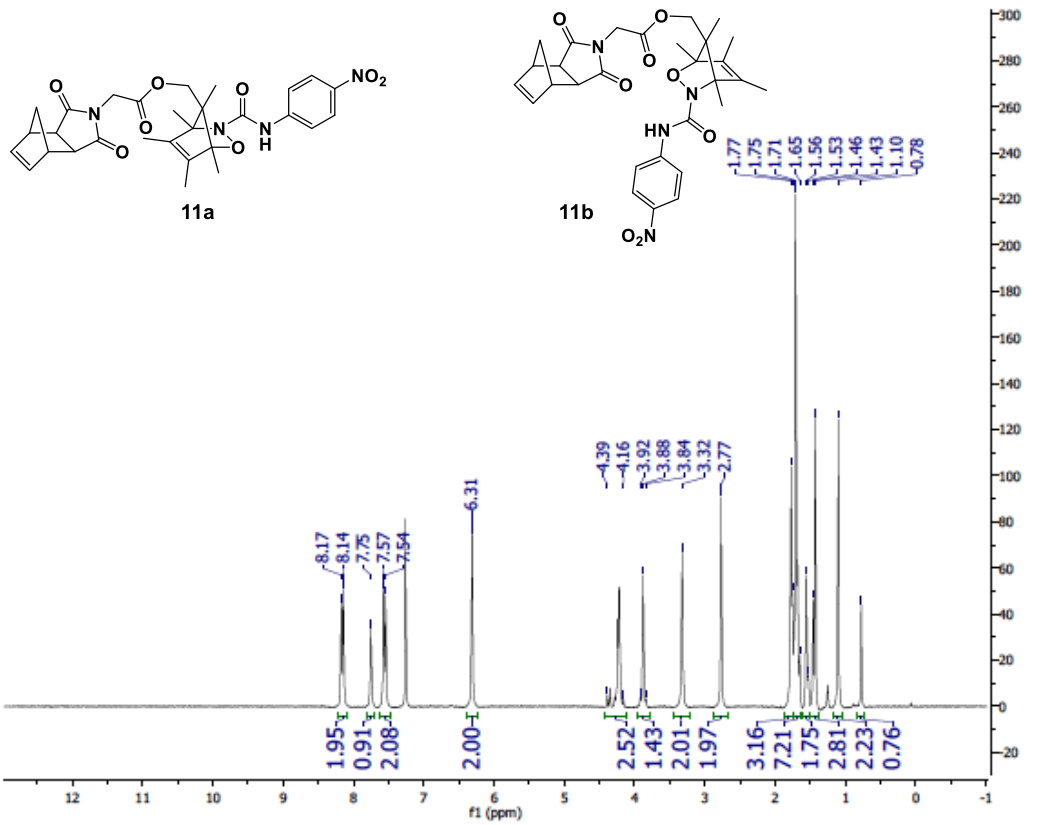
11a
11b
8.17
8.14
7.75
7.57
7.54
6.31
4.39
4.16
3.92
3.88
3.84
3.32
2.77
1.77
1.75
1.71
1.65
1.56
1.53
1.46
1.43
1.10
0.78
1.95
0.91
2.08
2.00
2.52
1.43
2.01
1.97
3.16
7.21
1.75
2.81
2.23
0.76
f1 (ppm)

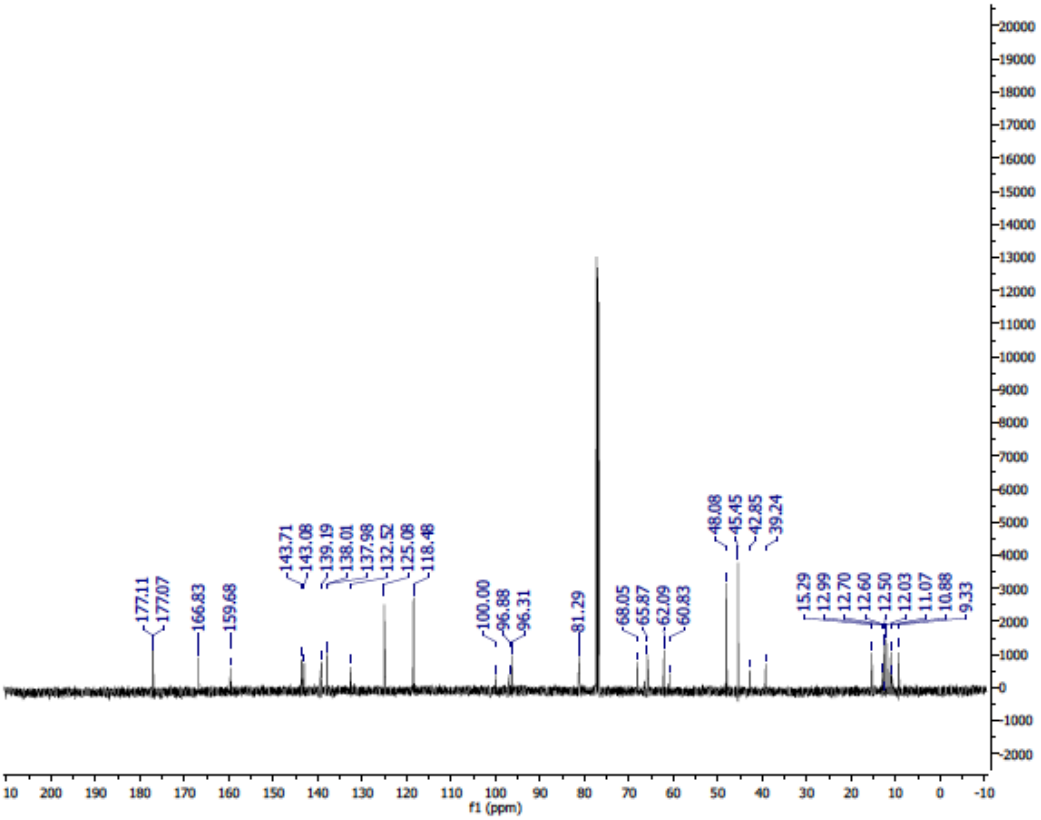
177.11
177.07
166.83
159.68
143.71
143.08
139.19
138.01
137.98
132.52
125.08
118.48
100.00
96.88
96.31
81.29
68.05
65.87
62.09
60.83
48.08
45.45
42.85
39.24
15.29
12.99
12.70
12.60
12.50
12.03
11.07
10.88
9.33
f1 (ppm)

2.5.14 *Representative NMR Stacked Plots of Small Molecule Isomerization at 60 °C*

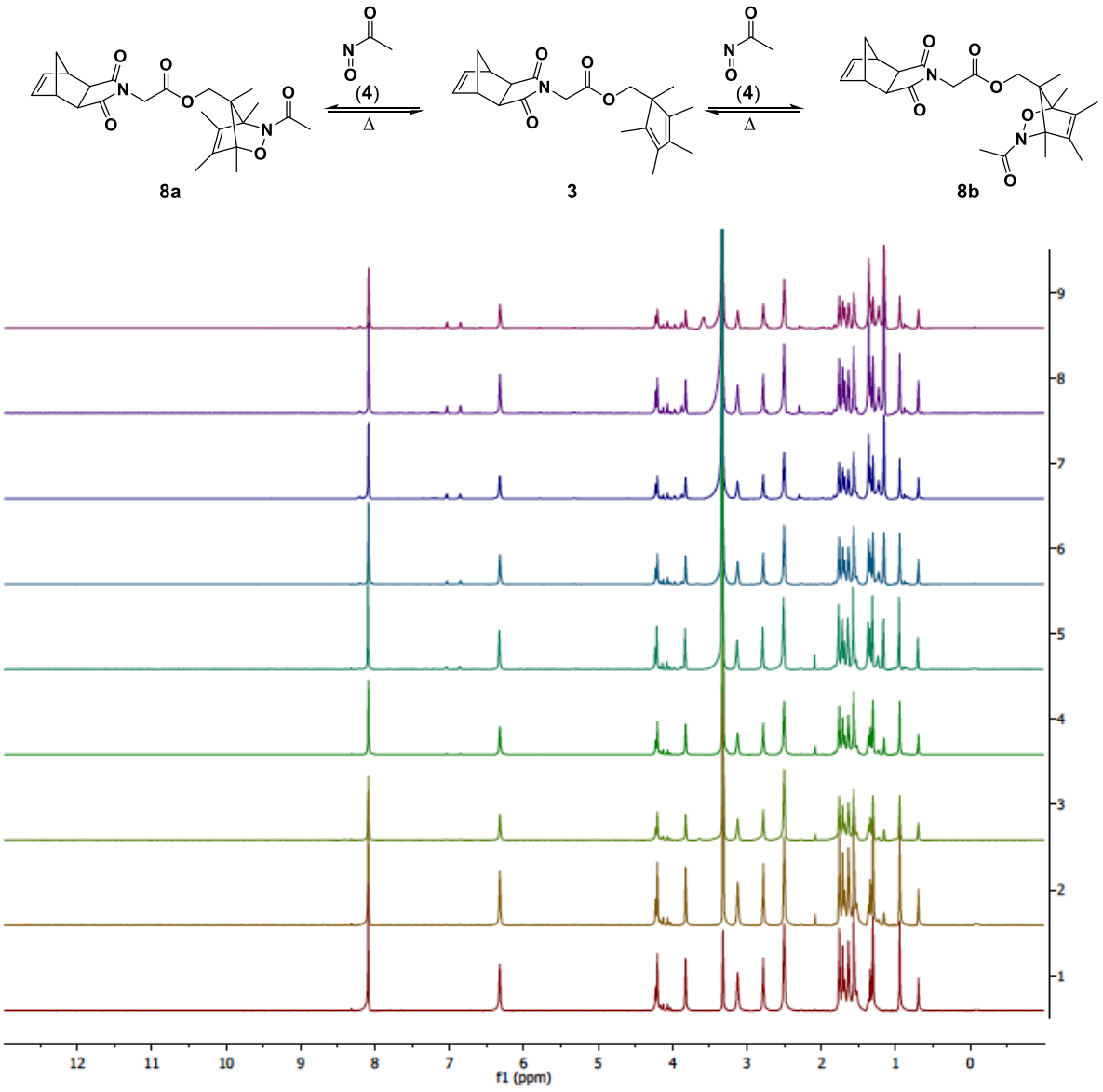

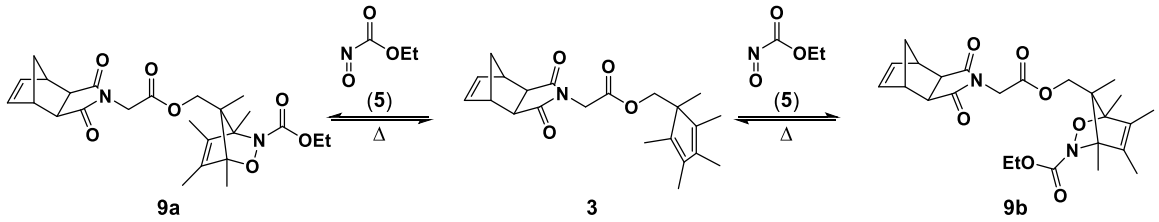

9a 3 9b

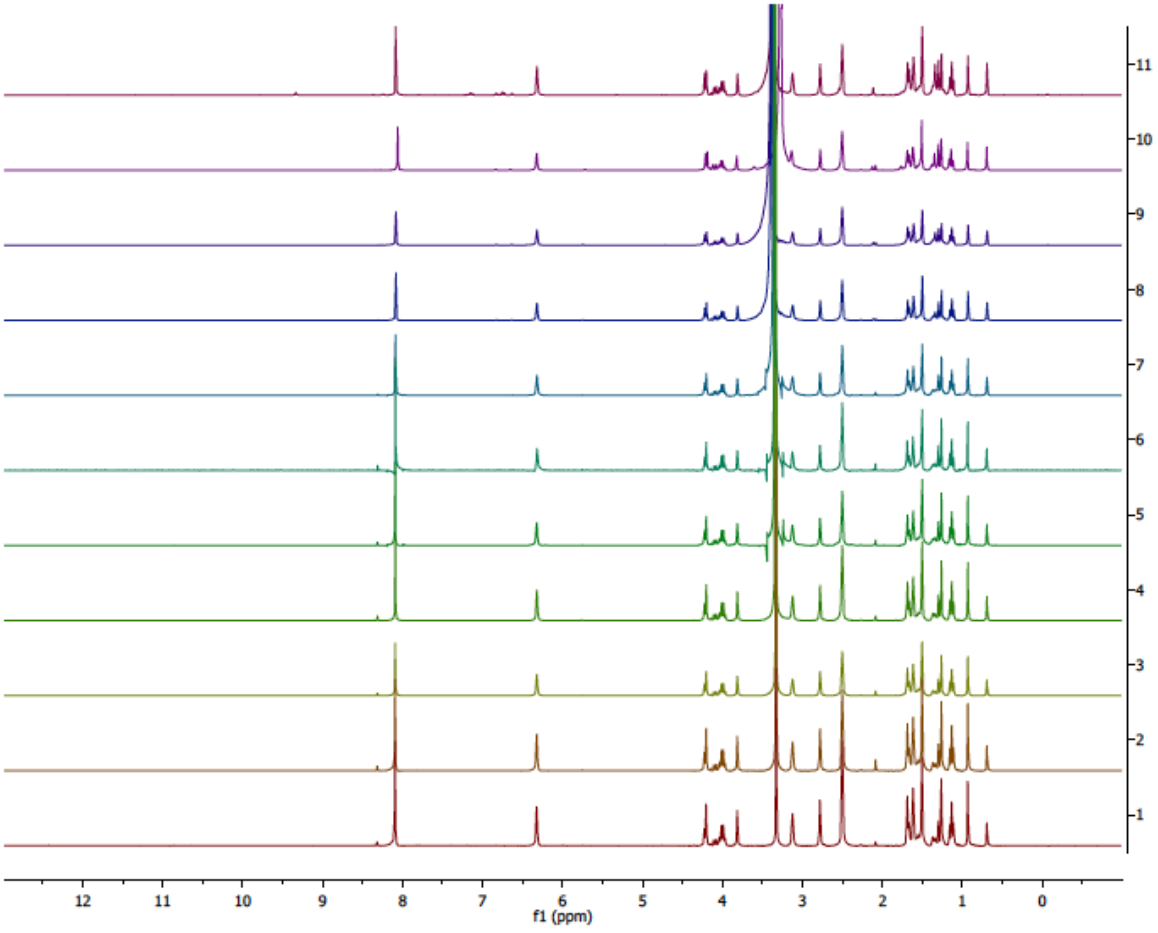

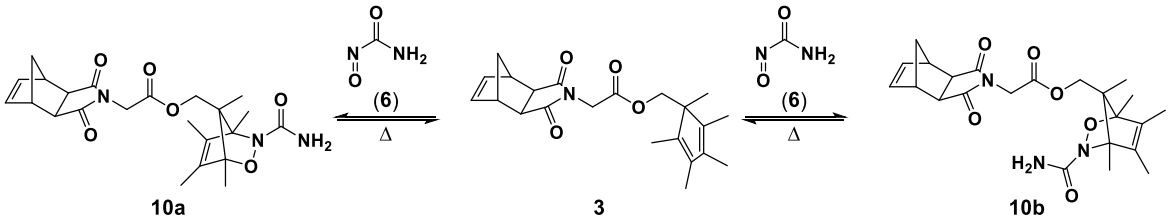
(6)
Δ
(6)
Δ
10a
3
10b

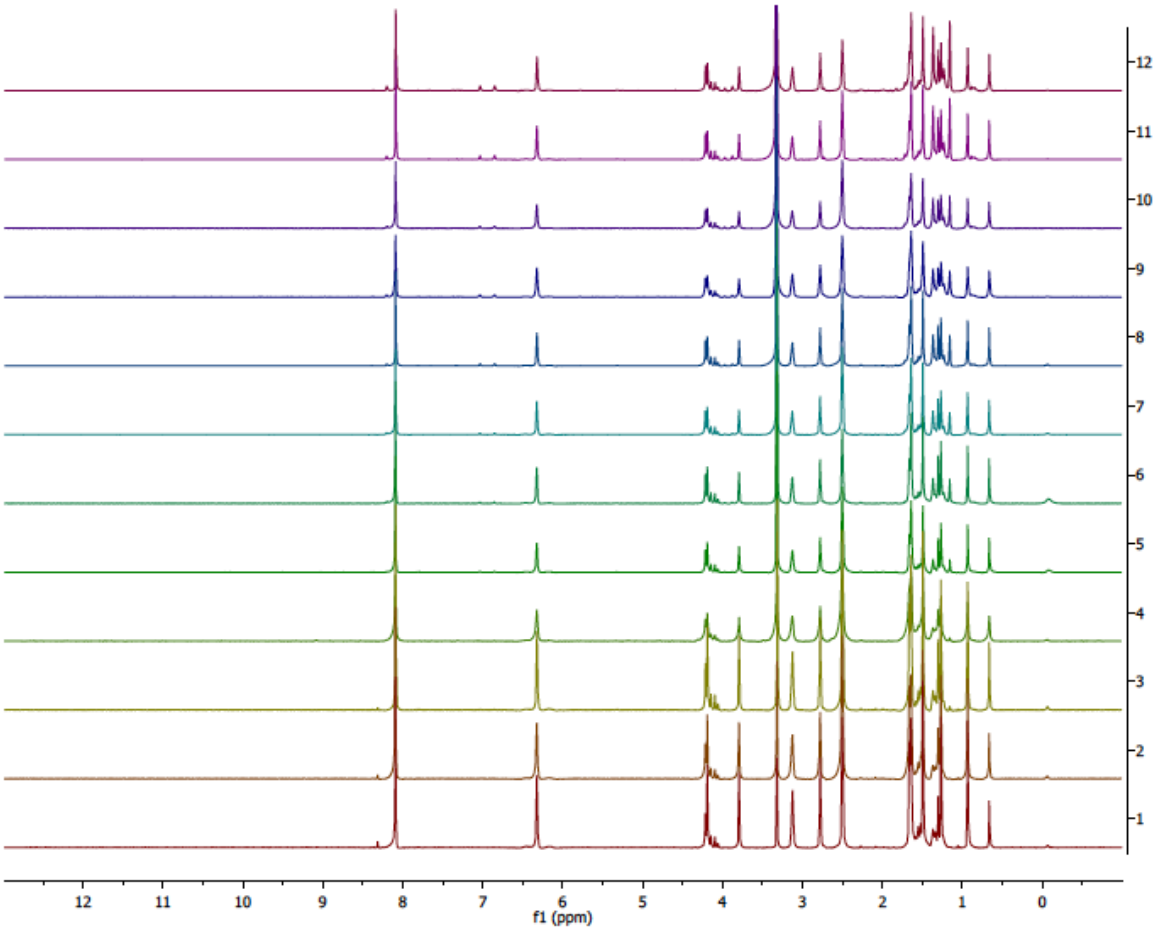
f1 (ppm)

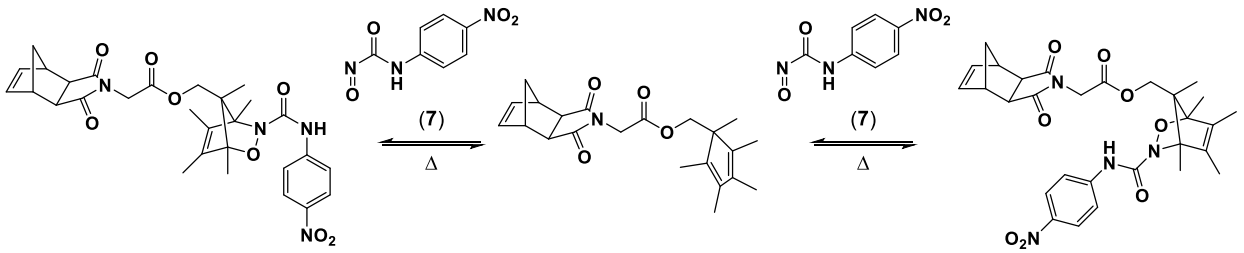

11a **3** **11b**

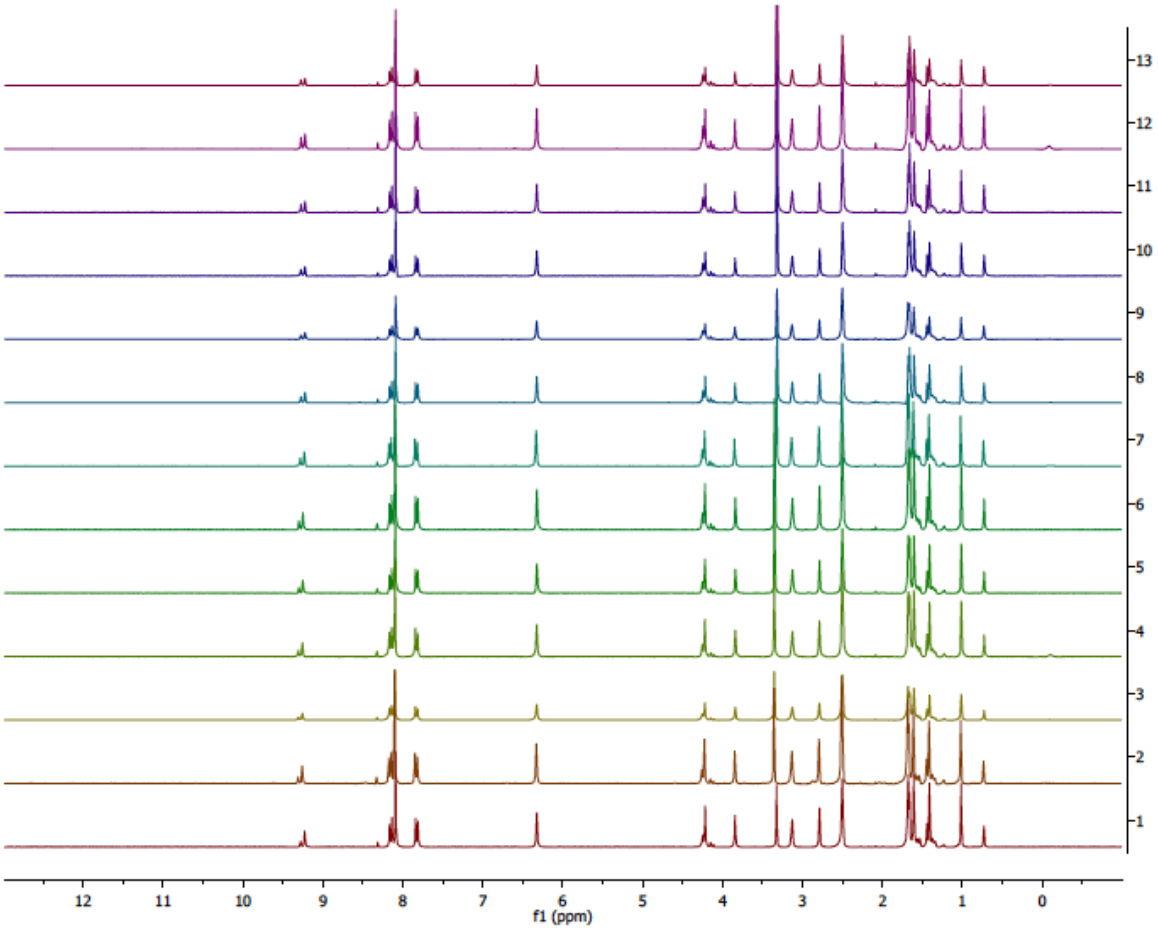

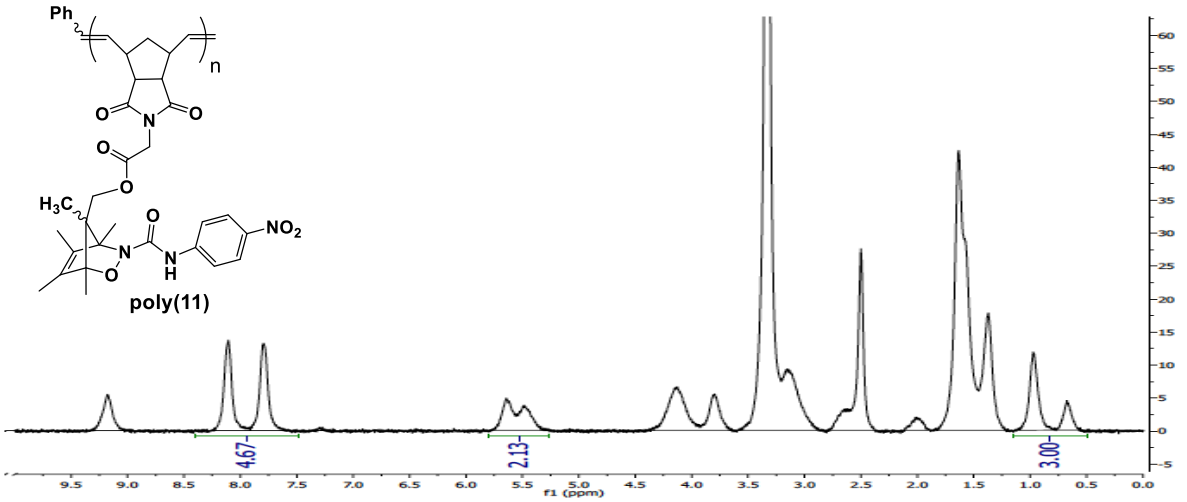
Ph
n
O
N
O
O
O
O
H3C
O
N
O
N
H
O
NO2
poly(11)
4.67
2.13
3.00
f1 (ppm)

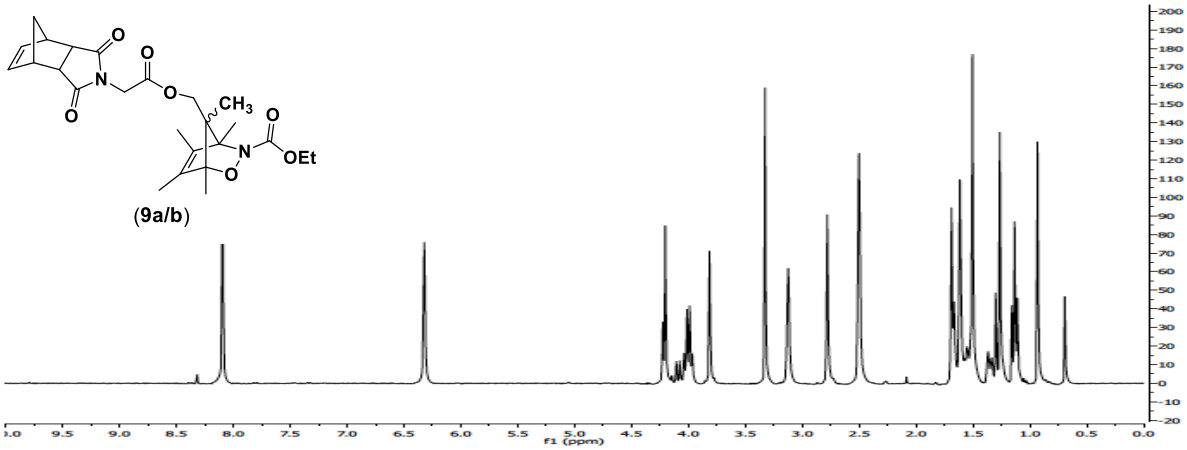
O
O
N
O
O
O
CH3
O
N
O
OEt
(9a/b)
f1 (ppm)

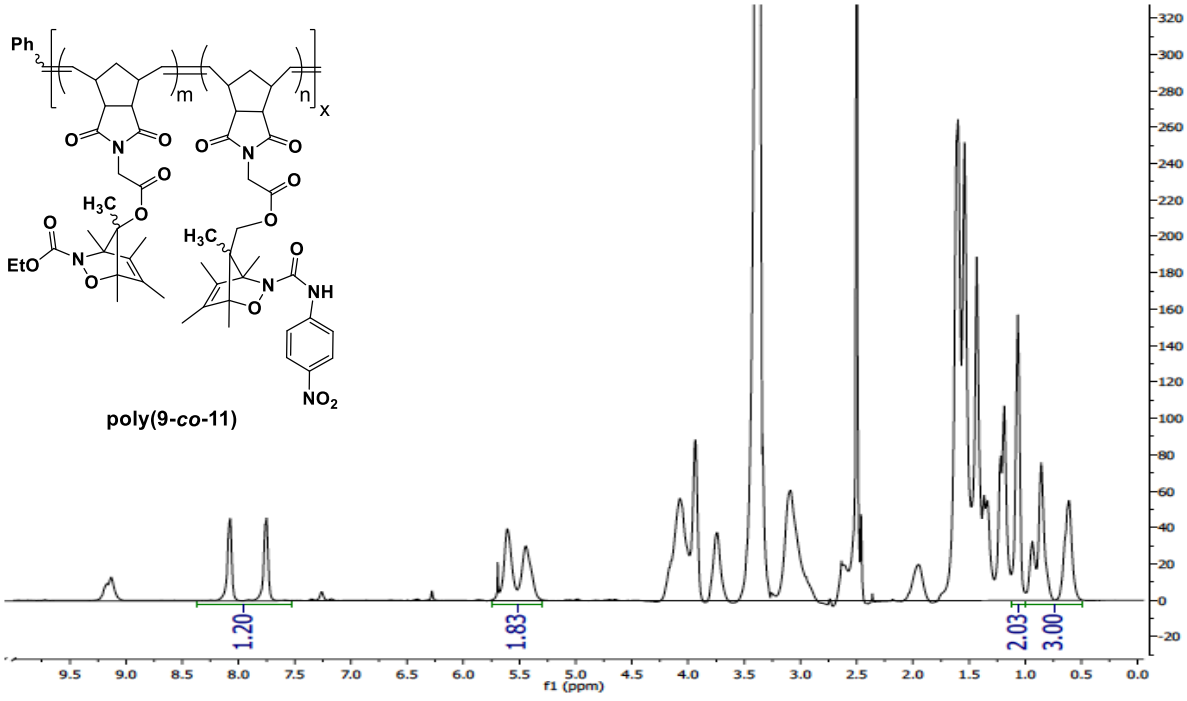
Ph
m
n
x
O
N
O
O
O
O
H3C
O
EtO
N
O
H3C
O
N
O
NH
NO2
poly(9-co-11)
1.20
1.83
2.03
3.00
f1 (ppm)

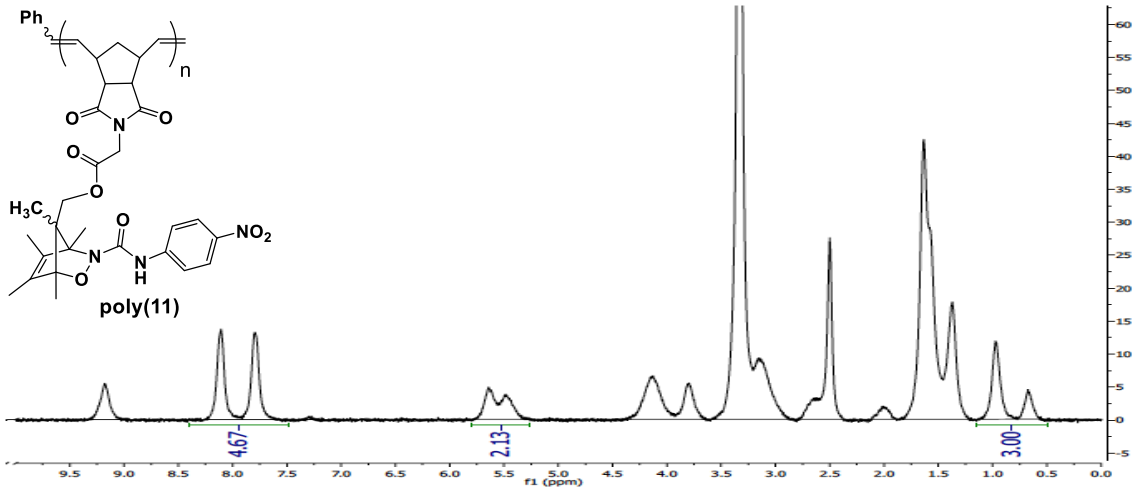
poly(11)
4.67
2.13
3.00
f1 (ppm)

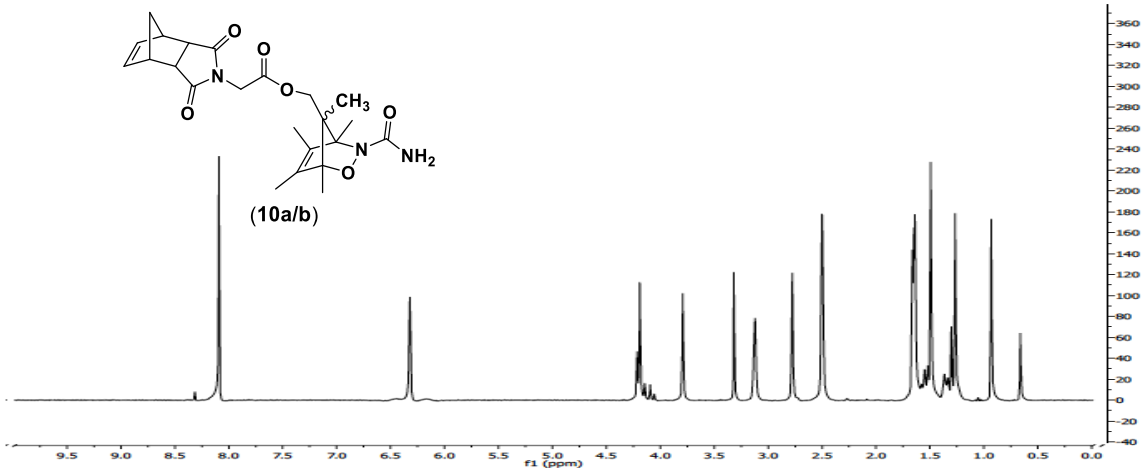
(10a/b)
f1 (ppm)

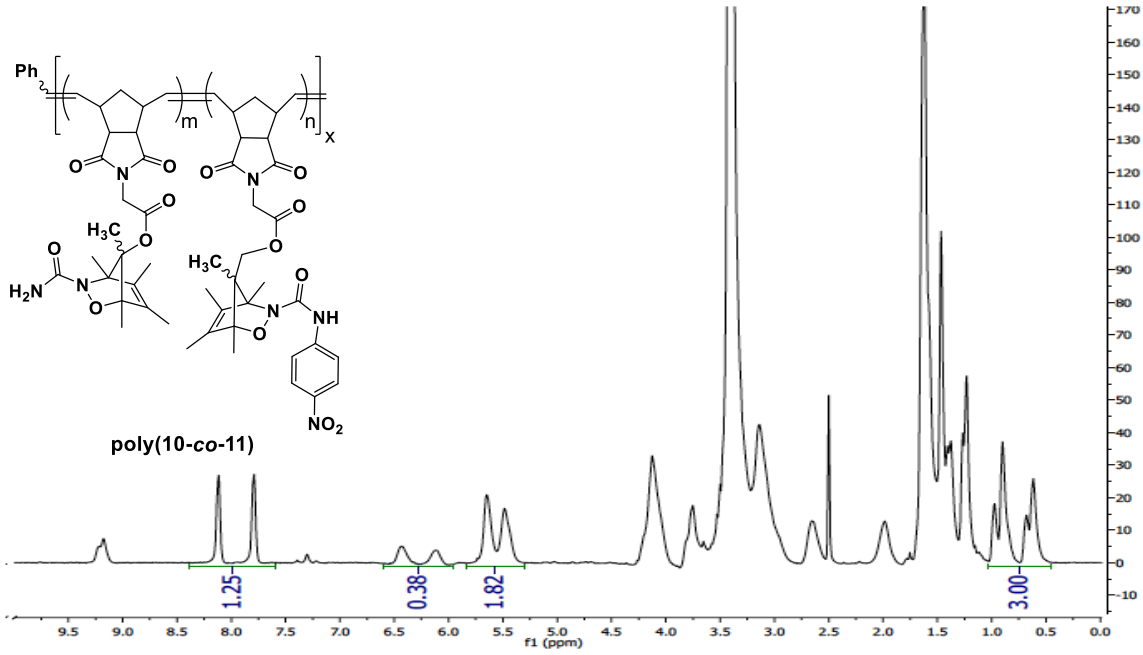
poly(10-co-11)
1.25
0.38
1.82
3.00
f1 (ppm)

2.5.15 *Experimental References*

1) Love, J. A.; Morgan, J. P.; Trnka, T. M.; Grubbs, R. H. *Angew. Chem. Int. Ed.* **2002**, *41*, 4035.
2) Conrad, R. M.; Grubbs, R. H. *Angew. Chem. Int. Ed.* **2009**, *48*, 8328.
3) Peterson, G. I.; Church, D. C.; Boydston, A. J. *Polymer* **2014**, *55*, 5980.
4) Jiang, Y.; Zhang, J.; Cao, Y.; Chai, X.; Zou, Y.; Wu, Q.; Zhang, D.; Jiang, Y.; Sun, Q. *Bioorg. Med. Chem. Lett.* **2011**, *21*, 4471.
5) Matsuo, K.; Nakagawa, H.; Adachi, Y.; Kameda, E.; Aizawa, K.; Tsumoto, H.; Suzuki, T.; Miyata, N. *Chem. Pharm. Bull.* **2012**, *60*, 1055.

Chapter 3. 1,2-OXAZINE LINKER AS A THERMAL TRIGGER FOR SELF-IMMOLATIVE POLYMERS

3.1 INTRODUCTION

Self-immolative polymers (SIPs) comprise an exciting class of functional macromolecules capable of head-to-tail depolymerization in response to an external stimulus.[1-3] The single triggering event that typically occurs at the chain end results in an amplified response as multiple repeat units are sequentially released from the activated polymer (Scheme 3.1). The selectivity and efficiency of triggering reactions are key to the successful deployment of SIPs in diverse applications including their potential use in sensory materials, drug delivery platforms, and lithographic plastics. Moreover, incorporation of triggering groups enables site-specificity during activation and potential tunability in the rate of activation. The variety of trigger designs for self-immolative polymers, dendrimers, and oligomers collectively utilize pH-, redox-, enzyme-, nucleophile-, and photo-mediated activation.[1b] While general thermal triggers for chemical reactions are well established,[4] many are not capable of activating SIPs and, to our knowledge, none have been demonstrated for this purpose.

Scheme 3.1. Generalized process for a SIP undergoing stimulus-triggered head-to-tail depolymerization.

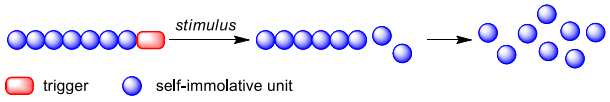

Thermally-activated SIPs may have practical advantages in the biomedical arena considering the techniques that are available for controlled localized heating. For example, photothermal[5] or magnetothermal[6] transduction, or focused ultrasound[7] may be viable methods for triggering depolymerization of SIPs with excellent spatiotemporal control. Additionally, passive activation at physiological temperatures may provide a simplified method for accomplishing sustained release of therapeutics, potentially mimicking continuous infusion with single, infrequent injections of drug-releasing SIPs.

Amidst relatively broad structural variations and sensitivities to stimuli, a unifying theme for SIP trigger reactivity is to unveil an electron-releasing functional group at the chain end of the SIP. The electron-releasing nature of the active chain end typically initiates a cascade of elimination or substitution reactions that depolymerize the macromolecule in a unidirectional, head-to-tail fashion. This mechanism of activation contrasts that of the thermal activation of low ceiling temperature polymers. For instance, when heated above ca. 150 °C, poly(phthalaldehyde) undergoes random mid-chain thermolysis and bidirectional depolymerizaiton.[8]

Inspired by the investigations of Kirby and King involving hydroxyurea and oxidized derivatives thereof, we envisioned substituted 1,2-oxazines may be good candidates for thermal triggers.[9] We anticipated the cycloreversion of a substituted 1,2-oxazine on the chain end of a SIP (e.g., **1**, Scheme 3.2) would result in a hydrolytically unstable carbamoylnitroso intermediate (**2**), as demonstrated for small molecule 1,2-oxazines.[9] Following hydrolysis of **2** and rapid decarboxylation of carbamic acid **3**, a free amine would be generated at the SIP chain end (e.g., **4**). A practical approach to installing oxazines involves oxidation of hydroxyureas and in situ trapping via [4+2] cycloaddition reactions with various dienes.[9,10] This cycloaddition was also recently shown to be a useful reaction for the conjugation of carbonylnitroso and diene end

group-functionalized polymers.[11] Herein, we describe the synthesis and evaluation of a viable thermal trigger for a versatile class of SIPs.

Scheme 3.2. Proposed mechanism of action of a thermally-activated SIP trigger.

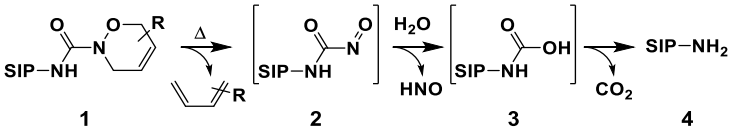

3.2 Results and Discussion

We considered polyurethane-based SIPs derived from *p*-aminobenzyl alcohol to be an attractive and versatile platform since they can be readily adapted for small-molecule release from side chain functionalities, turn-on fluorescence reporting, and solubility in water.[1] Thus, our first synthetic target was a polyurethane-based SIP with a hydroxyurea end cap. Beginning from phenyl carbamate **5** (Scheme 3.3), polymerization was conducted using Et_3N as a mediator at 60 °C in dry DMSO. We found these polymerization conditions to be more successful for our particular end group functionalization than Sn(IV)-mediated polymerizations,[2] albeit at the expense of slightly longer polymerization times. The hydroxyurea moiety was incorporated into the polymer by capping with NH_2OH after complete monomer consumption was observed as determined by ^{1}H NMR spectroscopy. Analysis via ^{1}H NMR spectroscopy of various experiments revealed the resulting SIP **6** to have average DPs of 8 – 12.

Scheme 3.3. Synthesis of SIP **6**.

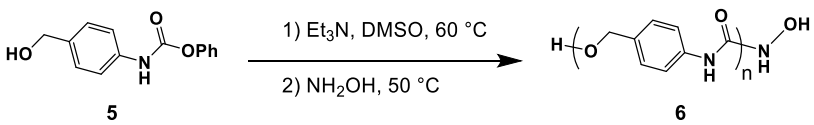

We next determined the extent to which formation and subsequent decomposition of the carbamoylnitroso end group would lead to SIP depolymerization. Toward this end, SIP **6** was subjected to conditions known to oxidize hydroxyureas directly to carbamoylnitroso intermediates.[10-12] Specifically, wet DMSO-d_6 (10% D_2O by volume) solutions of SIP **6** were treated with TBAP or CuCl and pyridine and monitored by ^{1}H NMR spectroscopy; key data are summarized in Table 3.1. Upon exposure to oxidizing conditions, we observed gradual depletion of the SIP **6** repeat units (entries 1 through 4) and generation of a mixture of products consistent with *p*-aminobenzyl alcohol (**7**), *p*-aminobenzaldehyde, and other unidentified compounds. As expected, using anhydrous DMSO-d_6 resulted in depolymerization to a lesser extent (entries 5 throught 8). Control experiments confirmed the need for oxidative conditions, indicating that hydrolysis was not occurring directly on the polymer main chain or end group (entries 9 and 10). These results indicated to us that if the carbamoylnitroso species could be liberated by cycloreversion of an oxazine on the chain end of a SIP, then thermally triggered depolymerization could be achieved. It is noteworthy that while a variety of hydroxyureas have been shown to undergo oxidative decomposition,[12] we are unaware of any reports on this reactivity being demonstrated for the activation of SIPs.

Table 3.1. Oxidation conditions for the depolymerization of SIP **6**.

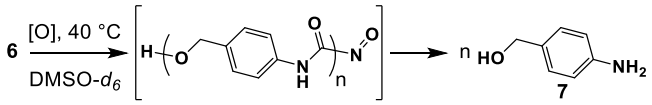

entry	additives	time (h)	% depolymerization
1	TBAP, D_2O	25	50
2	TBAP, D_2O	100	67
3	CuCl, pyridine, D_2O	25	42
4	CuCl, pyridine, D_2O	100	69
5	TBAP	25	11
6	TBAP	100	24
7	CuCl, pyridine	25	0
8	CuCl, pyridine	100	2
9	D_2O	25	1
10	D_2O	100	6

The % depolymerization = 100 - % SIP repeat units remaining, as determined by ^{1}H NMR spectroscopy using 1,4-dicyanobenzene as an internal standard.

We next focused on installing the oxazine at the triggering position of the SIP (Scheme 3.4). A cyclopentadiene derivative was targeted as the diene constituent of the oxazine as they are known to provide good stability and mild cycloreversion temperaures,[9,11] and a diblock copolymer architecture comprising an oxazine junction between the SIP and an adjoining hydrophilic block. We reasoned that this synthetic strategy would circumvent issues arising from incomplete chain end functionalization during the hydroxyurea installation and oxazine formation, since the resulting diblock copolymer would display disparate solubility from uncoupled SIP chains. Moreover, the diblock architecture may provide an entryway into self-assembled or mechanochemically-initiated SIPs featuring the oxazine trigger.[3b,13,14] Toward this end, initiator **9** was prepared from pentamethylcyclopentadiene and used for atom-transfer radical polymerization of DMA, providing poly(*N*,*N*-dimethylacrylamide) (PDMA) **10**. Treatment of **10** with **6** in a 1:2 ratio under oxidative conditions provided complete end capping

of **10** to yield diblock copolymer **11**. Attempted coupling with a 1:1 ratio of the two resulted in mixtures of free SIP and PDMA in addition to **11**. Removal of residual **6** was accomplished by precipitation into CH_2Cl_2 followed by filtration through Celite/alumina. Notably, the selective precipitation of the unreacted SIP circumvents issues associated with incomplete chain end functionalization or oxidation to the carbamoylnitroso species. GPC and ^{1}H NMR analysis supported the successful 1:1 conjugation of the SIP and PDMA blocks. To evaluate the extent to which hydrolysis may be giving rise to background triggering of the SIP, we prepared control polymer **14** in which the trigger moiety is absent.

Scheme 3.4. Synthesis of diblock copolymers **11** and **14**.

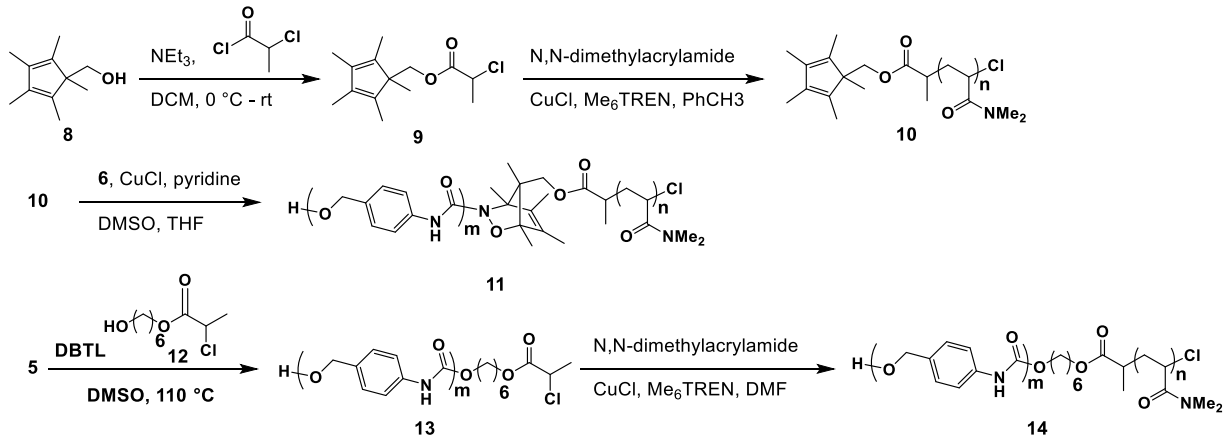

To avoid complications arising from insolubility of the SIP block after detachment from the PDMA, we conducted thermal triggering and depolymerization experiments in DMSO-d_6/D_2O mixtures (9:1 v/v). Figure 3.1 shows the amount of SIP depolymerization over time as **11** and **14** were heated at various temperatures. At a long-term storage temperature of 4 °C we saw negligible activity from **11** in solution over the course of 50 d. At RT, however, we observed gradual activation leading to 22% depolymerization after 65 d. As expected, at 40 °C more rapid activation and depolymerization was observed, reaching 61% depolymerization after ca. 71 d. At

60 and 85 °C, nearly full depolymerization was observed after ca. 47 and 5 d, respectively. We observed only 17% or 18% depolymerization when **14** was heated at RT or 40 °C for 81 d, respectively. At 60 and 85 °C, the rate of depolymerization was clearly much less for **14** than for the oxazine trigger variant (**11**), consistent with different mechanisms of activation between the two. The results from the control polymer suggested to us that hydrolysis plays a fairly significant role in the degradation of the SIP above 60 °C.

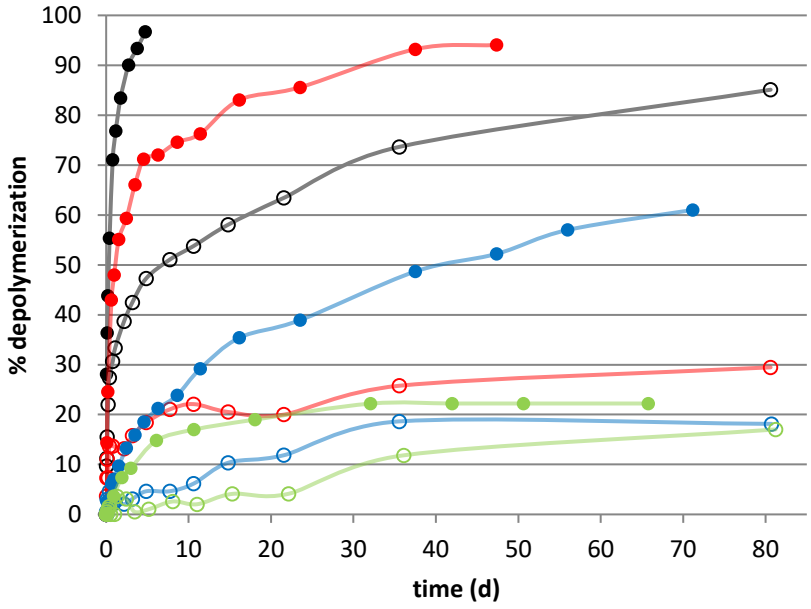

Figure 3.1. Thermal activation and depolymerization of SIPs **11** (filled circles) and **14** (empty circles) in DMSO-d_6/D_2O (9:1 v/v) at 85 °C (●,○), 60 °C (●,○), 40 °C (●,○), and RT (●,○). The % depolymerization = 100 - % SIP repeat units remaining, as determined by ^{1}H NMR spectroscopy using 1,4-dicyanobenzene as an internal standard. Average of two runs. The colored lines are for visual aid only.

Additional confirmation of the oxazine trigger reactivity was obtained from thermolysis of **11** in the presence of excess 1,3-cyclohexadiene (Figure 3.2). Specifically, heating **11** at 60 °C in

DMSO-d_6/D_2O (9:1 v/v) containing 300 equivalents (ca. 1.7% by volume) of 1,3-cyclohexadiene relative to oxazine trigger significantly suppressed the rate of depolymerization (see Supporting Information). Only 20% depolymerization was observed after 2 d, versus nearly 60% for **11** at the same time and temperature. These results are consistent with the intermediacy of a carbamoylnitroso species and formation of the more thermally stable cyclohexadiene adduct. ^{1}H NMR analysis also revealed increasing intensities of resonances centered at δ = 4.80 ppm that were consistent with bridgehead protons of the cyclohexadiene-based oxazine (see Supporting Information).

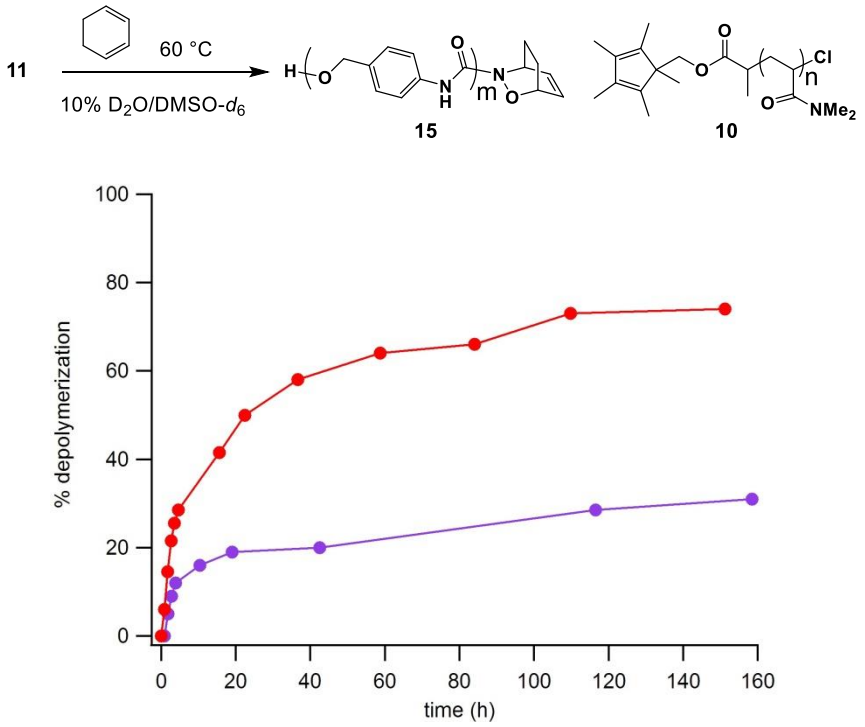

Figure 3.2. Thermal activation and depolymerization of SIP **11** in DMSO-d_6/D_2O (9:1 v/v) at 60 °C with (●) or without (●) 1,3-cyclopentadiene. The % depolymerization = 100 - % SIP repeat units remaining, as deter-mined by ^{1}H NMR spectroscopy using 1,4-dicyanobenzene as an internal standard. The colored lines are for visual aid only.

3.3 CONCLUSION

In summary, we have demonstrated a new class of SIP trigger that is responsive to mild thermal impetus. Our trigger comprises a bicyclic oxazine that is an efficient source of an electron rich functionality necessary for initiating depolymerization. Diene transfer studies support the proposed mechanism of a carbamoylnitroso intermediate. The temperature-dependent triggering provides an exciting approach for future on-demand SIP activation.

3.4 REFERENCES

1) For recent reviews, see: (a) Phillips, S. T.; Robbins, J. S.; DiLauro, A. M.; Olah, M. G. *J. Appl. Polym. Sci.* **2014**, DOI: 10.1002/APP.40992. (b) Phillips, S. T.; DiLauro, A. M. *ACS Macro Lett.* **2014**, *3*, 298. (c) Peterson, G. I.; Larsen, M. B.; Boydston, A. J. *Macromolecules* **2012**, *45*, 7317.

2) For the first example of a SIP, see: Sagi, A.; Weinstain, R.; Karton, N.; Shabat, D. *J. Am. Chem. Soc.* **2008**, *130*, 5434.

3) For recent SIP examples, see: (a) Fan, B.; Trant, J. F.; Wong, A. D.; Gillies, E. R. *J. Am. Chem. Soc.* **2014**, *136*, 10116. (b) Liu, G.; Wang, X.; Hu, J.; Zhang, G.; Liu, S. *J. Am. Chem. Soc.* **2014**, *136*, 7492. (c) Zhang, L.-J.; Deng, X.-X.; Du, F.-S.; Li, Z.-C. *Macromolecules* **2013**, *46*, 9554. (d) McBride, R. A.; Gillies, E. R. *Macromolecules* **2013**, *46*, 5157. (e) DiLauro, A. M.; Zhang, H.; Baker, M. S.; Wong, F.; Sen, A.; Phillips, S. T. *Macromolecules* **2013**, *46*, 7257. (f) Olah, M. G.; Robbins, J. S.; Baker, M. S.; Phillips, S. T. *Macromolecules* **2013**, *46*, 5924. (g) Lewis, G. G.; Robbins, J. S.; Phillips, S. T. *Macromolecules* **2013**, *46*, 5177. (h) DiLauro, A. M.; Abbaspourrad, A.; Weitz, D. A.; Phillips, S. T. *Macromolecules*

2013, *46*, 3309. (i) Robbins, J. S.; Schmid, K. M.; Phillips, S. T. *J. Org. Chem.* **2013**, *78*, 3159. (j) DiLauro, A. M.; Robbins, J. S.; Phillips, S. T. *Macromolecules* **2013**, *46*, 2963.

4) Sabongi, G. J. *Chemical Triggering: Reactions of Potential Utility in Industrial Processes*; Plenum Press: New York, 1987.

5) Alkilany, A. M.; Thompson, L. B.; Boulos, S. P.; Sisco, P. N.; Murphy, C. J. *Adv. Drug Del. Rev.* **2012**, *64*, 190.

6) Kumar, C. S. S. R.; Mohammad, F. *Adv. Drug Del. Rev.* **2011**, *63*, 789.

7) (a) Grüll, H.; Langereis, S. *J. Control. Release* **2012**, *161*, 317. (b) Haar, G.; Coussios, C. *Int. J. Hyperthermia* **2006**, *23*, 89.

8) (a) Coulembier, O.; Knoll, A.; Pires, D.; Gotsmann, B.; Duerig, U.; Frommer, J.; Miler, R. D.; Dubois, P.; Hedrick, J. L. *Macromolecules* **2010**, *43*, 572. (b) Knoll, A. W.; Pires, D.; Coulembier, O.; Dubois, P.; Hedrick, J. L.; Frommer, J.; Duerig, U. *Adv. Mater.* **2010**, *22*, 3361. (c) Kostler, S.; Zechner, B.; Trathnigg, B.; Fasl, H.; Kern, W.; Ribitsch, V. *J. Polym. Sci. Part A: Polym. Chem.* **2009**, *47*, 1499.

9) (a) Zeng, B.; Huang, J.; Wright, M. W.; King, S. B. *Bioorg. Med. Chem. Lett.* **2004**, *14*, 5565. (b) Xu, Y.; Alavanja, M.; Johnson, V. L.; Yasaki, G.; King, S. B. *Tetrahedron Lett.* **2000**, *41*, 4265. (c) Christie, C. C.; Kirby, G. W.; McGuigan, H.; Mackinnon, J. W. M. *J. Chem. Soc. Perkin Trans.* **1985**, *1*, 2469.

10) (a) Frazier, C.; Bugarin, A.; Engelking, J.; Read de Alaniz, J. *Org. Lett.* **2012**, *14*, 3620. (b) Chaiyaveij, D.; Cleary, L.; Batsanov, A.; Marder, T.; Shea, K.; Whiting, A. *Org. Lett.* **2011**, *13*, 3442.

11) Samoshin, A. V.; Hawker, C. J.; Read de Alaniz, J. *ACS Macro Lett.* **2014**, *3*, 753.

12) King, S. B. *Curr. Med. Chem.* **2003**, *10*, 437.

13) DeWit, M. A.; Gillies, E. R. *J. Am. Chem. Soc.* **2009**, *131*, 18327.

14) (a) Diesendruck, C. E.; Peterson, G. I.; Kulik, H. J.; Kaitz, J. A.; Mar, B. D.; May, P. A.; White, S. R.; Martínez, T. J.; Boydston, A. J.; Moore, J. S. *Nat. Chem.* **2014**, *6*, 623. (b) Peterson, G. I.; Boydston, A. J. *Macromol. Rapid Commun.* **2014**, *in press* (DOI: 10.1002/marc.201400271).

3.5 EXPERIMENTAL

3.5.1 *General Considerations*

Dry dimethylsulfoxide (DMSO), tetrahydrofuran (THF), toluene, and CH_2Cl_2 were obtained from a Glass Contour solvent purification system. Et_3N and *N*,*N*-dimethylacrylamide (DMA) were distilled after drying over CaH_2 overnight. Tetrabutylammonium periodate (TBAP) was dried with P_2O_5 overnight before use. House N_2 was passed through a drying tube before use. Self-immolative monomer **5** was prepared as previously described.[2] All other reagents and solvents were used as obtained from commercial sources. ^1H and ^{13}C NMR spectra were recorded on a Bruker AVance 300 and 500 MHz spectrometers. Chemical shifts are reported in delta (δ) units, expressed in parts per million (ppm) downfield from tetramethylsilane using the residual protio-solvent as an internal standard ($CDCl_3$, ^1H: 7.26 ppm and ^{13}C: 77.16 ppm; DMSO-d_6, ^1H: 2.50 ppm and ^{13}C: 39.5 ppm). GPC setup consisting of: a Shimadzu pump, 3 in-line columns, and Wyatt light scattering and refractive index detectors with 0.01 M LiBr in DMF as the mobile phase.

3.5.2 *Synthesis of **6**.*

A flame-dried round-bottom flask under N_2 was charged with 6 g (24.6 mmol, 1.0 mol. equiv.) of **5** and a stir bar. Dry DMSO (12.3 mL, **5** at 2.0 M) and dry Et_3N (3.5 mL, 24.7 mmol, 1.0 mol. equiv.) were then added. The solution was heated at 60 °C for 2.5 h. At that time, a small aliquot was removed and the degree of polymerization (DP) was determined by ^1H NMR spectroscopy by comparing the areas of the peaks corresponding to end groups and repeat units. To the reaction mixture was then added hydroxylamine (16.8 mmol, 5.0 mol. equiv. relative to end group) from a 1.0 M stock solution prepared in dry DMSO. The resulting mixture was stirred for 6 h at 50 °C. The reaction mixture was then poured into MeOH (approximately 10 times the volume of DMSO) and cooled in a refrigerator causing precipitation of the polymer. The precipitate was collected on a sintered-glass Büchner funnel and dried under vacuum. The yield was 89% by mass recovery. An average run yields 90-100% capped SIP. Technical note: The hydroxylamine solution was prepared by combining hydroxylamine hydrochloride (20 mmol) with anhydrous K_2CO_3 (40 mmol) in dry DMSO (20 mL, hydroxylamine at 1.0 M). The mixture was stored at room temperature (RT) for 12 h prior to use.

3.5.3 *Synthesis of **8**.*

To a flame-dried, N_2-purged three neck round-bottom flask, fit with a condenser, was added paraformaldehyde (580 mg) and dry THF (10.5 mL). The resulting suspension was refluxed under N_2 for 2 h and then cooled to RT. To a separate flame-dried, N_2-purged round bottom flask was added 1,2,3,4,5-pentamethylcyclopentadiene (0.6 mL, 3.83 mmol, 1.0 mol. equiv.), tetrabutylammonium iodide (140 mg, 0.38 mmol, 0.1 mol. equiv.), dry THF (8.0 mL), and a stir bar. The solution was cooled to 0 °C and n-butyllithium (2.33 M, 4.6 mmol, 1.2 equiv) was

added dropwise. A white precipitate immediately began to form. The suspension was stirred for 45 min at 0 °C, then paraformaldehyde from the previously refluxed solution (230 mg, 7.66 mmol, 2.0 mol. equiv.) was added and stirred for 18 h, letting the ice bath expire. The solvent was then removed under reduced pressure and the solids were redissolved/resuspended in diethyl ether. This mixture was washed sequentially with 1.0 M HCl, sat. $NaHCO_3$ aq., and H_2O. The organic solution was dried over Na_2SO_4 and the solvent was removed under reduced pressure. The crude mixture was then purified by flash column chromatography to give a transparent light yellow oil in 56% yield. ^{1}H NMR (300 MHz, $CDCl_3$) δ 3.50 (s, 2H), 1.77 (d, *J* = 18.8 Hz, 12H), 0.87 (s, 3H). ^{13}C NMR (126 MHz, $CDCl_3$) δ 138.0, 136.2, 65.3, 58.4, 16.8, 11.3, 9.7.

3.5.4 *Synthesis of **9**.*

A flame-dried round bottom flask under nitrogen was charged with **8** (679 mg, 4.08 mmol, 1.0 mol. equiv.), dry CH_2Cl_2 (18.0 mL), and a stir bar. The solution was cooled to 0 °C and Et_3N (0.63 mL, 4.49 mmol, 1.1 mol. equiv.) was added. A solution of 2-chloropropionyl chloride (0.44 mL, 4.49 mmol, 1.1 mol. equiv.) in dry CH_2Cl_2 (6.0 mL) was made prepared under a N_2 atmosphere and added dropwise to the solution containing **8**. The reaction mixture was stirred for 18 h, letting the ice bath expire. The reaction solvent was then removed under reduced pressure and the solids were redissolved/resuspended in diethyl ether. This mixture was washed sequentially with sat. $NaHCO_3$ aq., and H_2O. The organic solution was dried over Na_2SO_4 and the solvent was removed under reduced pressure to give a yellow/brown oil. The product was isolated by flash column chromatography to obtain a transparent yellow oil in 71% yield. ^{1}H NMR (300 MHz, $CDCl_3$) δ 4.31 (m, *J* = 13.9, 7.0 Hz, 1H), 4.05 (q, *J* = 10.7 Hz, 2H), 1.75 (s,

12H), 1.59 (d, J = 7.0 Hz, 3H), 0.96 (s, 3H). ^{13}C NMR (75 MHz, $CDCl_3$) δ 170.0, 138.4, 135.4, 68.9, 55.7, 52.9, 21.7, 16.8, 11.2, 10.3.

3.5.5 *Synthesis of **10**.*

Freshly distilled DMA (11.2 mL, 109 mmol, 350 mol. equiv. to initiator), CuCl (92 mg, 0.93 mmol, 3.0 mol. equiv.), and dry toluene (10.0 mL) were added to a Schlenk tube in a glove box. The reaction solution underwent three freeze-pump-thaw cycles, after which tris[2-(dimethylamino)ethyl]amine (Me_6TREN) (0.25 mL, 0.93 mmol, 3.0 mol. equiv.) was added and stirred for 30 min. Lastly, **9** (82 mg, 0.31 mmol, 1.0 mol. equiv.) was added and the polymerization was stirred for 5 h at RT. The reaction solution was diluted with THF and put through an alumina plug. The polymer solution was concentrated under vacuum and then dissolved in approximately 4 mL of CH_2Cl_2. A sat. ethylenediaminetetraacetic acid (EDTA) aq. solution (1.0 mL) was added and the layers were stirred vigorously so that remaining copper would be absorbed into the aqueous layer. Na_2SO_4 was then added to dry the solution. The remaining solids were removed by filtration and the solvent was removed from the solution under reduced pressure. The resulting oily polymer residue was then redissolved in a minimal volume of pyridine and precipitated into ether (approximately 10 times the volume of the polymer solution). The precipitate was collected on a sintered-glass Büchner funnel and dried under vacuum. An off-white powder was recovered in 65% yield (7.0 g). M_n =26.5 kDa, PDI = 1.07.

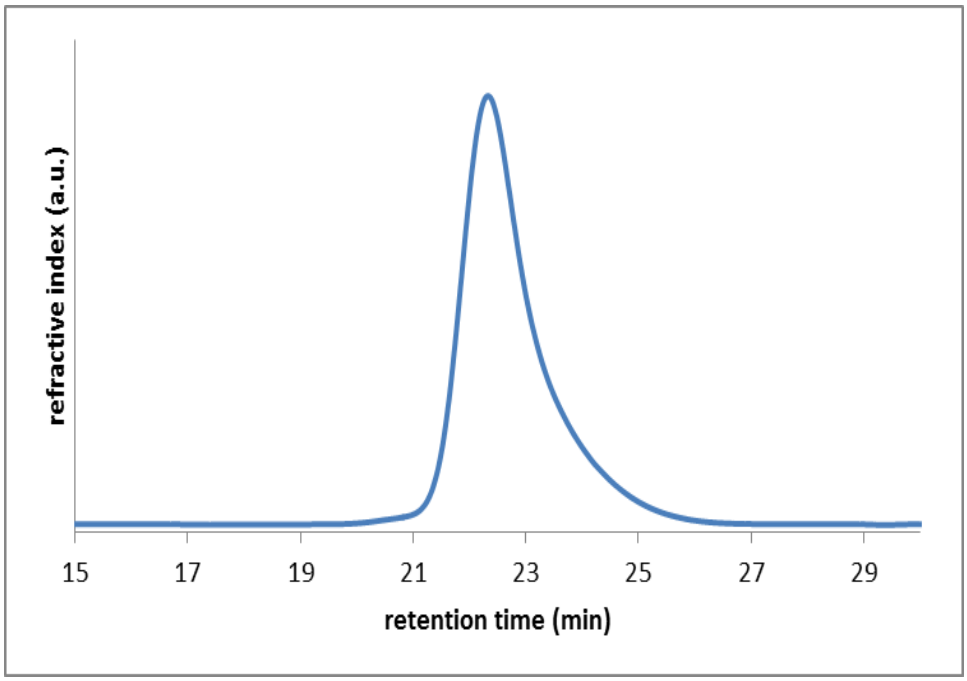

Figure 3.3. GPC trace of polymer **10**.

3.5.6 *Synthesis of **11***.

A flame-dried round-bottom flask was charged with SIP **6** (138 mg, 0.086 mmol, 2.0 mol. equiv.) and dry DMSO (10.0 mL). Once the SIP fully dissolved, **10** (1.08 g, 0.043 mmol, 1.0 mol. equiv.) and THF (10.0 mL) were added followed by CuCl (34 mg, 0.34 mmol, 0.8 mol. equiv.) and pyridine (7 μL, 0.086 mmol, 0.2 mol. equiv.). The reaction solution was stirred (open to air) for 24 h at RT. The solution was then precipitated into CH_2Cl_2 and filtered through a celite/alumina plug in a sintered-glass Büchner funnel. The CH_2Cl_2 was then removed under reduced pressure and the remaining DMSO/polymer solution was added into diethyl ether. The polymer oiled out on bottom of flask. After decanting away the ether solution, the polymer was dissolved in a minimal volume of CH_2Cl_2 and precipitated into ether. The precipitate was collected on a sintered-glass Büchner funnel then dried under vacuum. A slightly off-white powder was recovered in 37% yield (402 mg). M_n =31.3 kDa, PDI = 1.03.

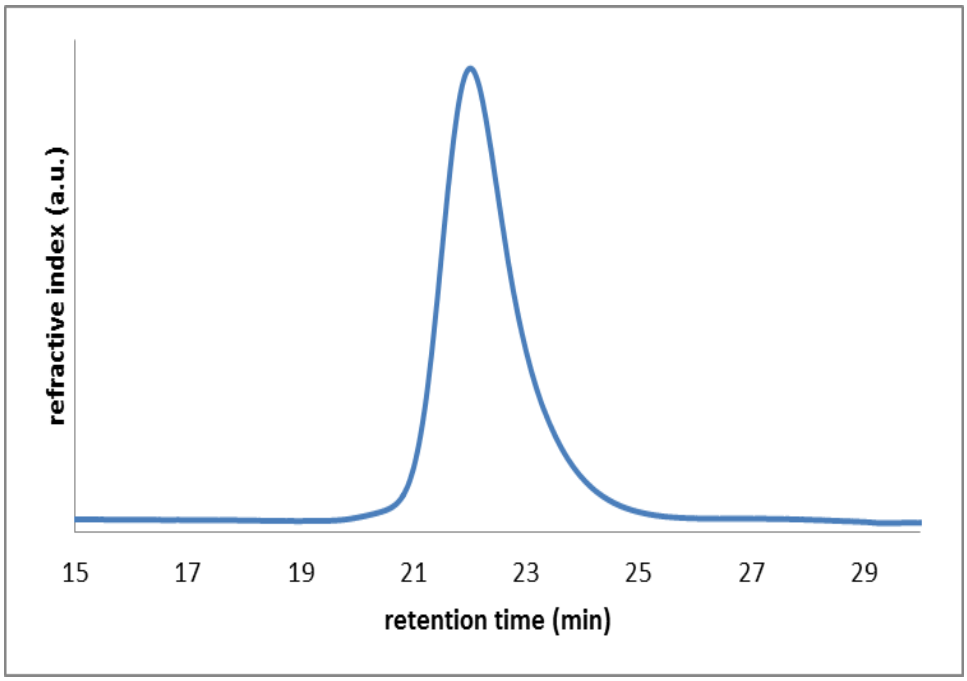

Figure 3.4. GPC trace of polymer **11**.

3.5.7 *Synthesis of **12**.*

A flame-dried round bottom flask under N_2 atmosphere was charged with 1,6-hexanediol (4.0 g, 33.84 mmol, 6.0 mol. equiv.), dry CH_2Cl_2 (24.0 mL), and a stir bar. The solution was cooled to 0 °C and Et_3N (0.79 mL, 5.64 mmol, 1.0 mol. equiv.) was added. A solution of 2-chloropropionyl chloride (0.55 mL, 5.64 mmol, 1.0 mol. equiv.) in dry CH_2Cl_2 (6.0 mL) was prepared under N_2 atmosphere and added dropwise to the solution containing the diol. The reaction mixture was stirred for 18 h, letting the ice bath expire. The reaction solvent was then removed under reduced pressure and the solids were redissolved/resuspended in diethyl ether. This mixture was washed sequentially with sat. $NaHCO_3$ aq., and H_2O. The organic solution was dried over Na_2SO_4 and the solvent was removed under reduced pressure. The product was isolated by flash column chromatography (50% EtOAc/Hex) to obtain a transparent colorless oil

in 52% yield. ^{1}H NMR (300 MHz, DMSO) δ 4.70 (q, *J* = 6.8 Hz, 1H), 4.33 (t, *J* = 5.2 Hz, 1H), 4.12 (t, *J* = 6.6 Hz, 2H), 3.37 (dd, *J* = 11.6, 6.3 Hz, 2H), 1.58 (m, 5H), 1.41 (m, 2H), 1.31 (m, 4H). ^{13}C NMR (126 MHz, DMSO) δ 169.5, 65.4, 60.6, 52.8, 32.3, 27.9, 25.1, 25.1, 21.2.

3.5.8 *Synthesis of **13**.*

A flame-dried round bottom flask under N_2 atmosphere was charged with self-immolative monomer **5** (300.0 mg, 1.23 mmol, 1.0 mol. equiv.), dry DMSO (0.6 mL), and a stir bar. Alcohol **12** (31.0 mg, 0.12 mmol, 0.1 mol. equiv.) and dibutyltin dilaurate (DBTL) (36.0 µL, 0.06 mmol, 0.06 mol. equiv.) were added. The reaction mixture was then placed on heat at 110 °C for 2 hours. The reaction mixture was then poured into MeOH (approximately 10 times the volume of DMSO) and cooled in a refrigerator causing precipitation of the polymer. The precipitate was collected on a sintered-glass Büchner funnel and dried under vacuum. The yield was 56% by mass recovery. The SIP was ca. 81% capped with alcohol **12** and had a DP of ca. 10.

3.5.9 *Synthesis of **14**.*

Freshly distilled DMA (1.5 mL, 15.0 mmol, 300 mol. equiv. to initiator), CuCl (14.8 mg, 0.15 mmol, 3.0 mol. equiv.), and dry DMF (1.5 mL) were added to a Schlenk tube in a glove box. The reaction solution underwent three freeze-pump-thaw cycles, after which Me_6TREN (40.2 µL, 0.15 mmol, 3.0 mol. equiv.) was added and stirred for 30 min. Lastly, **13** (87.2 mg, 0.05 mmol, 1.0 mol. equiv.) was added and the polymerization was stirred for 14 h at RT. The solution was then precipitated into diethyl ether. The solids were collected and redissolved in

CH_2Cl_2. This solution was filtered through a Celite/alumina plug in a sintered-glass Büchner funnel. The solution was then concentrated and again precipitated into diethyl ether. The precipitate was collected on a sintered-glass Büchner funnel and dried under vacuum. The polymer was obtained in 60% yield. M_n=14.9 kDa, PDI = 1.33.

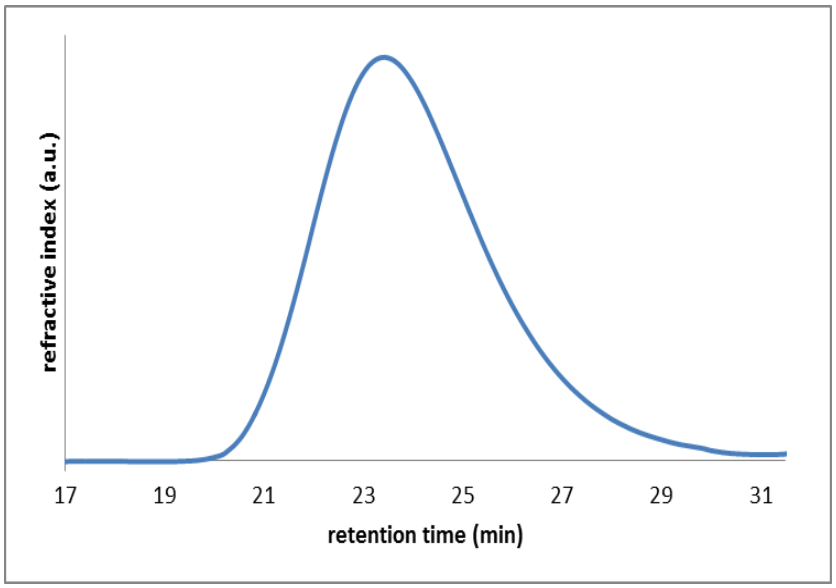

Figure 3.5. GPC trace of polymer **14**.

3.5.10 *Synthesis of **15**.*

A flame-dried round-bottom flask was charged with SIP **6** (100 mg, 0.091 mmol, 1.0 mol. Equiv.), 1,3-cyclohexadiene (0.36 mL, 4.55 mmol, 50 mol. Equiv.) and a stir bar. The mixture was dissolved in dry DMSO (1.6 mL) and THF (0.4 mL). CuCl (7.12 mg, 0.072 mmol, 0.8 mol. Equiv.) and pyridine (1.45 µL, 0.2 mol. Equiv.) were then added. After 16 h of stirring (open to air) at RT, the reaction mixture was poured into MeOH (approximately 10 times the volume of DMSO) and cooled in a refrigerator causing precipitation of the polymer. The precipitate was collected on a sintered-glass Büchner funnel, washed with CH_2Cl_2 and dried under vacuum. The product was obtained in 65% yield with 60% of the chain ends bearing the desired adduct.

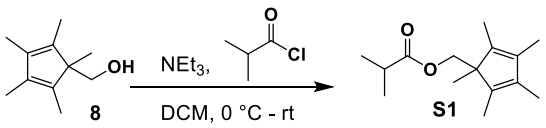

3.5.11 *Synthesis of **S1***.

A flame-dried round bottom flask under N_2 was charged with **8** (1.316 g, 7.91 mmol, 1.0 mol. equiv.), dry CH_2Cl_2 (24.0 mL), and a stir bar. The solution was cooled to 0 °C and Et_3N (1.67 mL, 11.86 mmol, 1.5 mol. equiv.) was added followed by the dropwise addition of isobutyryl chloride (1.25 mL, 11.86 mmol, 1.5 mol. equiv.). The reaction mixture was stirred for 24 h, letting the ice bath expire. The reaction solvent was then removed under reduced pressure and the solids were redissolved/resuspended in diethyl ether. This mixture was washed sequentially with sat. $NaHCO_3$ aq., and H_2O. The organic solution was dried over Na_2SO_4 and the solvent was removed under reduced pressure to give a yellow/organe oil. The product was isolated by flash column chromatography to obtain the product in 86 % yield. ^{1}H NMR (300 MHz, 1:9 D_2O/DMSO) δ 3.90 (s, 2H), 2.42 – 2.25 (m, 1H), 1.68 (s, 12H), 0.95 (d, J = 7.0 Hz, 6H), 0.85 (s, 3H). ^{13}C NMR (75 MHz, 1:9 D_2O/DMSO) δ 175.8, 138.2, 134.3, 65.7, 55.4, 33.3, 18.5, 16.5, 10.7, 9.8.

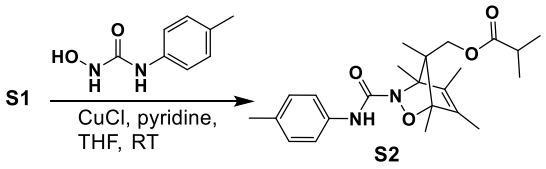

3.5.12 *Synthesis of **S2.***

Into a round-bottom flask, *N*-hydroxy-*N'*-(*p*-methylphenyl)urea (300 mg, 1.8 mmol, 1.0 mol. equiv.), obtained as previously described,[i] was dissolved in THF (15 mL). Then, a solution of **S1** (510 mg, 2.16 mmol, 1.2 mol. equiv.) in THF (3 mL) was added to the reaction mixture. Finally,

CuCl (35 mg, 0.36 mmol, 0.2 mol. equiv.) and pyridine (7 μL, 0.09 mmol, 0.05 mol. equiv.) were added to the solution. The reaction was stirred (open to air) at RT for 27 h. The reaction solvent was then removed under reduced pressure and the solids were taken up in ethyl acetate. This mixture was washed twice with ethylenediaminetetraacetic acid (aq) and then H_2O. The organic solution was dried over Na2SO4 and the solvent was removed under reduced pressure. The product was isolated by flash column chromatography to obtain the product in 65 % yield. ^{1}H NMR (300 MHz, DMSO) δ 8.45 (s, 1H), 7.34 (d, J = 8.4 Hz, 2H), 7.04 (d, J = 8.3 Hz, 2H), 3.73 (m, 2H, isomers), 2.56 (m, 1H), 2.23 (s, 3H), 1.69 (s, 3H), 1.67 (s, 3H), 1.59 (s, 3H), 1.40 (s, 3H), 1.09 (d, *J* = 6.9 Hz, 6H), 1.01 & 0.72 (s, 3H, isomers). ^{13}C NMR (75 MHz, DMSO) δ 175.8, 161.0, 137.1, 135.8, 132.2, 132.1, 128.8, 120.4, 94.9, 80.8, 66.1, 61.2, 33.4, 20.4, 18.7, 12.6, 12.2, 11.5, 10.8, 9.0.

3.5.13 *General Method for Oxidation Experiments with SIP **6**.*

SIP **6** (20 mg, 0.0083 mmol, 1.0 mol. Equiv.) was dissolved in anhydrous DMSO-d_6 (0.45 mL) under a N_2 atmosphere and transferred to a NMR tube. Next, either TBAP (5.4 mg, 0.012 mmol, 1.5 mol. Equiv.) or CuCl (0.4 mg, 0.004 mmol, 0.5 mol. Equiv.) and pyridine (0.2 μL, 0.002 mmol, 0.25 mol. Equiv.) were added. Lastly, 1,4-dicyanobenzene (ca. 0.7 mg as an internal standard), and D_2O (0.05 mL) were added and the NMR tube was capped and sealed with electrical tape. The sample was then heated at 40 °C and the depolymerization was monitored by ^{1}H NMR spectroscopy. The % of SIP repeat units remaining was determined by monitoring the benzylic protons of the carbamate repeat unit (δ = 5.05 ppm) versus the internal standard. Control experiments without D_2O (using 0.5 mL of DMSO-d_6) and with only the SIP and D_2O were also completed under the same conditions.

3.5.14 *General Method for Monitoring the Thermally Triggered Depolymerization of **11**.*

Diblock copolymer **11** (20 mg) was dissolved in anhydrous DMSO-d_6 (0.9 mL, SIP repeat units at 7 mM concentration) and transferred to a screw cap NMR tube. D_2O (0.1 mL) and 1,4-dicyanobenzene (1 mg as an internal standard) were then added. A time-zero ^{1}H NMR spectrum was collected. The NMR tube was then immersed in a pre-heated oil bath set to the desired temperature and the depolymerization progress was monitored at various time points by ^{1}H NMR spectroscopy.

3.5.15 *Diene Transfer with **11**.*

Diblock copolymer **11** (20 mg, 1.0 mol. equiv.) was dissolved in anhydrous DMSO-d_6 (0.88 mL) and transferred to a screw cap NMR tube. D_2O (0.1 mL), 1,3-cyclohexadiene (0.019 mL, 300 mol. equiv.) and 1,4-dicyanobenzene (1 mg as an internal standard) were then added. A time-zero ^{1}H NMR spectrum was collected. The NMR tube was then immersed in a pre-heated oil bath set to 60 °C and the depolymerization progress was monitored at various time points by ^{1}H NMR spectroscopy.

3.5.16 *Extended Time Plot of Thermolysis of SIP**11**.*

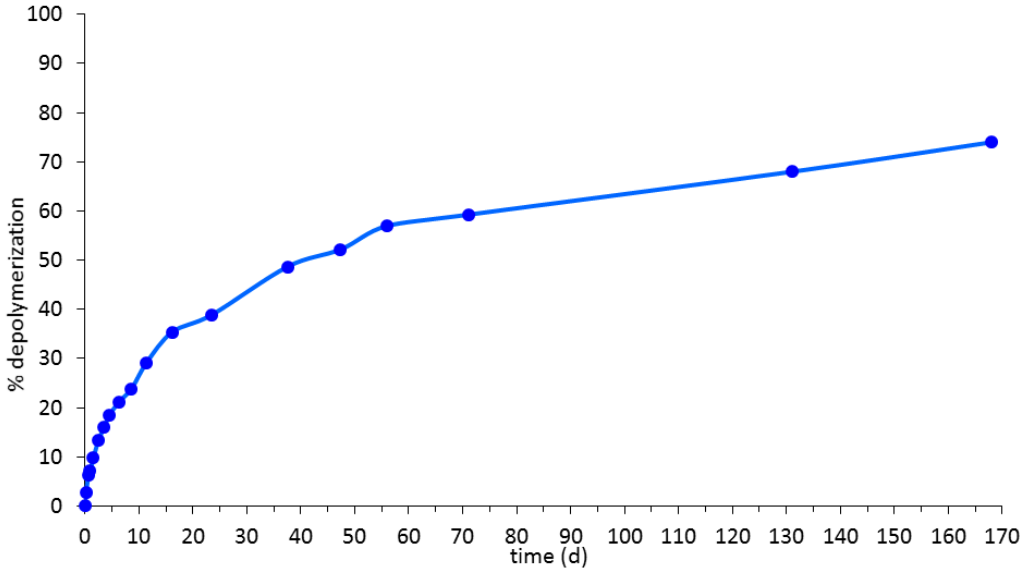

Figure 3.6. Extended time plot of the thermal activation and depolymerization of SIP **11** in DMSO-d_6/D_2O (9:1 v/v) at 40 °C.

3.5.17 *NMR Spectra*

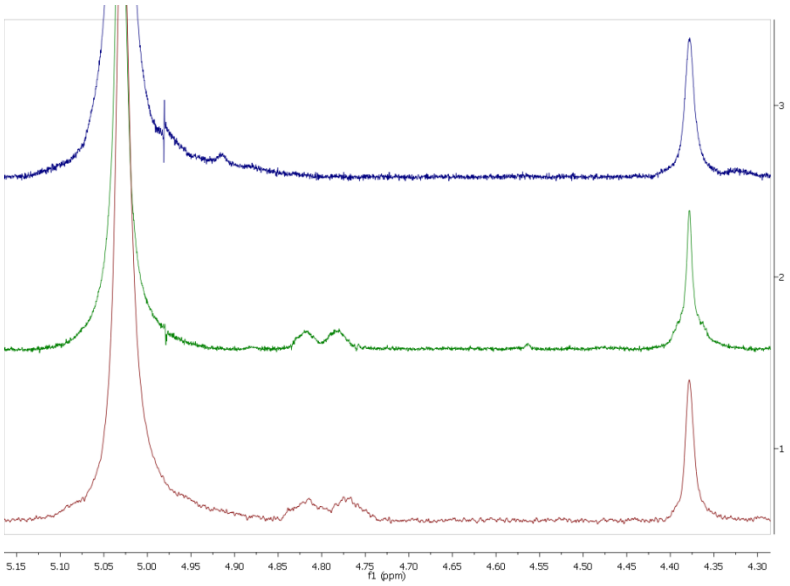

Figure 3.7. ^{1}H NMR spectra of (top) diblock copolymer **11** prior to the diene transfer experiment, (middle) **11** after heating in the presence of 1,3-cyclohexadiene for 19 h, and (bottom) SIP **15**.

The stacked NMR spectra for the diene transfer experiment are shown in **Figure S3**. The spectra show the benzylic CH_2 end group of the SIP at 4.37 ppm, the benzylic CH_2 repeat unit of the SIP at 5.03 ppm, and the bridgehead C*H* protons of the 1,3-cyclohexadiene adduct at 4.80 ppm (if present). The appearance of the peaks at 4.80 ppm in the middle plot confirms that the adduct has been produced in the diblock diene transfer experiment.

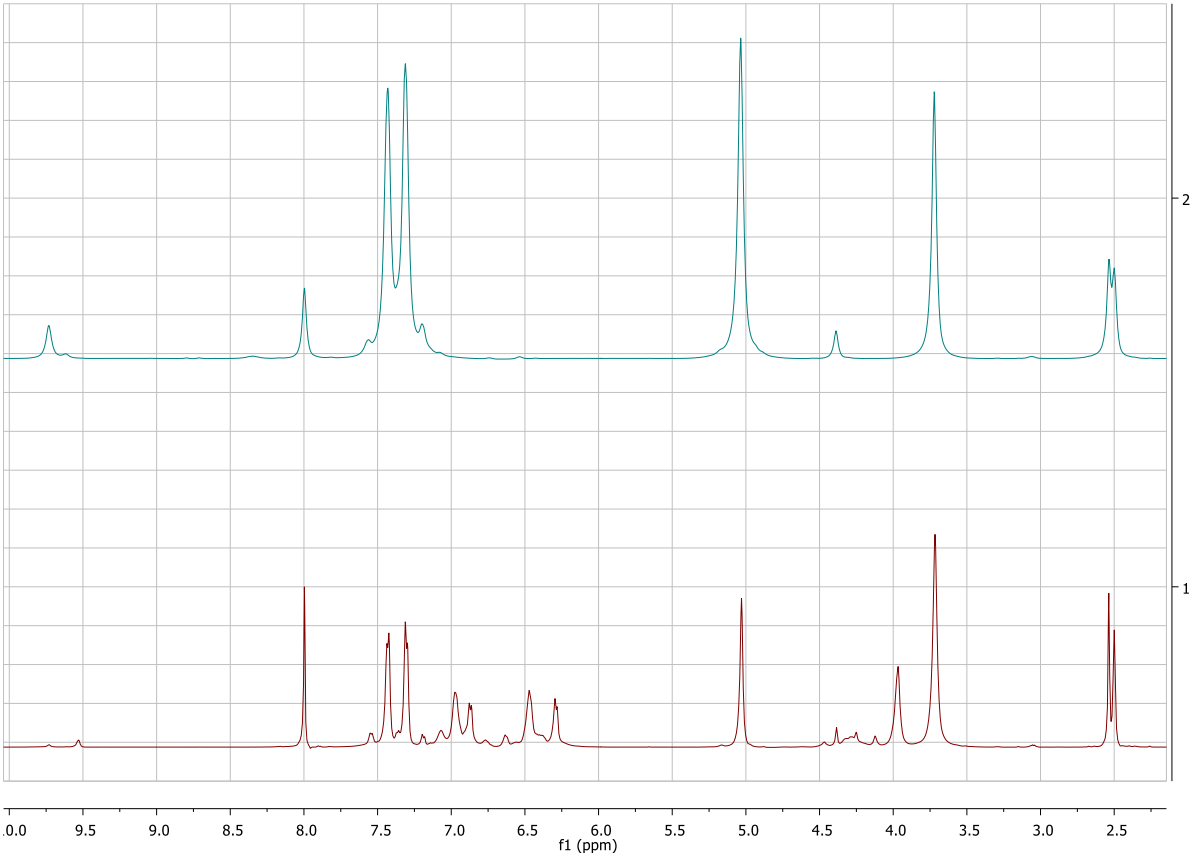

Figure 3.8. ^{1}H NMR spectra of (top) SIP **6** in 10% D_2O/DMSO-d_6 with CuCl and pyridine, prior to heating, and (bottom) the same solution after heating for 100 h (Table 1, entry 4). The % depolymerization was determined by integrating the benzyl repeat unit of the SIP (blue box) versus the internal standard 1,4-dicyanobenzene (red box).

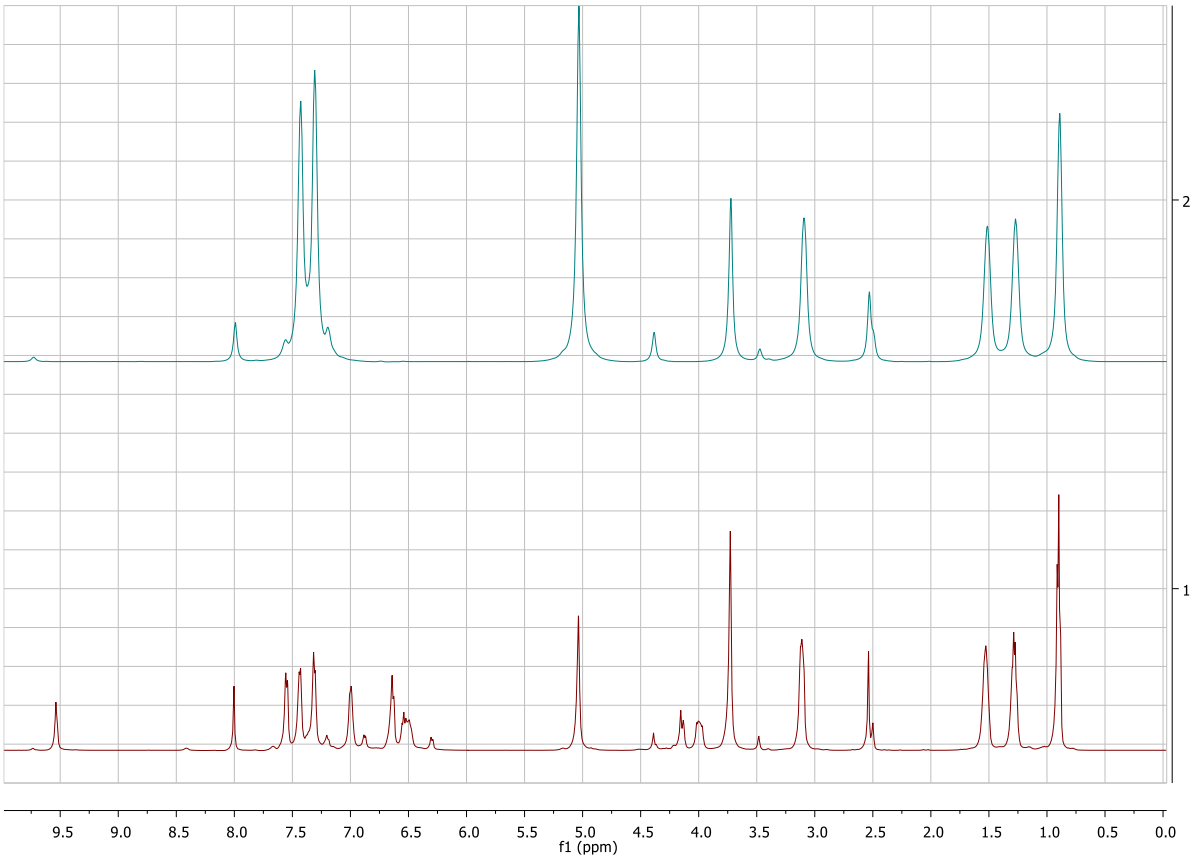

Figure 3.9. ^{1}H NMR spectra of (top) SIP **6** in 10% D_2O/DMSO-d_6 with TBAP, prior to heating, and (bottom) the same solution after heating for 100 h (Table 1, entry 2). The % depolymerization was determined by integrating the benzyl repeat unit of the SIP (blue box) versus the internal standard 1,4-dicyanobenzene (red box).

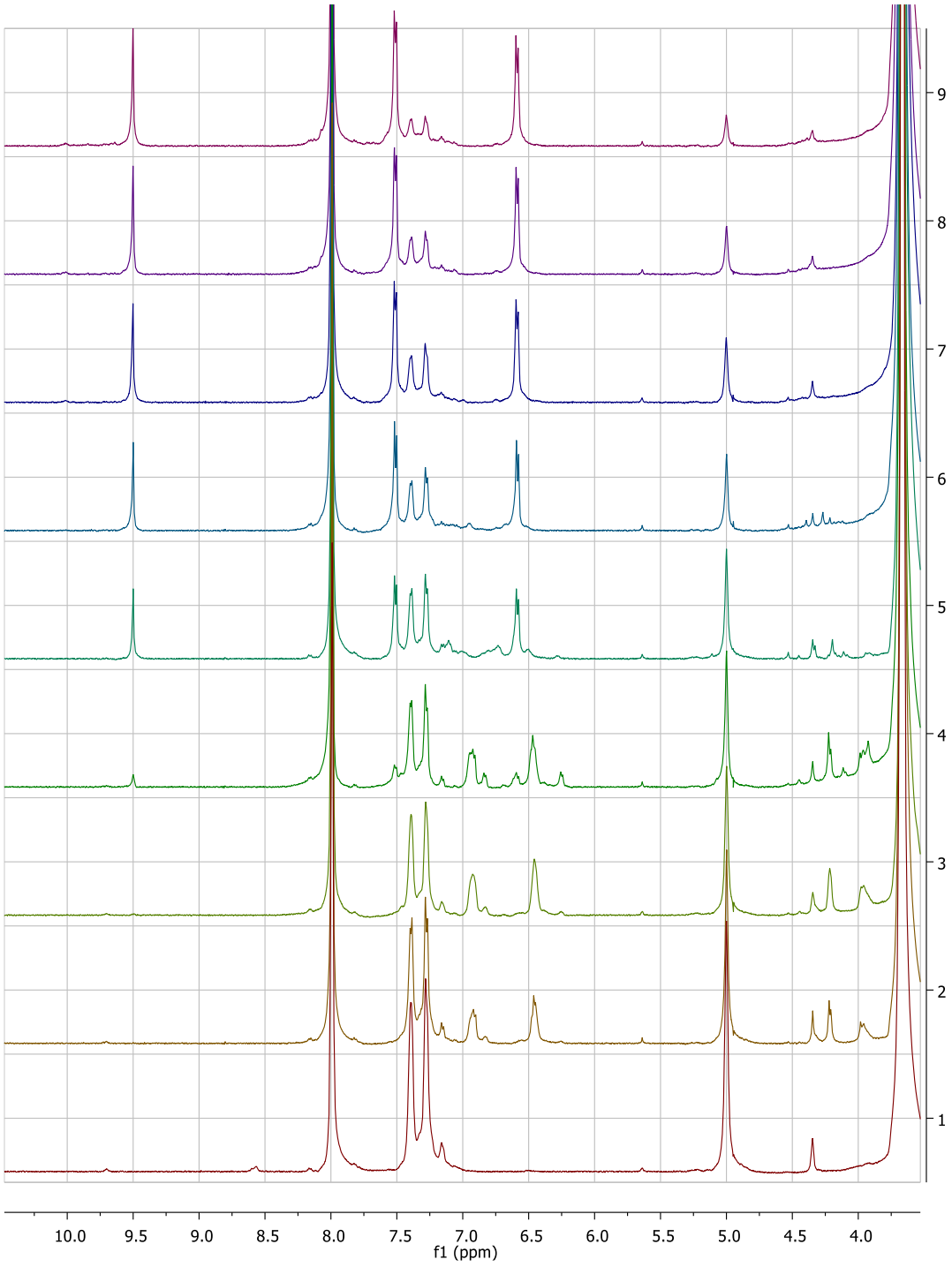

Figure 3.10. ^{1}H NMR spectra of SIP **11** in 10% D_2O/DMSO-d_6 heated at 85 °C. Spectra correspond to reaction time points of: 0, 1.3, 3.2, 5.3, 10, 19, 28, 42.1, and 65.6 h. The spectra are consistent with formation of the *p*-aminobenzyl alcohol and the cyclopentadiene-based end

group (δ = 3.9 ppm). Oxidation of *p*-aminobenzyl alcohol is presumed due to peaks consistent with the formation of *p*-aminobenzaldehyde. End-group formation was compared against small molecule analogues.

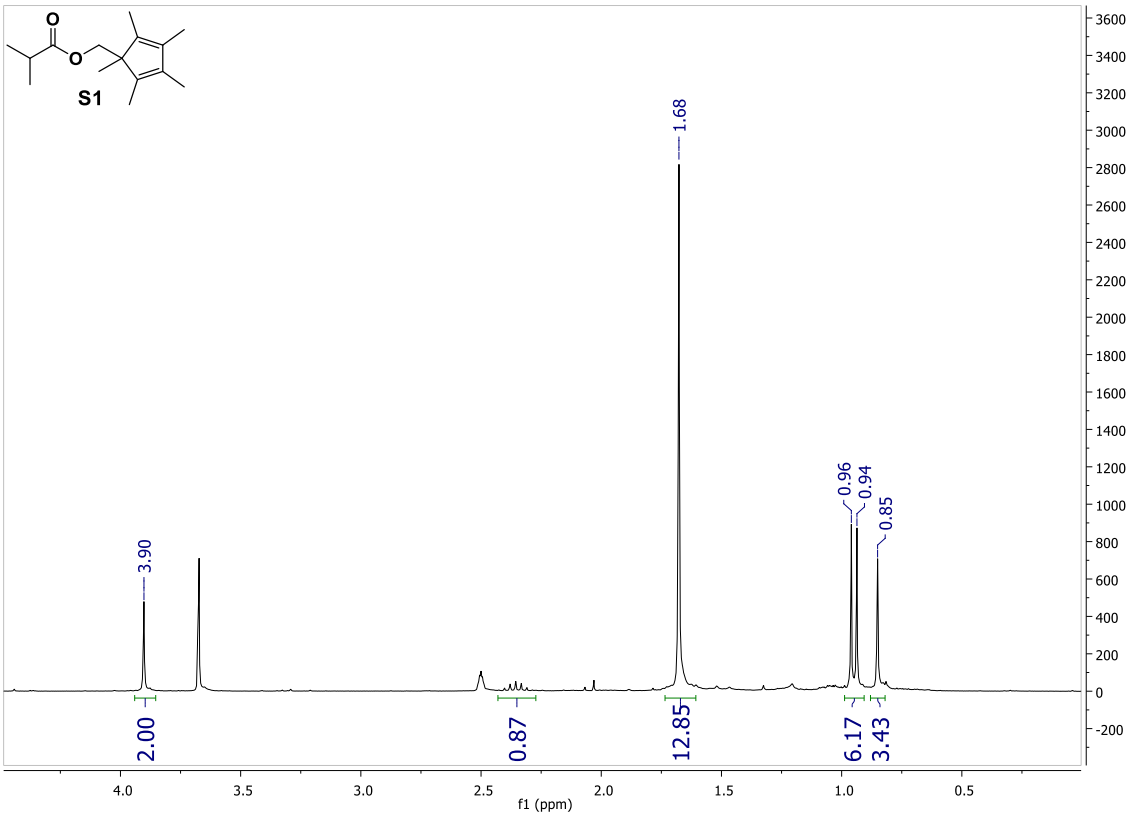
S1
1.68
0.96
0.94
0.85
3.90
2.00
0.87
12.85
6.17
3.43
f1 (ppm)

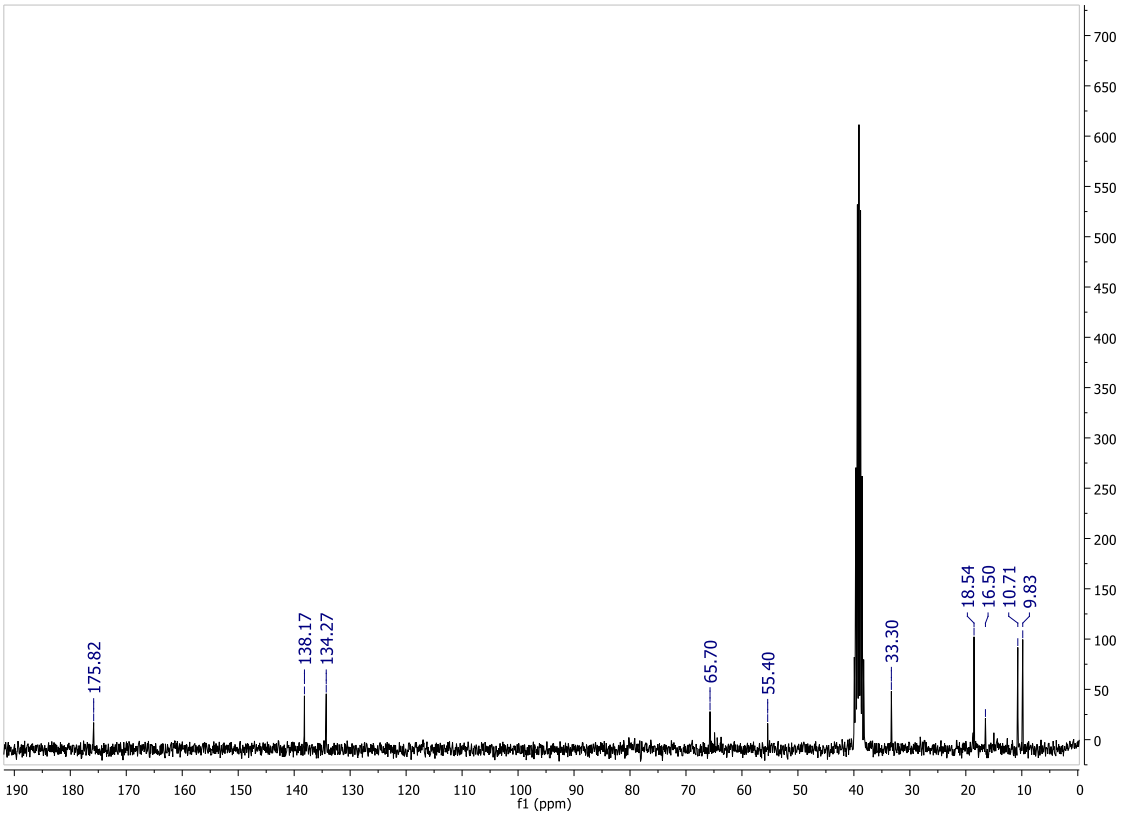
175.82
138.17
134.27
65.70
55.40
33.30
18.54
16.50
10.71
9.83
f1 (ppm)

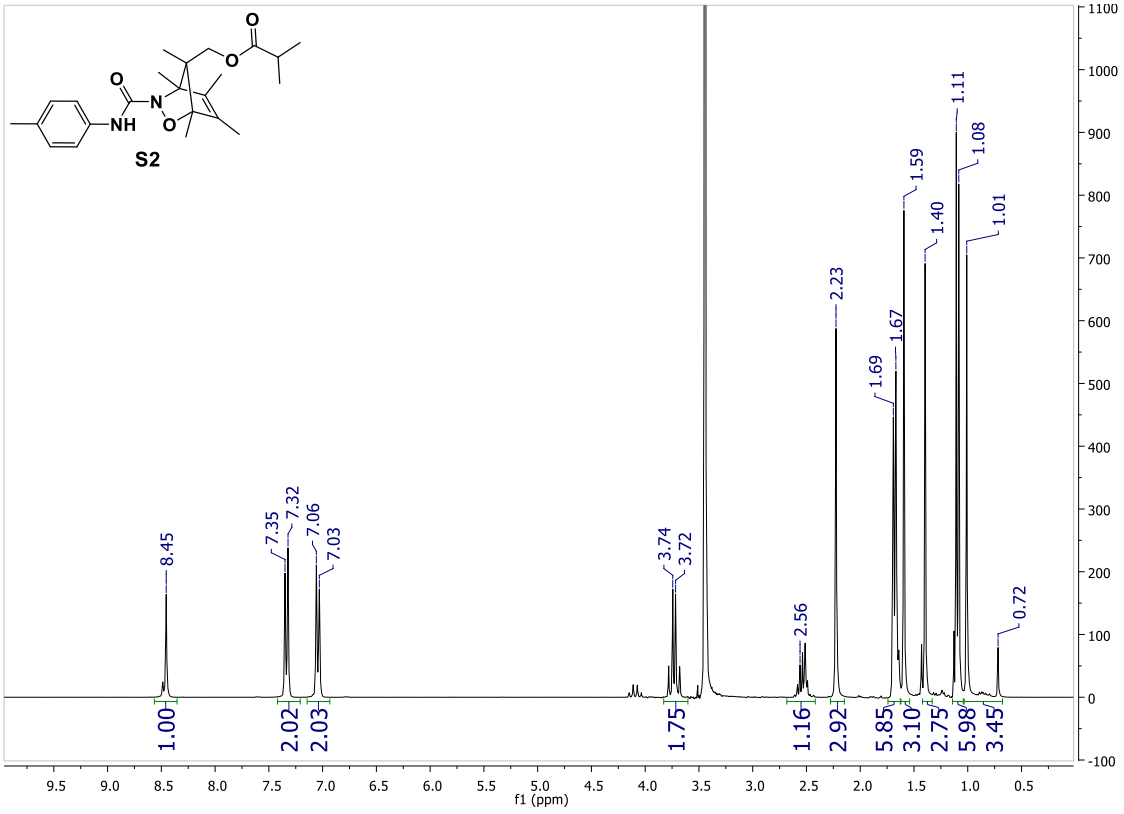
S2
8.45
7.35
7.32
7.06
7.03
3.74
3.72
2.56
2.23
1.69
1.67
1.59
1.40
1.11
1.08
1.01
0.72
1.00
2.02
2.03
1.75
1.16
2.92
5.85
3.10
2.75
5.98
3.45
f1 (ppm)

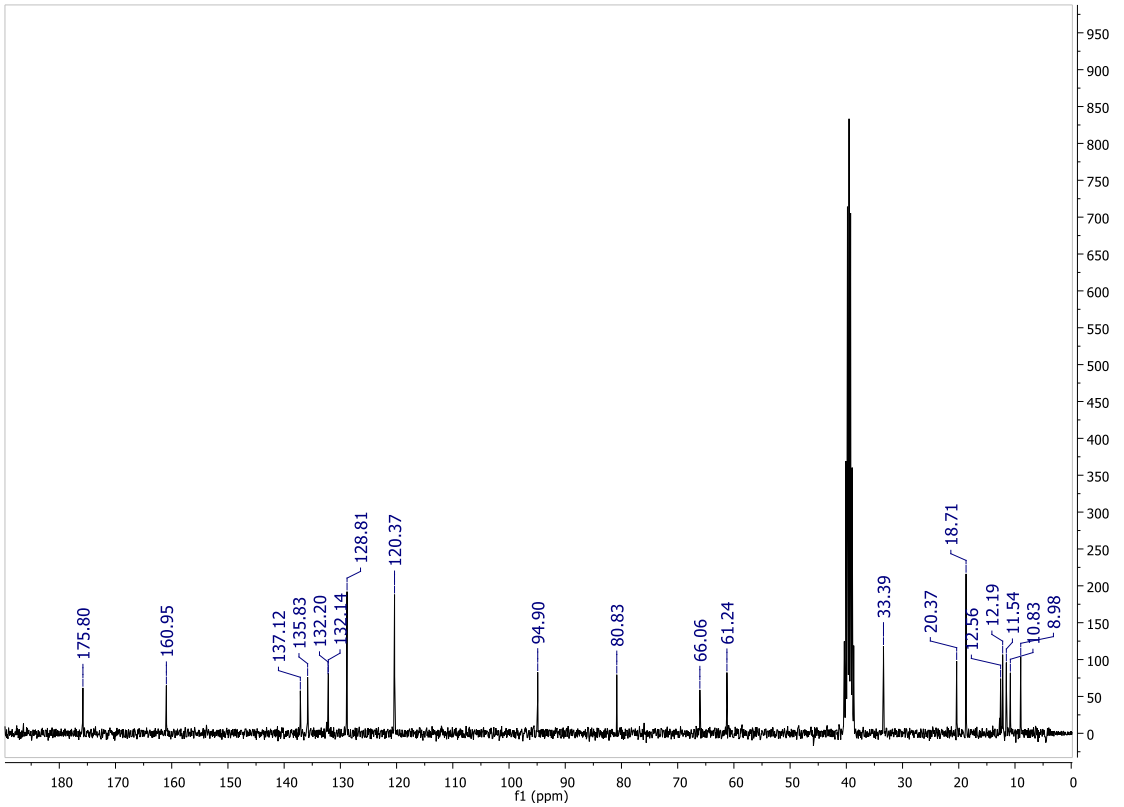
175.80
160.95
137.12
135.83
132.20
132.14
128.81
120.37
94.90
80.83
66.06
61.24
33.39
20.37
18.71
12.56
12.19
11.54
10.83
8.98
f1 (ppm)

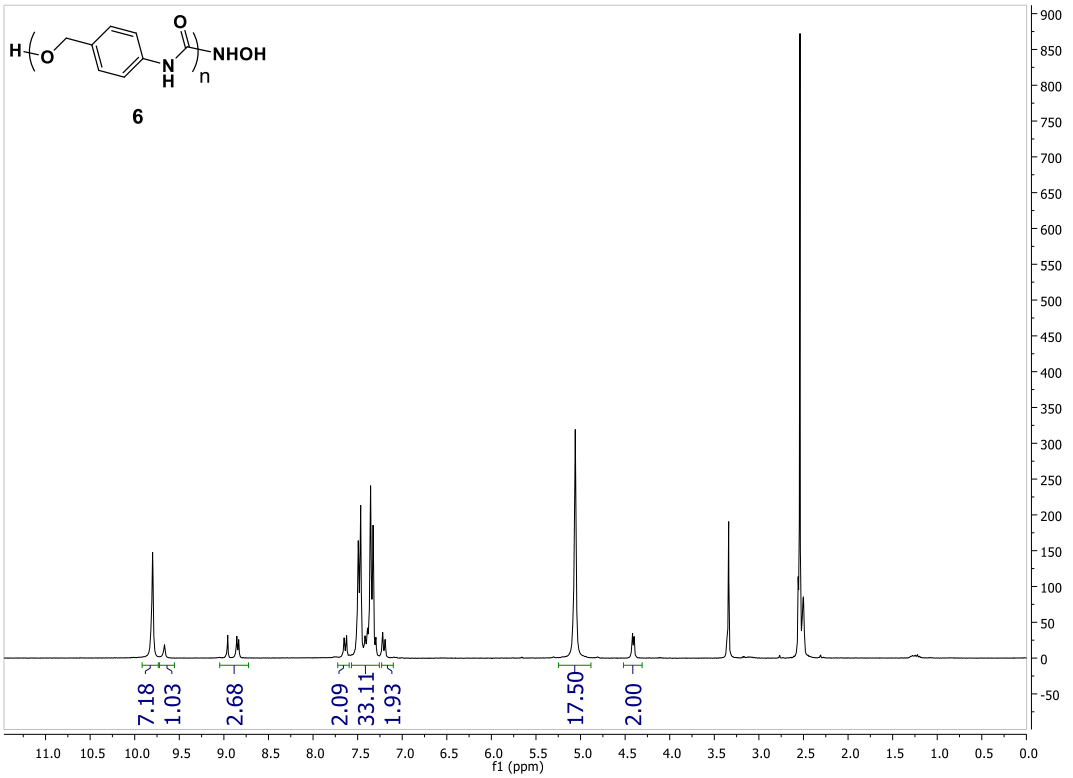
H
O
O
NHOH
N
H
n
7.18
1.03
2.68
2.09
33.11
1.93
17.50
2.00
f1 (ppm)

6

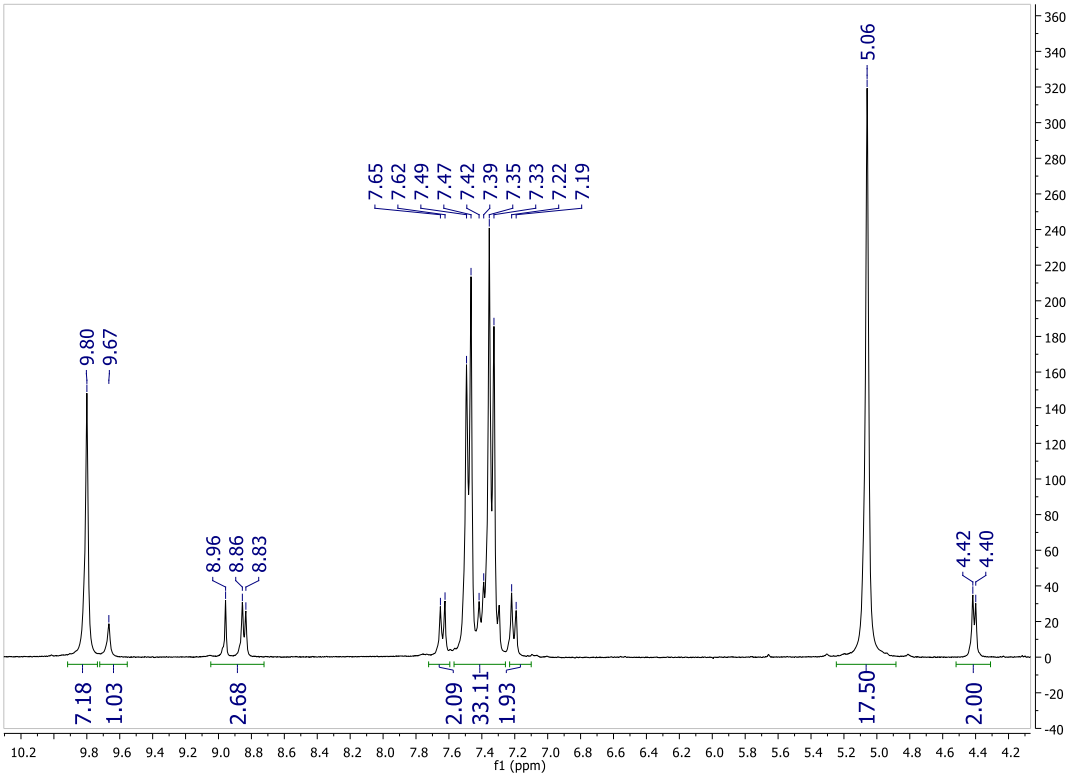
9.80
9.67
8.96
8.86
8.83
7.65
7.62
7.49
7.47
7.42
7.39
7.35
7.33
7.22
7.19
5.06
4.42
4.40
7.18
1.03
2.68
2.09
33.11
1.93
17.50
2.00
f1 (ppm)

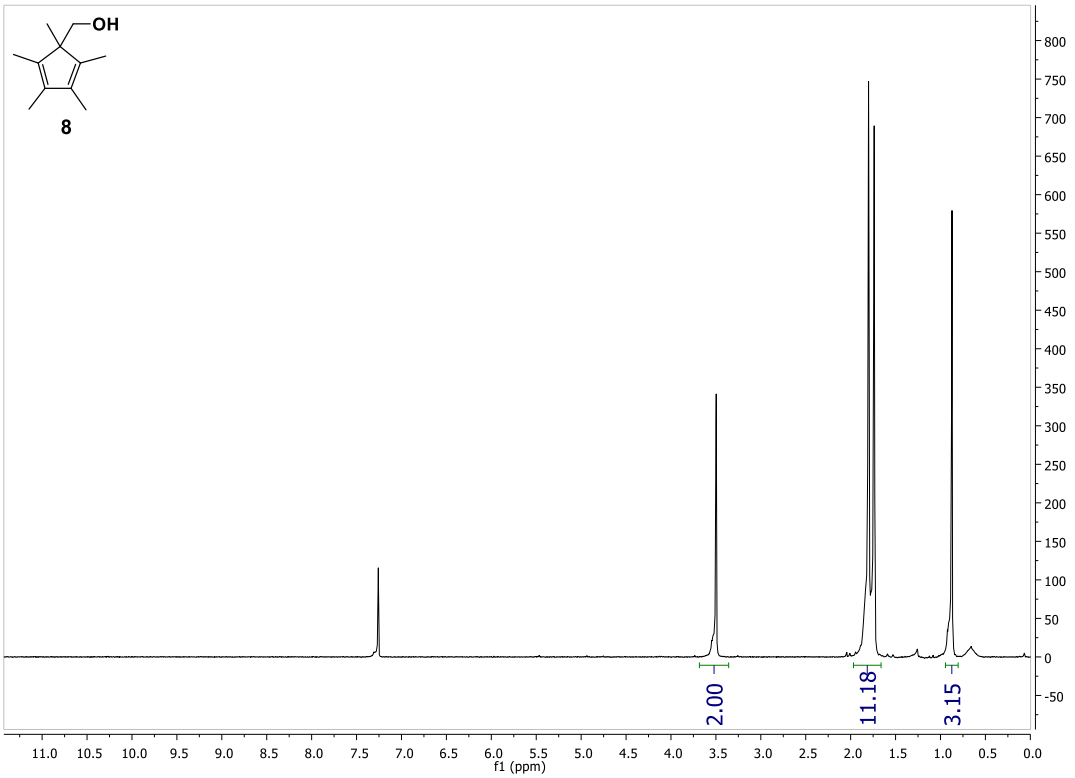
OH
8
2.00
11.18
3.15
f1 (ppm)

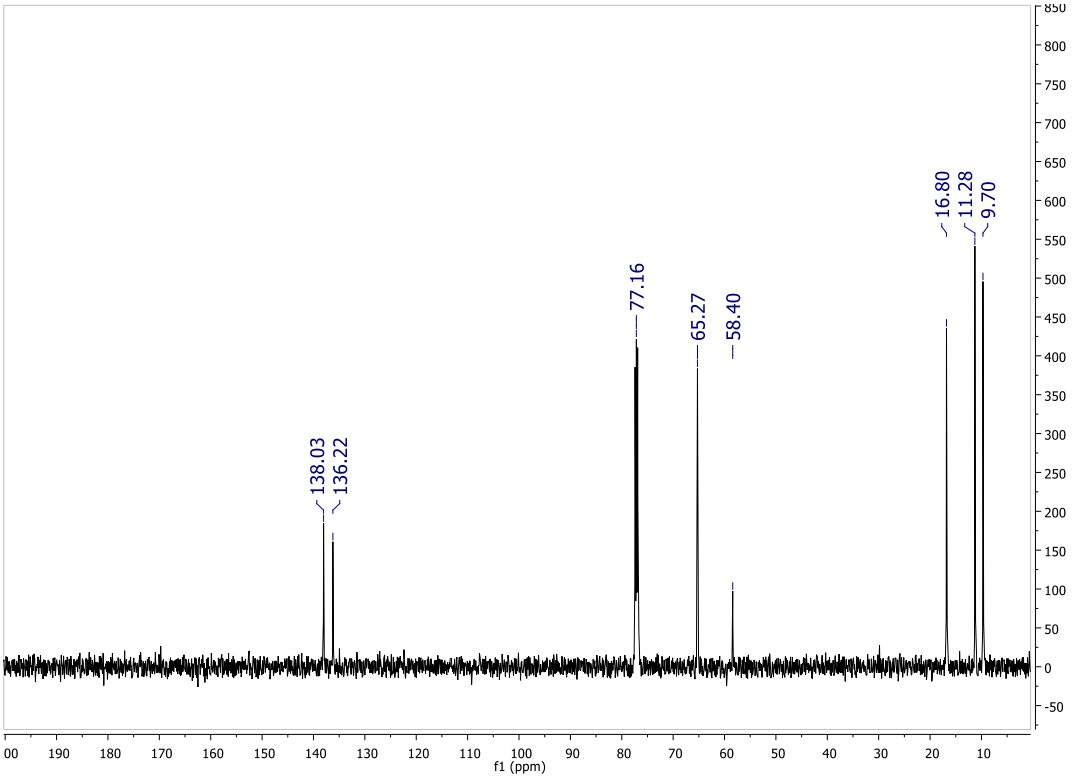
138.03
136.22
77.16
65.27
58.40
16.80
11.28
9.70
f1 (ppm)

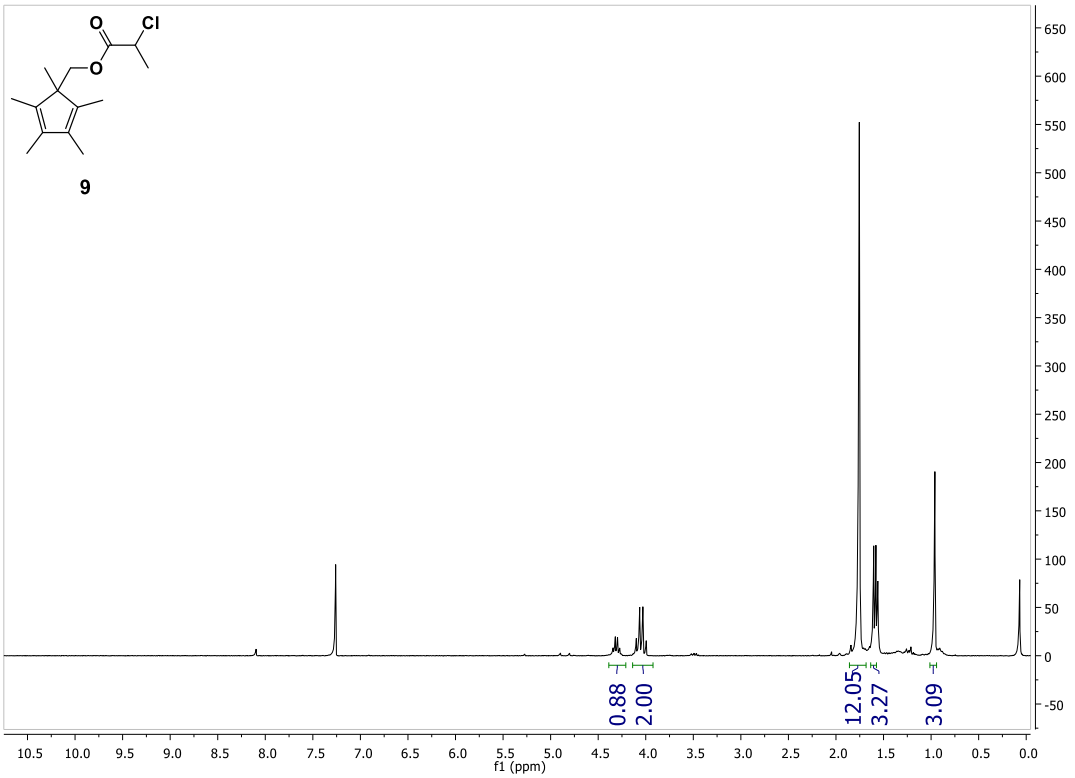
O
Cl
O
9
0.88
2.00
12.05
3.27
3.09
f1 (ppm)

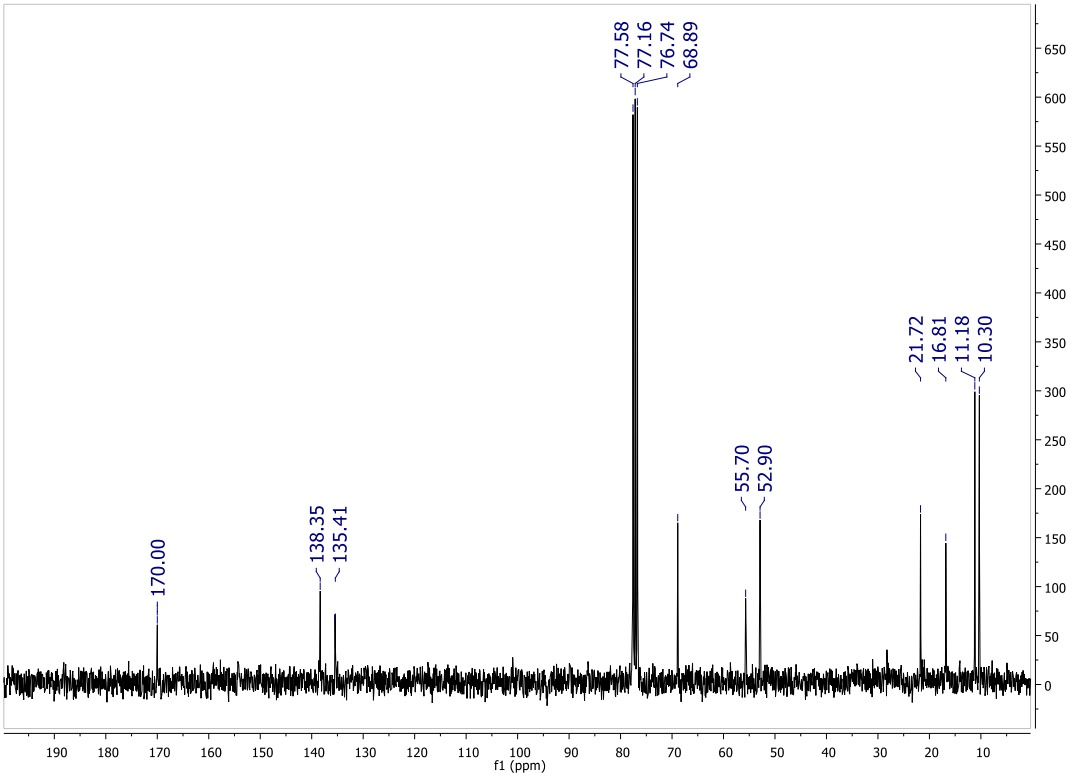
77.58
77.16
76.74
68.89
170.00
138.35
135.41
55.70
52.90
21.72
16.81
11.18
10.30
f1 (ppm)

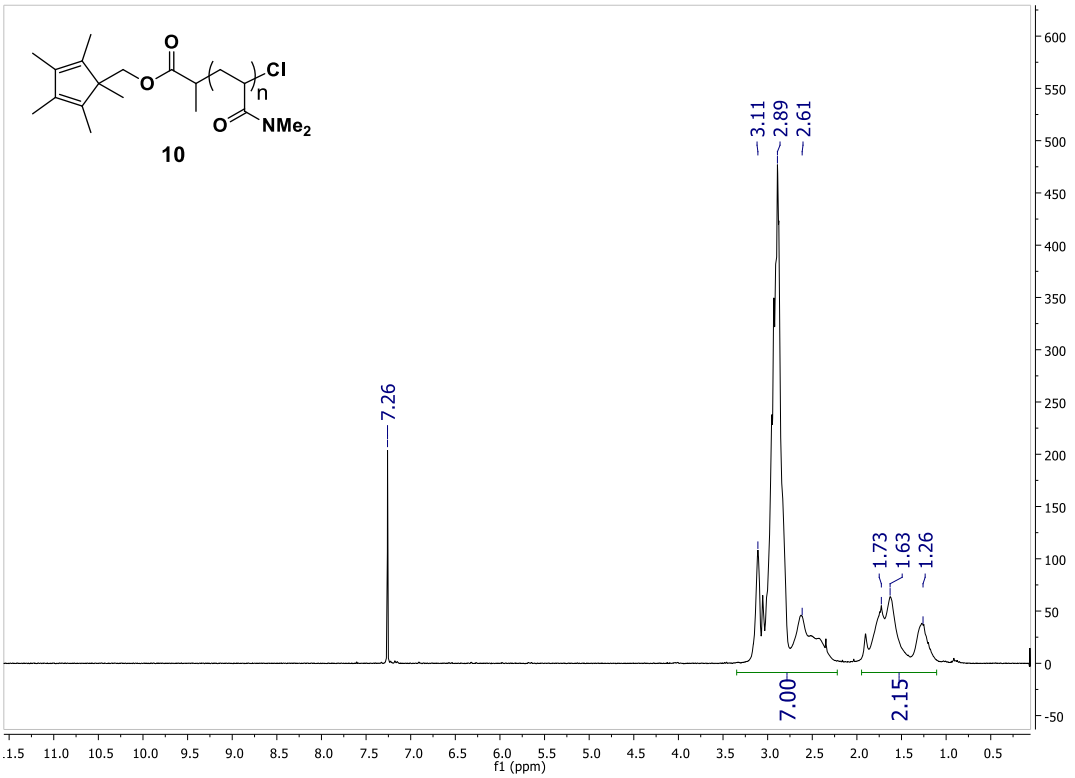
10
7.26
3.11
2.89
2.61
1.73
1.63
1.26
7.00
2.15
f1 (ppm)

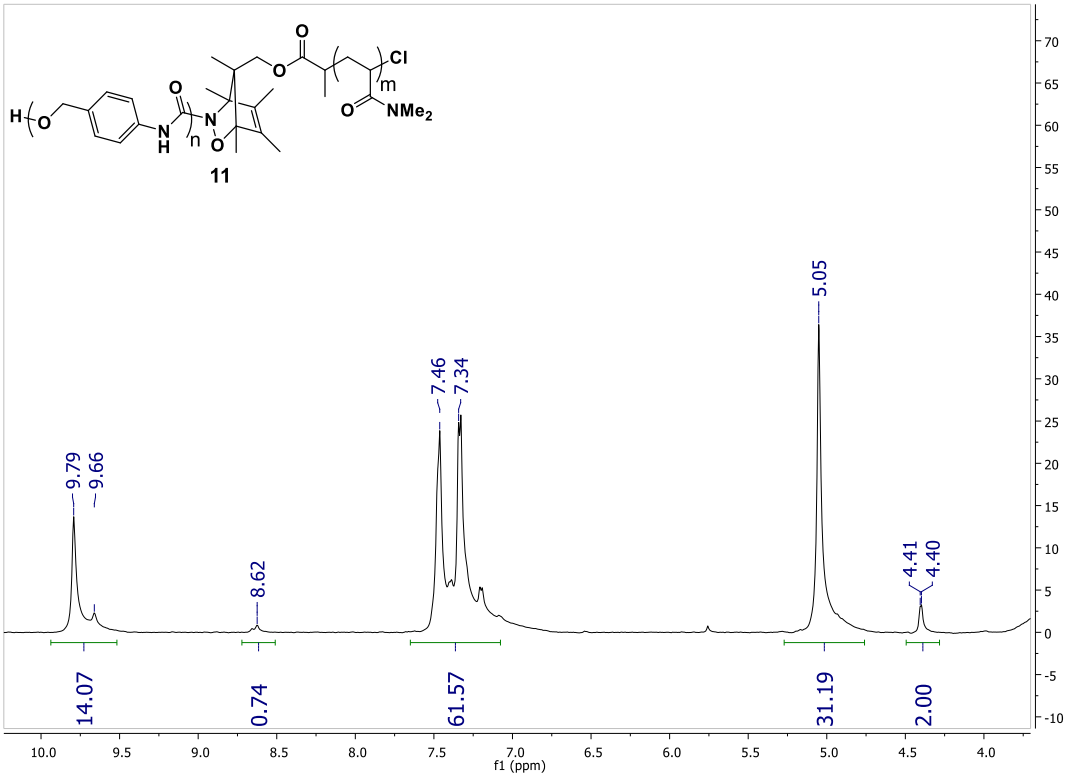
11
9.79
9.66
8.62
7.46
7.34
5.05
4.41
4.40
14.07
0.74
61.57
31.19
2.00
f1 (ppm)

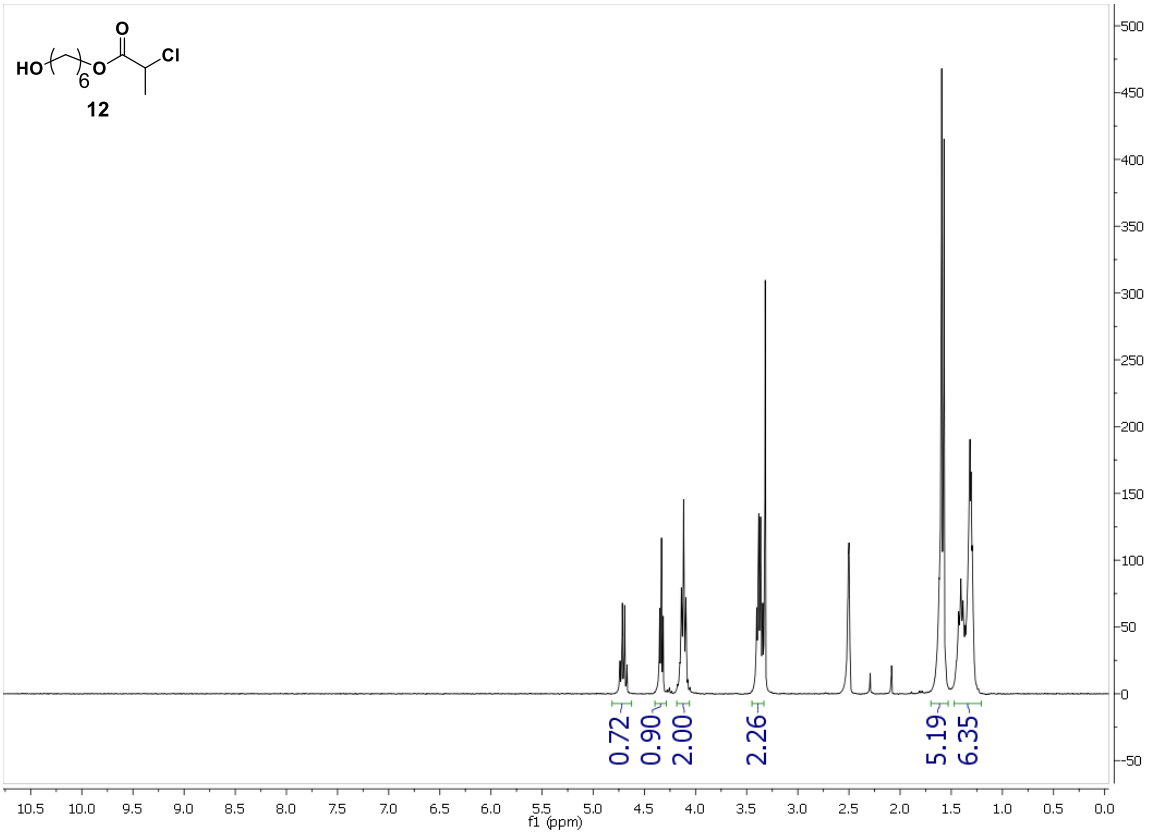
HO
6
O
O
Cl
12
0.72
0.90
2.00
2.26
5.19
6.35
f1 (ppm)

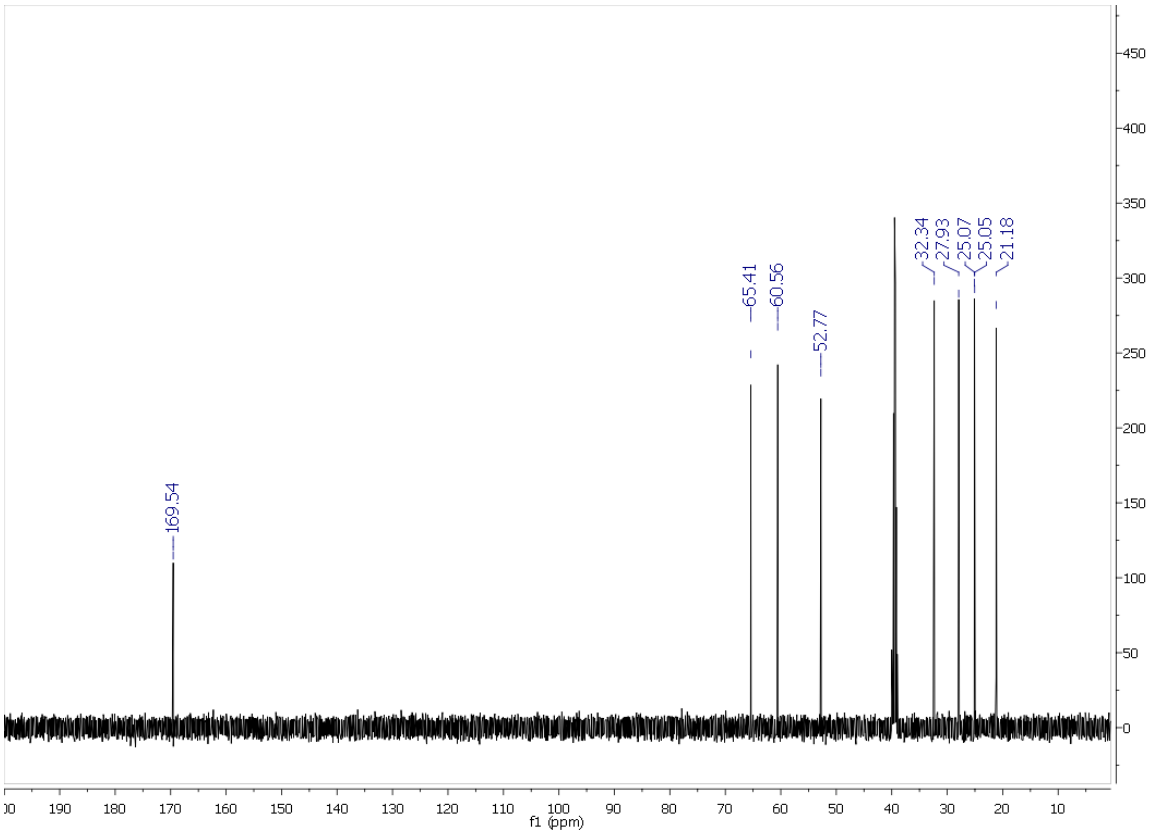
169.54
65.41
60.56
52.77
32.34
27.93
25.07
25.05
21.18
f1 (ppm)

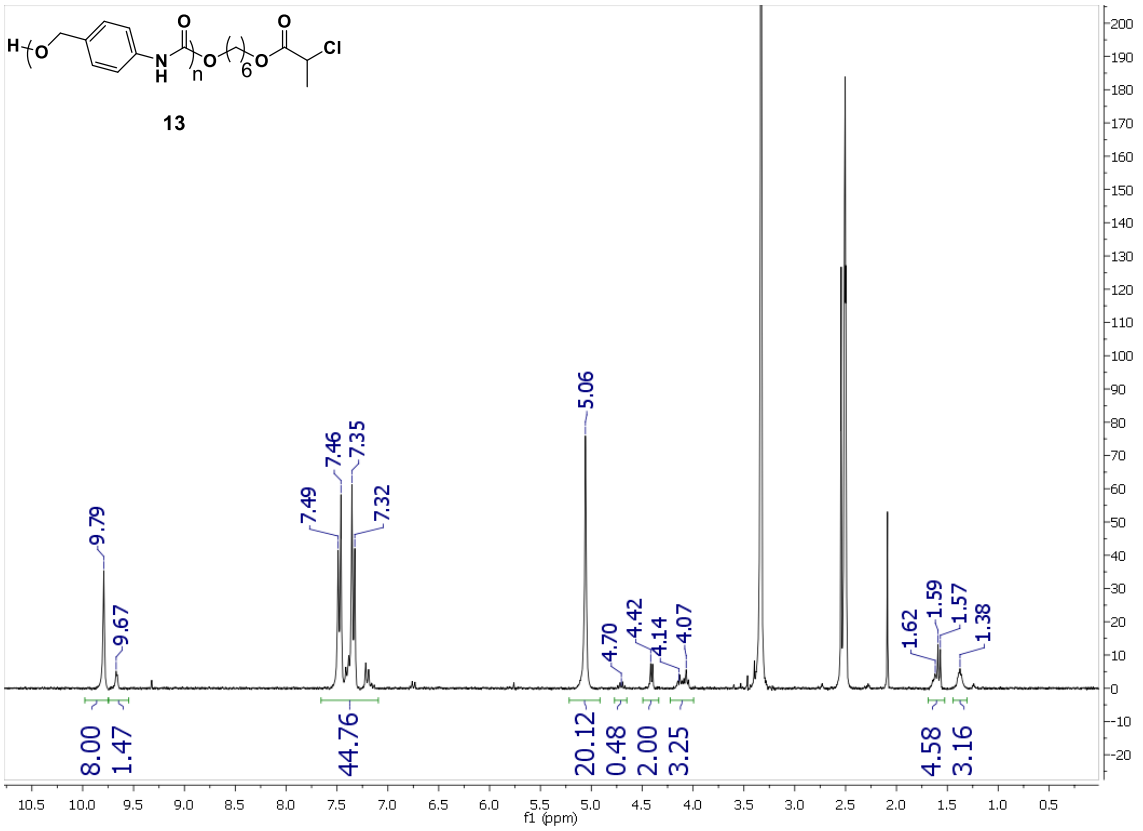
13
9.79
9.67
7.49
7.46
7.35
7.32
5.06
4.70
4.42
4.14
4.07
1.62
1.59
1.57
1.38
8.00
1.47
44.76
20.12
0.48
2.00
3.25
4.58
3.16
f1 (ppm)

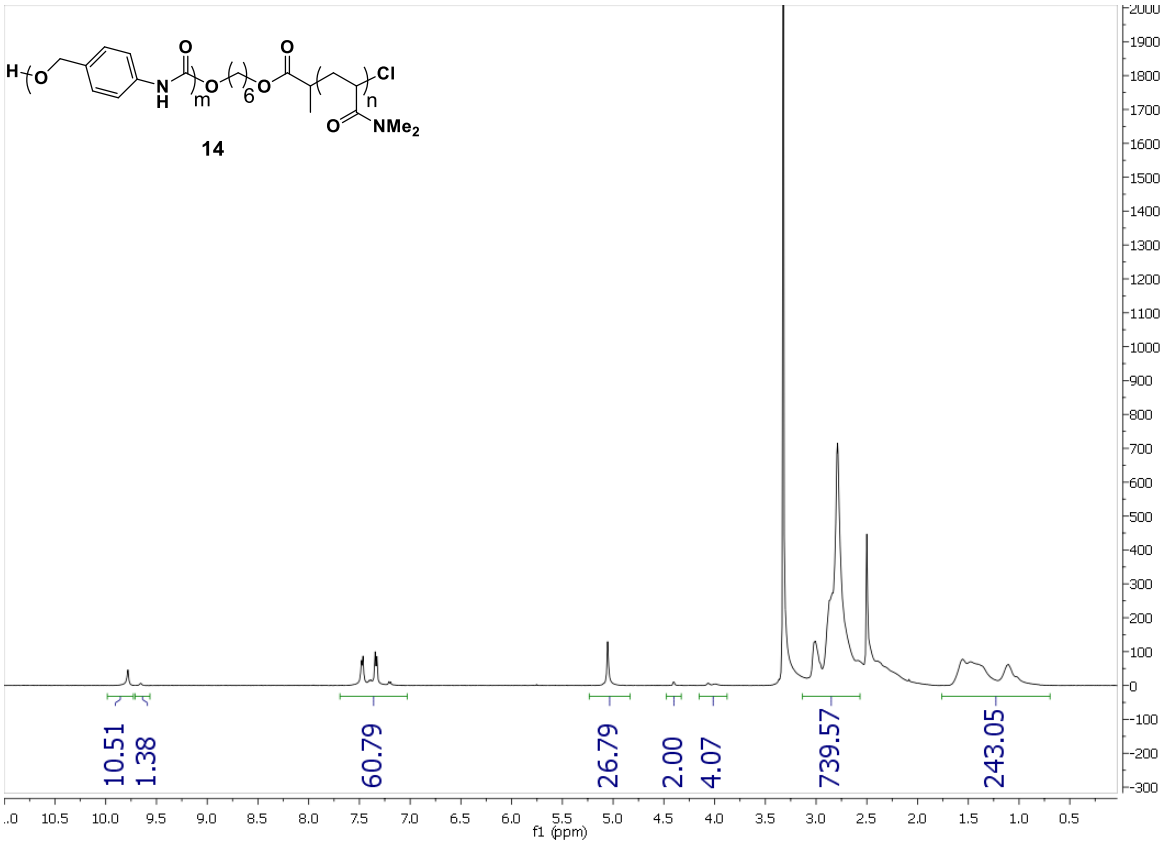
14
10.51
1.38
60.79
26.79
2.00
4.07
739.57
243.05
f1 (ppm)

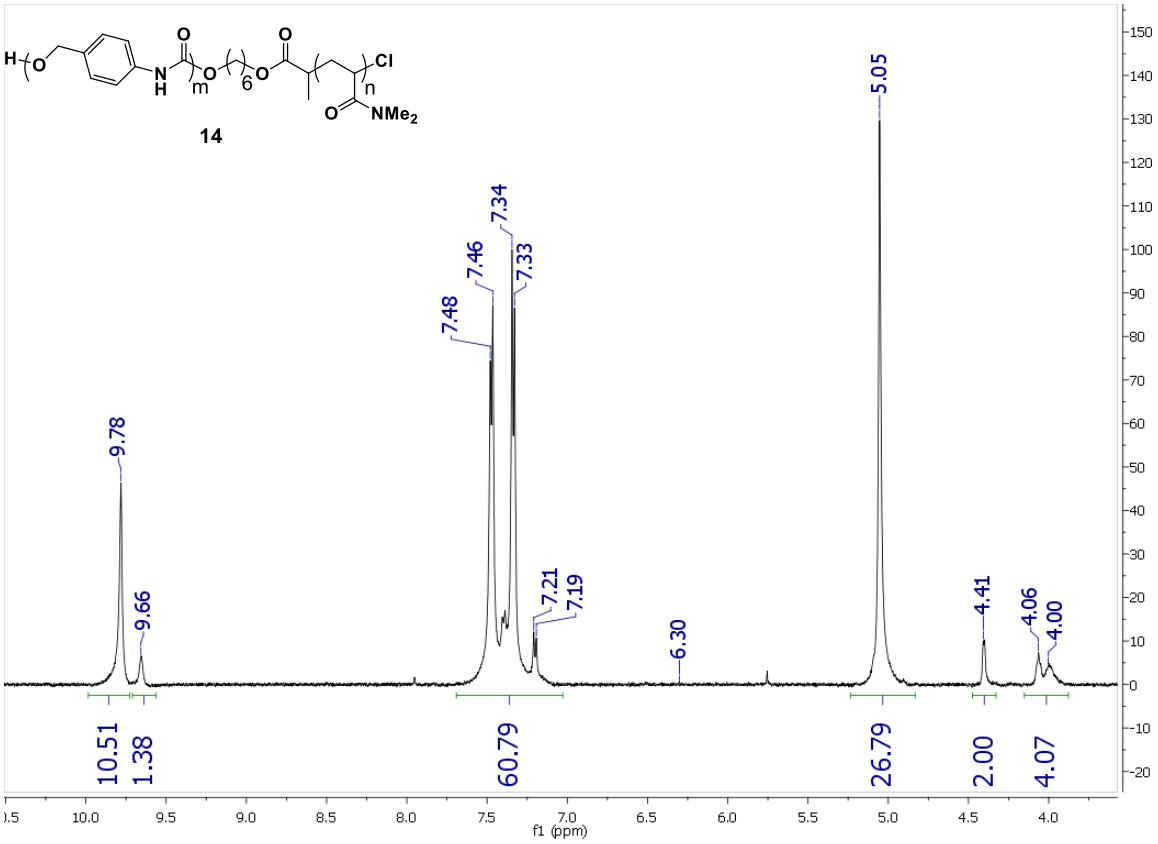
14
9.78
9.66
7.48
7.46
7.34
7.33
7.21
7.19
6.30
5.05
4.41
4.06
4.00
10.51
1.38
60.79
26.79
2.00
4.07
f1 (ppm)

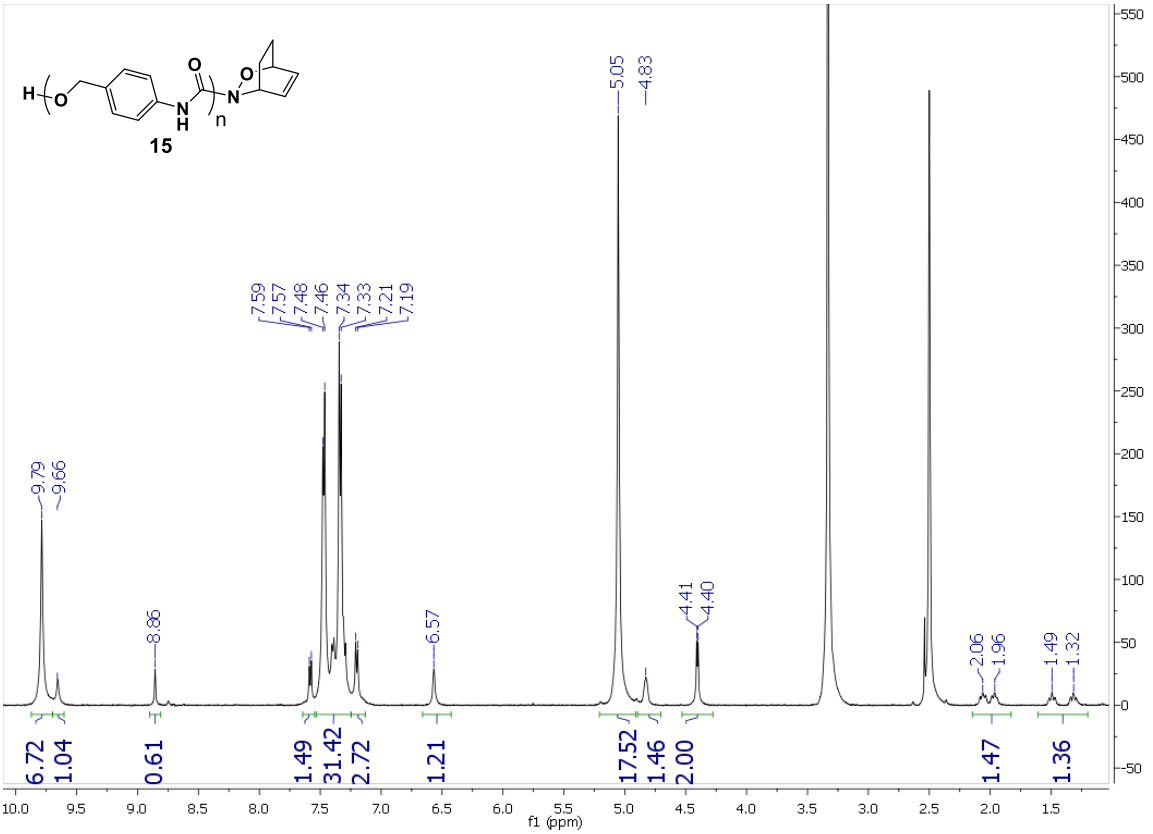
15
9.79
9.66
8.86
7.59
7.57
7.48
7.46
7.34
7.33
7.21
7.19
6.57
5.05
4.83
4.41
4.40
2.06
1.96
1.49
1.32
6.72
1.04
0.61
1.49
31.42
2.72
1.21
17.52
1.46
2.00
1.47
1.36
f1 (ppm)

3.5.18 *Experimental References*

1) Uesato, S.; Hashimoto, Y.; Nishino, M.; Nagaoka, Y.; Kuwajima, H. *Chem. Pharm. Bull.* **2002**, *50*, 1280.

2) Sagi, A.; Weinstain, R.; Karton, N.; Shabat, D. *J. Am. Chem. Soc.* **2008**, *130*, 5434.

Chapter 4. AMPHIPHILIC POLYMERS CAPABLE OF CONCOMITANT RELEASE OF HNO AND SMALL MOLECULE ORGANICS

4.1 INTRODUCTION

Nitroxyl (HNO) has garnered considerable interest for its potential in the treatment of heart failure and its notable anticancer properties.[1] Often compared with its more widely studied redox congener, nitric oxide (NO), growing evidence suggests that the mechanism of action of HNO is fundamentally unique.[2] Unfortunately, systematic investigations on the cellular and biological responses to controlled exposure to HNO have largely been thwarted by a notable lack of delivery platforms for the highly reactive species. Attribution of therapeutic effects can also be convoluted due to the fact that some HNO donors react to give NO in parallel, and the distribution of HNO to NO can be dependent upon environmental factors such as pH.[2] A significant challenge to the realization of HNO-based therapeutics is the rate at which HNO dimerizes ($k = 8 \times 10^6\ M^{-1}s^{-1}$), which precludes its use as a discrete agent.[3] Moreover, monitoring the production of HNO for accurate correlations with cellular and biological responses is also complicated by its inherent reactivity and lack of native diagnostic handles.

An exciting advance toward HNO therapeutics, however, has been the recent development of HNO donors, such as organic small molecule conjugates.[4] The potential for synergistic interaction between HNO and organic small molecule therapeutics, such as NSAIDs, further

motivates the development of modular HNO delivery platforms.[5] Recognizing the complementarity and potential advantages of polymer-based therapeutics,[6] we took aim at amphiphilic polymers for controlled release of HNO from modular oxazine functionalities.

Recently, we and others have demonstrated the use of oxazine units as dynamic junctions within polymer constructs.[7] The envisioned reactivity, previously described by Kirby and King, involves cycloreversion of the oxazine unit to release a diene and nitrosocarbonyl species (Scheme 4.1).[8] The nitrosocarbonyl species is then susceptible to hydrolysis to release HNO. Depending upon the nature of the carbonyl species, subsequent decarboxylation is also a viable outcome, which can lead to production of an additional small molecule payload (e.g., a reporter molecule or therapeutic agent).

Scheme 4.1. Idealized mechanism of HNO formation from thermally-labile 1,2-oxazines.

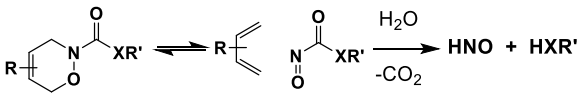

We envisioned that incorporating high quantities of this class of oxazine unit into a water soluble polymer would facilitate the delivery of HNO under physiological conditions. Additionally, polymeric carriers are particularly attractive for biological applications as these systems can be engineered to enable advanced capabilities, including site-specific cellular targeting, stabilization of small molecule cargo, systemic transport throughout the body, and controlled kinetic profiles for release of conjugates. Herein, we describe the synthesis and characterization of amphiphilic polymers capable of HNO delivery, quantitation of HNO released over time, and temperature-dependent kinetic profiles for release of HNO and a reporter molecule.

4.2 Results and Discussion

To our knowledge, polymerization of monomers bearing 1,2-oxazine units has not been widely explored. We previously reported the homopolymerization of monomer **1** (Scheme 4.2), which was prepared as a mixture of *syn*- and *anti*-isomers.[7a] To move toward water soluble variants, we developed a ROMP graft-through approach to incorporate both oxazine and PEG side chains into a statistical copolymer structure.[9] Specifically, copolymerization of monomers **1** and **2** in a 1:3 molar ratio provided a water soluble copolymer (**3**) in good isolated yield. Analysis of **3** by size-exclusion chromatography (SEC) revealed a M_n = 34.6 kDa ($Đ$ = 1.04), and ^{1}H NMR analysis indicated a 1:2.8 ratio of **1** and **2** had been incorporated into the polymer. These values correspond to an average of 16 oxazine units per polymer chain. Importantly, the oxazine cycloreversion and carbonylnitroso hydrolysis reaction rates are each known to be highly structure-dependent,[7,8] thus potentiating tunable release kinetics from the modular design of polymer **3**.

Scheme 4.2. Copolymerization of monomers **1** and **2**.

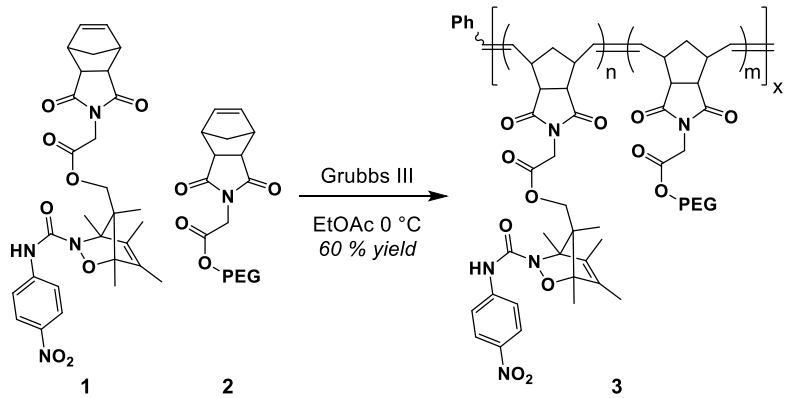

With polymer **3** at hand, we were able to study the breakdown of the oxazine units in phosphate buffered water. Thermally-driven cycloreversion of the oxazine units in polymer **3**, and hydrolysis of the ensuing carbamoylnitroso species (as generalized in Scheme 4.1), was expected to give easily detectable 4-nitroaniline (4-NA). The oxazine adducts in polymer **3** displayed a UV-vis absorption λ_{max} at 330 nm, versus 390 nm for 4-NA. Thus, we used UV-vis spectroscopy to assess oxazine reactivity at various temperatures. A representative set of UV-vis spectra are shown in Figure 4.1 and reveal a steady decrease in the amount of oxazine adduct with concomitant increase in the absorbance that corresponds to 4-NA. Confirmation of 4-NA production was further corroborated by ^{1}H NMR spectroscopy (see Supporting Information).

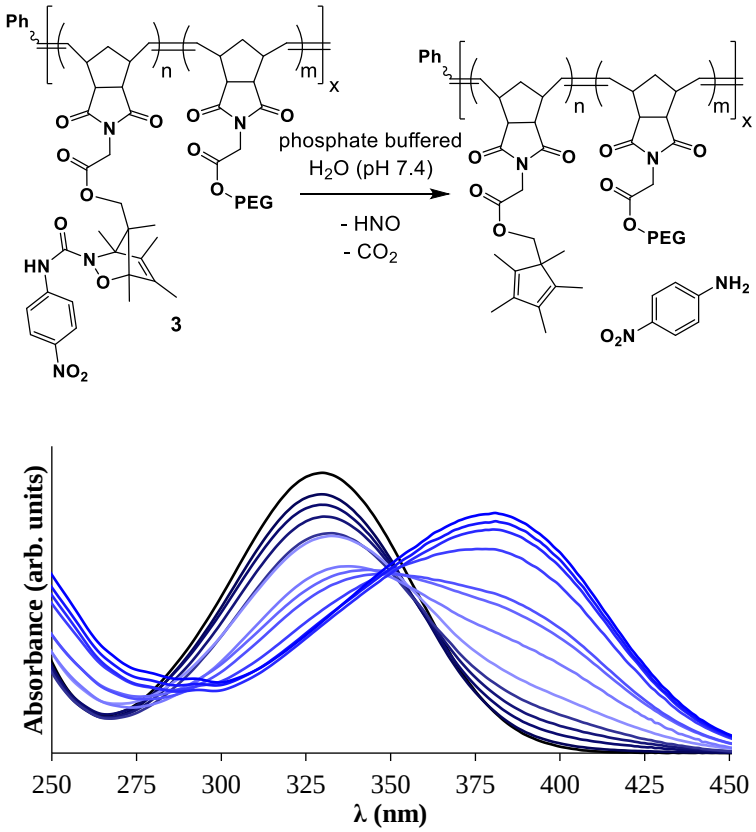

Figure 4.1. UV-vis spectra taken during thermolysis of polymer **3** at 60 °C in pH 7.4 phosphate buffered H_2O (total reaction time = 32 days).

As expected, we observed a strong temperature dependence on the relative rate of 4-NA production from polymer **3** (Figure 4.2). At a cold storage temperature of 4 °C, we observed an expectedly slow release profile (blue circles), reaching a value of 11% after 231 d. Similarly, at 22 °C we observed less than 20% production of 4-NA after 100 d, and 33% of the theoretical maximum amount of 4-NA was released over the 231-d course. Increasing the temperature to 37 °C increased the rate of 4-NA production considerably. At this temperature, a steady release profile was observed over 231 d, resulting in release of 93% of the theoretical limit of 4-NA. This signified the ability for sustained release of HNO and small molecule organics at

physiological temperatures. As expected, increasing the temperature to 60 °C resulted in considerably faster breakdown of the oxazine adduct and release of 4-NA, which indicated to us that localized heating techniques (e.g., photothermal transduction) may be a viable method for augmenting the oxazine activation in these systems. At 60 °C, 97% release of 4-NA was achieved within 21 d.

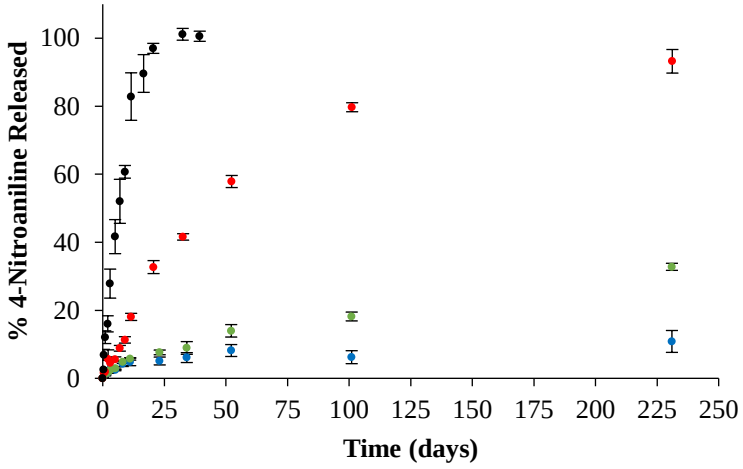

Figure 4.2. Release of 4-NA (% of theoretical maximum) from polymer **3** in pH 7.4 phosphate buffered H_2O at various temperatures. 4-NA release was determined by UV-vis spectroscopy, monitored at 415 nm. Blue = 4 °C, orange = 22 °C, red = 37 °C, black = 60 °C. Data points are an average of three runs, error bars represent one standard deviation.

We next sought to confirm that HNO was indeed being released during the thermolysis of polymer **3**, and to quantify the production of HNO in comparison with that of 4-NA. Toward this end, HNO production from polymer **3** was analyzed by gas chromatographic (GC) headspace analysis to quantify the amount of nitrous oxide (N_2O, the dehydrated dimerization product of

HNO) observed over time. As a control and standard, we analyzed 2-bromo-N-hydroxybenzenesulfonamide (2-bromo Piloty's Acid, or 2-BrPA) under the same conditions. Our GC results were consistent with steady production of HNO from polymer **3**. Moreover, the production of HNO from polymer **3** exhibited strong correlation with release of 4-NA (Figure 4.3). This suggested to us that concomitant release of HNO and therapeutics or indirect reporter molecules is viable with our polymer design.

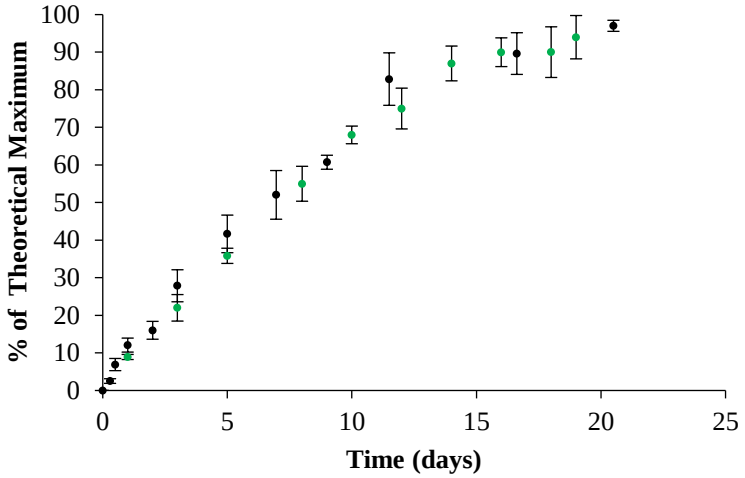

Figure 4.3. Production of HNO and 4-NA from polymer 3 in pH 7.4 phosphate buffered H_2O at 60 °C. Analysis of 4-NA (black) was done via UV-vis spectroscopy. Analysis of HNO (green) was done in parallel by GC headspace analysis of N_2O and reported relative to 2-BrPA. Data points are an average of three runs, error bars represent one standard deviation.

We found that the polymer composition and monomer sequence were easily modulated, owing to the versatile nature of living ROMP.[10] We explored constructs that might give advantageous materials properties for therapeutic applications with consideration of the extended release profiles we observed from copolymer **3**. Specifically, we targeted block copolymers that

could enable self-assembly into higher order structures. Of particular interest to us was hydrogel formation observed from ABA triblock copolymers prepared from monomers **1** and **2** (Figure 4.4).

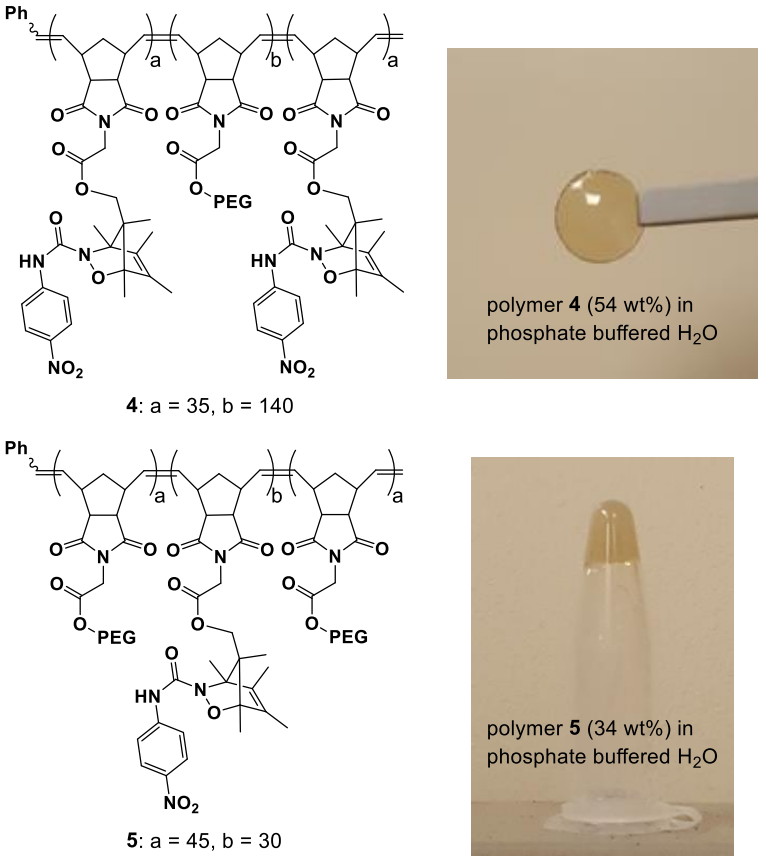

Figure 4.4. Representative block copolymer structures and their resulting hydrogels.

Triblock copolymers, in which the outer blocks consisted of the oxazine-based units, resulted in relatively robust hydrogels. For example, polymer **4** at 54 wt% provided a hydrogel that could be bent or twisted without tearing (Figure 4.5). Characterization of the material by rheology revealed a storage modulus (G') of 1.4 MPa (0.05% strain, 1 Hz) at 37 °C (Figure 4.5A and B). Changing the composition of the triblock copolymer such that the outer blocks consisted

of the PEG units (**5**) resulted in a hydrogel with less polymer content when fully hydrated and a lower storage modulus (Figure 4.5C and D). At 34 wt%, polymer **5** yielded a hydrogel with G' = 7.2 kPa (0.05% strain, 1 Hz) at 37 °C. The steady-state flow experiment indicated non-Newtonian characteristics with the apparent viscosity decreasing with increasing shear rate (Figure 4.5E). Furthermore, cyclic strain experiments also indicated self-healing properties of the gel, as it recovered quickly from deformations at high strain (Figure 4.5F). Notably, these materials represent some of the first examples of mechanically robust, physically cross-linked polynorbornene-based hydrogels.[11] Dissolution of the polymers from the hydrogels into THF and analysis by SEC was consistent with physical, as opposed to covalent, crosslinking within the networks.

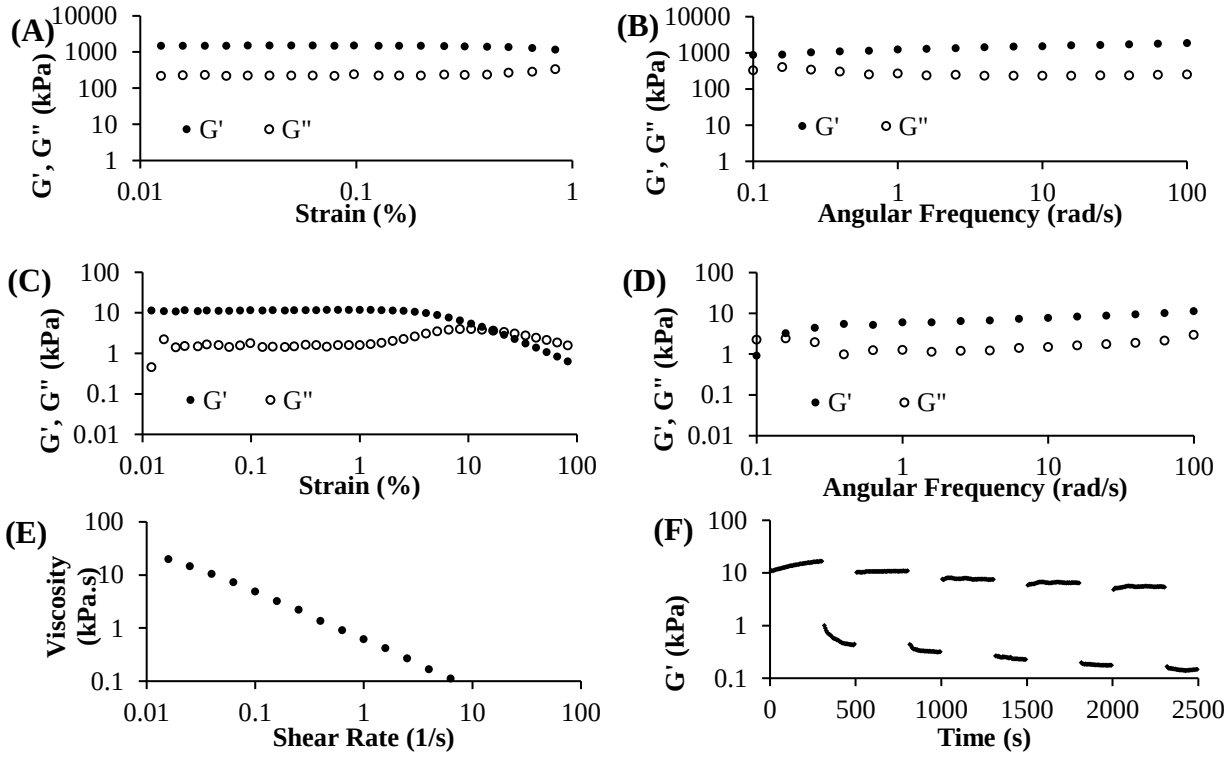

Figure 4.5. (A) Strain-dependent dynamic storage and loss moduli (G' and G") of 54 wt% **4**, frequency = 1 Hz (B) Frequency-dependent G' and G" of 54 wt% **4**. (C) Strain-dependent G' and

G” of 34 wt% **5**, frequency = 1 Hz (D) Frequency-dependent G’ and G” of 34 wt% **5**. (E) Linear decrease in viscosity as a function of increasing shear rate indicative of shear thinning behavior of 34 wt% **5**. (F) Alternating strain experiment of 34 wt% **5** (alternating 0.05% strain for 300 s, 100% strain for 180 s). All experiments were done at 37 °C.

Given that the oxazine moieties used herein appear to release 4-NA and HNO with high fidelity and a 1:1 stoichiometric ratio, we sought to also characterize the 4-NA release kinetics from hydrogels produced from **4**. We assessed the release of 4-NA from the hydrogel at 60 °C by UV-Vis spectroscopy (Figure 4.6). Over the course of 23 days, 62% of the theoretical maximum amount of 4-NA was released from the hydrogels. After this period, the structural integrity of the gels failed and dissolution of the material was observed. In fact, we observe gradual expansion of the gels from diameter = 8 mm to 12 mm prior to dissolution.

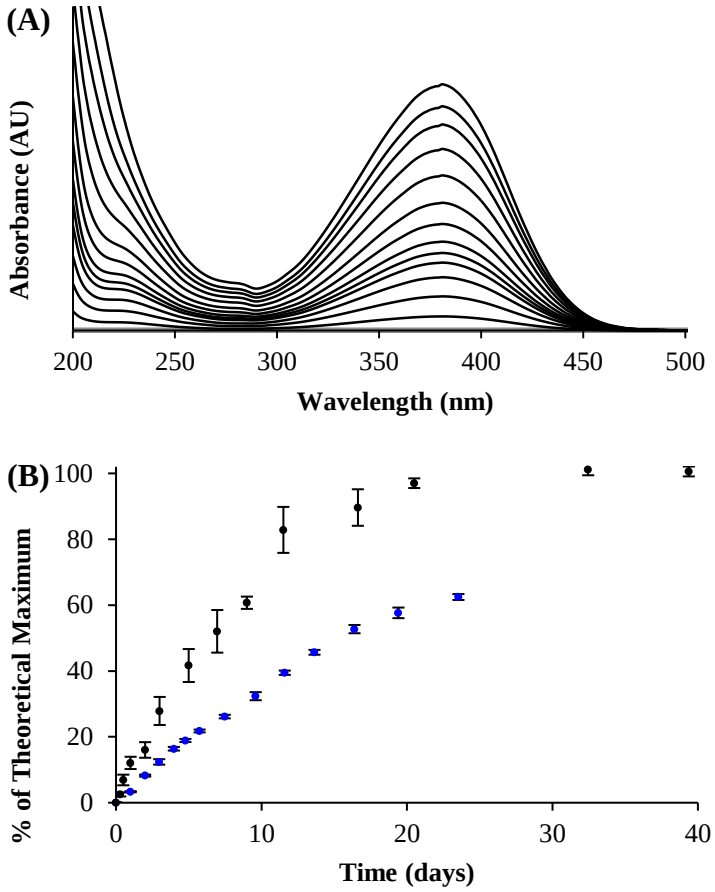

Figure 4.6. (A) UV-vis spectra recorded during thermolysis of hydrogel **4** at 60 °C showing increase in signal intensity corresponding to 4-NA over time. Fresh buffer was used after each time point and relative absorption intensity was corrected to represents the cumulative 4-NA released. Total time = 23 d. (B) Release of 4-nitroaniline (% of theoretical maximum) from polymer **3** (black) and hydrogel **4** (blue) in pH 7.4 PBS at 60 °C. Release of 4-NA was determined by UV-vis spectroscopy, monitored at 381 nm.

4.3 Conclusion

In conclusion, we have demonstrated the first examples of HNO release from covalent polymer-donor conjugates. The oxazine-based donors enable release of HNO at the exclusion of

NO, and concomitant release of a small organic molecule at physiologically relevant temperatures. The features further affirm the potential of these materials for delivery of therapeutics and assessment of HNO release kinetics. Additionally, the versatile polynorbornene ROMP graft-through technique offers exceptional tunability of the polymer properties, which can be tailored for specific application.

4.4 References

1) (a) Paolocci, N.; Jackson, M.; Lopez, B.; Miranda, K.; Tocchetti, C.; Wink, D.; Hobbs, A.; Fukuto, J. *Pharmacology & Therapeu.tics* **2007**, *113*, 442. (b) Switzer, C.; Flores-Santana, W.; Mancardi, D.; Donzelli, S.; Basudhar, D.; Ridnour, L.; Miranda, K.; Fukuto, J.; Paolocci, N.; Wink, D. *Biochimica et Biophysica Acta* **2009**, *1787*, 835. (c) Paolocci, N.; Keceli, G.; Wink, D. A.; Kass, D. A. "From Heaven to Heart: Nitroxyl (HNO) in the Cardiovascular System and Beyond." In The Chemistry and Biology of Azanone (HNO); Marti, M.A., Doctorovich, F., Farmer, P., Ed.; Elsevier, **2016**; 353.

2) (a) Fukuto, J.; Bartberger, M.; Dutton, A.; Paolocci, N.; Wink, D.; Houk, K. *Chem. Res. Toxicol.* **2005**, *18*, 790. (b) Irvine, J.;Ritchie, R.; Favaloro, J.; Andrews, K.; Widdop, R.; Kemp-Harper, B. *Trends in Pharmacological Sciences* **2008**, *29*, 601.

3) (a) Shafirovich, V.; Lymar, S. V. *Proc. Natl. Acad. Sci. U.S.A.* **2002**, *99*, 7340.

4) (a) Miranda, K. M.; Nagasawa, H. T.; Toscano, J. P. *Top. Med. Chem.* **2005**, *5*, 649. (b) DuMond, J. F.; King, S. B. Antioxid. Redox Signal. 2011, *14*, 1637. (c) Miao, Z.; King, S. B. Nitric Oxide 2016, *57*, 1. (d) Guthrie, D. A.; Nourian, S.; Toscano, J. P. "Hydroxylamines with Organic-Based Leaving Groups as HNO Donors." In The Chemistry and Biology of Azanone (HNO); Marti, M.A., Doctorovich, F., Farmer, P., Ed.; Elsevier, 2016; 37.

5) (a) Huang, A.; Velázquez, C. A.; Abdellatif, K. R. A.; Chowdhury, M. A.; Reisz, J. A.; DuMond, J. F.; King, S. B.; Knaus, E. E. *J. Med. Chem.* **2011**, *54*, 1356. (b) Basudhar, D.; Bharadwaj, G.; Cheng, R. Y.; Jain, S.; Shi, S.; Heinecke, J. L.; Holland, R. J.; Ridnour, L. A.; Caceres, V. M.; Regina, C. S.; Paolocci, N.;Velázquez-Martínez, C. A.; Wink, D. A.; Miranda, K. M. *J. Med. Chem.* **2013**, *56*, 7804.

6) (a) Blum, A. P.; Kammeyer, J. K.; Rush, A. M. Callmann, C. E.; Hahn, M. E.; Gianneschi, N. C. *J. Am. Chem. Soc.* **2015**, 137, 2140. (b) Crucho, C. I. C. *Chem. Med. Chem.* **2015**, *10*, 24-38; (c) Dong, R.; Pang, Y.; Su, Y.; Zhu, X. *Biomater. Sci.* **2015**, *3*, 937. (d) Hoffman, A. S. *Adv. Drug Deliv. Rev.* **2012**, *64*, 18. (e) Hoare, T. R.; Kohane, D. S. *Polymer* **2008**, *49*, 1993. (f) Keefer, L. K. *Current Topics in Medicinal Chemistry* **2005**, *5*, 625.

7) (a) Kensy, V. K.; Peterson, G. I.; Church, D. C.; Yakelis, N. A.; Boydston, A. J. *Org. Biomol. Chem.* **2016**, *14*, 5617. (b) Peterson, G. I.; Church, D. C.; Yakelis, N. A.; Boydston, A. J. *Polymer* **2014**, *55*, 5980. (c) Samoshin, A. V.; Hawker, C. J.; Read de Alaniz, J. *ACS Macro Lett.* **2014**, *3*, 753.

8) (a) Kirby, G.; Sweeny, J. *J. Chem. Soc., Perkins Trans 1* **1981**, *12*, 3250. (b) Christie, C.; Kirby, G.; McGuigan, H.; Mackinnon, J. *J. Chem. Soc., Perkins Trans. 1* **1985**, *11*, 2469. (c) Kirby, G.; McGuigan, H.; Mackinnon, J.; McLean, D.; Sharma, R. P. *J. Chem. Soc., Perkins Trans. 1* **1985**, *7*, 1437. (d) Atkinson, R. N.; Storey, B. M.; King, S. B. *Tet. Lett.*, **1996**, *37*, 9287. (e) Xu, Y.; Alavanja, M.; Johnson, V. L.; Yasaki, G.; Kings, S. B. *Tet. Lett.*, **2000**, *41*, 4265.

9) Bielawski, C. W.; Grubbs, R. H. *Angew. Chem. Int. Ed.* **2000**, *39*, 2903.

10) (a) Xia, Y.; Olsen, B. D.; Kornfield, J. A.; Grubbs, R. H. *J. Am. Chem. Soc.* **2009**, *131*, 18525. (b) Bielawski, C. W.; Grubbs, R. H. *Prog. Polym. Sci.* **2007**, *32*, 1.

11) Belger, C.; Weis, J. G.; Egap, E.; Swager, T. *Macromolecules* **2015**, *48*, 7990.

4.5 EXPERIMENTAL

4.5.1 *General Considerations*

Dry THF, pyridine, and CH_2Cl_2 were obtained from a Glass Contour solvent purification system. All other reagents and solvents were used as obtained from commercial sources. Grubbs 3rd generation catalyst, $(iMesH_2)(C_5H_5N)_2(Cl)_2Ru{=}CHPH$, was synthesized according to literature procedure.[1] Compounds **S1** and **1** were synthesized as previously reported.[2,3] ^1H and ^{13}C NMR spectra were recorded on a Bruker AVance 300 or 500 MHz spectrometer. Chemical shifts are reported in delta (δ) units, expressed in parts per million (ppm) downfield from tetramethylsilane using the residual protio-solvent as an internal standard ($CDCl_3$, ^1H: 7.26 ppm and ^{13}C: 77.16 ppm; D_2O, ^1H: 4.79 ppm). GPC setup consists of: an Agilent 1260 Infinity II HPLC pump, three in-line MZ-Gel 10 μm size-exclusion columns (pore sizes = 10^3, 10^3, and 10^5 Å), miniDAWN-TREOS 3-angle multi-angle laser light scatter and OptiLab T-rEx refractive index detectors (each from Wyatt Technologies Corporation). The mobile phase consisted of THF. No calibration standards were used, and dn/dc values were obtained for each injection assuming 100% mass elution from the columns. UV-Vis experiments were conducted on an Agilent 8453 Diode Array UV-Vis Spectrophotometer. Gas chromatography was performed on a Varian CP-3800 instrument equipped with a 1041 manual injector, electron capture detector, and a 2 m × 2 mm × $^1/_8$ in ShinCarbon ST packed column. Grade 5.0 nitrogen was used as both the carrier (8 mL/min) and the make-up (22 mL/min) gas. For all the measurements, the column oven temperature was kept constant at 150 °C, and the injector oven and the detector oven were held at 200 °C and 300 °C, respectively. A 100 μL gastight syringe with a sample-lock was used

for all gas injections. A TA Instruments Discovery HR-2 Hybrid Rheometer with an 8 mm stainless steel parallel Peltier Plate upper geometry was used for all rheology experiments. The temperature was maintained at 37 °C using the lower Peltier Plate temperature system. Dynamic storage modulus (G') and loss modulus (G") of the hydrogels were measured by oscillatory shear experiments. Dynamic strain sweep experiments were conducted at a frequency of 1 Hz, and the linear viscoelastic regime was determined. Dynamic frequency sweep experiments were conducted within the linear viscoelastic regime (at a strain amplitude of γ = 0.05 %) as a function of angular frequency from 0.1 to 100 (rad/s). Steady-state flow experiment was conducted by a shear ramp from 0.01 to 100 (1/s) for equilibrium duration of 5 s to measure apparent viscosity as function of shear rate.

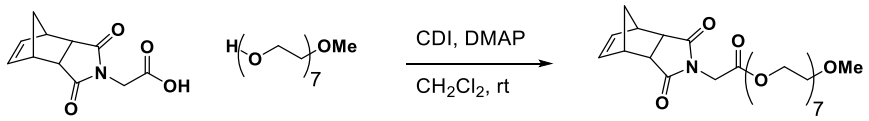

S1 **2**

4.5.2 *Synthesis of **2**.*

Into a flame-dried, N_2-purged round bottom flask, *N*,*N*-carbonyldiimidazole (1.7 g, 10.7 mmol, 1.3 eq.) were added a magnetic stir bar and 20 mL of CH_2Cl_2. To this solution, **S1** (2.4 g, 10.7 mmol, 1.3 eq.) was added portion-wise. The reaction mixture was stirred at room temperature for 45 min. After this time, DMAP (100 mg, 0.82 mmol, 0.1 eq.) and poly(ethylene glycol) methyl ether (350 Da) (3.0 mL, 8.2 mmol, 1.0 eq.) in 20 mL of CH_2Cl_2 were added to the reaction mixture. The reaction mixture was then stirred at room temperature for 18 h. The reaction mixture was then concentrated under reduced pressure and filtered through an alumina/Celite plug, using CH_2Cl_2 (60 mL) as eluent. The solution was then concentrated under

reduced pressure to afford the desired product. (95% yield) ^{1}H NMR (500 MHz, $CDCl_3$) δ 6.23 (s, 1H), 4.25 – 4.20 (m, 1H), 4.18 (s, 1H), 3.57 (d, J = 4.8 Hz, 15H), 3.30 (s, 1H), 3.24 (s, 1H), 2.68 (s, 1H), 1.65 (d, J = 10.0 Hz, 1H), 1.45 (d, J = 10.0 Hz, 1H). ^{13}C NMR (126 MHz, $CDCl_3$) δ 176.5, 166.5, 137.6, 71.5, 70.1, 68.3, 64.4, 58.5, 47.5, 45.0, 42.4, 38.9.

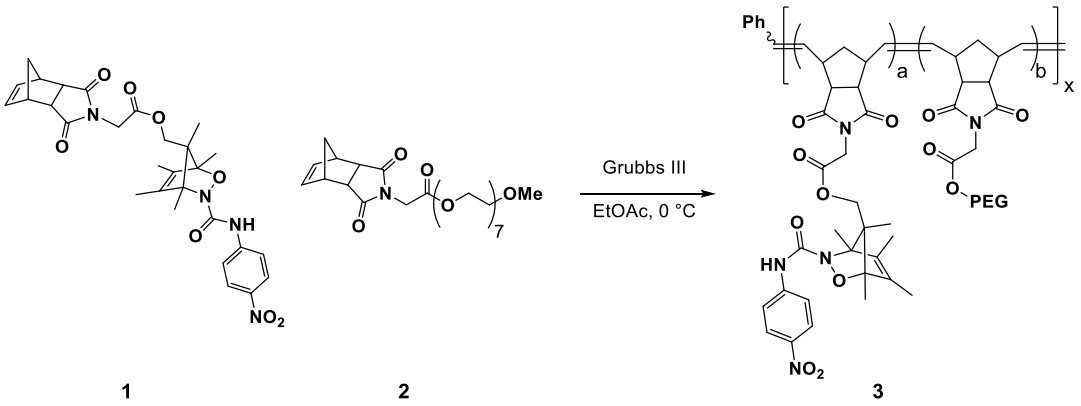

1 **2** **3**

4.5.3 *Synthesis of **3**.*

Into a flame-dried, N_2-purged round bottom flask, monomers **1** (75 mg, 0.13 mmol, 15 eq.), **2** (216 mg, 0.39 mmol, 45 eq.), a magnetic stir bar and 15 mL of N_2-purged EtOAc were added. The mixture was stirred until complete dissolution was obtained (judged visually), and then the solution was cooled to 0 °C in an ice bath and Grubbs 3rd generation catalyst (6.3 mg, 0.0087 mmol, 1.0 eq.) in 0.87 mL of N_2-purged EtOAc was quickly added via syringe. The reaction solution was stirred for 2 h, during which time the ice bath expired. Ethyl vinyl ether (2.4 mL) was then added to the reaction mixture and the solution was stirred for an additional 10 min. The solution volume was then reduced to ca. 2 mL under reduced pressure and then added dropwise into cold diethyl ether causing precipitation of polymer **3**. The resulting ethereal solution was decanted away from the polymer residue. The polymer was then dissolved in a minimal amount of CH_2Cl_2 and filtered through an alumina/Celite plug using CH_2Cl_2 as eluent. The solution was

again concentrated under reduced pressure and precipitated into diethyl ether. The resulting ethereal solution was decanted away and the polymer residue was washed with diethyl ether, providing the desired product as a soft, tacky solid (173 mg, 60% yield). M_n = 41.9 kDa, Đ = 1.09. A 1:3.18 ratio of **1** to **2** in the polymer was determined by ^{1}H NMR spectroscopy. This corresponds to an average oxazine content per polymer chain of 18. The oxazine content was determined by examining the relative ratio of –OMe peak at δ = 3.37 ppm to the integration of the –Me peak attached to the bridging carbon of the combined *anti* and *syn* oxazine isomers (δ = 1.07 and 0.77 ppm, respectively).

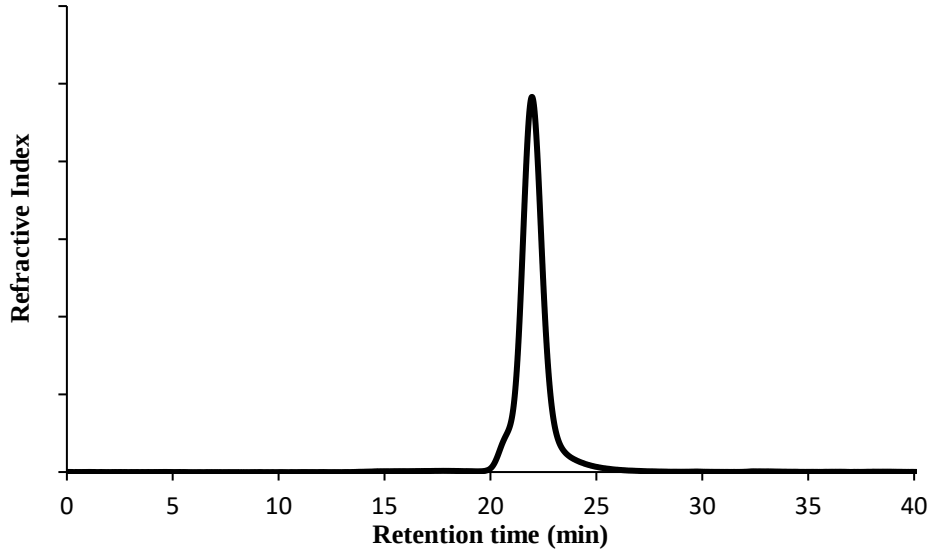

Figure 4.7. GPC trace of polymer **3**

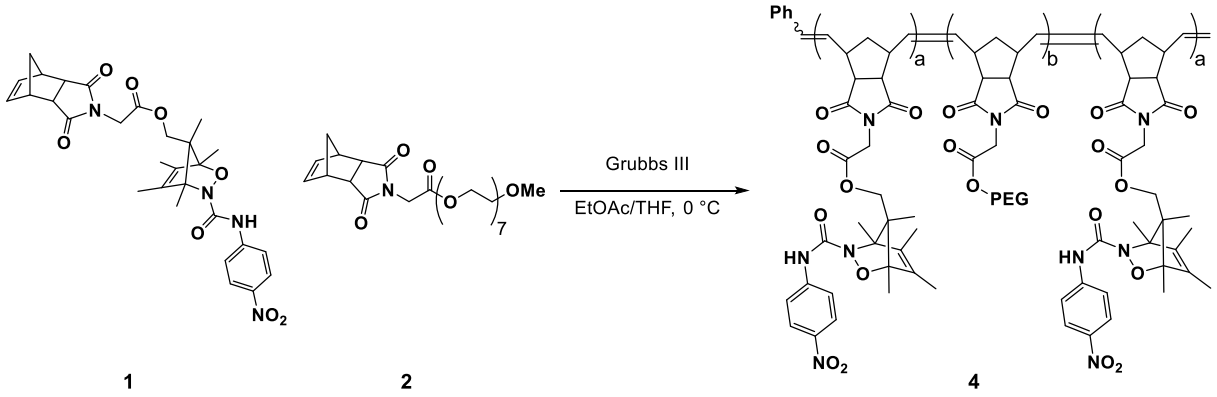

1 2 4

4.5.4 *Synthesis of **4**.*

Into a flame-dried, N_2-purged round bottom flask were added monomer **1** (325 mg, 0.57 mmol, 35 eq.), a magnetic stir bar, 24 mL of N_2-purged EtOAc, and 24 mL of N_2-purged THF. Once complete dissolution was achieved (judged visually), the solution was cooled to 0 °C in an ice bath and Grubbs 3rd generation catalyst (13.8 mg, 0.019 mmol, 1.0 eq.) in 0.7 mL of N_2-purged THF was quickly added. The reaction solution was then stirred for 40 min. Compound **2** (1.26 g, 2.28 mmol, 140 eq.) in 4 mL of N_2-purged EtOAc was added and the reaction mixture was stirred for an additional 40 min. Finally, **1** (325 mg, 0.57 mmol, 35 eq.) in 2 mL of N_2-purged THF was added and the reaction mixture was stirred for an additional 40 min. Ethyl vinyl ether (6 mL) was then added to the reaction mixture and the resulting solution was stirred for 10 min. The solution volume was then concentrated under reduced pressure and then filtered through an alumina/Celite plug using CH_2Cl_2 as eluent. The solution was again concentrated under reduced pressure and precipitated into cold diethyl ether. The resulting ethereal solution was decanted away and the polymer residue was washed with diethyl ether, providing the desired product as a soft, tacky solid (1.36 g, 71% yield). Mn = 115.7 kDa, Đ = 1.03. A 1 : 2.26 ratio of **1 to 2** in the polymer was confirmed by ^{1}H NMR spectroscopy. Average oxazine content per polymer chain is ~65. The oxazine content was determined by examining the relative ratio of –

OMe peak at 3.37 ppm to the integration of the –Me peak attached to the bridging carbon of the combined *anti* and *syn* oxazine isomers (δ = 1.07 and 0.77 ppm, respectively).

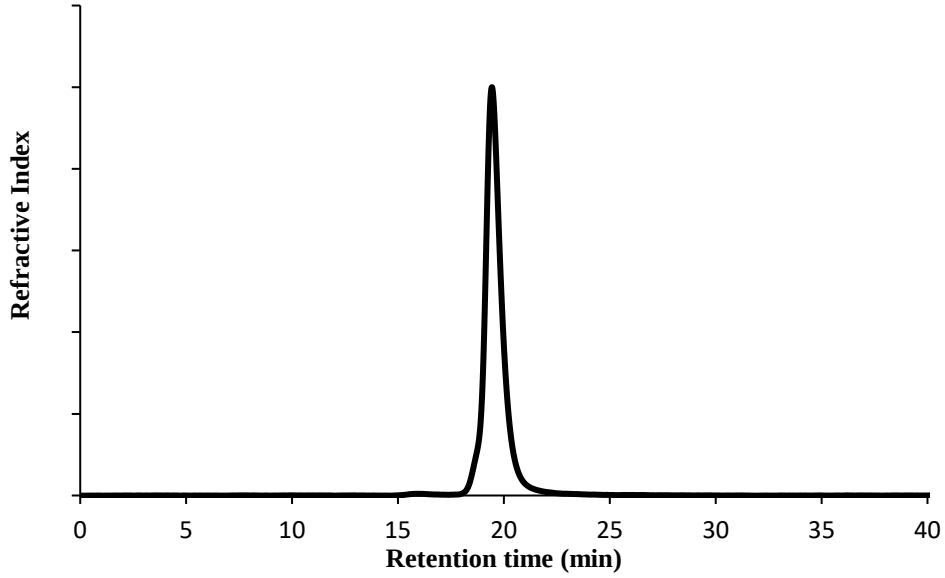

Figure 4.8. GPC trace of polymer **4**.

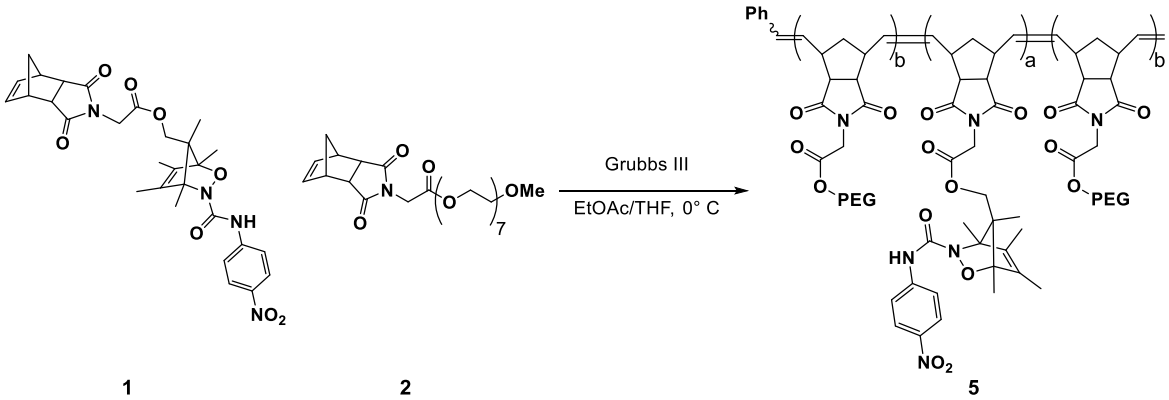

4.5.5 *Synthesis of **5**.*

Into a flame-dried, N_2-purged round bottom flask were added monomer **2** (521 mg, 0.94 mmol, 45 eq.), a magnetic stir bar, and 40 mL of N_2-purged EtOAc. Once complete dissolution was achieved (judged visually), the solution was cooled to 0 °C in an ice bath and Grubbs 3rd

generation catalyst (15.3 mg, 0.021 mmol, 1.0 eq.) in 0.7 mL of N_2-purged THF was quickly added. The reaction solution was then stirred for 40 min. Compound **1** (355 mg, 0.63 mmol, 30 eq.) in 2 mL of N_2-purged EtOAc was added and the reaction mixture was stirred for an additional 40 min. Finally, **2** (521 mg, 0.94 mmol, 45 eq.) in 2 mL of N_2-purged EtOAc was added and the reaction mixture was stirred for an additional 40 min. Ethyl vinyl ether (6 mL) was then added to the reaction mixture and the resulting solution was stirred for 10 min. The solution volume was then concentrated under reduced pressure and then filtered through an alumina/Celite plug using CH_2Cl_2 as eluent. The solution was again concentrated under reduced pressure and precipitated into cold diethyl ether. The resulting ethereal solution was decanted away and the polymer residue was washed with diethyl ether, providing the desired product as a soft, tacky solid (1.07 g, 76% yield). Mn = 65.9 kDa, Đ = 1.02. A 1 : 3.34 ratio of **1 to 2** in the polymer was confirmed by ^{1}H NMR spectroscopy. The oxazine content was determined by examining the relative ratio of –OMe peak at 3.37 ppm to the integration of the –Me peak attached to the bridging carbon of the combined *anti* and *syn* oxazine isomers (δ = 1.07 and 0.77 ppm, respectively).

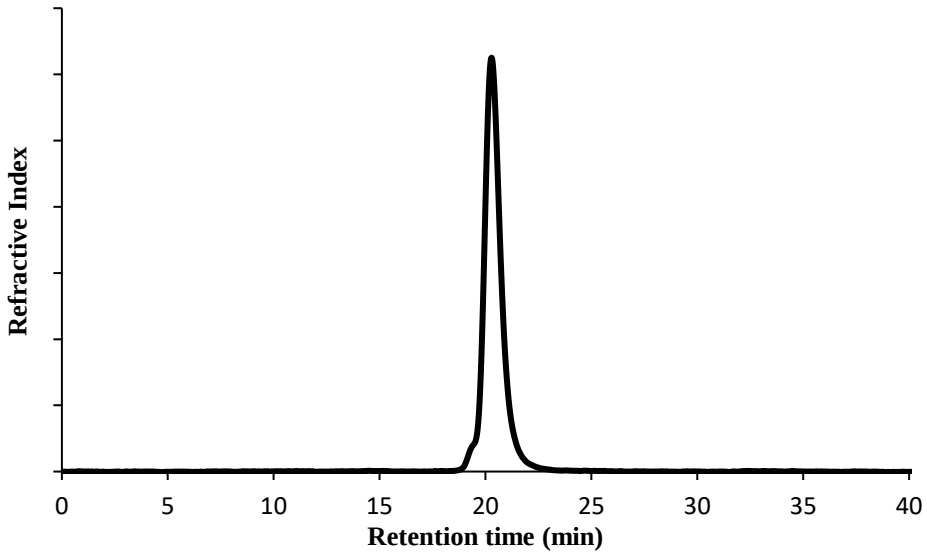

Figure 4.9. GPC trace of polymer **5**.

4.5.6 *General Method for Monitoring the Release of 4-Nitroaniline from **3**.*

Polymer **3** (12 mg) was dissolved in 3 mL of Milli-Q filtered H_2O with vigorous stirring for 6 hours to make a 1.12×10^{-4} M stock solution. Then, 2.7 mL of the polymer stock solution was combined with0.5 mL of 100 mM pH 7.4 phosphate buffer before dilution to 100 mL using Milli-Q filtered H_2O. This gave a final polymer concentration of 3×10^{-6} M in 0.5 mM pH 7.4 phosphate buffer. The resulting solution was then filtered through a 0.45-μm pore size PTFE syringe filter. The polymer solution was then portioned out (5 mL) into screw-cap scintillation vials and then each vial was sealed with a PTFE-lined screw cap. The vials were then submerged into a pre-heated oil bath where applicable. At specified time points, UV-vis spectroscopy was conducted on the aqueous polymer solution. Each experiment was conducted in triplicate.

4.5.7 *General Method for Preparing Hydrogels from **4**.*

From a 400 mg/mL stock solution of polymer **4** in THF, 0.17 mL was added to a tared 2 mL GC vial. The solvent was then evaporated under steady flow of N_2 over 18 h. Then, the dry mass of the polymer film was recorded. Phosphate buffered water (1 mL, 10 mM, pH 7.4) was then added to the film. After 24 h, the vials were carefully broken to allow for removal of the films. The films were then submerged in 1 mL of fresh phosphate buffered water for an additional 24 h. The hydrated mass of the films were then recorded. Then, 8-mm disks were cut out from the films for rheology and 4-nitroaniline release studies.

4.5.8 *General Method for Preparing Hydrogels from **5**.*

From a 800 mg/mL stock solution of polymer **5** in CH_2Cl_2, 0.1 mL was added to a tared Eppendorf tube. The solvent was then evaporated under steady flow of N_2 over 18 h. Then, the

dry mass of the polymer was recorded. Phosphate buffered water (0.5 mL, 10 mM, pH 7.4) was then added. After 24 h, excess water was removed and the mass of the resulting hydrogel was recorded.

4.5.9 *Nitrous Oxide (N_2O) Quantification by Headspace Gas Chromatography*

Samples were prepared in 6 mL Wheaton Clr headspace vials with volumes pre-measured for sample uniformity (actual vial volume ranges from 5.8 - 6.3 mL). Vials were charged with 3 mL of 0.5 mM phosphate buffer at pH 7.4 and fit with rubber septa and 20 mm aluminum seals. The vials were purged with argon and thermally equilibrated for at least 10 minutes at 60 °C in a dry block heater. Stock solutions of 2-bromo-*N*-hydroxybenzenesulfonamide (2-bromo-Piloty's acid, 2-BrPA) and polymer **3** were prepared in acetonitrile and DI water, respectively, and used immediately after preparation. From these stock solutions a series of 2-BrPA samples and a series of polymer **3** samples were prepared in thermally equilibrated vials with final concentrations of 100 and 6.4 μM respectively. The theoretical maximum percentage of HNO produced from this concentration of polymer **3**, which contains on average 15.7 units of oxazine per polymer chain, is equivalent to that produced from 100 μM 2-BrPA. Vials were then incubated at 60 °C over 19 days and periodically, 60 μL of the headspace of each vial was sampled by three successive injections using a gastight syringe with a sample lock. The N_2O yields for polymer **3** were averaged and are reported as HNO yields relative to analogous measurements for the 2-BrPA standard.

4.5.10 *4-Nitroaniline Detection by ^{1}H-NMR Spectroscopy*

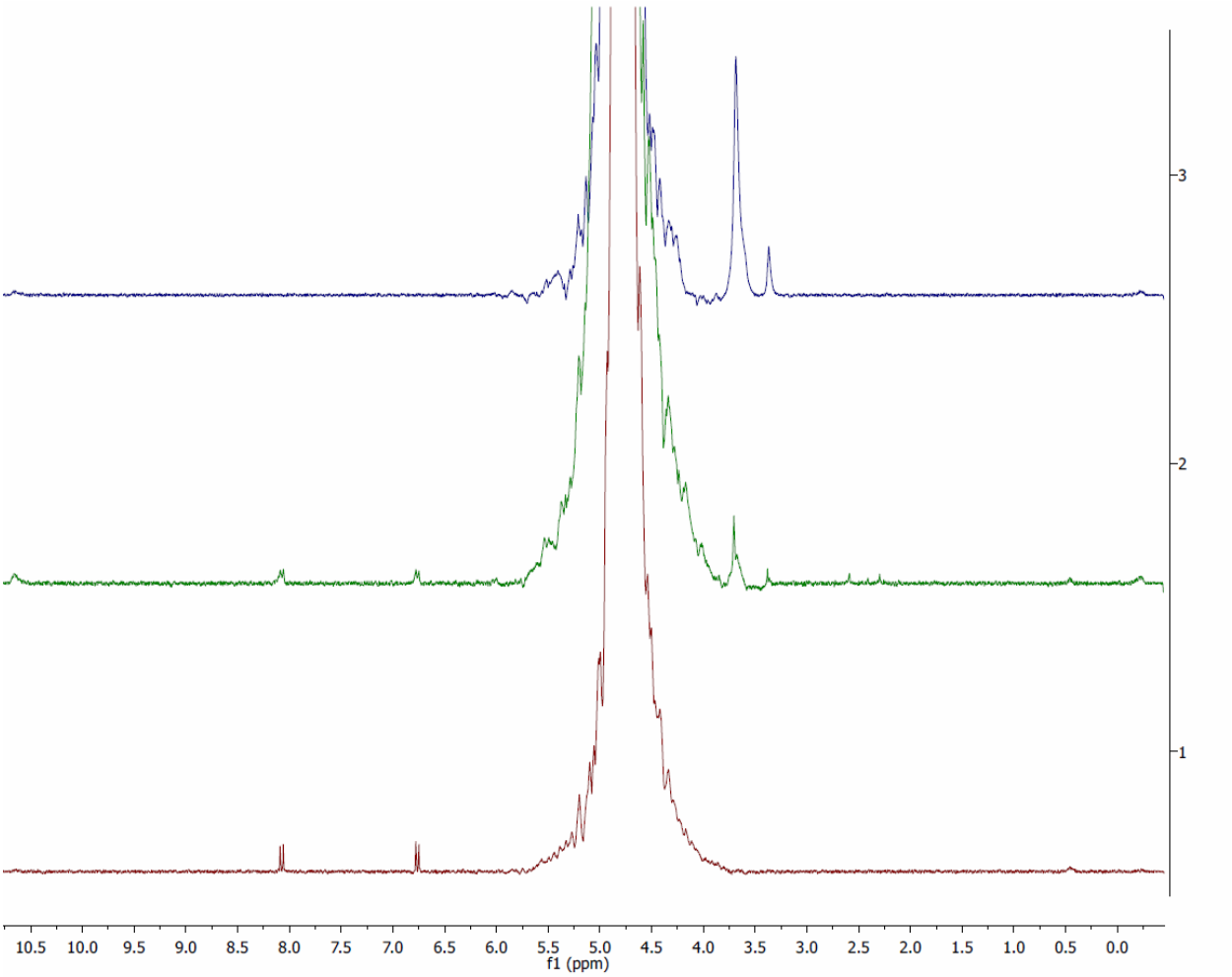

Figure 4.10. Polymer **3** in phosphate buffered water containing 10% D_2O by volume (top). Thermolysis of polymer **3** at 80 °C for 24 hours (middle). 4-Nitroaniline in phosphate buffered water containing 10% D_2O by volume (bottom)

4.5.11 *NMR Spectra*

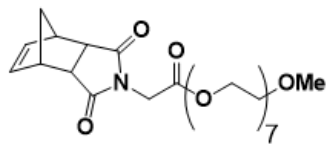

2

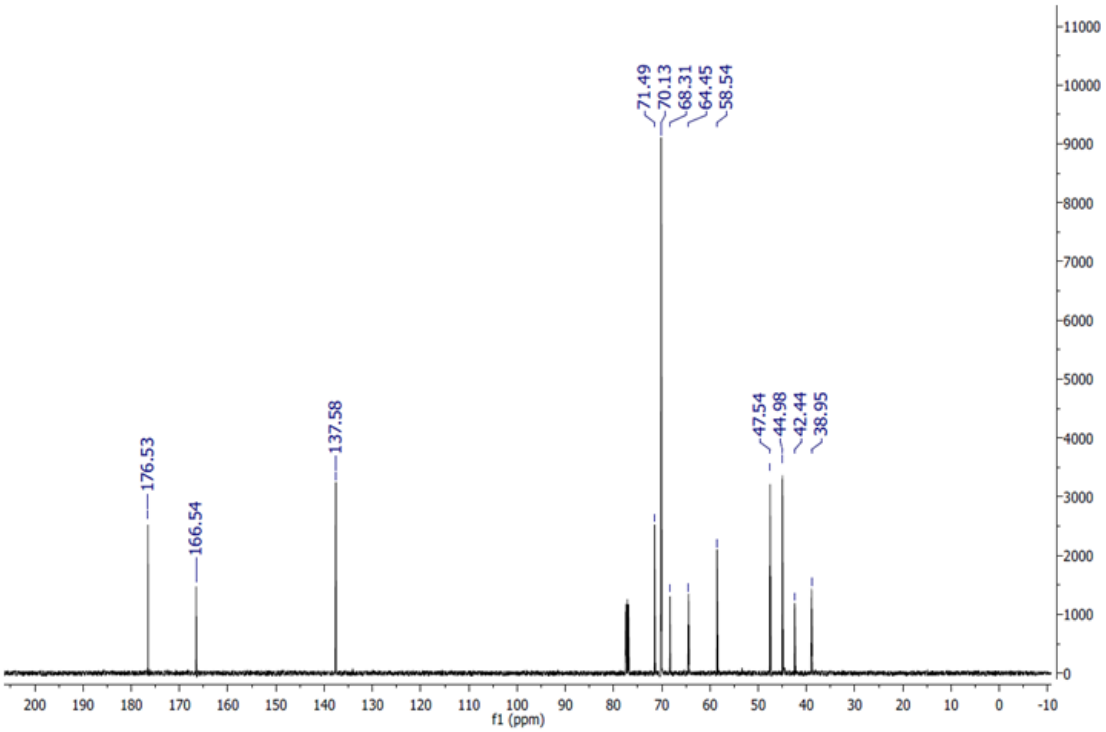

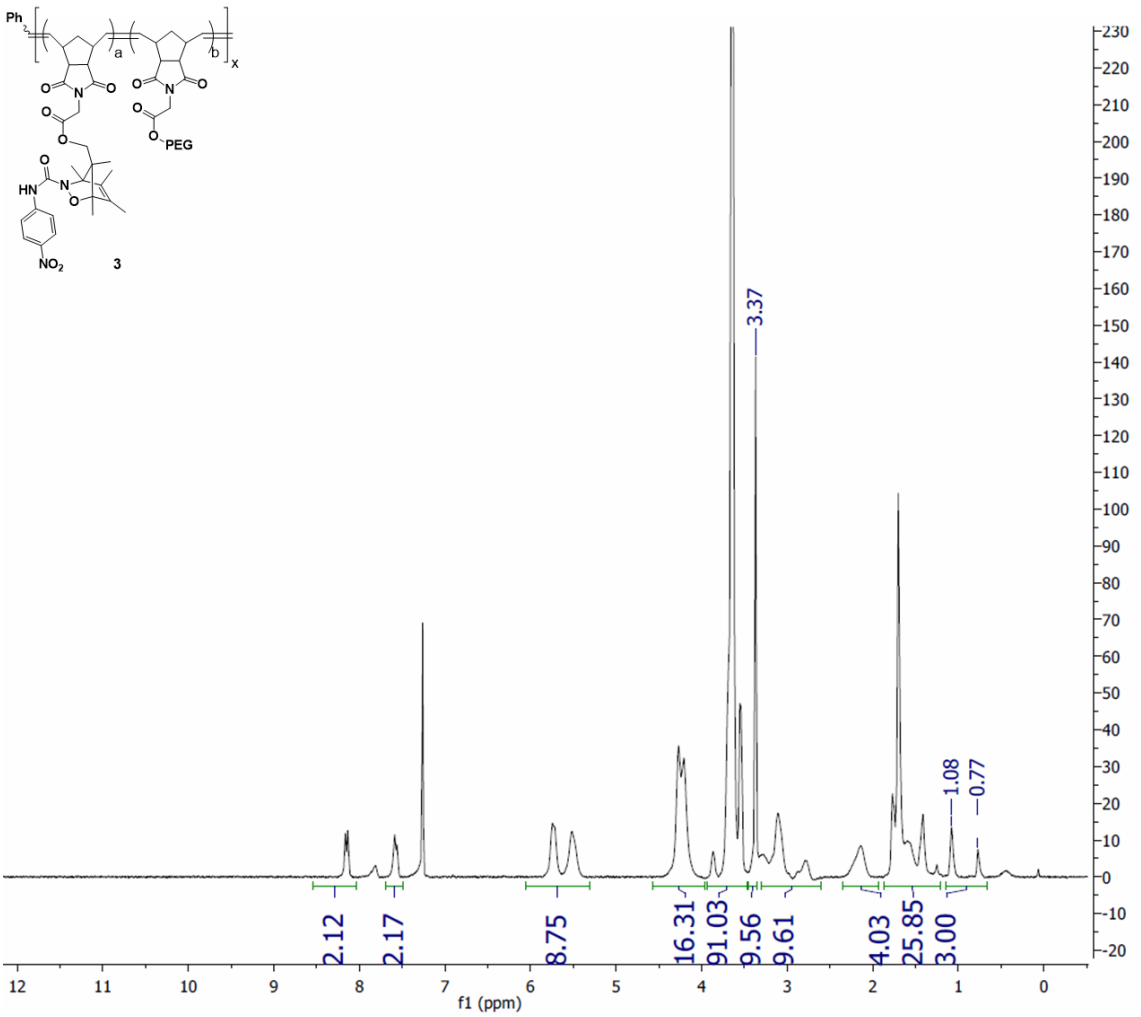
Ph
a
b
x
PEG
HN
NO2
3
3.37
1.08
0.77
2.12
2.17
8.75
16.31
91.03
9.56
9.61
4.03
25.85
3.00
f1 (ppm)

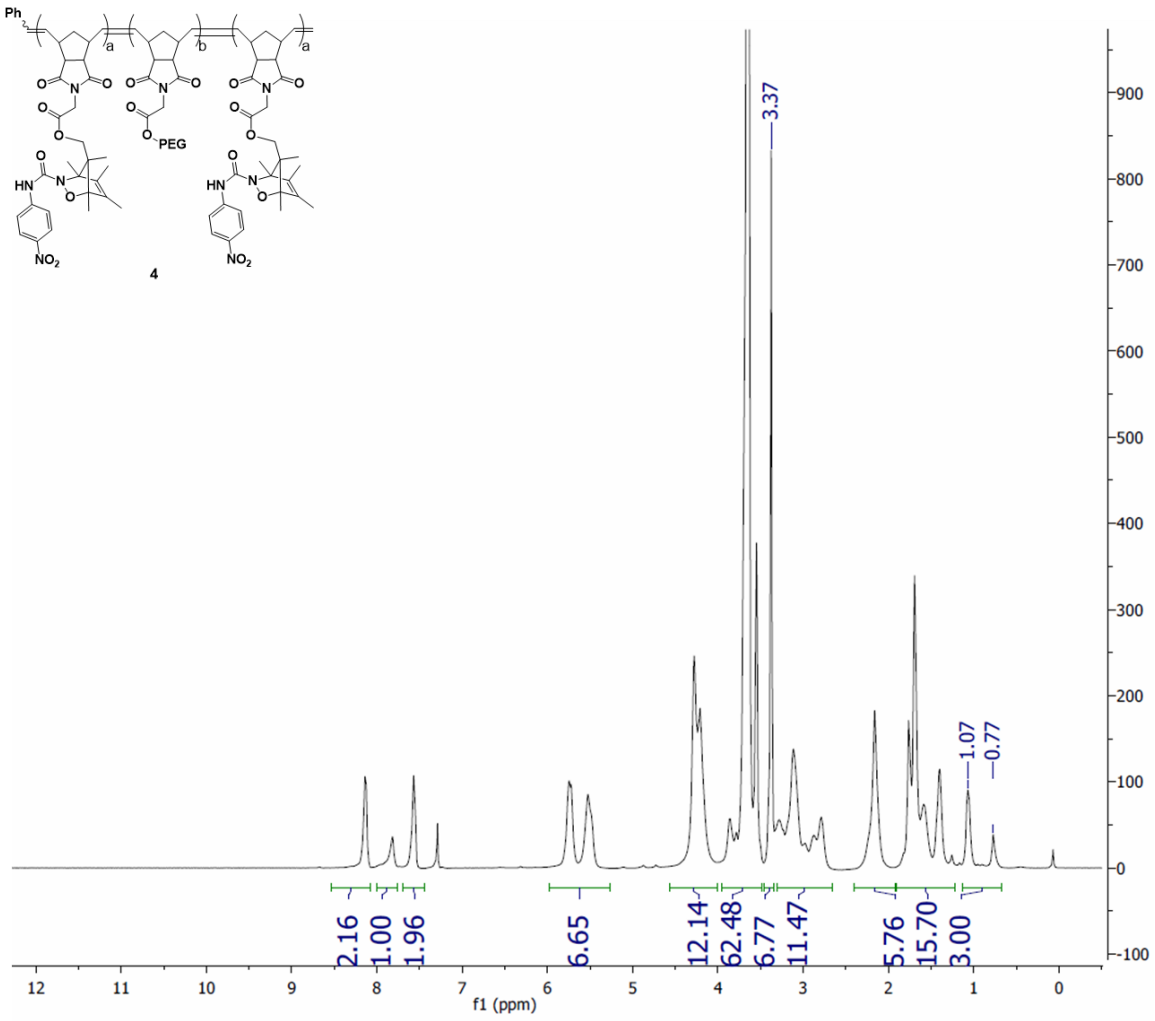
Ph
a
b
a
PEG
HN
NO2
4
3.37
1.07
0.77
2.16
1.00
1.96
6.65
12.14
62.48
6.77
11.47
5.76
15.70
3.00
f1 (ppm)

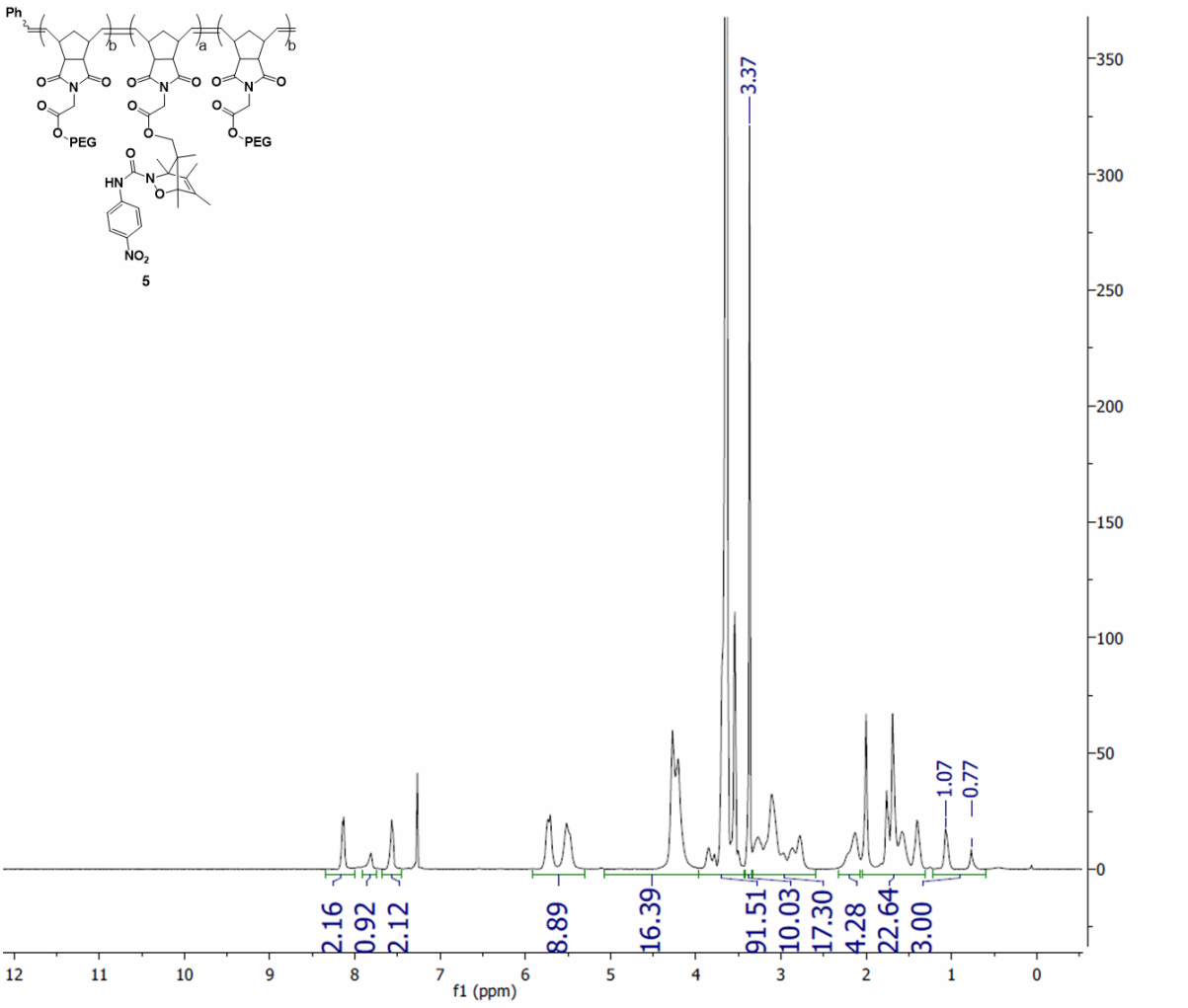

4.5.12 *Experimental References*

1) Love, J. A.; Morgan, J. P.; Trnka, T. M.; Grubbs, R. H. *Angew. Chem. Int. Ed.* **2002**, *41*, 4035.

3) Conrad, R. M.; Grubbs, R. H. *Angew. Chem. Int. Ed.* **2009**, *48*, 8328.

4) Kensy, V. K.; Peterson, G. I.; Church, D. C.; Yakelis, N. A.; Boydston, A. J. *Org. Biomol. Chem.* **2016**, *14*, 5617.

Chapter 5. EXOGENOUS PHOTOTHERMAL ACTIVATION OF 1,2-OXAZINES AND OTHER FUTURE WORK

5.1 EXOGENOUS PHOTOTHERMAL ACTIVATION OF 1,2-OXAZINES

Previously it has been demonstrated that HNO and small molecule undergo sustained and concomitant release at physiological temperatures, which is ideal for passive administration of a therapeutic. Predictably, at higher temperatures, an increase in the rate of release is also observed. However, to access these higher temperatures for therapeutic applications, an exogenous source of hyperthermia must be utilized.

Generating localized hyperthermia within the body from an exogenous source has attracted copious amounts of attention for the treatment of various diseases, such as cancer, due to its non-invasive and targeted nature. Ultrasound, magnetic, radio frequency, microwave and near-infrared (NIR) stimuli have all been used in conjunction with synthetic materials to induce localized heating effects.[1] These techniques have been used to directly ablate and eradicate diseased tissues or initiate phase changes in a polymeric carrier to expel encapsulated therapeutics in a site- and time-specific manner.

Recent advancements in light generation and the synthesis of light absorbing chromophores have greatly enhanced the profile of photothermal therapy (PTT) for biomedical applications.[2] Typically, materials for PTT are designed to absorb in the NIR region due to minimal absorption of the surrounding tissues within this spectral window, resulting in greater bodily penetration.

Organic dyes are an exciting class of PTT agents due to the ability to synthetically modify their electronic structure and thereby wavelength at which they absorb.[3] Recent research in this area has demonstrated that encapsulating these dyes within polymeric nanoparticles has successfully resulted in tumor ablation or release of encapsulated therapeutic upon uptake of the

nanoparticles.[4] We therefore wanted to explore whether these dyes could be harnessed for the triggered activation of the oxazine moiety.

5.1.1 *Photothermal Dye Doped Micelles*

One route envisioned toward exogenous activation of the oxazine-containing polymer within the body is the encapsulation of a photothermal dye within the hydrophobic core of a diblock copolymer micelle. By this route, passive accumulation of the micelle within a tumor would occur through the enhanced permeation and retention effect. Upon entering the tumor, the affected area would then be irradiated with a NIR laser to trigger photothermal transduction and oxazine activation to release the desired payload. Recent work by Smith and coworkers have demonstrated that croconaine dyes (**Croc**) are effective PTT agents as they are biocompatible, absorb in the NIR region, and produce no singlet oxygen upon irradiation which otherwise may degrade therapeutic payload within the micelle.[5] They demonstrated that photothermal activation of the dye encapsulated within the hydrophobic layer of a thermosensitive liposome caused a thermally-induced phase transition and leakage of a fluorescent reporter molecule from the aqueous interior.

Towards this end, diblock copolymer **1** was synthesized via the ring opening metathesis polymerization (ROMP) technique. A solution of polymer **1** and **Croc** in DMF was then dialyzed against pH 7.4 0.5 mM phosphate buffered water, causing the hydrophobic oxazine block to aggregate and encapsulate the **Croc** dye into self-assembled spherical micelles (Scheme 5.1).

Scheme 5.1. Synthesis of **Croc** doped micelles from **1**.

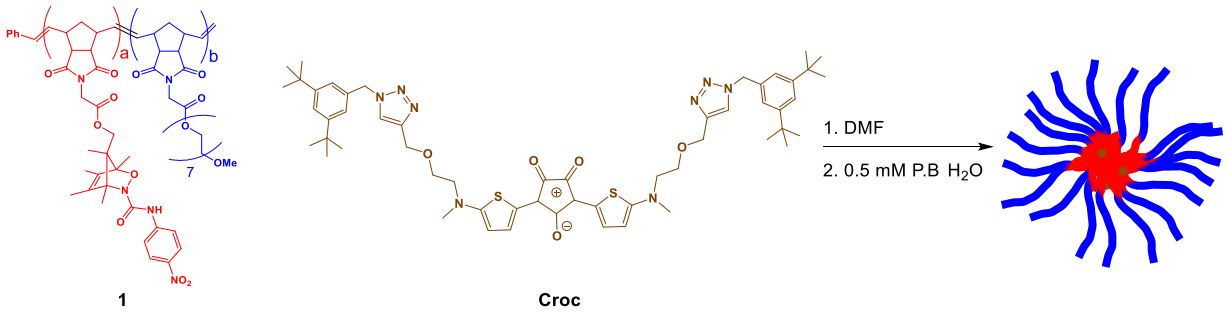

UV-vis spectroscopy of the resulting aqueous solution (Figure 5.1) displayed peaks for the oxazine moiety and dye within the hydrophobic core at 330 nm and 802 nm respectively, in accordance with literature precedent.[5] Transmission Electron Miscroscopy (TEM) images (Figure 5.2) support the existence of self-assembled structures with uniform spherical morphologies and average diameter of 19.6 ± 1.4 nm.

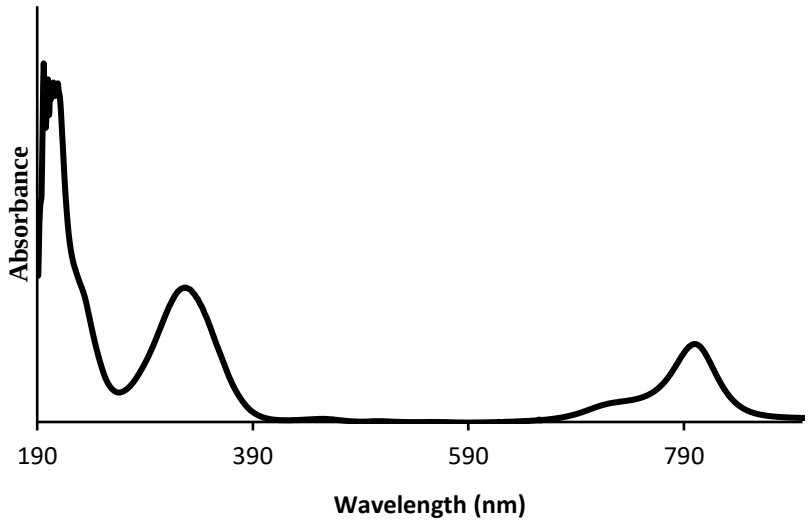

Figure 5.1. UV-vis spectrum of micelles from **1** and encapsulated **Croc** dye.

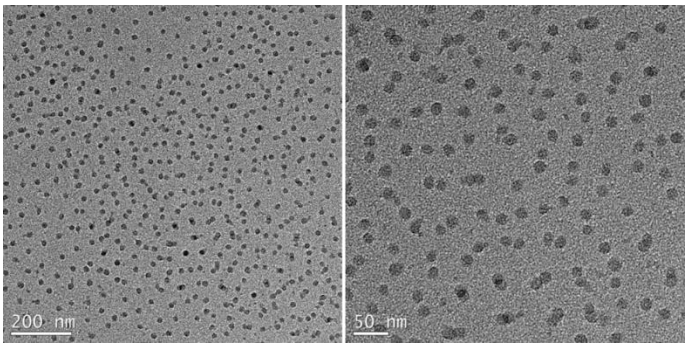

Figure 5.2. TEM images of **Croc** doped micelles made from polymer **1**.

Release of 4-nitroaniline (4-NA) was observed upon bulk heating of the micelles at 60 °C (Figure 5.3), suggesting that release of the 4-NA reporter molecule should be unencumbered by sequestration in the hydrophobic core. However, subsequent irradiation with a NIR laser at power densities ranging from 0.44 – 1.74 W/cm^2 displayed no oxazine activation nor 4-NA release, despite bulk solution temperatures of ~50 ^{0}C being reached.

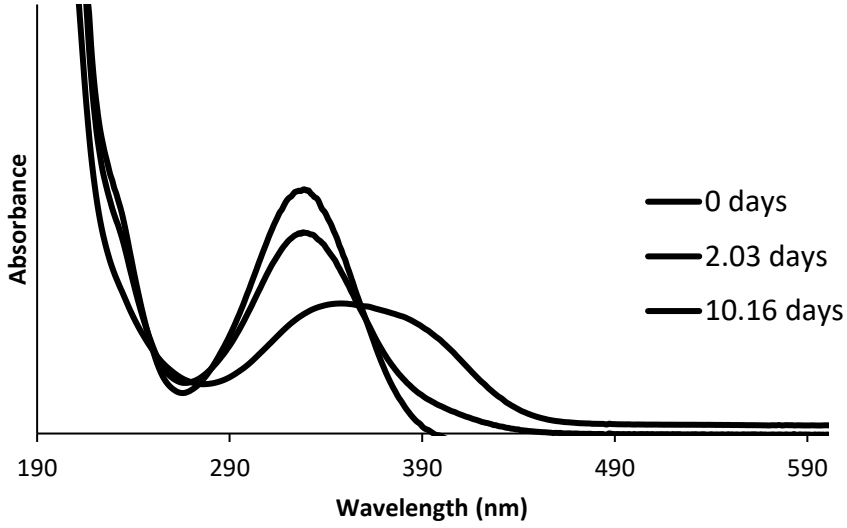

Figure 5.3. UV-vis spectra tracking release of 4-NA release from micelles made from polmer **1** at 60 °C in phosphate buffered H_2O.

5.1.2 *Photothermal Dye Doped Hydrogels*

An alternative approach was envisioned in which the the **Croc** dye could be incorporated into the hydrophobic domains of a hydrogel formulation. By this route, the **Croc**-doped hydrogel could be placed in a discrete location inside the body without risk of rapid clearance. Irradiation with a NIR light source could then be applied to cause an on-demand burst release of the therapeutic, directly at the targeted area. To this end, triblock copolymer **2** was doped with different concentrations of **Croc** dye (Scheme 5.2).

Scheme 5.2. Synthesis of **Croc** doped hydrogels from **2**.

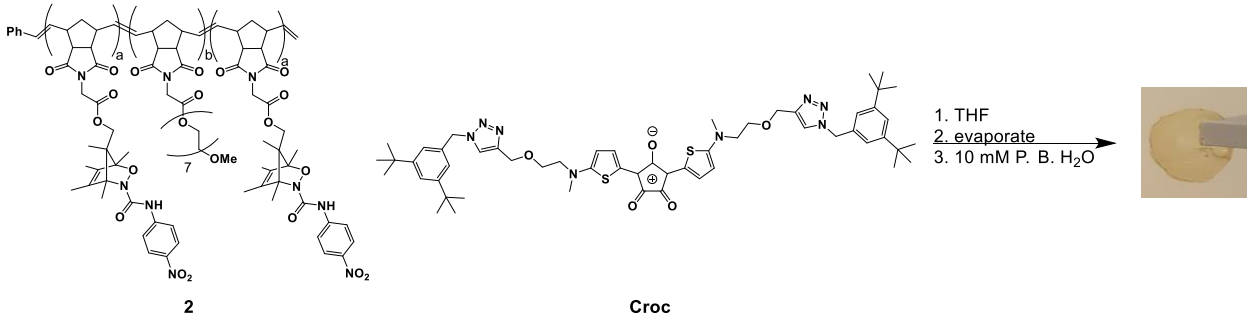

As a preliminary investigation into the effects of dye concentration and laser irradiation on photothermal output, dye-doped polymer films were irradiated with 808 nm light at 1.72 W/cm^2 (Figure 5.4). When no dye is present in the film, a baseline temperature of 47.6 °C was observed when irradiated with the NIR laser (Table 5.1). A hydrogel with 0.09 wt% of **Croc** dye displayed a slight increase in temperature of Δ +2 °C over the course of 60 seconds. However, when a hydrogel containing 0.9 wt% dye was irradiated, an instantaneous increase in temperature of Δ +50 °C was observed, accompanied by thermal deformation of the hydrogel. To determine whether these exposure times were sufficient to cause oxazine activation, each film was then

soaked in phosphate buffered water for 1 hour, at which point the solutions were analyzed by UV-vis spectroscopy.

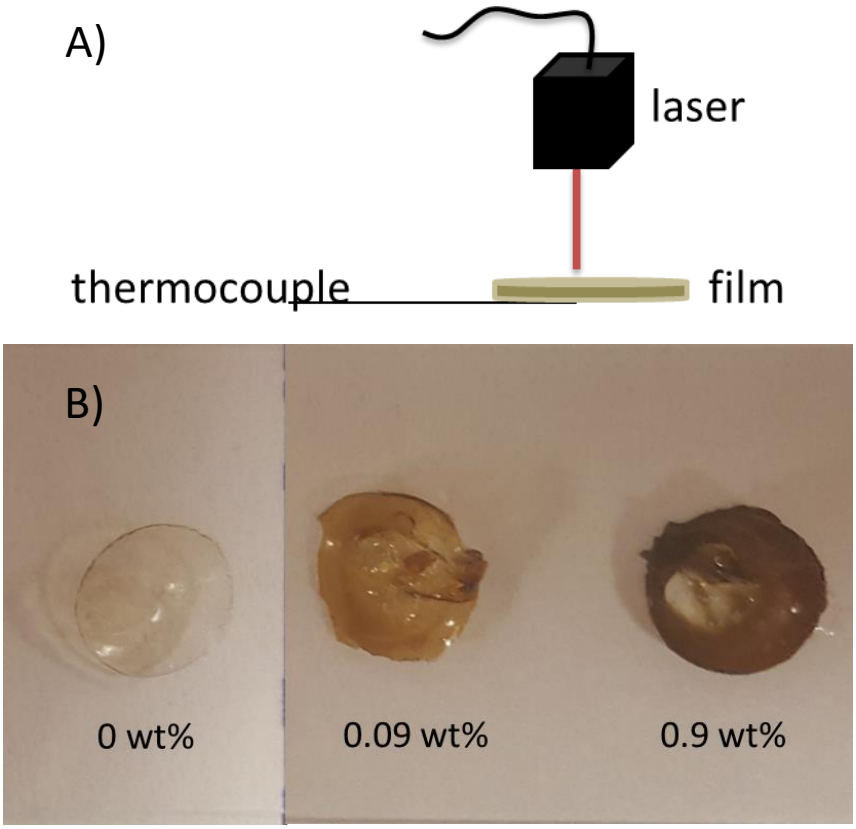

Figure 5.4. A) General setup for NIR irradiation of **Croc** doped hydrogel from **2**. B) Pictures of **Croc** doped hydrogels with different weight percent of dye. Picture taken after laser irradiation.

Table 5.1. 4-NA release from hydrogels as a function of **Croc** weight percent.

Entry	**Croc** wt%	Power Density (W/cm^2)	Irradiation time (s)	T (°C)	% 4-NA released[b]
1	0	1.72	60	47.6	0.8
2	0.09	1.72	60	49.8	1.1
3	0.9	1.72	10[a]	100	1.5

[a]Less irradiation time due to rapid thermal deformation of the hydrogel.
[b]Results are from a single experiment.

A slight increase in the % 4-NA released from 0.8% to 1.1% was observed for a hydrogel doped with 0.09 wt% **Croc** dye relative to a non-doped hydrogel, corresponding with the slight increase in temperature upon irradiation. At the higher dye loading (0.9 wt%), a further increase in the % 4-NA released (1.5%) was observed. While this increase in % 4-NA released seems moderate at best considering the tremendous change in temperature, this hydrogel was irradiated only for 10 seconds due to the rapid thermal deformation of the gel. As a comparison, it takes nearly 12 hours of bulk heating hydrogels made from **2** at 60 °C to achieve ~1.5% 4-NA release. These preliminary results suggest that rapid oxazine activation is possible in conjunction with photothermal heating of an encapsulated dye.

Future work should be done to fully characterize the small molecule release profile from **Croc**-doped films upon NIR laser irradiation. Submerging the films in an aqueous environment upon irradiation better mimics physiological conditions and should better dissipate the heat that is generated by the laser itself. Activation of 1,2-oxazines that would otherwise be inaccessible at physiological temperatures as well as those that release relevant therapeutics should be used to fully explore the capabilities of this potential drug delivery platform.

5.2 Effect of Oxazine Composition on Hydrogel Mechanical Properties

The mechanical properties of a hydrogel are greatly influenced by the type of bonding that holds the gel matrix together. *Chemically*-crosslinked hydrogels use covalent bonds to generate the hydrogel matrix and are generally mechanically very robust. The mechanical integrity of *physically*-crosslinked hydrogels relies on chain entanglements or secondary forces such as ionic, hydrogen-bonding or hydrophobic interactions.[6] Due to the weak, yet dynamic, interactions that sustain the network of this class of hydrogel, many display non-Newtonian characteristics such

as self-healing and shear-thinning capabilities. However, these hydrogels can also suffer from dilution upon injection into the body and subsequent dissipation.[7]

The polynorbornene-based triblock copolymers that have been examined thus far presumably rely on secondary interactions, such as hydrophobic interactions, to form the hydrogel network, as no cross-linker is present during hydrogel formation. However, further exploration of these hydrogels is necessary in order to understand whether modification of the oxazine moiety will alter the hydrogel properties in addition to any changes in the thermal activation of the oxazine moiety itself.

To probe whether oxazine N-substituents affect the mechanical properties of the hydrogels, triblock copolymer **3**, containing ethoxy-functionalized 1,2-oxazines, was synthesized. The swelling extent and material properties of the resulting hydrogel were qualitatively compared to hydrogels made from **2** with 4-nitroaniline pendant groups as well as a hydrogel made from **4,** which has pendant acetylsalicylic acid groups.

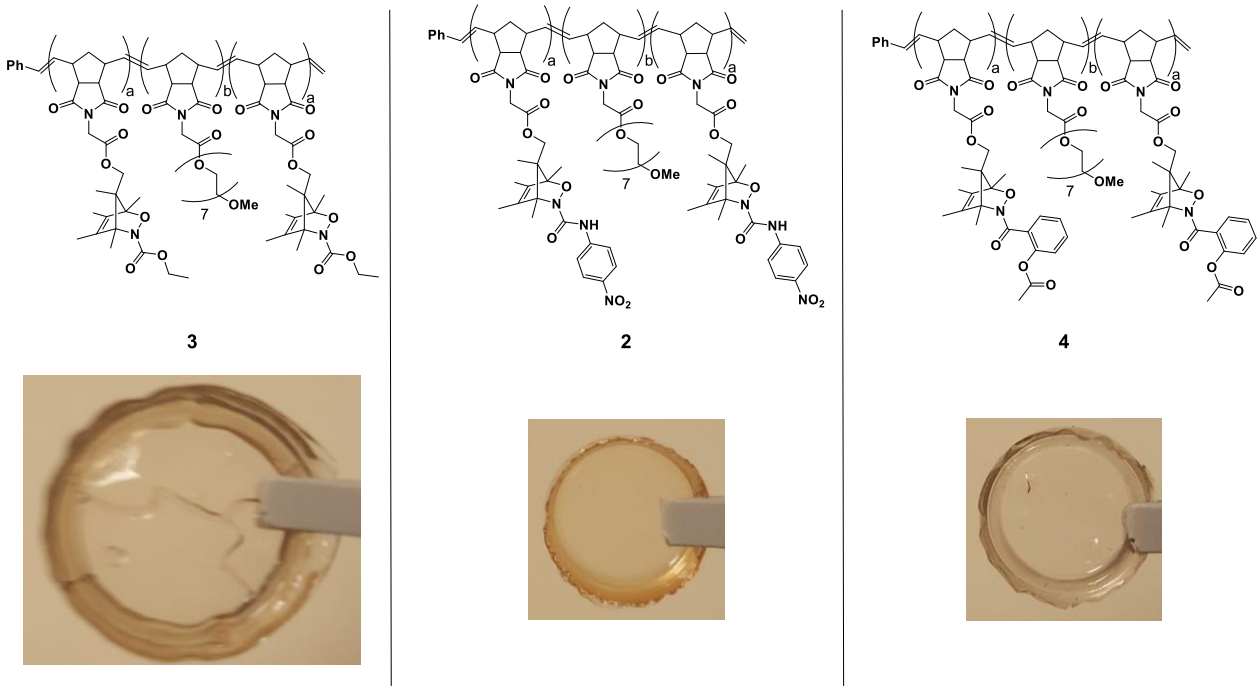

Figure 5.5. Hydrogels formed from triblock copolymers **2**, **3** and **4**. Tip of forceps can be used as an approximate scale bar.

Polymer **3** formed a 23 wt% hydrogel while polymers **2** and **4** absorbed less water and formed 54 wt% hydrogels. The high water content of hydrogels from **3** seems consistent with a loose gel matrix that easily expands upon absorption of water. Figure 5.5 qualitatively demonstrates the difference in sizes of the gels. Furthermore, hydrogels composed of **2** and **4** could be bent and twisted with no bulk failure of the gel while hydrogels composed of **3** were easily torn under identical motions. These results also suggest that the aromatic moieties in **2** and **4**, which are absent in polymer **3**, may play a key role in the tough mechanical properties of the hydrogels.

5.3 Conclusions and Outlook of 1,2-Oxazines for Thermal Functional Materials

Our research thus far demonstrates that 1,2-oxazines are versatile moieties when engineered into polymer constructs, with potential downfield applications ranging from thermally degradeable materials to drug delivery. Small molecule studies demonstrate that the DA/rDA equilibrium can be readily tuned by modifying the N-acyl substituent of the oxazine, suggesting that an impressive breadth of tunability can be achieved with these moieties for dynamic covalent materials.[8]

Depending on the N-acyl substituent used, a hydrolysis pathway of the resulting nitrosocarbonyl intermediate becomes prevalent, resulting in irreversible adduct dissociation and HNO release. We have demonstrated that this pathway can be utilized for controlled polymer degradation or as a sustained HNO and small molecule delivery platform under physiological conditions.

In order to continue pushing the potential of thermally responsive 1,2-oxazine functional materials, robust and cost-efficient polymer scaffolds are needed. In particular, polyurethanes (Scheme 5.3) may produce hydrogels with desirable mechanical properties and biocompatibility.[9] Additionally, extensive profiling of oxazine functionalization and its corresponding effects on the DA/rDA equilibrium is vital to realize the full scope of applications for this dynamic moiety.

Scheme 5.3. Proposed polymer synthesis for 1,2-oxazines in polyurethane-based scaffolds.

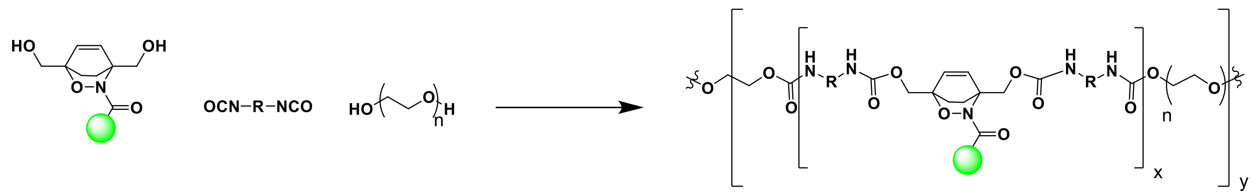

5.4 References

1) Beik, J.; Abed, Z.; Ghoreishi, F. S.; Hosseini-Nami, S.; Mehrzadi, S.; Shakeri-Zadeh, A.; Kamrava, S. K. *J. Control. Release* **2016**, *235*, 205.
2) Zhang, Y.; Ang, C. Y.; Zhao, Y. *Polym. J.* **2015**, *48*, 1.
3) Yuan, A.; Wu, J.; Tang, X.; Zhao, L.; Hu, Y. *J. Pharm. Sci.* **2013**, *102*, 6.
4) (a) Cheng, L.; He, W.; Gong, H.; Wang, C.; Chen, Q.; Cheng, Z.; Liu, Z. *Adv. Funct. Mater.* **2013**, *23* , 5893; (b) Jian, W. H.; Yu, T. W.; Chen, C. J.; Huang, W. C.; Chiu, H. C.; Chiang, W. H. *Langmuir* **2015**, *31*, 6202; (c) Li, M.; Teh, C.; Ang, C. Y.; Tan, S. Y.; Luo, Z.; Qu, Q.; Zhang, Y.; Korzh, V.; Zhao, Y. *Adv. Funct. Mater*. **2015**, *25*, 5602; (d) Zhang, Y.; Ang, C. Y.; Li, M.; Tan, S. Y.; Qu, Q.; Zhao, Y. *ACS Appl. Mater. Interfaces* **2016**, *8*, 6869.
5) (a) Spence, G. T.; Hartland, G. V.; Smith, B. D. *Chem. Sci.* **2013**, *4*, 4240; (b) Spence, G. T.; Lo, S. S.; Ke, C.; Destecroix, H.; Davis, A. P.; Hartland, G. V.; Smith, B. D. *Chem. - A Eur. J.* **2014**, *20*, 12628; (c) Guha, S.; Shaw, S. K.; Spence, G. T.; Roland, F. M.; Smith, B. D. *Langmuir* **2015**, *31*, 7826.
6) Hoffman, A. S. *Adv. Drug Deliv. Rev.* **2012**, *64*, 18.
7) Hoare, T. R.; Kohane, D. S. *Polymer* **2008**, *49*, 1993.
8) Kensy, V. K.; Peterson, G. I.; Church, D. C.; Yakelis, N. A.; Boydston, A. J. *Org. Biomol. Chem.* **2016**, 14, 5617.

9) Cherng, J. Y.; Hou, T. Y.; Shih, M. F.; Talsma, H.; Hennink, W. E. *Int. J. Pharm.* **2013**, *450*, 145.

5.5 EXPERIMENTAL

5.5.1 *General Considerations*

Dry THF, pyridine, and CH_2Cl_2 were obtained from a Glass Contour solvent purification system. All other reagents and solvents were used as obtained from commercial sources. Grubbs 3rd generation catalyst, $(iMesH_2)(C_5H_5N)_2(Cl)_2Ru{=}CHPH$, was synthesized according to literature procedure.[1] **S1**, **S3** and **S4** were synthesized as mentioned in chapter 2. **S2** and **2** were synthesized as mentioned in chapter 4. ^1H and ^{13}C NMR spectra were recorded on a Bruker AVance 300 or 500 MHz spectrometer. Chemical shifts are reported in delta (δ) units, expressed in parts per million (ppm) downfield from tetramethylsilane using the residual protio-solvent as an internal standard ($CDCl_3$, ^1H: 7.26 ppm and ^{13}C: 77.16 ppm; D_2O, ^1H: 4.79 ppm). GPC setup consists of: an Agilent 1260 Infinity II HPLC pump, three in-line MZ-Gel 10 μm size-exclusion columns (pore sizes = 10^3, 10^3, and 10^5 Å), miniDAWN-TREOS 3-angle multi-angle laser light scatter and OptiLab T-rEx refractive index detectors (each from Wyatt Technologies Corporation). The mobile phase consisted of THF. No calibration standards were used, and dn/dc values were obtained for each injection assuming 100% mass elution from the columns. UV-Vis experiments were conducted on an Agilent 8453 Diode Array UV-Vis Spectrophotometer.

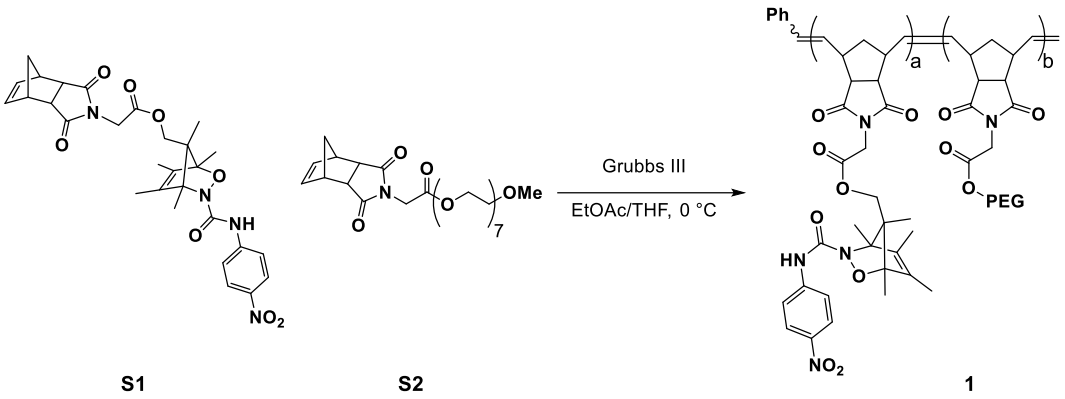

S1 **S2** **1**

5.5.2 *Synthesis of **1***

Into a flame-dried, N_2-purged round bottom flask were added monomer **S1** (150 mg, 0.26 mmol, 30 eq.), a magnetic stir bar, 8 mL of N_2-purged EtOAc, and 8 mL of N_2-purged THF. Once complete dissolution was achieved (judged visually), the solution was cooled to 0 °C in an ice bath and Grubbs 3rd generation catalyst (6.3 mg, 0.009 mmol, 1.0 eq.) in 0.7 mL of N_2-purged THF was quickly added. The reaction solution was then stirred for 40 min. Compound **S2** (147 mg, 0.26 mmol, 30 eq.) in 2 mL of N_2-purged EtOAc was added and the reaction mixture was stirred for an additional 40 min. Ethyl vinyl ether (6 mL) was then added to the reaction mixture and the resulting solution was stirred for 10 min. The solution volume was then concentrated under reduced pressure and then filtered through an alumina/Celite plug using CH_2Cl_2 as eluent. The solution was again concentrated under reduced pressure and precipitated into cold diethyl ether. The resulting ethereal solution was decanted away and the polymer residue was washed with diethyl ether, providing the desired product as a soft, tacky solid (180 mg, 61% yield). Mn = 38.1 kDa, Đ = 1.01. A 1 : 1.10 ratio of **S1** to **S2** in the polymer was confirmed by ^{1}H NMR spectroscopy. Average oxazine content per polymer chain is ~32. The oxazine content was determined by examining the relative ratio of –OMe peak at 3.37 ppm to the integration of the –

Me peak attached to the bridging carbon of the combined *anti* and *syn* oxazine isomers (δ = 1.07 and 0.77 ppm, respectively).

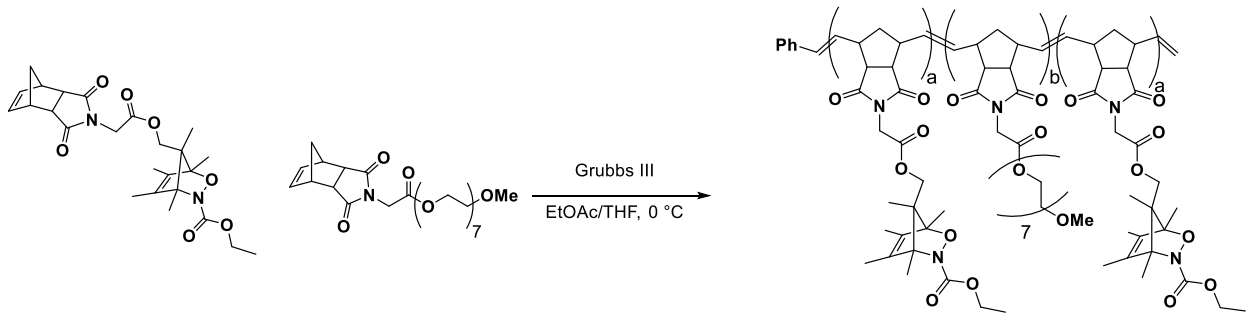

S3 **S2** **3**

5.5.3 *Synthesis of **3***

Into a flame-dried, N_2-purged round bottom flask were added monomer **S3** (120 mg, 0.51 mmol, 35 eq.), a magnetic stir bar, 20 mL of N_2-purged EtOAc, and 20 mL of N_2-purged THF. Once complete dissolution was achieved (judged visually), the solution was cooled to 0 °C in an ice bath and Grubbs 3rd generation catalyst (10.2 mg, 0.014 mmol, 1.0 eq.) in 0.7 mL of N_2-purged THF was quickly added. The reaction solution was then stirred for 40 min. Compound **S2** (565 mg, 1.02 mmol, 140 eq.) in 2 mL of N_2-purged EtOAc was added and the reaction mixture was stirred for an additional 40 min. Finally, **S3** (120 mg, 0.51 mmol, 35 eq.) in 2 mL of N_2-purged THF was added and the reaction mixture was stirred for an additional 40 min. Ethyl vinyl ether (6 mL) was then added to the reaction mixture and the resulting solution was stirred for 10 min. The solution volume was then concentrated under reduced pressure and then filtered through an alumina/Celite plug using CH_2Cl_2 as eluent. The solution was again concentrated under reduced pressure and precipitated into cold diethyl ether. The resulting ethereal solution was decanted away and the polymer residue was washed with diethyl ether, providing the desired product as a soft, tacky solid (400 mg, 50% yield). Mn = 87.0 kDa, Đ = 1.05. A 1 : 1.78 ratio of

S3 to **S2** in the polymer was confirmed by ^{1}H NMR spectroscopy. Average oxazine content per polymer chain is ~16.5. The oxazine content was determined by examining the relative ratio of –OMe peak at 3.37 ppm to the integration of the –Me peak attached to the bridging carbon of the combined *anti* and *syn* oxazine isomers (δ = 1.23 and 1.01 ppm, respectively).

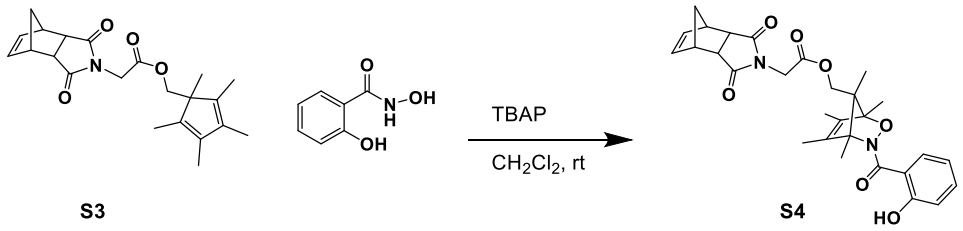

5.5.4 *Synthesis of **S5***

Into a round bottom flask, salicylhydroxamic acid (132 mg, 0.86 mmol, 1.2 eq.), **S3** (268 mg, 0.72 mmol, 1.0 eq.), CH_2Cl_2 (4 mL) and a magnetic stir bar were added. Tetrabutylammonium periodate (373 mg, 0.86 mmol, 1.2 eq.) was then added. The reaction was allowed to stir at room temperature for 3 hours. Ethyl acetate (10 mL) was added and the reaction mixture was washed with sat. sodium bisulfite (2 × 10 mL), sat. $NaHCO_3$ (1 × 10 mL0, 1 M HCl (1 × 10 mL) and diH_2O (1 × 10 mL). The organic layer was dried over Na_2SO_4, filtered through a thin pad of Celite, and concentrated under reduced pressure. Product was isolated via flash column chromatography (gradient 20 - 40% EtOAc/hexanes) as a mixture with an unknown impurity that co-eluted off column (293 mg recovered). No further purification was done.

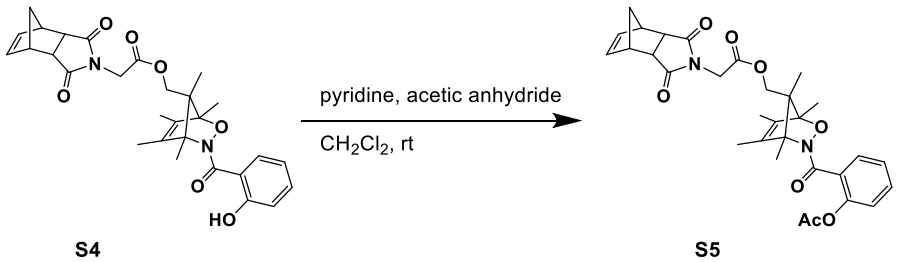

5.5.5 *Synthesis of **S6***

Into a round bottom flask, **S4** (186 mg, 0.86 mmol, 1.2 eq.), acetic anhydride (0.10 mL, 1.08 mmol, 3.0 eq.), pyridine (0.11 mL, 1.44 mmol, 4.0 eq.) and CH_2Cl_2 (0.5 mL) and a magnetic stir bar were added. The reaction was stirred at room temperature for 3 hours. Reaction mixture was concentrated under reduced pressure. Product was isolated via flash column chromatography (gradient 30% EtOAc/hexanes) as a white solid (109 mg, 54% yield). ^{1}H NMR (500 MHz, $CDCl_3$) δ 7.40 (dd, J = 13.6, 7.6 Hz, 2H), 7.19 (t, J = 7.1 Hz, 1H), 7.15 – 6.98 (m, 1H), 6.31 (s, 2H), 4.55 – 4.18 (m, 3H), 3.90 (s, 1H), 3.32 (s, 2H), 2.76 (s, 2H), 2.38 – 2.20 (m, 3H), 1.94 – 1.40 (m, 14H), 1.11 (s, 2H), 0.78 (s, 1H).

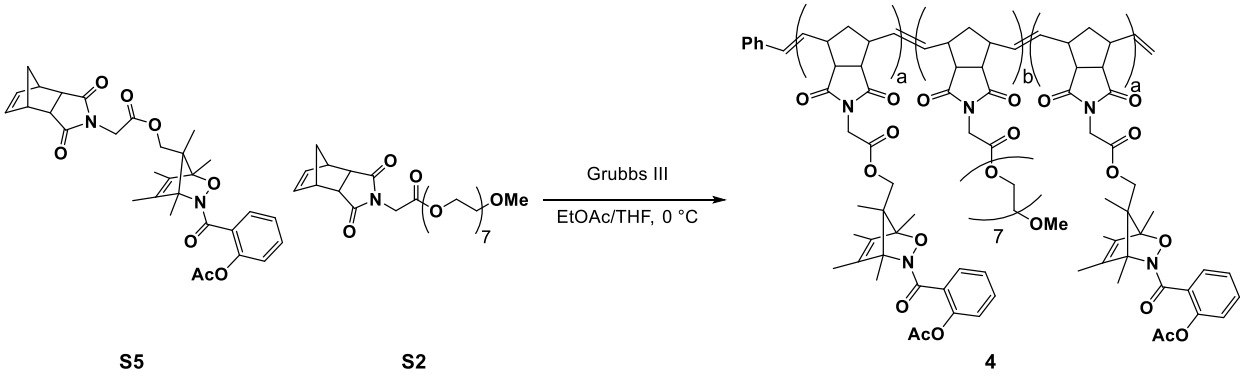

S5 **S2** **4**

5.5.6 *Synthesis of **4***

Into a flame-dried, N_2-purged round bottom flask were added monomer **S5** (54 mg, 0.19 mmol, 33 eq.), a magnetic stir bar, 9 mL of N_2-purged EtOAc, and 9 mL of N_2-purged THF. Once complete dissolution was achieved (judged visually), the solution was cooled to 0 °C in an ice bath and Grubbs 3rd generation catalyst (4.1 mg, 0.0057 mmol, 1.0 eq.) in 0.7 mL of N_2-purged THF was quickly added. The reaction solution was then stirred for 40 min. Compound **S2** (210 mg, 1.02 mmol, 130 eq.) in 1 mL of N_2-purged EtOAc was added and the reaction mixture was stirred for an additional 40 min. Finally, **S5** (54 mg, 0.19 mmol, 33 eq.) in 1 mL of N_2-

purged THF was added and the reaction mixture was stirred for an additional 40 min. Ethyl vinyl ether (6 mL) was then added to the reaction mixture and the resulting solution was stirred for 10 min. The solution volume was then concentrated under reduced pressure and then filtered through an alumina/Celite plug using CH_2Cl_2 as eluent. The solution was again concentrated under reduced pressure and precipitated into cold diethyl ether. The resulting ethereal solution was decanted away and the polymer residue was washed with diethyl ether, providing the desired product as a soft, tacky solid (130 mg, 41% yield). Mn = 60.0 kDa, Đ = 1.05. A 1 : 2.25 ratio of **S5** to **S2** in the polymer was confirmed by ^{1}H NMR spectroscopy. Average oxazine content per polymer chain is ~16.5. The oxazine content was determined by examining the relative ratio of –OMe peak at 3.36 ppm to the integration of the –Me peak attached to the bridging carbon of the combined *anti* and *syn* oxazine isomers (δ = 1.08 and 0.75 ppm, respectively).

5.5.7 *General Procedure for Preparation of **Croc**-doped Micelles from **1***

From a 4 mg/mL stock solution of polymer **1** in DMF and a 92 µg/mL solution of **Croc** dye in DMF, 1 mL and 0.5 mL respectively were combined with 3.5 mL of pure DMF. The solution was then transferred to a 25 mm x 16 mm Fisher Scientific seamless cellulose dialysis tubing (12,000 – 16,000 MWCO) and sealed. Polymer solution was dialyzed against 300 mL 0.5 mM phosphate buffered H_2O for 18 hours at 4 °C three times.

5.5.8 *General Procedure for Preparation of **Croc**-doped Hydrogels from **2***

From a 400 mg/mL stock solution of polymer **4** in THF, 0.17 mL was added to a tared 2 mL GC vial. Appropriate volume from 1 mg/mL stock solution of **Croc** dye in THF was then added. The solvent was then evaporated under steady flow of N_2 over 18 h. Then, the dry mass of the polymer film was recorded. Phosphate buffered water (1 mL, 10 mM, pH 7.4) was then added to

the film. After 24 h, the vials were carefully broken to allow for removal of the films. The films were then submerged in 1 mL of fresh phosphate buffered water for an additional 24 h. The hydrated mass of the films were then recorded. Then, 8-mm disks were cut out from the films for rheology and 4-nitroaniline release studies.

5.5.9 *General Procedure for Laser Irradiation of **Croc**-doped Hydrogels*

An 8 mm disc of **Croc**-doped hydrogel from **2** was placed on top of a thermocouple. Each disc was irradiated from above with an 808 nm laser at 1.72 W/cm^2 for 60 s. The temperature was recorded upon stabilization. After irradiation, the gels were soaked in 3 mL of 10 mM phosphate buffered water for 1 hour. The solution was analyzed by UV-vis. The % of total 4-NA released was determined using the theoretical max of 4-NA from *entire* hydrogel sample (not irradiated area).

5.5.10 *General Procedure for Preparation of Hydrogels from **2**, **3**, and **4***

From a 400 mg/mL stock solution of desired polymer in THF, 0.17 mL was added to a tared 2 mL GC vial. The solvent was then evaporated under steady flow of N_2 over 18 h. Then, the dry mass of the polymer film was recorded. Phosphate buffered water (1 mL, 10 mM, pH 7.4) was then added to the film. After 24 h, the vials were carefully broken to allow for removal of the films. The films were then submerged in 1 mL of fresh phosphate buffered water for an additional 24 h. The hydrated mass of the films were then recorded. Then, 8-mm disks were cut out from the films for rheology and 4-nitroaniline release studies.

5.5.11 *NMR Spectra*

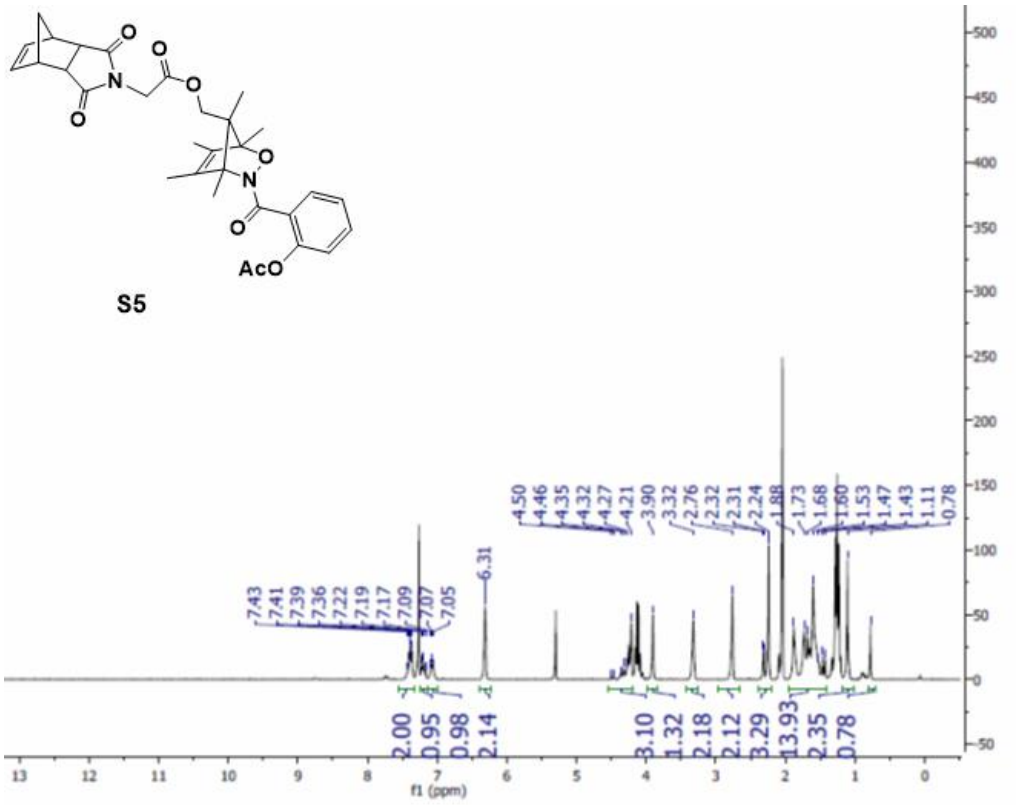

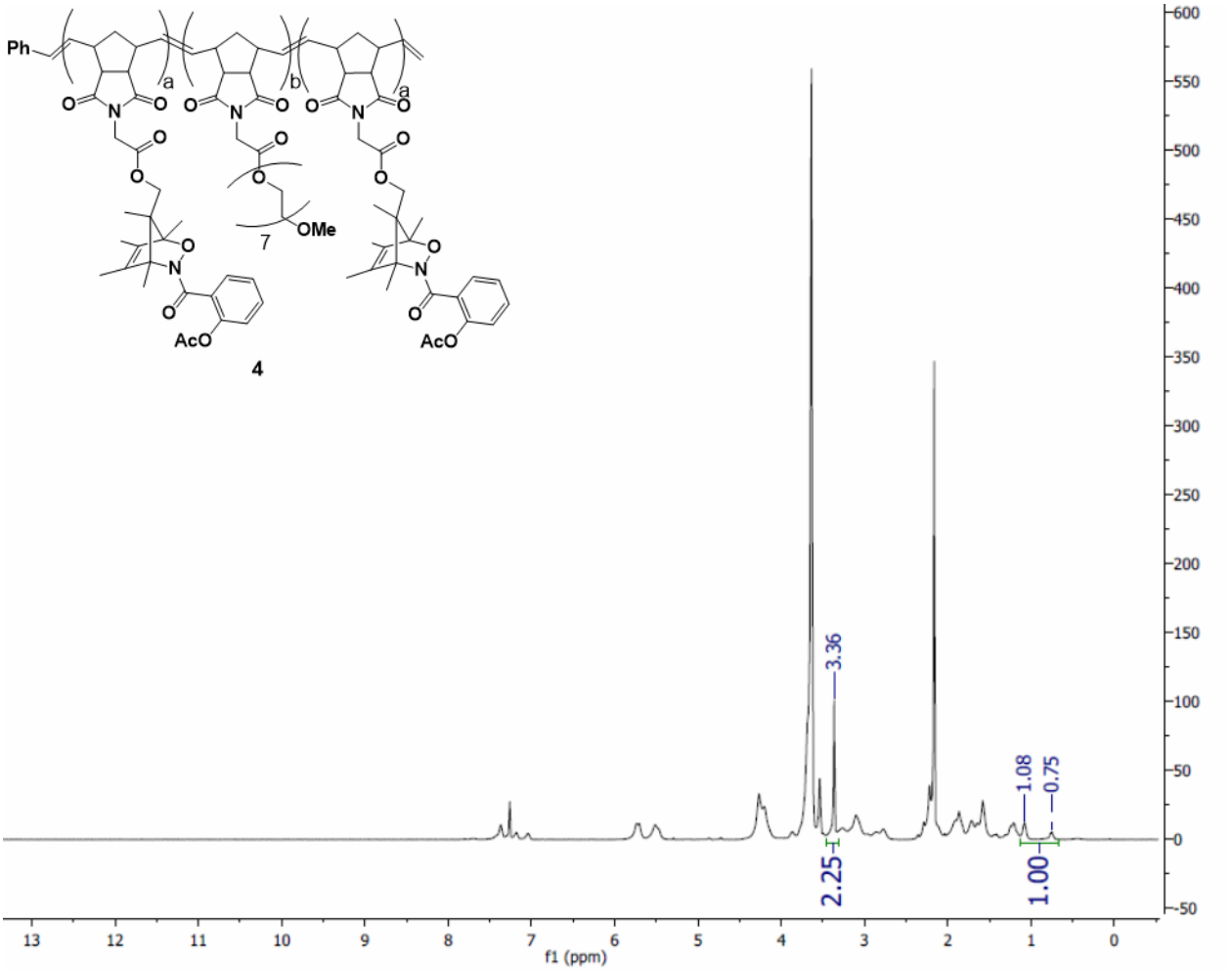
Ph
a
b
a
7
OMe
AcO
AcO
4
3.36
1.08
0.75
2.25
1.00
f1 (ppm)

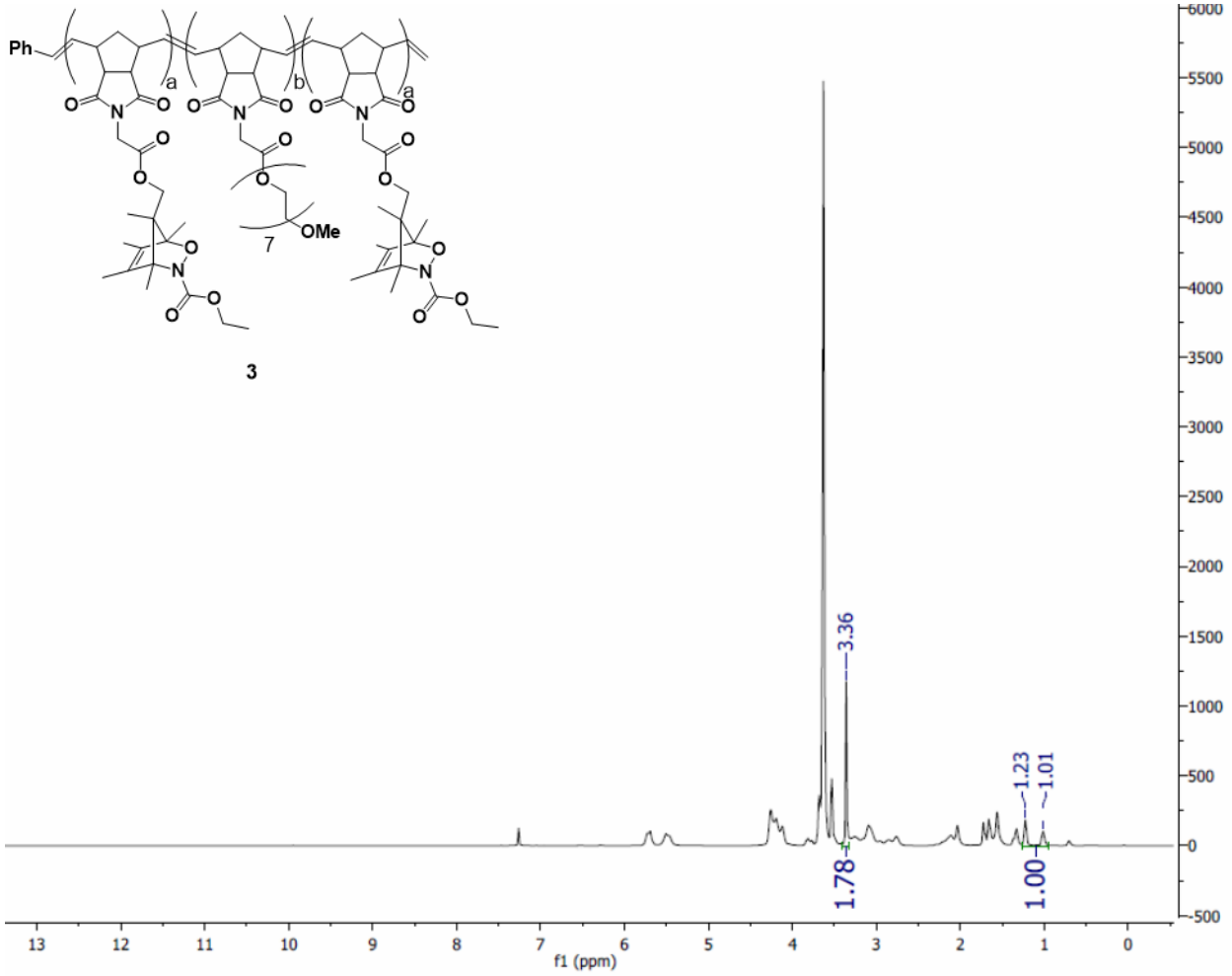
Ph
a
b
a
7
OMe
3
3.36
1.23
1.01
1.78
1.00
f1 (ppm)

Chapter 6. COMPARISON OF MECHANOCHEMICAL CHAIN SCISSION RATES FOR LINEAR VERSUS THREE-ARM STAR POLYMERS IN STRONG ACOUSTIC FIELDS

6.1 INTRODUCTION

Mechanochemistry involves transduction of mechanical input into chemical output by coupling force vectors with productive geometric distortions of functional groups.[1] Polymer mechanochemistry, specifically, uses macromolecular scaffolds to direct and distribute mechanical forces as a function of shape and composition of the polymer framework.[2,3] Perhaps the simplest chemical output that can arise from tensile forces within a polymer main chain is bond scission leading to fragmentation of the polymer. Understanding mechanochemical chain scission has important implications for multiple disciplines, considering that a number of physicochemical properties depend upon polymer molecular weight.

Studies focusing on the influence of polymer structure on mechanochemical reactivity have unveiled key correlations.[4-7] One of the most basic tenets for linear polymers in elongational flow fields is a linear relationship between chain scission rate and molecular weight.[8] Variations in polymer shape, however, give rise to changes in molecular weight distribution, which in turn can influence scission rates. For example, star polymers display an enhanced shear stability in comparison with linear polymer analogues of the same total molecular weight (M_{total}).[5,9] This effect is ascribed to the star polymers having a lower effective molecular weight that is roughly

equivalent to two of the arms. This spanning region has a molecular weight (M_{span}) that is much lower than the M_{total}, thus the slower rate of chain scission.[5c]

One of the challenges to determining rate constants for specific chain scission events is that daughter fragments typically have molecular weights greater than the limiting molecular weight (M_{lim}) for chain scission. Therefore, commonly employed analyses of changes in ensemble averages for a polymer sample, such as molecular weight or viscosity, are not explicitly linked to chain scission in a single species (Scheme 6.1). For example, Striegel and coworkers have studied ultrasound-induced chain scission in a series of star polymers and observed an apparent *increase* in observed rate constant upon prolonged sonication.[5c] This was explained by an increase in the number of polymer species present that were above M_{lim} as the star polymer shed arms, and an inability to distinguish between the reacting species when monitoring the average molecular weight of the mixture. Herein, we describe a quantitative assessment of rate constants for mechanochemical chain scission in complementary series of star and linear polymers, and resolution of scission events between parent and daughter species.

Scheme 6.1. Generalized depiction of chain scission sequences in parent star and daughter species.

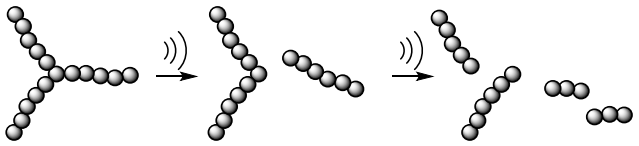

6.2 Results and Discussion

To begin, we synthesized a series of well-defined linear and three-arm polymer counterparts as depicted in Figure 6.1. The linear analogues were designed to represent the "two-arm" daughter fragments resulting from hypothetical single arm cleavage of the corresponding three-arm star polymer. Observed trends were found to be independent of either planar or tetrahedral core geometries (vide infra). We used a "core-first" approach and atom-transfer radical polymerization to produce a series of polymers each with narrow polydispersity index (PDI).[10] Kinetic analyses were conducted using the method described by Florea.[11] This method involves following the RI signal intensity of a single section of the insipient portion of the gel-permeation chromatogram over the course of the sonication experiment. This approach more effectively distinguishes initial chain scission from scission of daughter fragments than the average molecular weight analysis developed by Malhotra and used by Striegel.[5c,12] A caveat of the Florea method, however, is that adequate resolution of polymer species by GPC must be achieved.

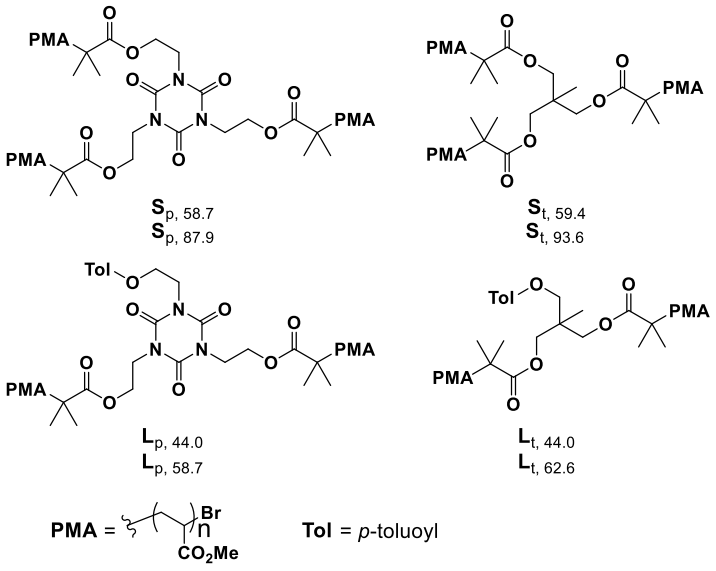

Figure 6.1. Structures of star and linear polymers used in this study. Subscripts indicate core geometry (planar or tetrahedral) and M_n values. All PDIs were found to be < 1.1

Each linear and star polymer was subjected to sonication in DMF and aliquots were analyzed by GPC over time. As a representative example, GPC traces of $\mathbf{S}_{t,59.4}$ are depicted in Figure 6.2 (top). The peak maximum (P_{max}) retention time before sonication was found to be 20.4 min (indicated by the dashed red line). Monitoring the RI signal intensity at that retention time over the course of the sonication experiment provided a first-order rate constant (k_{RI}) for the consumption of the polymer species with a molecular weight of M_p. The P_{max} for each initial polymer remained consistent throughout the set of three runs, indicating to us that column drift was not significant.[13]

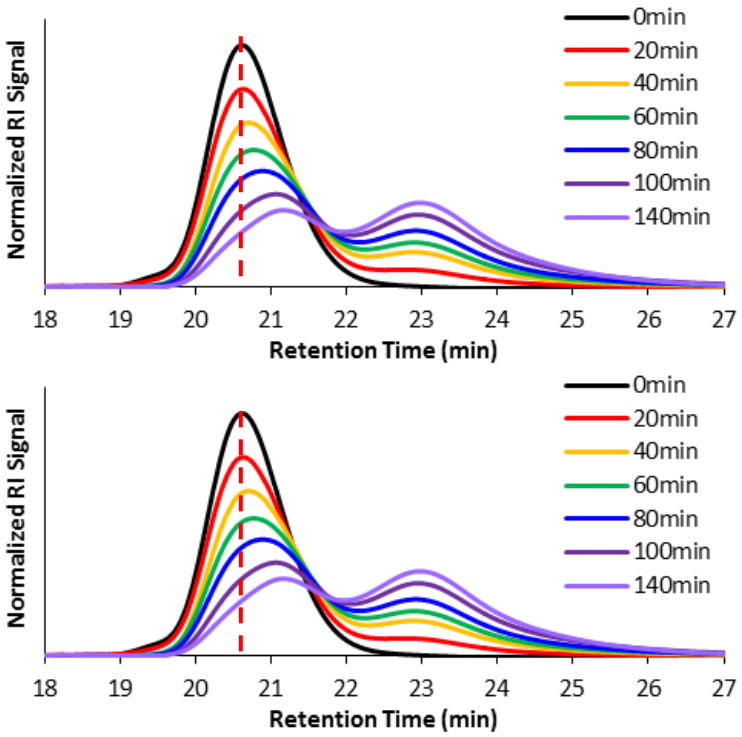

Figure 6.2. (top) GPC traces of $\mathbf{S}_{t,59.4}$ during ultrasonication. Sonication conditions: polymer concentration of 5 mg/mL in DMF, 13.8 W/cm^2, duty cycle of 1 s on 9 s off, N_2 atmosphere, 4 °C monitored internally. (bottom) Resolved GPC traces from nonlinear regression analysis of the chromatograms in the top plot. Dashed red lines indicate the retention time at which RI signal intensity was recorded for kinetic analyses.

Applying the same sonication conditions and analyses to each of the polymers in the series provided k_{RI} values as listed in Table 6.1. The trends are consistent with those observed by Striegel in which the M_{arm}, as opposed to M_{total}, of the polymer dictates the rate of chain scission.[5c] While two sequential chain scission events are operative in the mechanochemical degradation of three-arm star polymers, k_{RI} for consumption of each star polymer closely matches that of the corresponding linear counterpart of equal M_{arm}. For polymers with M_{arm} of ca. 20 kDa, k_{RI} were all similar, ranging from 1.02 to 1.26 × 10^{-2} min^{-1}. Moreover, the differences in

k_{RI} correlated well with the slight differences in M_{arm}. The same general trend was observed from the polymers bearing ~30 kDa arms, with k_{RI} clustered between 2.38 and 2.66 × 10^{-2} min^{-1}. Notably, an increase in *linear* polymer M_{total} from $\mathbf{L}_{t,44.0}$ to $\mathbf{L}_{t,62.6}$ resulted in an approximately doubled value of k_{RI}. In contrast, increasing M_{total} via a branch point to form a star polymer (cf. $\mathbf{L}_{t,44.0}$ versus $\mathbf{S}_{t,59.4}$) actually resulted in a slight reduction in k_{RI}, consistent with the reduction in M_{arm}.

Table 6.1. Summary of k_{RI} for mechanochemical chain scission of three-arm star and linear polymers.[a]

Polymer	M_{total} (kDa)	M_{arm} (kDa)	k_{RI} (× 10^{-2} min^{-1})
$\mathbf{S}_{p,58.7}$	58.7	19.6	1.02 ± 0.02
$\mathbf{S}_{t,59.4}$	59.4	19.8	1.10 ± 0.02
$\mathbf{L}_{p,44.0}$	44.0	22.0	1.26 ± 0.03
$\mathbf{L}_{t,44.0}$	44.0	22.0	1.25 ± 0.08
$\mathbf{S}_{p,87.9}$	87.9	29.3	2.44 ± 0.17
$\mathbf{L}_{p,58.7}$	58.7	29.3	2.38 ± 0.12
$\mathbf{S}_{t,93.6}$	93.6	31.2	2.66 ± 0.14
$\mathbf{L}_{t,62.6}$	62.6	31.3	2.63 ± 0.06

[a]M_{total} (M_n values) determined by GPC analysis using multi-angle laser light scattering (MALS) to give M_w values from which M_n values were calculated. M_{arm} were assumed to be one-third M_{total} for stars, and one-half *M*total for linear polymers. Rate constants were calculated from linear regression of the Ln(RI signal intensity) at the P_{max} retention time of the virgin sample versus ultrasonication "on time" and are an average of three runs ± one standard deviation.

A nonlinear regression analysis was used to resolve each GPC trace, which verified that the daughter fragments were not significantly contributing to the peak height at the retention time

used for determining k_{RI} (Figure 6.2, bottom). Using the resolved peaks, we calculated rate constants for scission of the initial polymer based upon the resolved initial P_{max} retention time RI intensity (k_{res}), and total peak area (k_{area}) for that species. We found k_{RI} to be in good agreement with k_{res} and k_{area} for each polymer.[13]

To investigate site-selective mechanophore activation as a function of polymer shape, we also prepared and analyzed a linear ($\mathbf{L}_{DA,61.6}$) and star polymer ($\mathbf{S}_{DA,85.9}$) pair that each contained an anthracene-maleimide Diels-Alder adduct mechanophore (Figure 6.3). Importantly, the average M_{arm} was similar in each polymer. The mechanophore, which has been extensively studied by Bielawski and coworkers, is capable of mechanochemical UV-vis and photoluminescence (PL) "turn-on" response upon mechanically-facilitated cycloreversion to generate an anthracene moiety.[14]

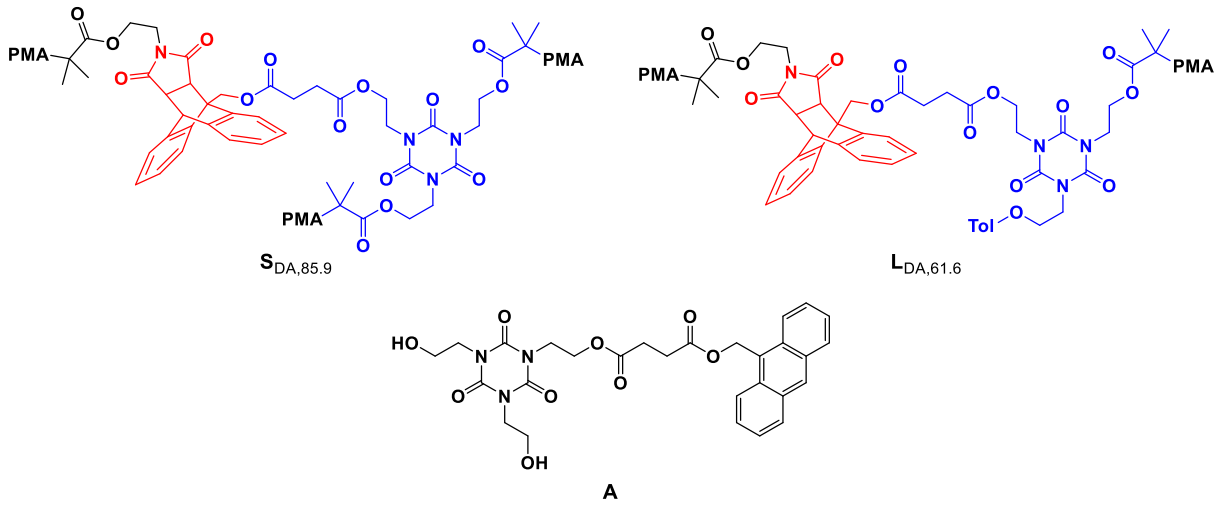

Figure 6.3. Mechanophore-containing star ($\mathbf{S}_{DA,85.9}$) and linear ($\mathbf{L}_{DA,61.6}$) polymers, and PL control compound **A**. Mechanophore is highlighted in red, core is highlighted in blue.

After subjecting $\mathbf{L}_{DA,61.6}$ and $\mathbf{S}_{DA,85.9}$ each to sonication as described above, the formation of anthracene was confirmed by UV-vis (Figure 6.4A) and photoluminescence (PL) spectroscopies (Figure 6.4B). Although the UV-vis spectra were consistent with formation of anthracene, control experiments revealed increases in solution optical density upon sonication of PMA (absent mechanophore). Although background corrections could be made, the optical density was dependent upon the extent of chain scission, which occurred at different rates and via different mechanisms for unfunctionalized PMA versus mechanophore-containing polymers (vide infra). PL experiments, however, confirmed consistent emission intensity over 60 min of sonication time (Figure 6.4C) for an anthracene-containing control (**A**) sonicated in the presence of $\mathbf{L}_{P,58.7}$. This confirmed the stability of anthracene to sonication, and circumvents issues with increased optical density upon sonication of polymer solutions. Additionally, we observed a linear correlation between PL intensity and concentration of **A** over the concentration range relevant to our kinetic studies. (Figure 6.4D).

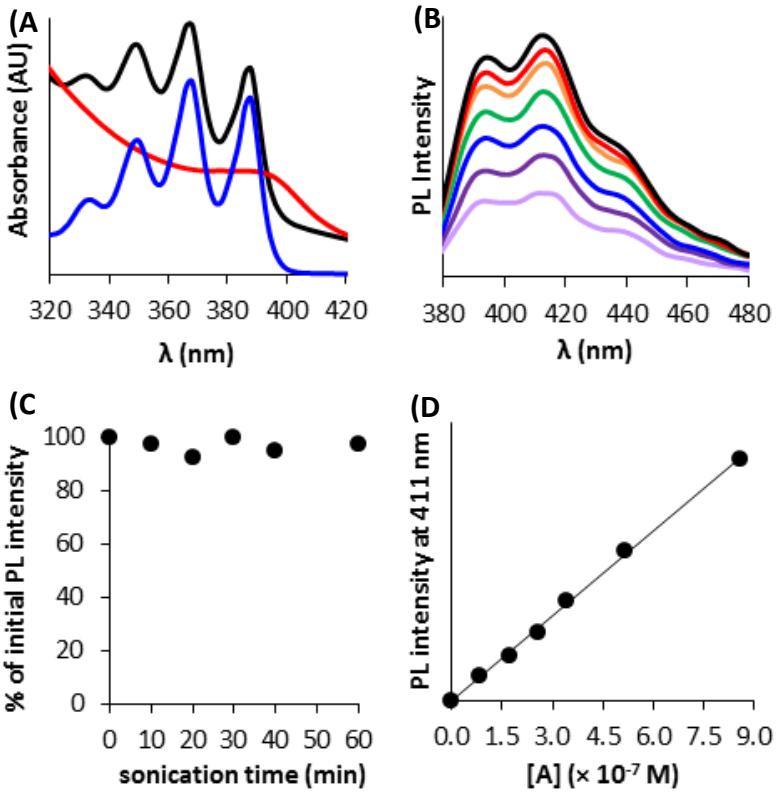

Figure 6.4. (A) UV-vis spectra in DMF of $\mathbf{S}_{DA,85.9}$ before (red) and after (black) sonication, and a small molecule control (blue);[13] (B) PL spectra in DMF of $\mathbf{L}_{DA,61.6}$ upon increasing sonication time (10 – 40 min, 5-min increments bottom-to-top); (C) % of initial PL intensity with increasing sonication time of a mixture of $\mathbf{L}_{p,58.7}$ and **A** in DMF; (D) PL intensity versus concentration of **A** in the presence of $\mathbf{L}_{p,58.7}$ ($R^2 = 0.9981$).

Monitoring the consumption of initial polymer via GPC-RI, and production of anthracene via PL spectroscopy (to give k_{PL}), provided corroborating data for consistent chain scission rate constants between the two polymer structures. As in the previous series, we found k_{RI} for the linear and star analogues to be very similar, consistent with their similar M_{arm} values (Table 6.2). Additionally, the k_{PL} values for each polymer were also similar to one another, and to the k_{RI}

values. The similarity between the k_{RI} and k_{PL} values are consistent with high selectivity for initial chain scission occurring at the mechanophore.

Table 6.2. Rate constants for mechanochemical chain scission for $\mathbf{S}_{DA,85.9}$ and $\mathbf{L}_{DA,61.6}$.[a]

Polymer	M_{total} (kDa)	M_{arm} (kDa)	k_{RI} ($\times 10^{-2}$ min^{-1})	k_{PL} ($\times 10^{-2}$ min^{-1})
$\mathbf{S}_{DA,85.9}$	85.9	28.6	3.13 ± 0.11	3.20 ± 0.14
$\mathbf{L}_{DA,61.6}$	61.6	30.8	3.27 ± 0.38	3.26 ± 0.09

[a]M_{total}, M_{arm}, and k_{RI} were determined as described above. Rate constants via PL (k_{PL}) were calculated from linear regression of the Ln(PL intensity at 411 nm) versus ultrasonication "on time". Rate constants are an average of three runs ± one standard deviation.

The inclusion of the mechanophore resulted in a discernable increase in k_{RI}, (cf. Tables 6.1 and 6.2). Specifically, polymers with M_{arm} values near 30 kDa clearly had k_{RI} values less than those observed from the mechanophore-containing polymers. To our knowledge, direct comparisons of rate constants for this mechanophore versus PMA homopolymers have not been reported. However, the relative increase in rate constant upon inclusion of the mechanophore in these studies is consistent with those reported by Moore and coworkers for investigation of cyclobutane-based mechanophores.[8b]

6.3 Conclusion

In summary, we report precise investigations of mechanochemical chain scission rates in linear and three-arm star polymers. Our results are consistent with previous chain scission

models in which the scission rate is governed by the length of any two arms emanating from the core. By resolving daughter fragments from the analysis and incorporating a fluorogenic "turn-on" mechanophore, we have provided kinetic analysis for specific scission events. These results provide quantitative guidelines for augmenting the mechanochemical reaction rates of macromolecules through control of the overall polymer architecture. Importantly, we observed nearly identical rate constants for activation of a mechanophore incorporated into structurally varied polymers of significantly different molecular weights.

6.4 References

1) For select reviews, see: a) Seidel, C. A. M.; Kuhnemuth, R. *Nat. Nanotechnol.* **2014**, *9*, 164. b) Cravotto, G.; Gaudino, E. C.; Cintas, P. *Chem. Soc. Rev.* **2013**, *42*, 7521. c) Sepelak, V.; Duvel, A.; Wilkening, M.; Becker, K.-D.; Heitjans, P. *Chem. Soc. Rev.* **2013**, *42*, 7507. d) Wang, G.-W. *Chem. Soc. Rev.* **2013**, *42*, 7668. e) Gilman, J. J. *Science* **1996**, *274*, 65.

2) For recent reviews, see: a) Brantley, J. N.; Bailey, C. B.; Wiggins, K. M.; Keatinge-Clay, A. T.; Bielawski, C. W. *Polym Chem.* **2013**, *4*, 3916. b) May, P. A.; Moore, J. S. *Chem. Soc. Rev.* **2013**, *42*, 7497. c) Wiggins, K. M.; Brantley, J. N.; Bielawski, C. W. *Chem. Soc. Rev.* **2013**, *42*, 7130. d) Groote, R.; Jakobs, R. T. M.; Sijbesma, R. P. *Polym. Chem.* **2013**, *4*, 4846. e) Brantley, J. N.; Wiggins, K. M.; Bielawski, C. W. *Polym. Int.* **2013**, *62*, 2. f) Ariga, K.; Mori, T.; Hill, J. P. *Adv. Mater.* **2012**, *24*, 158. g) Boulatov, R. *Pure Appl. Chem.* **2011**, *83*, 25. h) Caruso, M. M.; Davis, D. A.; Shen, Q.; Odom, S. A.; Sottos, N. R.; White, S. R.; Moore, J. S. *Chem. Rev.* **2009**, *109*, 5755. i) Beyer, M. K.; Clausen-Schaumann, H. *Chem. Rev.* **2005**, *105*, 2921.

3) For recent examples, see: a) Diesendruck, C. E.; Peterson, G. I.; Kulik, H. J.; Kaitz, J. A.; Mar, B. D.; May, P. A.; White, S. R.; Martinez, T. J.; Boydston, A. J.; Moore, J. S. *Nat. Chem.* **2014**, *DOI: 10.1038/nchem.1938*. b) Brantley, J. N.; Bailey, C. B.; Cannon, J. R.; Clark, K. A.; Vanden Bout, D. A.; Bodbelt, J. S.; Keatinge-Clay, A. T.; Bielawski, C. W. *Angew. Chem. Int. Ed.* **2014**, *DOI: 10.1002/anie.201306988.* c) Lee, C. K.; Diesendruck, C. E.; Lu, E.; Pickett, A. N.; May, P. A.; Moore, J. S.; Braun, P. V. *Macromolecules*, **2014**, *DOI: 10.1021/ma500195h*. d) Grady, M. E.; Beiermann, B. A.; Moore, J. S.; Sottos, N. R *ACS Appl. Mater. Inter.* **2014**, *DOI: 10.1021/am406028q.* e) Larsen, M. B.; Boydston, A. J. *J. Am. Chem. Soc.* **2014**, *136*, 1276. f) Gossweiler, G. R.; Hewage, G. B.; Soriano, G.; Wang, Q.; Welshofer, G. W.; Zhao, X.; Craig, S. L. *ACS Macro Lett.* **2014**, *3*, 216. g) Beiermann, B. A.; Kramer, S. L. B.; May, P. A.; Moore, J. S.; White, S. R. and Sottos, N. R *Adv. Funct. Mater.* **2014**, *24*, 1529. h) Chen, Y.; Zhang, H.; Fang, X.; Lin, Y.; Xu, Y.; Weng, W. *ACS Macro Lett.* **2014**, *3*, 141.

4) For selected examples of linear polymers, see: a) Klukovich, H. M.; Kouznetsova, T. B.; Kean, Z. S.; Lenhardt, J. M.; Craig, S. L. *Nat. Chem*. **2013**, *5*, 110. b) Berkowski, K. L. Potisek, S. L.; Hickenboth, C. R; Moore, J. S. *Macromolecule*s **2005**, *38*, 8975. c) Odell, J. A.; Keller, A. *J. Polym. Sci., Polym. Phys.* **1986**, *24*, 1889. d) Encina, M. V.; Lissi, E.; Sarasua, M.; Gargallo, L.; Radic, D. *J. Polym. Sci., Polym. Lett. Ed.* **1980**, *18*, 757. e) Schmid, G.; Rommel, O.; Z. *Physikal. Chem.* **1939**, *185*, 97.

5) For star polymers, see: a) Duan, M.; Fang, S.; Zhang, L.; Wang, F.; Zhang, P.; Zhang, J. *e-Polymers* **2011**, *11*, 1618. b) Xue, L.; Agarwal, U. S.; Lemstra, P. J. *Macromolecules* **2005**, *38*, 8825. c) Striegel, A. M.; *J. Biochem. Biophys. Methods* **2003**, *56*, 117. d) Kim, O. K.; Little, R. C.; Patterson, R. L.; Ting, R. Y. *Nature* **1974**, *250*, 408.

6) For selected examples of brush/graft polymers, see: a) Li, Y.; Nese, A.; Lebedeva, N. V.; Davis, T.; Matyjaszewski, K.; Sheiko, S. S. *J. Am. Chem. Soc.* **2011**, *133*, 17479. b) Sheiko, S. S.; Sun, F. C.; Randall, A.; Shirvanyants, D.; Rubinstein, M.; Lee, H-i.; Matyjaszewski, K. *Nature* **2006**, *440*, 191. c) Agarwal, U. S.; Mashelkar, R. A. *J. Non-Newtonian Fluid. Mech.* **1994**, *54*, 1.

7) For selected examples of mechanochemistry in cross-linked networks, see: a) Larsen, M. B.; Boydston, A. J. *J. Am. Chem. Soc.* **2013**, *135*, 8189. b) Klukovich, H. M.; Kouznetsova, T. B.; Kean, Z. S.; Lenhardt, J. M.; Craig, S. L. *Nat. Chem.* **2013**, *5*, 110. c) Baytekin, H.T.; Baytekin, B.; Grzybowski, B. A. *Angew. Chem. Int. Ed.* **2012**, *51*, 3596. d) Kingsbury, C. M.; May, P. A.; Davis, D. A.; White, S. R.; Moore, J. S.; Sottos, N. R. J. *Mater. Chem.* **2011**, *21*, 8381.

8) a) Vijayalakshmi, S. P.; Madras, G. *Polym. Degrad. Stab.* **2005**, *90*, 116. b) Kryger, M. J.; Munaretto, A. M.; Moore, J. S. *J. Am. Chem. Soc.* **2011**, *133*, 18992. c) Basedow, A. M.; Ebert, K. H. *Adv. Poly. Sci.* **1977**, *22*, 83. d) Jellinek, H. H. G. *J. Polymer Sci.* **1959**, *37*, 485.

9) a) Marsalko, T. M.; Majoros, I.; Kennedy, J. P. *J. Macromol. Sci., Pure Appl. Chem.* **1997**, *34*, 775. b) Covitch, M. J. *Society of Automotive Engineers, Special Publication* **1998**, *1390*, 14.

10) Matyjaszewski, K.; Xia, J. *Chem. Rev.* **2001**, *101*, 2921.

11) Florea, M. *J. Appl. Polym. Sci.* **1993**, *50*, 2039.

12) Malhotra, S. L. J. Macromol. Sci., Part A 1986, 23, 729. b) Malhotra, S. L. *J. Macromol. Sci., Part A* **1982**, *18*, 1055.

13) See supporting information.

14) a) Konda, S. S. M.; Brantley, J. N.; Varghese, B. T.; Wiggins, K. M.; Bielawski, C. W.; Makarov, D. E. *J. Am. Chem. Soc.* **2013**, *135*, 12722. b) Wiggins, K. M.; Syrett, J. A.; Haddleton, D. M.; Bielawski, C. W. *J. Am. Chem. Soc.* **2011**, *133*, 7180.

6.5 EXPERIMENTAL

6.5.1 *General Considerations*

Dry DMF, pyridine, and CH_2Cl_2 were obtained from a Glass Contour solvent purification system. Et_3N and methyl acrylate were distilled under N_2 after drying over CaH_2 overnight. All other reagents and solvents were used as obtained from commercial sources. Compound **1** was prepared according to literature procedure. ^1H and ^{13}C NMR spectra were recorded on a Bruker AVance 300 or 500 MHz spectrometer. Chemical shifts are reported in delta (δ) units, expressed in parts per million (ppm) downfield from tetramethylsilane using the residual protio-solvent as an internal standard ($CDCl_3$, ^1H: 7.26 ppm and ^{13}C: 77.2 ppm; CD_3CN, ^1H: 1.94 ppm and ^{13}C: 118.3 ppm). LRMS was performed on a Bruker Esquire equipped with either an electrospray ionization (ESI) or IonSense SVP100 DART source. GPC setup consists of: a Shimadzu pump, three in-line MZ-Gel 10 μm size-exclusion columns (10^3, 10^3, and 10^5 Å), DAWN-HELEOS II 18-angle multi-angle laser light scatter and OptiLab T-rEx refractive index detectors (each from Wyatt Technologies Corporation), and an Agilent Technologies UV-vis detector. The mobile phase consisted of 0.01 M LiBr in DMF. No calibration standards were used, and dn/dc values were obtained for each injection assuming 100% mass elution from the columns. Sonication experiments were done using a 20 kHz Sonics VSX series sonication probe (1.2 cm tip diameter) calibrated according to literature procedures.[1] Fluorescence spectroscopy was conducted using a

Perkin Elmer Luminescence Spectrometer LS 50 B. UV-vis spectra were recorded on a Varian Cary 500 scan UV-Vis-NIR Spectrophotometer.

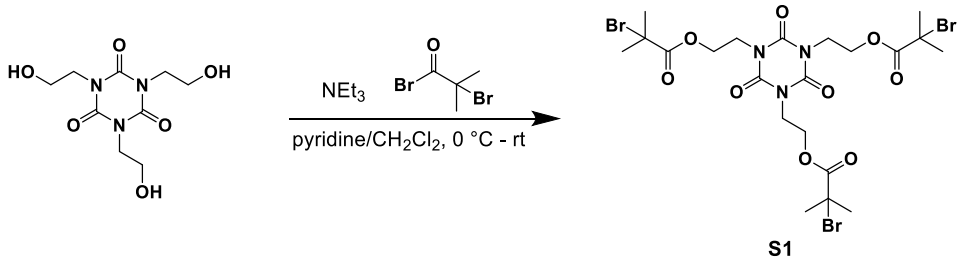

6.5.2 *Synthesis of **S1***

Into a flame-dried round bottom flask, 1,3,5-tris(2-hydroxyethyl)isocyanurate (200 mg, 0.76 mmol, 1.0 equiv.) was dissolved in dry pyridine (21 mL). The reaction mixture was placed in an ice bath. NEt_3 (0.35 mL, 2.50 mmol, 3.3 equiv.) was then added to the mixture. A solution of α-bromoisobutyryl bromide (0.31 mL, 2.50 mmol, 3.3 equiv.) in dry CH_2Cl_2 (3 mL) was then added dropwise. The reaction mixture was stirred for 22 h, during which time the ice bath expired. The solvent was then removed under reduced pressure. The crude residue was taken up in ether. The organic layer was washed successively with sat. $NaHCO_3$ (3 × 10 mL) and DI H_2O (2 × 10 mL). The organic layer was dried over Na_2SO_4, filtered through a thin pad of Celite, and concentrated under reduced pressure. The product was isolated via flash column chromatography (50% EtOAc/hexanes) to obtain a colorless transparent oil in 65% yield. ^1H NMR (500 MHz, $CDCl_3$) δ 4.37 (t, J = 5.1 Hz, 6H), 4.19 (t, J = 5.1 Hz, 6H), 1.85 (s, 18H). ^{13}C NMR (126 MHz, $CDCl_3$) δ 171.5, 148.8, 62.6, 55.7, 41.7, 30.7. LRMS (ESI): $[M+Na]^+$ calcd for $NaC_{21}H_{30}Br_3N_3O_9$, 729.94; found 729.2.

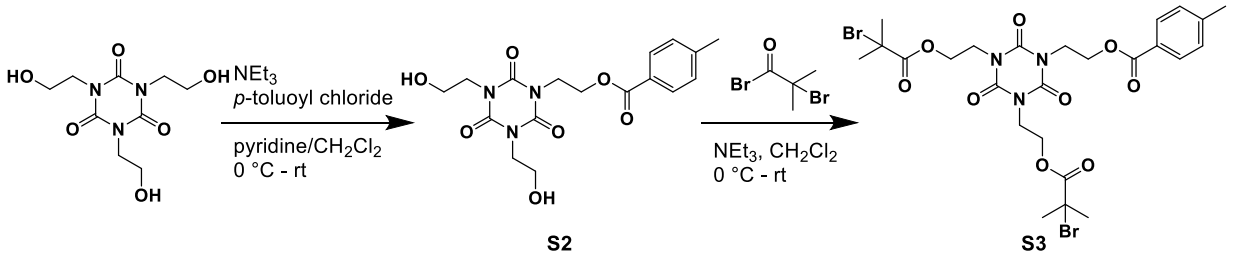

6.5.3 *Synthesis of **S2***

Into a flame-dried round bottom flask, 1,3,5-tris(2-hydroxyethyl)isocyanurate (1.30 g, 5.0 mmol, 1.0 equiv.) was dissolved in dry pyridine (58 mL). The reaction mixture was placed in an ice bath. NEt_3 (0.56 mL, 4.0 mmol, 0.80 equiv.) was then added to the mixture. Then, *p*-toluoyl chloride (0.53 mL, 4.0 mmol, 0.80 equiv.) was added dropwise. The reaction mixture was stirred for 20 h, during which time the ice bath expired. The solvent was then removed under reduced pressure and the crude residue was taken up in ether. The product was isolated using flash column chromatography (80% EtOAc/hexanes) to obtain the diol as a light yellow solid in 50% yield. ^{1}H NMR (500 MHz, $CDCl_3$) δ 7.89 (d, J = 8.2 Hz, 2H), 7.25 (d, J = 8.5 Hz, 2H), 4.58 – 4.55 (m, 2H), 4.37 – 4.33 (m, 2H), 4.08 (t, J = 5.2 Hz, 4H), 3.78 (t, J = 5.3, 4H), 2.91 (s, 2H), 2.42 (s, 3H).^{13}C NMR (126 MHz, $CDCl_3$) δ 166.9, 150.2, 149.5, 144.2, 129.8, 129.3, 126.9, 61.8, 60.2, 45.2, 42.2, 21.8. LRMS (ESI): $[M+Na]^+$ calcd for $NaC_{17}H_{21}N_3O_7$, 402.13, found 402.1.

6.5.4 *Synthesis of **S3***

Into a flame-dried round bottom flask, diol **S2** (199 mg, 0.40 mmol, 1.0 eq) was dissolved in dry CH_2Cl_2 (11 mL). The reaction solution was placed in an ice bath. NEt_3 (0.12 mL, 0.88 mmol, 2.20 equiv.) was then added to the solution. A solution of α-bromoisobutyryl bromide (0.10 mL, 0.88 mmol, 2.20 eq) in dry CH_2Cl_2 (2 mL) was then added dropwise. The reaction solution was stirred for 22 h, during which time the ice bath expired. The crude residue was

taken up in ether and was washed successively with sat. $NaHCO_3$ (3 × 10 mL) and DI H_2O (2 × 10 mL). The organic layer was dried over Na_2SO_4, filtered through a thin pad of Celite, and concentrated under reduced pressure. The product was isolated via flash column chromatography (30% EtOAc/hexanes) to obtain a colorless transparent oil in 52% yield. ^1H NMR (500 MHz, $CDCl_3$) δ 7.85 (d, J = 7.9 Hz, 2H), 7.21 (d, J = 7.9 Hz, 2H), 4.52 (t, J = 4.8 Hz, 2H), 4.34 (t, J = 4.8 Hz, 4H), 4.28 (t, J = 4.8, 2H), 4.20 (t, J = 4.7 Hz, 4H), 2.38 (s, 3H), 1.87 (s, 12H). ^{13}C NMR (126 MHz, $CDCl_3$) δ 171.6, 166.5, 148.9, 143.99, 129.8, 129.2, 127.0, 62.6, 61.4, 55.7, 42.2, 41.7, 30.7, 21.8. LRMS (ESI): $[M+Na]^+$ calcd for $NaC_{25}H_{31}Br_2N_3O_9$, 700.03; found 700.3.

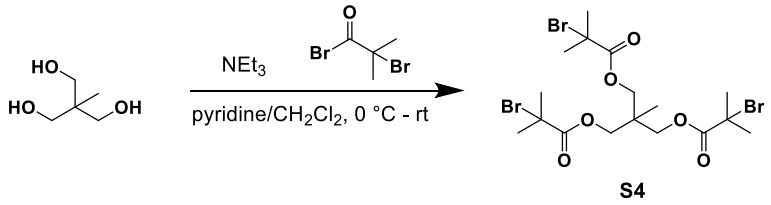

S4

6.5.5 *Synthesis of **S4***

Into a flame-dried round bottom flask, 1,1,1-tris(hydroxymethyl)ethane (100 mg, 0.83 mmol, 1.0 equiv.) was dissolved in dry pyridine (22 mL). The reaction mixture was placed in an ice bath. NEt_3 (0.38 mL, 2.75 mmol, 3.30 equiv.) was then added to the solution. A solution of α-bromoisobutyryl bromide (0.34 mL, 2.74 mmol, 3.30 equiv.) in dry CH_2Cl_2 (3 mL) was then added dropwise. The reaction mixture was stirred for 24 h, during which time the ice bath expired. The solvent was removed under reduced pressure. The crude residue was taken up in ether and washed successively with sat. $NaHCO_3$ (3 × 10 mL) and DI H_2O (2 × 10 mL). The organic layer was dried over Na_2SO_4, filtered through a thin pad of Celite, and concentrated under reduced pressure. The product was isolated via flash column chromatography (10%

EtOAc/hexanes) to obtain a colorless transparent oil in 61% yield. ^{1}H NMR (500 MHz, $CDCl_3$) δ 4.15 (s, 6H), 1.92 (s, 18H), 1.16 (s, 3H). ^{13}C NMR (126 MHz, $CDCl_3$) δ 171.2, 66.7, 55.5, 39.8, 30.8, 17.2. LRMS (ESI): $[M+Na]^+$ calcd for $NaC_{17}H_{27}Br_3O_6$, 588.92; found 589.2.

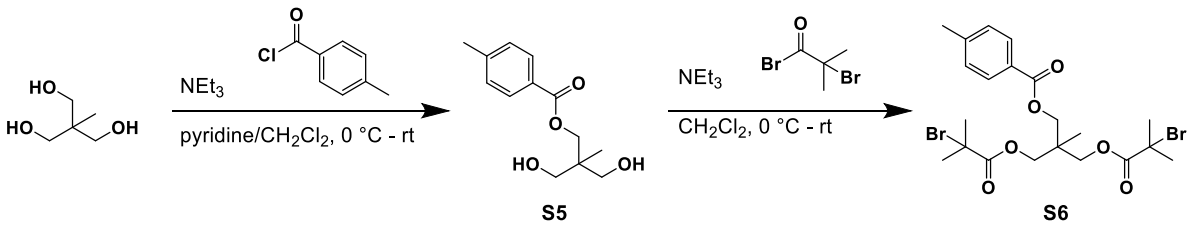

6.5.6 *Synthesis of **S5***

Into a flame-dried round bottom flask, 1,1,1-tris(hydroxymethyl)ethane (500 mg, 4.16 mmol, 1.0 equiv.) was dissolved in dry pyridine (20 mL). The reaction mixture was placed in an ice bath. NEt_3 (0.56 mL, 4.0 mmol, 0.80 equiv.) was then added to the mixture. A solution of *p*-toluoyl chloride (0.53 mL, 4.0 mmol, 0.80 equiv.) in dry CH_2Cl_2 (15 mL) was then added dropwise. The reaction mixture was stirred for 17 h, during which time the ice bath expired. The solvent was then removed under reduced pressure. The product was isolated via flash column chromatography (50% EtOAc/hexanes) to obtain product as a white solid in 56% yield. ^{1}H NMR (500 MHz, $CDCl_3$) δ 7.92 (d, J = 9.3 Hz, 2H), 7.24 (d, J = 9.3 Hz, 2H), 4.39 (s, 2H), 3.62 (m, 4H), 3.16 (m, 2H), 2.40 (s, 3H), 0.92 (s, 3H). ^{13}C NMR (126 MHz, $CDCl_3$) δ 167.6, 144.2, 129.8, 129.3, 129.30, 129.28, 127.1, 67.9, 66.8, 41.2, 21.8, 17.03. LRMS (ESI): $[M+Na]^+$ calcd for $NaC_{13}H_{18}O_4$, 261.11; found 261.0.

6.5.7 *Synthesis of **S6***

Into a flame-dried round bottom flask, diol **S5** (558 mg, 2.34 mmol, 1.0 equiv.) was dissolved in dry CH_2Cl_2 (24 mL). The reaction solution was placed in an ice bath. NEt_3 (0.72

mL, 5.14 mmol, 2.20 equiv.) was then added to the solution. A solution of α-bromoisobutyryl bromide (0.63 mL, 5.14 mmol, 2.20 eq) in dry CH_2Cl_2 (6 mL) was then added dropwise. The reaction solution was stirred for 17 h, during which time the ice bath expired. The solvent was then removed under reduced pressure and the crude residue was taken up in ether and then washed successively with sat. $NaHCO_3$ (3 × 10 mL) and DI H_2O (2 × 10 mL). The organic layer was dried over Na_2SO_4, filtered through a thin pad of Celite, and concentrated under reduced pressure. The product was isolated via flash column chromatography (30% EtOAc/hexanes) to obtain product as a colorless transparent oil in 52% yield. ^{1}H NMR (500 MHz, $CDCl_3$) δ 7.91 (d, *J* = 8.2 Hz, 2H), 7.24 (d, *J* = 8.2 Hz, 2H), 4.31 (s, 2H), 4.24 (s, 4H), 2.41 (s, 3H), 1.93 (s, 12H), 1.21(s, 3H). ^{13}C NMR (126 MHz, $CDCl_3$) δ 171.4, 166.3, 144.1, 129.8, 129.3, 127.1, 67.1, 66.1, 55.6, 39.7, 30.8, 21.8, 17.4. LRMS (ESI): $[M+Na]^+$ calcd for $NaC_{21}H_{28}Br_2O_6$, 559.01; found 559.1.

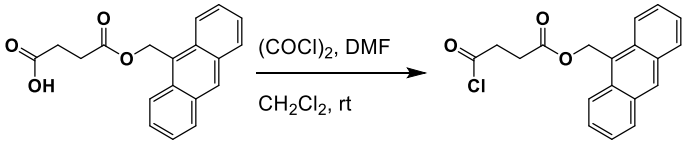

S7 **S8**

6.5.8 *Synthesis of **S8***

Compound **S7** was prepared according to literature procedure.[2] Into a flame-dried round bottom flask, compound **S7** (274 mg, 0.89 mmol, 1.0 equiv.) was dissolved in dry CH_2Cl_2 (9 mL). Oxalyl chloride (0.38 mL, 4.45 mmol, 5 equiv.) was then added to the solution followed by two drops of dry *N*,*N*-dimethylformamide. The reaction solution was stirred for 45 min at room temperature. The solvent was then removed under reduced pressure. The product was used immediately for subsequent acylation.

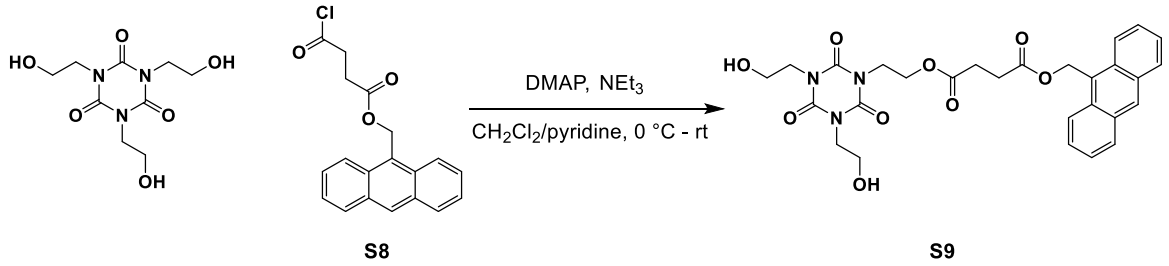

S8 **S9**

6.5.9 *Synthesis of **S9***

Into a flame-dried round bottom flask, 1,3,5-tris(2-hydroxyethyl)isocyanurate (799 mg, 3 mmol, 6.0 equiv.) and DMAP (6 mg, 0.051 mmol, 0.10 equiv.) were dissolved in dry pyridine (12 mL). The reaction mixture was placed in an ice bath. NEt_3 (0.078 mL, 0.56 mmol, 1.10 eq) was then added to the solution. A solution of acid chloride **S8** (167 mg, 0.51 mmol, 1.0 equiv.) dissolved in dry CH_2Cl_2 (10 mL) was then added dropwise over 4 h. The reaction solution was stirred for 18 h, during which time the ice bath expired. The solvent was then removed under reduced pressure and the product was isolated via flash column chromatography (70% EtOAc/hexanes) to obtain a yellow viscous oil in 53% yield. ^{1}H NMR (500 MHz, CD_3CN) δ 8.61 (s, 1H), 8.35 (d, J = 8.9 Hz, 2H), 8.09 (d, J = 8.4 Hz, 2H), 7.67 – 7.52 (m, 4H), 6.12 (s, 2H), 4.17 (t, J = 5.4 Hz, 2H), 4.00 (t, J = 5.4 Hz, 2H), 3.93 (t, J = 5.9 Hz, 4H), 3.64 (t, J = 5.9 Hz, 4H), 2.52 (m, 4H). ^{13}C NMR (126 MHz, CD_3CN) δ 173.3, 150.4, 132.3, 131.8, 130.0, 129.9, 127.6, 126.2, 125.0, 61.8, 59.7, 59.6, 45.6, 42.1, 29.7, 29.6. LRMS (ESI): $[M+Na]^+$ calcd for $NaC_{28}H_{29}N_3O_9$, 574.18; found 574.3.

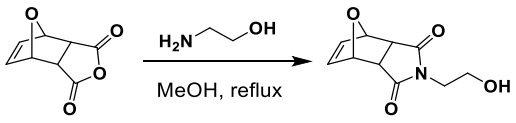

S10

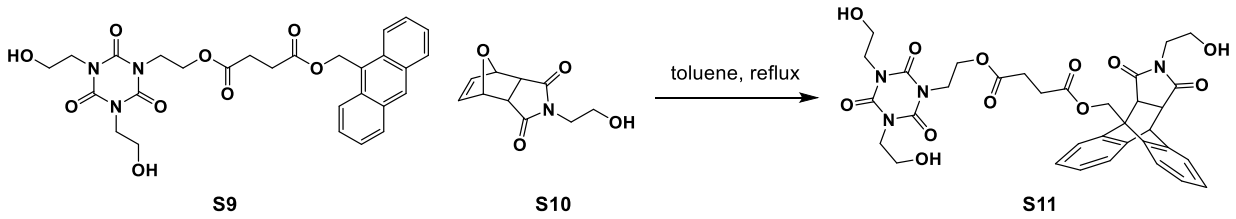

S9 S10 S11

6.5.10 *Synthesis of **S11***

Compound **S10** was prepared according to literature procedure.[3] Into a round bottom flask, compounds **S9** (151 mg, 0.27 mmol, 1.0 equiv.) and **S10** (56 mg, 0.27 mmol, 1.0 equiv.) were dissolved in toluene (2.5 mL). The flask was then fitted with a water-jacketed reflux condenser, and the reaction mixture was stirred at reflux for 22 h. The flask was then removed from heat and the solvent was removed under reduced pressure. The resulting oily residue was dissolved in minimal MeOH and precipitated into ether to provide pure product as a white solid (81% yield). ^{1}H NMR (500 MHz, CD_3CN) δ 7.45 (dd, J = 5.7, 3.0 Hz, 1H), 7.38 (dd, J = 5.7, 3.0 Hz, 1H), 7.29 (dd, J = 5.4, 2.5 Hz, 1H), 7.24 – 7.11 (m, 5H), 5.41 (s, 2H), 4.76 (d, J = 3.2 Hz, 1H), 4.30 – 4.16 (m, 2H), 4.08 – 4.04 (m, 2H), 3.93 (t, J = 5.9 Hz, 4H), 3.64 (t, J = 5.9 Hz, 4H), 3.31 (dd, J = 8.4, 3.2 Hz, 1H), 3.26 (d, J = 8.3 Hz, 1H), 3.10 (t, J = 6.5 Hz, 2H), 2.84 (t, J = 6.3 Hz, 2H), 2.67 (t, J = 6.5 Hz, 2H), 2.58 (t, J = 6.4 Hz, 2H). ^{13}C NMR (126 MHz, CD_3CN) δ 177.4, 176.8, 173.2, 173.1, 150.5, 150.4, 143.1, 142.2, 140.3, 139.5, 127.8, 127.7, 127.5, 127.3, 126.0, 125.1, 124.2, 123.2, 62.8, 61.9, 59.6, 58.8, 46.3, 45.6, 42.2, 41.0, 29.8, 29.7. LRMS (ESI): $[M+Na]^+$ calcd for $NaC_{34}H_{36}N_4O_{12,}$ 715.22; found 715.5.

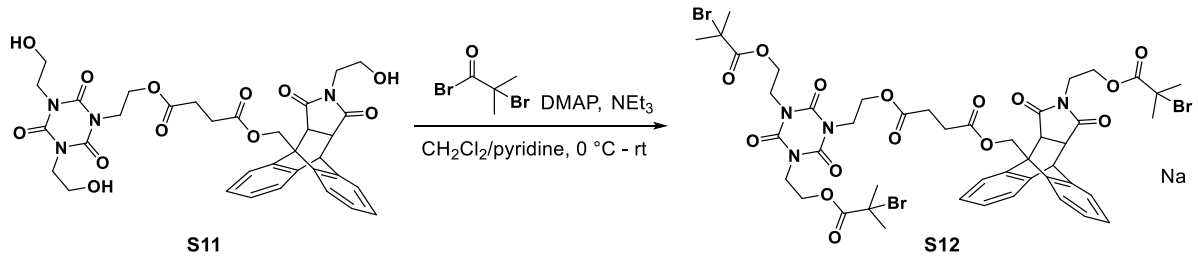

S11 S12

6.5.11 *Synthesis of **S12***

Into a flame-dried round bottom flask, triol **S11** (152 mg, 0.22 mmol, 1.0 equiv.) and DMAP (8.0 mg, 0.066 mmol, 0.30 equiv.) were dissolved in dry pyridine (6 mL). The reaction mixture was placed in an ice bath and NEt_3 (0.10 mL, 0.72 mmol, 3.30 equiv.) was then added to the mixture. A solution of α-bromoisobutyryl bromide (0.089 mL, 0.72 mmol, 3.30 equiv.) in dry CH_2Cl_2 (2 mL) was then added dropwise. The reaction solution was stirred for 18 h, during which time the ice bath expired. The solvent was then removed under reduced pressure. The crude residue was taken up in EtOAc and then washed successively with sat. $NaHCO_3$ (3 × 10 mL) and DI H_2O (2 × 10 mL). The organic layer was dried over Na_2SO_4, filtered through a thin pad of Celite, and concentrated under reduced pressure. The product was isolated using flash column chromatography (30% EtOAc/hexanes) to obtain a colorless transparent oil (52% yield). ^{1}H NMR (500 MHz, CD_3CN) δ 7.46 (dd, J = 5.4, 3.2 Hz, 1H), 7.39 (dd, J = 5.3, 3.4 Hz, 1H), 7.30 (dd, J = 5.5, 2.9 Hz, 1H), 7.19 (m, 5H), 5.42 (d, J = 8.9 Hz, 2H), 4.78 (d, J = 3.1 Hz, 1H), 4.32 (t, J = 5.3 Hz, 4H), 4.22 (t, J = 5.6 Hz, 2H), 4.14 (t, J = 5.3 Hz, 4H), 4.05 (t, J = 4.9 Hz, 2H), 3.58 (dd, J = 10.2, 5.6 Hz, 2H), 3.39 (dd, 3.2 Hz, 1H), 3.16 (m, 3H), 2.67 (t, J = 6.3 Hz, 2H), 2.58 (t, J = 6.2 Hz, 2H), 1.85 (s, 18H). ^{13}C NMR (126 MHz, CD_3CN) δ 177.0, 176.4, 173.1, 173.0, 172.3, 172.0, 150.2, 143.1, 142.2, 140.3, 139.5, 139.0, 127.9, 127.8, 127.6, 127.4, 126.1, 125.1, 124.3, 123.3, 63.5, 63.1, 62.8, 61.9, 57.5, 57.3, 48.6, 46.3, 42.4, 42.2, 37.3, 31.0, 31.0, 29.9, 29.8. LRMS (ESI): $[M+Na]^+$ calcd for $NaC_{46}H_{51}Br_3N_4O_{15,}$ 1161.08; found 1161.8.

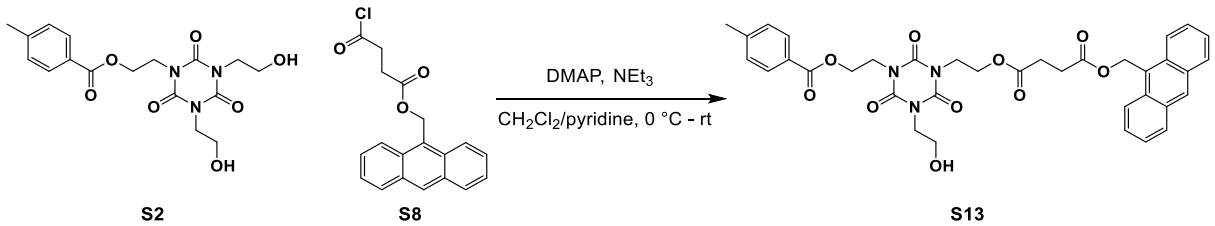

S2 S8 S13

6.5.12 *Synthesis of **S13***

Into a flame-dried round bottom flask, diol **S2** (835 mg, 1.68 mmol, 6.0 equiv.) and DMAP (3 mg, 0.028 mmol, 0.10 equiv.) were dissolved in dry pyridine (4.5 mL). The reaction solution was placed in an ice bath and NEt_3 (0.043 mL, 0.30 mmol, 1.10 eq) was then added to the solution. A solution of acid chloride **S8** (91 mg, 0.28 mmol, 0.10 equiv.) in dry CH_2Cl_2 (5.6 mL) was then added dropwise. The reaction solution was stirred for 20 h, during which time the ice bath expired. The solvent was then removed under reduced pressure. The crude residue was taken up in EtOAc and then washed successively with sat. $NaHCO_3$ (3 × 10 mL) and DI H_2O (2 × 10 mL). The organic layer was dried over Na_2SO_4, filtered through a thin pad of Celite, and concentrated under reduced pressure. The yellow crude oil mixture was further purified by flash column chromatography in 50% EtOAc/hexanes. An inseparable impurity co-eluted with the product. The mixture was carried through in the synthesis of **S14**. LRMS (ESI): $[M+Na]^+$ calcd for $NaC_{36}H_{35}N_3O_{10,}$ 692.22; found 692.5.

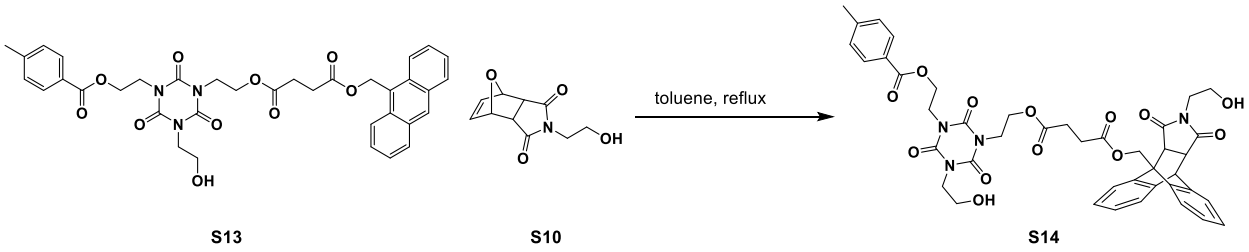

6.5.13 *Synthesis of **S14***

Into a round bottom flask, alcohols **S13** (95 mg, 0.14 mmol, 1.0 equiv.) and **S10** (29 mg, 0.14 mmol, 1.0 equiv.) were dissolved in toluene (2 mL). The flask was then fitted with a water-jacketed reflux condenser, and the reaction mixture was stirred at reflux for 22 h. The flask was then removed from heat and the solvent was removed under reduced pressure. The resulting oily

residue was dissolved in minimal EtOAc and precipitated into ether to provide pure product as a white solid (40% yield). ^{1}H NMR (500 MHz, CD_3CN) δ 7.84 (d, J = 8.0 Hz, 2H), 7.44 (dd, J = 5.2, 3.2 Hz, 1H), 7.37 (dd, J = 5.2, 3.3 Hz, 1H), 7.27 (m, 3H), 7.23 – 7.12 (m, 5H), 5.41 (s, 2H), 4.76 (d, J = 3.0 Hz, 1H), 4.43 (t, J = 5.1 Hz, 2H), 4.21 (m, 4H), 4.04 (t, J = 5.0 Hz, 2H), 3.91 (t, J = 5.9 Hz, 2H), 3.61 (dd, J = 11.6, 5.7 Hz, 2H), 3.29 (dd, J = 8.3, 3.1 Hz, 1H), 3.24 (d, J = 7.9 Hz, 1H), 3.09 (t, J = 6.4 Hz, 2H), 2.84 (m, 3H), 2.65 (t, J = 6.5 Hz, 2H), 2.55 (t, J = 6.4 Hz, 2H), 2.36 (s, 3H). ^{13}C NMR (126 MHz, CD_3CN) δ 177.4, 176.7, 173.1, 173.0, 167.1, 150.4, 150.3, 145.0, 143.1, 142.2, 140.3, 139.5, 130.4, 130.1, 128.2, 127.8, 127.7, 127.6, 127.3, 126.0, 125.1, 124.2, 123.3, 62.8, 62.5, 61.9, 59.6, 58.9, 48.5, 46.3, 45.6, 42.5, 42.2, 41.0, 29.8, 29.7, 21.6. LRMS (ESI): $[M+Na]^+$ calcd for $NaC_{42}H_{42}N_4O_{13}$, 833.26; found 833.8.

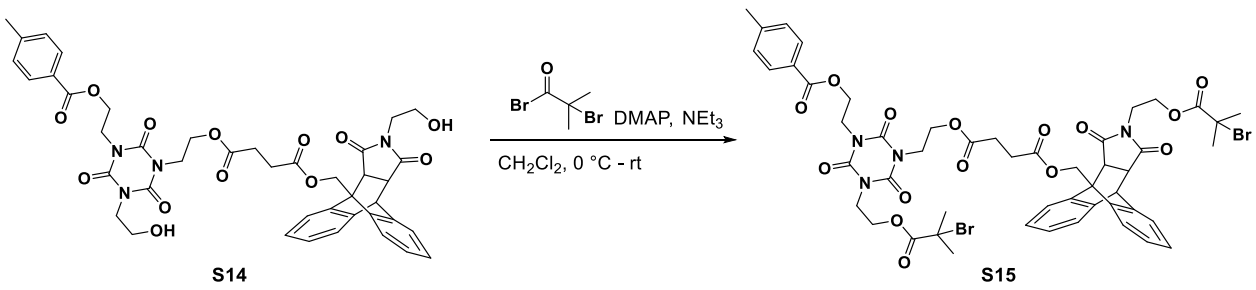

S14 **S15**

6.5.14 *Synthesis of **S15***

Into a flame-dried round bottom flask, diol **S14** (45 mg, 0.055 mmol, 1.0 equiv.) and DMAP (1.0 mg, 0.011 mmol, 0.20 equiv.) were dissolved in dry CH_2Cl_2 (1.6 mL). The reaction mixture was placed in an ice bath and NEt_3 (0.016 mL, 0.12 mmol, 2.2 equiv.) was then added to the solution. A solution of α-bromoisobutyryl bromide (0.015 mL, 0.12 mmol, 2.2 equiv.) in dry CH_2Cl_2 (0.50 mL) was then added dropwise. The reaction solution was stirred for 22 h, during which time the ice bath expired. The solvent was then removed under reduced pressure. The

crude residue was taken up in EtOAc and washed successively with sat. $NaHCO_3$ (3 × 10 mL) and DI H_2O (2 × 10 mL). The organic layer was dried over Na_2SO_4, filtered through a thin pad of Celite, and concentrated under reduced pressure. The product was isolated using flash chromatography (30% EtOAc/hexanes) to obtain a colorless oil (41% yield). ^1H NMR (500 MHz, CD_3CN) δ 7.84 (d, J = 8.2 Hz, 2H), 7.45 (dd, J = 5.8, 2.9 Hz, 1H), 7.37 (dd, J = 5.8, 3.0 Hz, 1H), 7.31 – 7.25 (m, 3H), 7.22 – 7.14 (m, 5H), 5.44 – 5.36 (m, 2H), 4.77 (d, J = 3.2 Hz, 1H), 4.43 (t, J = 5.3 Hz, 2H), 4.28 (t, J = 5.4 Hz, 2H), 4.20 (dd, J = 10.8, 5.6 Hz, 4H), 4.12 (t, J = 5.4 Hz, 2H), 4.03 (td, J = 5.5, 1.8 Hz, 2H), 3.62 – 3.52 (m, 2H), 3.32 (dd, J = 8.5, 3.2 Hz, 1H), 3.27 (td, J = 5.7, 1.8 Hz, 3H), 2.65 (dd, J = 9.8, 4.0 Hz, 2H), 2.54 (dd, J = 9.8, 4.1 Hz, 2H), 2.37 (s, 3H), 1.84 (d, J = 7.9 Hz, 12H). ^{13}C NMR (126 MHz, CD_3CN) δ 177.0, 176.39, 173.1, 173.0, 172.2, 172.0, 167.0, 150.2, 145.0, 143.1, 142.2, 140.2, 139.4, 130.4, 130.1, 127.9, 127.8, 127.6, 127.4, 126.1, 125.1, 124.3, 63.4, 63.1, 62.7, 62.4, 61.8, 57.4, 57.3, 48.6, 46.2, 42.5, 42.3, 42.1, 37.3, 30.9, 30.9, 29.84, 29.76, 21.7. LRMS (ESI): $[M+Na]^+$ calcd for $NaC_{50}H_{52}Br_2N_4O_{15}$, 1131.17; found 1131.6.

6.5.15 *Representative Example Polymerization Procedure*

In a nitrogen-filled drybox, initiator **S1** (9.5 mg, 0.013 mmol, 1.0 equiv.), methyl acrylate (1.13 mL, 12.48 mmol, 960 equiv.), dry DMF (0.56 mL) and a magnetic stir bar were added into a scintillation vial. A solution of CuBr (3.7 mg, 0.026 mmol, 2.0 equiv.) and PMDETA (5.4 µL, .026 mmol, 2.0 equiv.) in DMF (0.56 mL) was then added to reaction mixture. The vial was sealed with a Teflon-lined screw cap and the reaction solution was stirred at room temperature for 13 h. The viscous solution was then added dropwise into an excess of MeOH causing the polymer to precipitate from solution. The solvent was decanted and the resulting polymer

residue was rinsed with MeOH (3 × 20 mL). The polymer was dissolved in CH_2Cl_2 (10 mL) and filtered through a plug of alumina to remove residual copper. The solvent was removed under reduced pressure and the resulting polymeric residue was dried under reduced pressure. General structures are shown in Figure 6.6, and data from GPC analysis is given in Table 6.3.

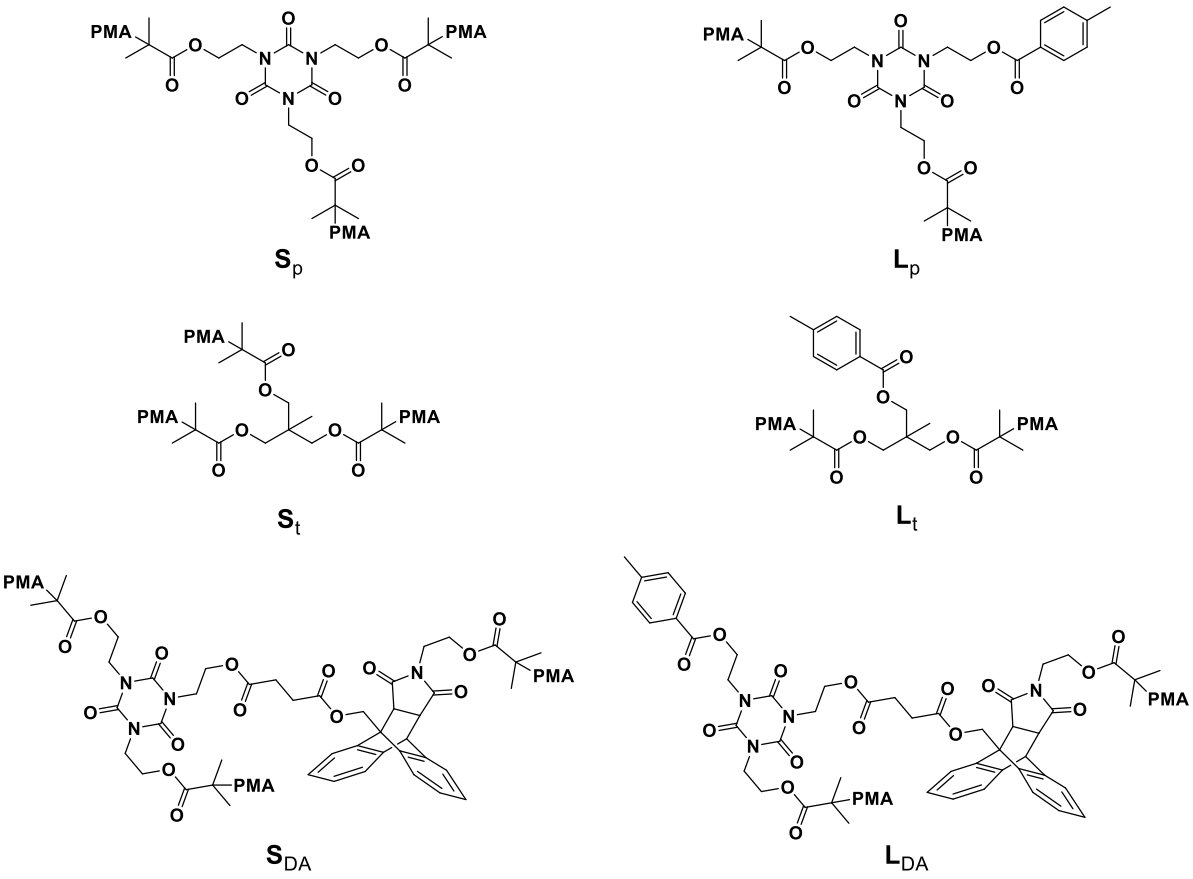

Figure 6.5. General structures of star and linear polymers used in the current study.

Table 6.3. GPC data for star and linear polymers before sonication.

Polymer	M_n (kDa)	M_w (kDa)	PDI
$\mathbf{S}_{p,58.7}$	58.7	59.9	1.02
$\mathbf{S}_{t,59.4}$	59.4	60.6	1.02
$\mathbf{L}_{p,44.0}$	44.0	45.8	1.04
$\mathbf{L}_{t,44.0}$	44.0	44.4	1.01
$\mathbf{S}_{p,87.9}$	87.9	88.8	1.01
$\mathbf{L}_{p,58.7}$	58.7	59.3	1.01
$\mathbf{S}_{t,93.6}$	93.6	97.3	1.04
$\mathbf{L}_{t,62.6}$	62.6	64.5	1.03
$\mathbf{S}_{DA,\ 85.9}$	85.9	87.6	1.02
$\mathbf{L}_{DA,61.6}$	61.6	63.5	1.03

6.5.16 *Sonication Procedure*

Sonication experiments were done in a flame-dried, N_2-purged Suslick flask, with the sonication horn (1 cm diameter) already attached to Suslick flask. Each arm of the Suslick flask was fitted with a rubber septum. In a separate flame-dried round bottom flask, the polymer sample was dissolved in dry DMF at a concentration of 5 mg/ml. The polymer solution was then transferred to the Suslick flask under dry N_2 via syringe. The entire apparatus (sonication horn + Suslick flask) was then transferred to a cold room (4 °C) for the duration of sonication experiment. Polymer solutions were sonicated at 13.8 W/cm^2 for a pulse of 1s on, 9s off. Aliquots of 0.5 mL were withdrawn from the reaction periodically and analyzed by GPC. Final GPC analysis data are given in Table 6.4. ^{1}H NMR spectra of the polymers before and after sonication showed consistent resonances for the core structure. This indicated to us that the core remained intact during sonication, and chain scission was occurring within the polymer arm. Representative spectra are shown in Figure 6.6.

Table 6.4. GPC data for star and linear polymers after sonication.

Polymer	M_n (kDa)	M_w (kDa)	PDI
$\mathbf{S}_{p,58.7}$	22.6	30.2	1.34
$\mathbf{S}_{t,59.4}$	26.1	31.9	1.23
$\mathbf{L}_{p,44.0}$	21.0	23.6	1.12
$\mathbf{L}_{t,44.0}$	19.8	23.3	1.19
$\mathbf{S}_{p,87.9}$	41.1	53.2	1.30
$\mathbf{L}_{p,58.7}$	29.7	35.9	1.21
$\mathbf{S}_{t,93.6}$	36.7	51.0	1.40
$\mathbf{L}_{t,62.6}$	29.0	35.1	1.20
$\mathbf{S}_{DA,\ 85.9}$	42.7	51.0	1.20
$\mathbf{L}_{DA,61.6}$	33.0	38.7	1.17

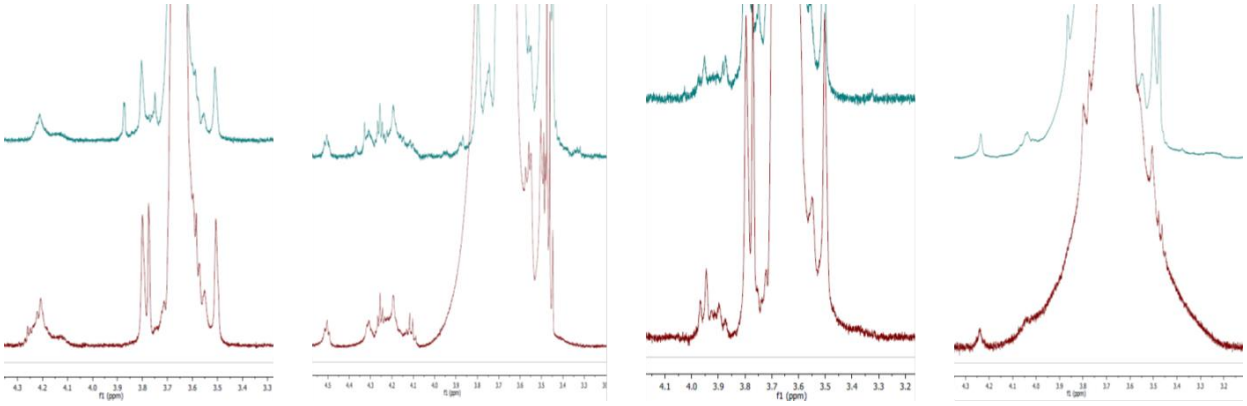

Figure 6.6. Representative ^{1}H NMR spectra before (red) and after (blue) sonication. From left to right: $\mathbf{S}_{p,58.7}$, $\mathbf{L}_{p,44.0}$, $\mathbf{S}_{t,59.4}$, $\mathbf{L}_{t,44.0}$.

6.5.17 *Data Analysis*

During sonication experiments, aliquots were withdrawn and injected directly into the GPC system, which uses a manual injector with a loop volume of 143 µL. Polymer peaks in the RI traces were normalized to constant area. The peak maximum (P_{max}) retention time of each virgin polymer was recorded. The RI intensity at that retention time for each normalized GPC trace taken during sonication was then used to generate a first-order kinetic plot. Three independent

experiments were conducted for each polymer sample, with aliquots being drawn at the same time intervals for each run. The rate constants (k_{RI}) determined from each run were averaged, and standard deviations were calculated. Plots shown below provide the average value for each data point, with error bars representing the standard deviation for each. Column drift was also investigated and found to be small (Table 6.5). Specifically, the standard deviation for the P_{max} retention time for the time zero samples were found to be < 0.2 min for each polymer sample.

Table 6.5. Average peak maxima for time zero GPC traces.

Polymer	Mean P_{max} Retention Time (min)	Standard Deviation (min)
$\mathbf{S}_{p,58.7}$	20.498	0.028
$\mathbf{S}_{t,59.4}$	20.551	0.100
$\mathbf{L}_{p,44.0}$	20.898	0.009
$\mathbf{L}_{t,44.0}$	21.014	0.187
$\mathbf{S}_{p,87.9}$	19.756	0.041
$\mathbf{L}_{p,58.7}$	20.408	0.024
$\mathbf{S}_{t,93.6}$	19.682	0.033
$\mathbf{L}_{t,62.6}$	20.166	0.016
$\mathbf{S}_{DA,\ 85.9}$	19.640	0.000
$\mathbf{L}_{DA,61.6}$	20.151	0.060

To verify that the daughter fragments were not contributing to the RI signal intensity of the reactant polymer, the overlapping peaks were resolved using a non-linear regression analysis. For linear and star polymers, GPC peaks were assumed to be the sum of two or three polynomial modified Gaussian functions, respectively.[4] The Microsoft Excel Solver function was used to minimize the sum of squared differences between the experimental and fit data. Peak resolution was completed for a single run of each polymer type. For comparison, the experimental and

corresponding resolved GPC traces for each experiment are shown below. The red vertical lines indicate the retention time used for rate constant determination. The resolved data were used to calculate rate constants based upon the RI intensities (k_{res}), and the total area of the reactant polymer peak (k_{area}). The peak resolution studies suggest that the daughter fragments do not significantly contribute to the intensity at the initial P_{max} retention time, which is further supported by the consistency of the rate constants determined from the experimental and resolved data (summarized in Table 6.6).

Table 6.6. Summary of rate constants for consumption of parent polymer via mechanochemical chain scission.[a]

Polymer	M_{total} (kDa)	M_{arm} (kDa)	k_{RI} (× 10^{-2} min^{-1})	k_{res} (× 10^{-2} min^{-1})	k_{area} (× 10^{-2} min^{-1})
$\mathbf{S}_{p,58.7}$	58.7	19.6	1.02 ± 0.02	0.99	0.95
$\mathbf{S}_{t,59.4}$	59.4	19.8	1.10 ± 0.02	1.12	1.09
$\mathbf{L}_{p,44.0}$	44.0	22.0	1.26 ± 0.03	1.24	1.20
$\mathbf{L}_{t,44.0}$	44.0	22.0	1.25 ± 0.08	1.15	1.12
$\mathbf{S}_{p,87.9}$	87.9	29.3	2.44 ± 0.17	2.31	2.29
$\mathbf{L}_{p,58.7}$	58.7	29.3	2.38 ± 0.12	2.35	2.35
$\mathbf{S}_{t,93.6}$	93.6	31.2	2.66 ± 0.14	2.48	2.43
$\mathbf{L}_{t,62.6}$	62.6	31.3	2.63 ± 0.06	2.74	2.72
$\mathbf{S}_{DA,\ 85.9}$	85.9	28.6	3.13 ± 0.11	3.33	3.30
$\mathbf{L}_{DA,61.6}$	61.6	30.8	3.27 ± 0.38	3.00	2.87

[a]For GPC traces and kinetic plots refer to Appendix A

6.5.18 *Determination of Rate Constants for $\mathbf{S}_{DA}$ and $\mathbf{L}_{DA}$ by Photoluminescence Spectroscopy*

For polymers containing the Diels-Alder adduct mechanophore, rate constants were also determined by photoluminescence spectroscopy. A 50 µL aliquot was drawn at various time points during the sonication experiment. The aliquot was then diluted to 5 mL total volume using a volumetric flask and filtered through a 0.45 µm filter. Finally the photoluminescence emission

spectrum was collected from 370 to 600 nm using an excitation wavelength of 360 nm (Figure 6.7). The time zero emission spectrum was subtracted from each subsequent data file, as a background correction. The emission intensity at 411 nm was used to determine photoluminescence rate constant (k_{PL}) for the formation of anthracene. The experiment was conducted in triplicate for each mechanophore-containing polymer, and the rate constants were averaged and standard deviations calculated. Shown below are the photoluminescence spectra for a representative run and first-order kinetic plots for $\mathbf{S}_{DA,85.9}$ and $\mathbf{L}_{DA,61.6}$.

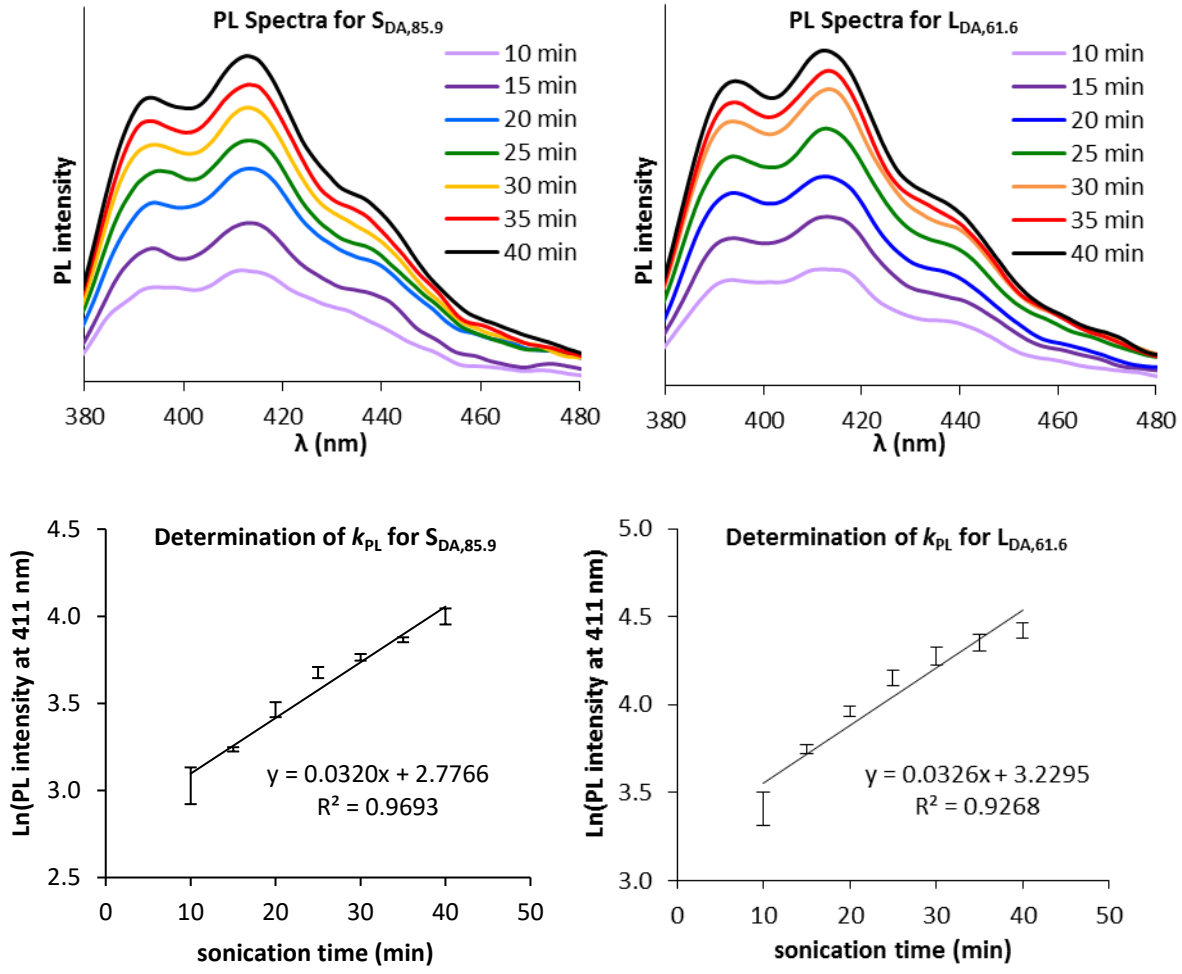

Figure 6.7. Determination of k_{PL} of $\mathbf{S}_{DA,85.9}$ and $\mathbf{L}_{DA,61.6}$ from the corresponding PL spectra.

6.5.19 *Photoluminescence Control Experiments*

As a sonication control experiment, a mixture of $\mathbf{L}_{p,58.7}$ (64 mg) and **A** (**S9** above, 0.61 mg, 0.0011 mmol) in DMF (12.8 mL, 5 mg/mL polymer solution) was sonicated as described above for kinetic studies. The PL spectrum was recorded from 370 to 600 nm using an excitation wavelength of 360 nm. The total integrated emission intensity was plotted as a % of initial value versus sonication time (Figure 5C of the Main Text, and Figure 6.8 left, below). These results confirm the stability of product anthracene moieties to sonication and that the UV-absorbing material formed upon degradation of unfunctionalized PMA does not influence the PL output intensities. The PL intensity at 411 nm (excitation at 360 nm) for a mixture of $\mathbf{L}_{p,58.7}$ and **A** was also recorded over a concentration range for **A** consistent with the theoretical concentrations of anthracene produced in the kinetic studies (Figure 5D in the Main Text, and Figure 6.8 right, below). A linear correlation was observed.

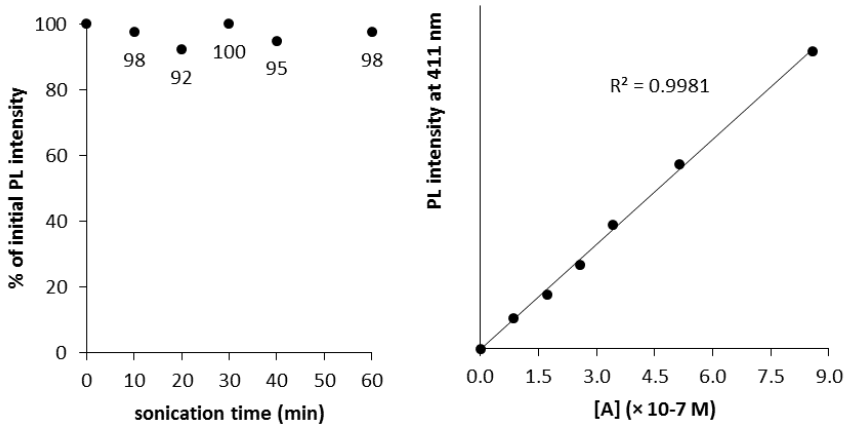

Figure 6.8. (left) % of initial PL intensity with increasing sonication time of a mixture of $\mathbf{L}_{p,58.7}$ and **A** in DMF, and (right) linear correlation between PL intensity and concentration of **A** in the presence of $\mathbf{L}_{p,58.7}$.

6.5.20 *Determination of Mechanophore Activation by UV-vis*

UV-vis absorption spectra were also used to confirm the formation of anthracene upon sonication of the mechanophore-containing polymers. A representative set of spectra are show in Figure 6.9 below.

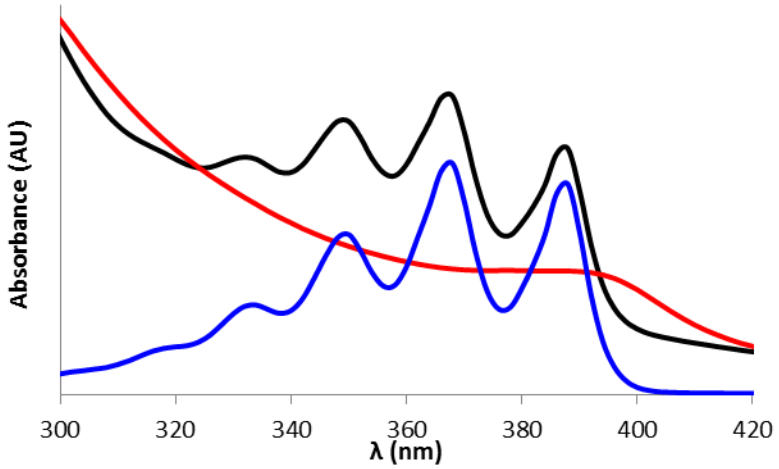

Figure 6.9. UV-vis absorption spectrum in DMF of **S9** (blue line), and $\mathbf{S}_{DA,85.9}$ before (red line) and after (black line) sonication. The characteristic features observed in the blue and black traces are consistent with anthracene formation upon sonication of $\mathbf{S}_{DA,85.9}$.

6.5.21 *NMR Spectra*

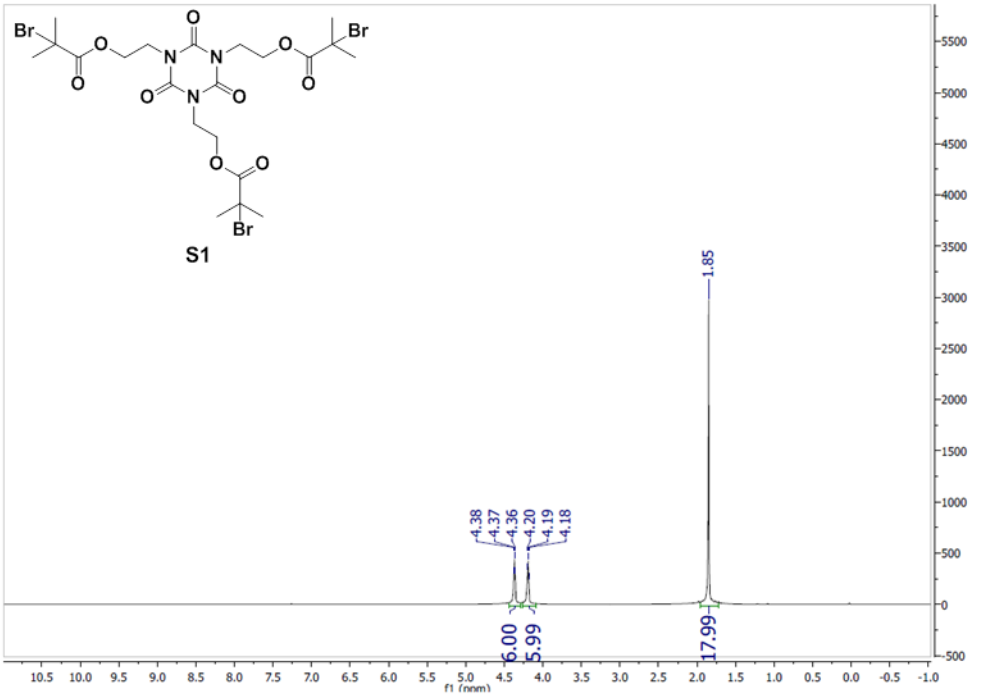

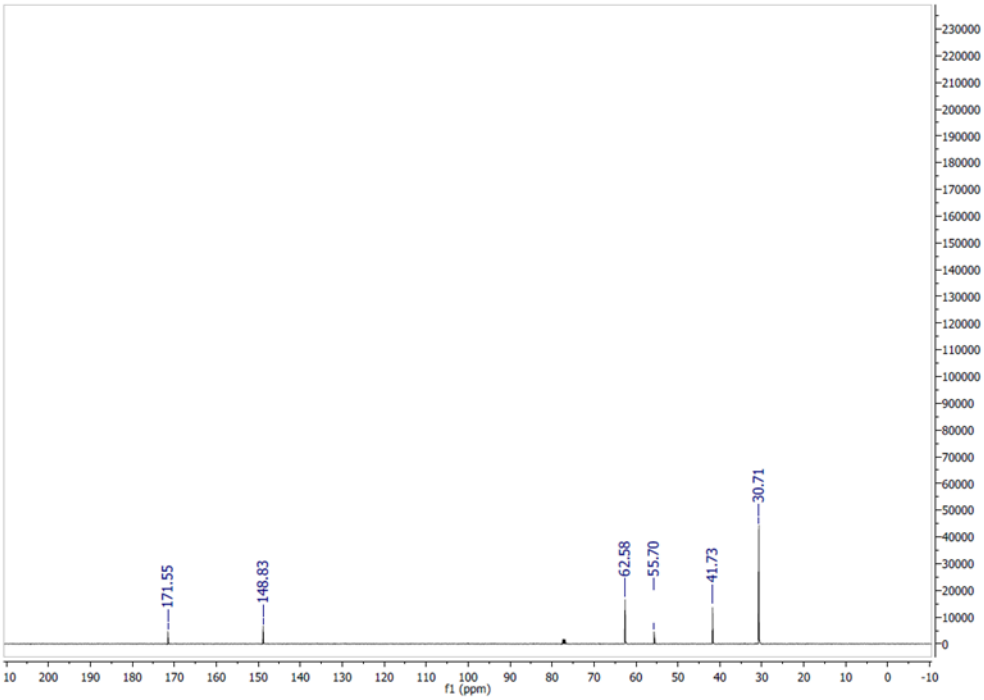

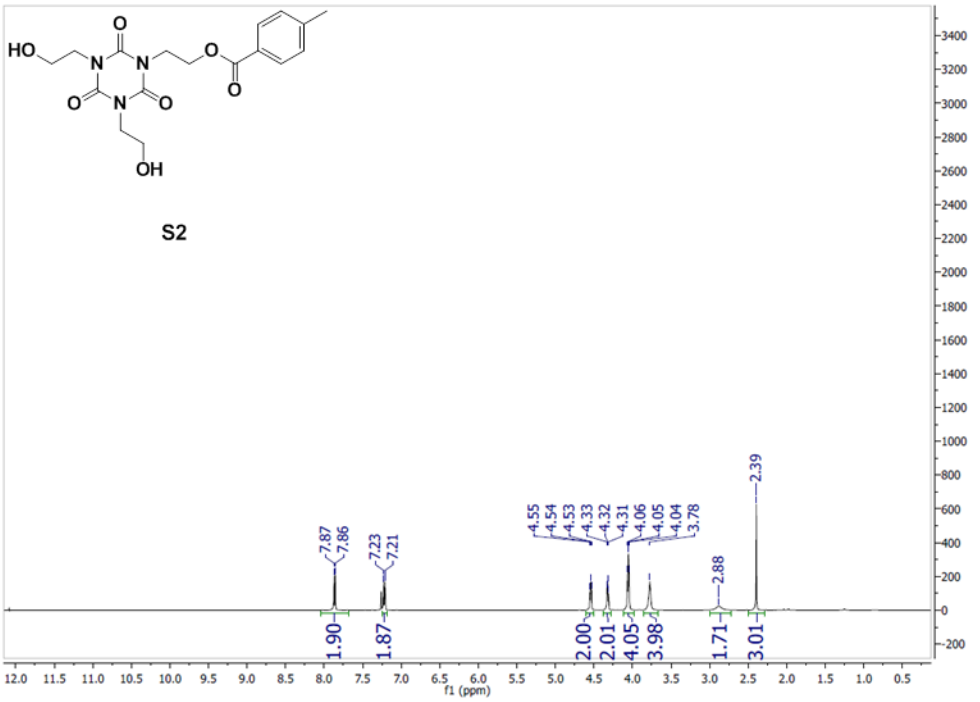
HO
O
N
N
O
O
N
O
O
O
OH
S2
7.87
7.86
7.23
7.21
4.55
4.54
4.53
4.33
4.32
4.31
4.06
4.05
4.04
3.78
2.88
2.39
1.90
1.87
2.00
2.01
4.05
3.98
1.71
3.01
f1 (ppm)

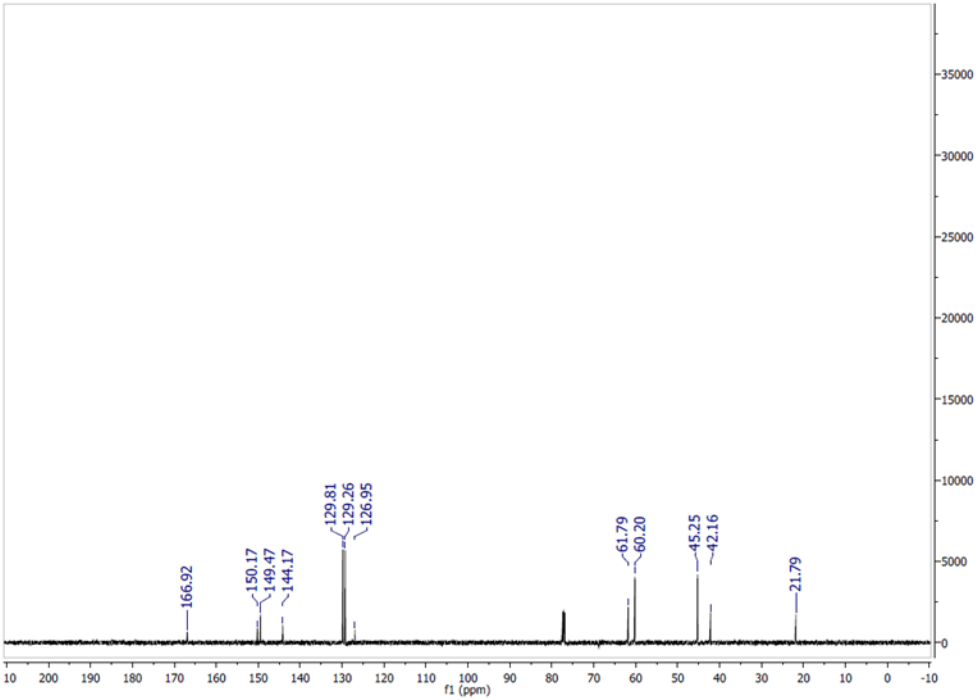
166.92
150.17
149.47
144.17
129.81
129.26
126.95
61.79
60.20
45.25
42.16
21.79
f1 (ppm)

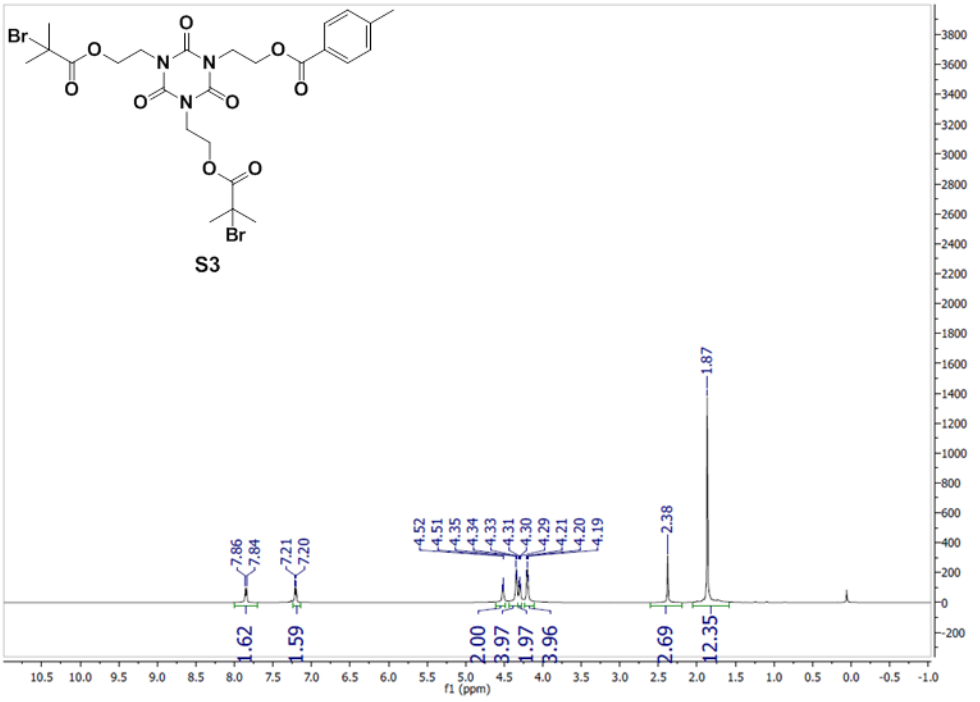
Br
O
O
N
N
N
O
O
O
O
O
O
O
Br
S3
7.86
7.84
7.21
7.20
4.52
4.51
4.35
4.34
4.33
4.31
4.30
4.29
4.21
4.20
4.19
2.38
1.87
1.62
1.59
2.00
3.97
1.97
3.96
2.69
12.35
f1 (ppm)

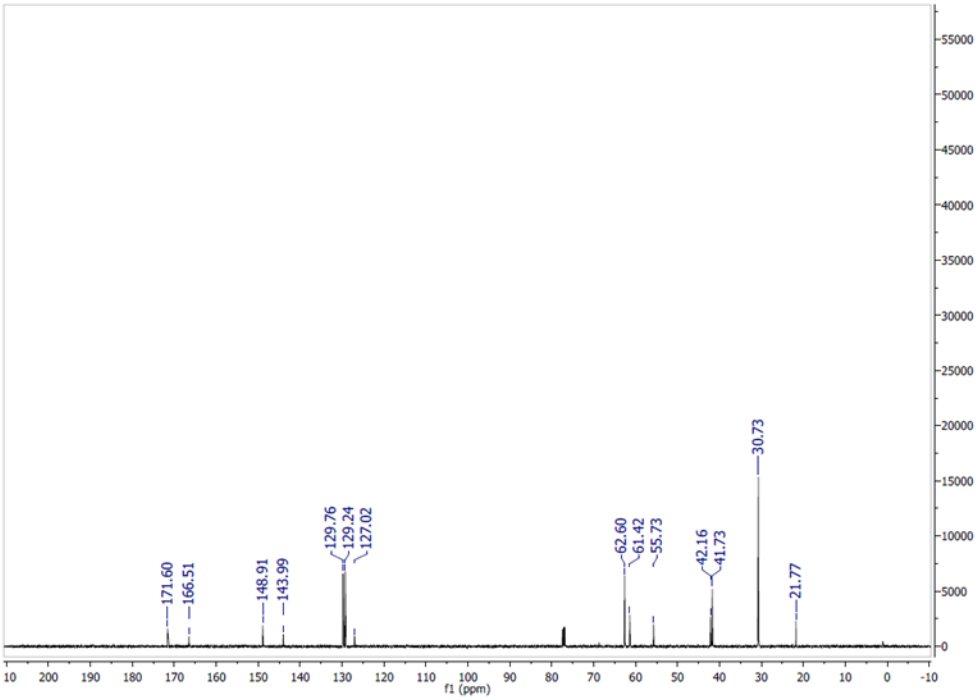
171.60
166.51
148.91
143.99
129.76
129.24
127.02
62.60
61.42
55.73
42.16
41.73
30.73
21.77
f1 (ppm)

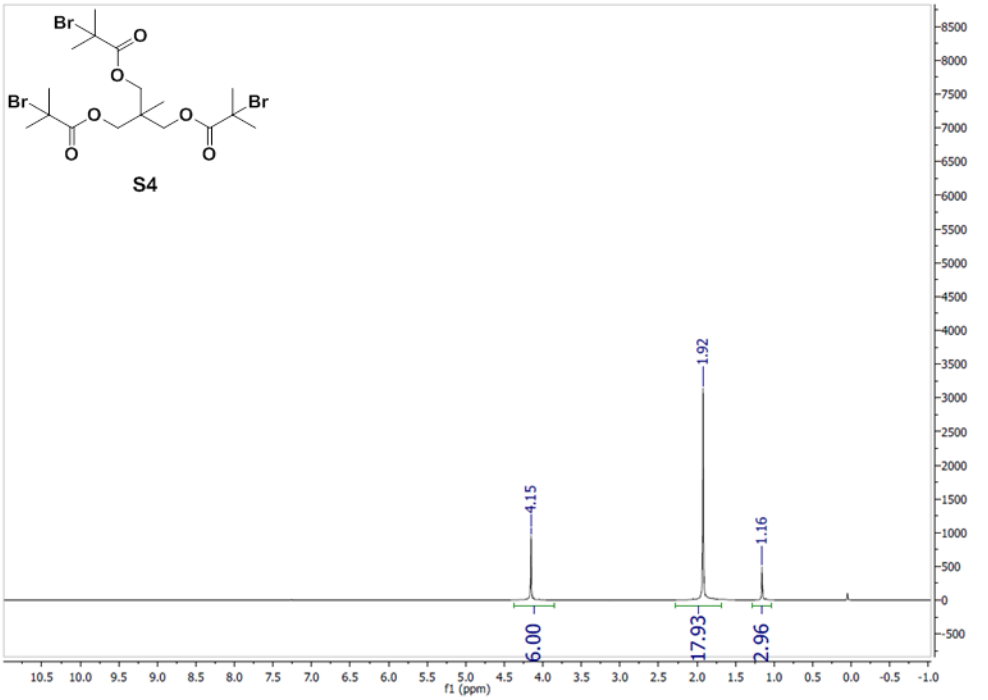
Br
O
O
Br
O
O
O
Br
O
S4
1.92
4.15
1.16
6.00
17.93
2.96
f1 (ppm)

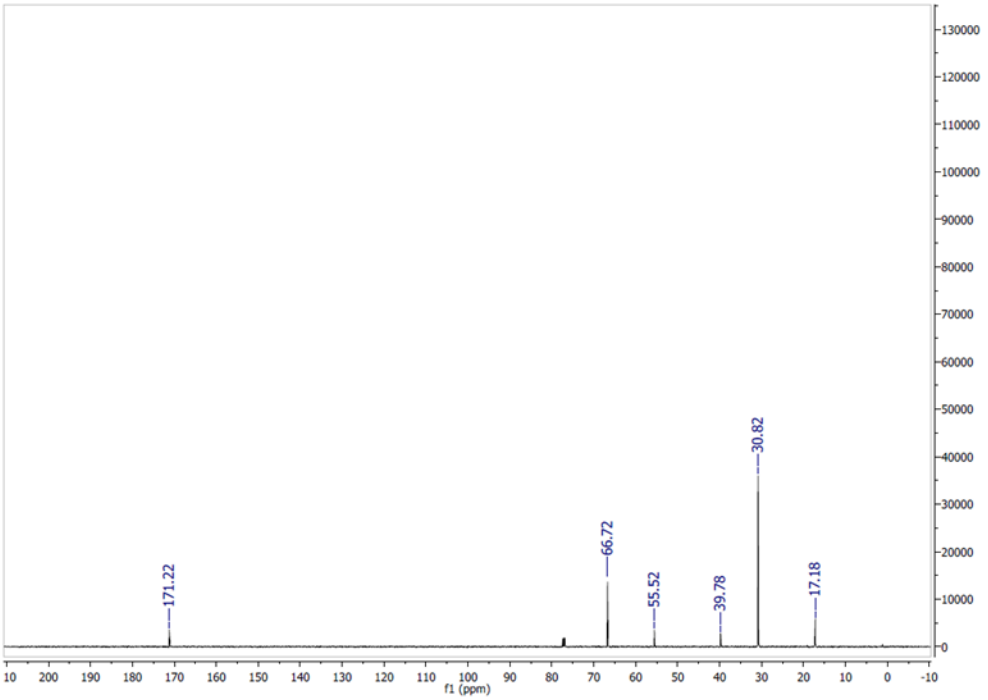
171.22
66.72
55.52
39.78
30.82
17.18
f1 (ppm)

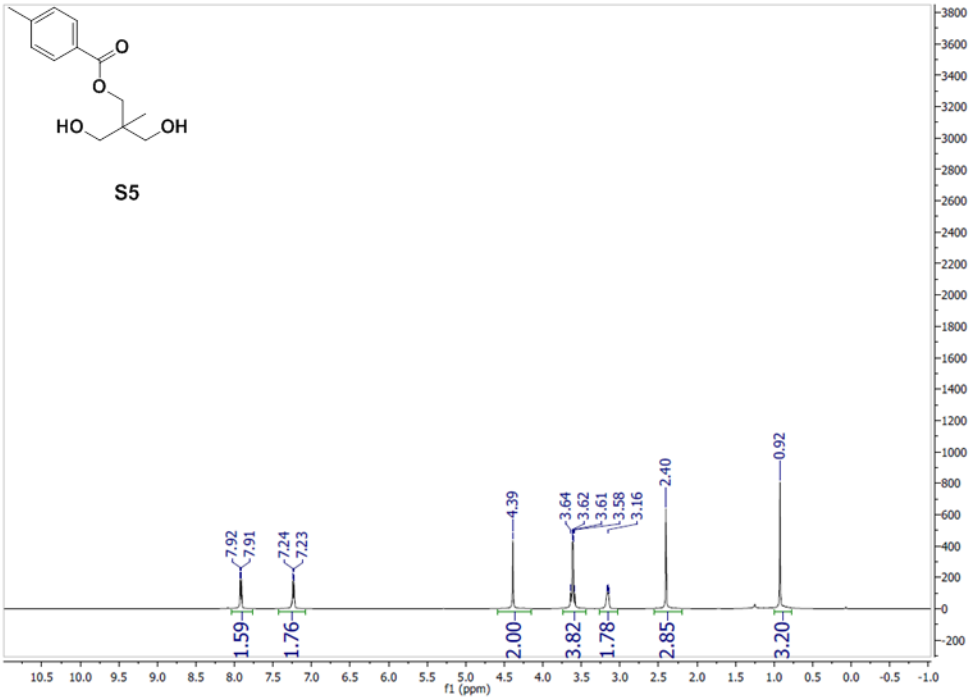
HO
OH
O
O
S5
7.92
7.91
7.24
7.23
4.39
3.64
3.62
3.61
3.58
3.16
2.40
0.92
1.59
1.76
2.00
3.82
1.78
2.85
3.20
f1 (ppm)

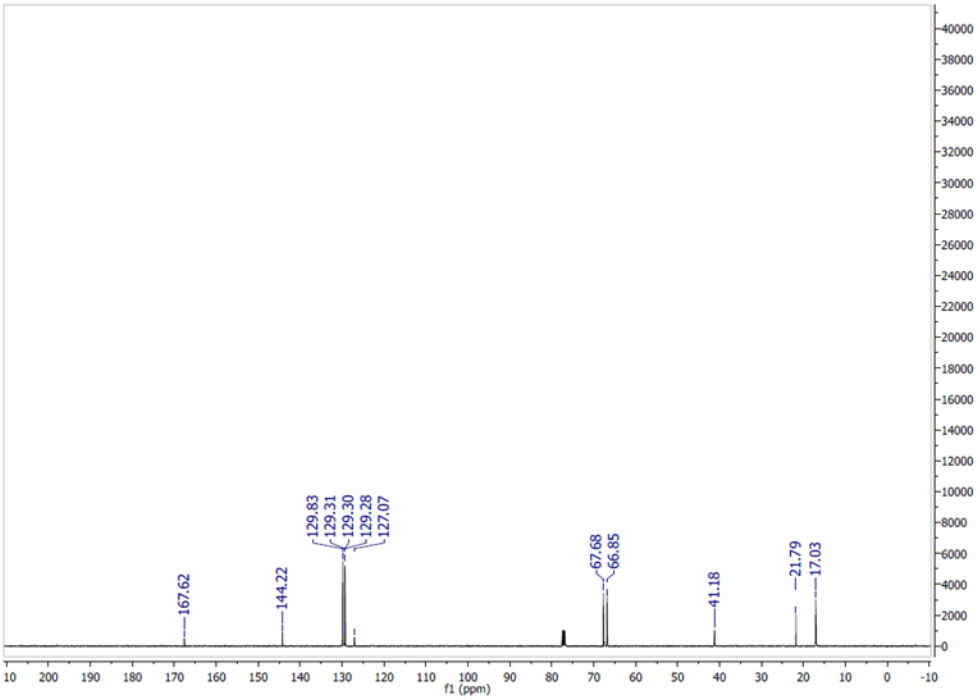
167.62
144.22
129.83
129.31
129.30
129.28
127.07
67.68
66.85
41.18
21.79
17.03
f1 (ppm)

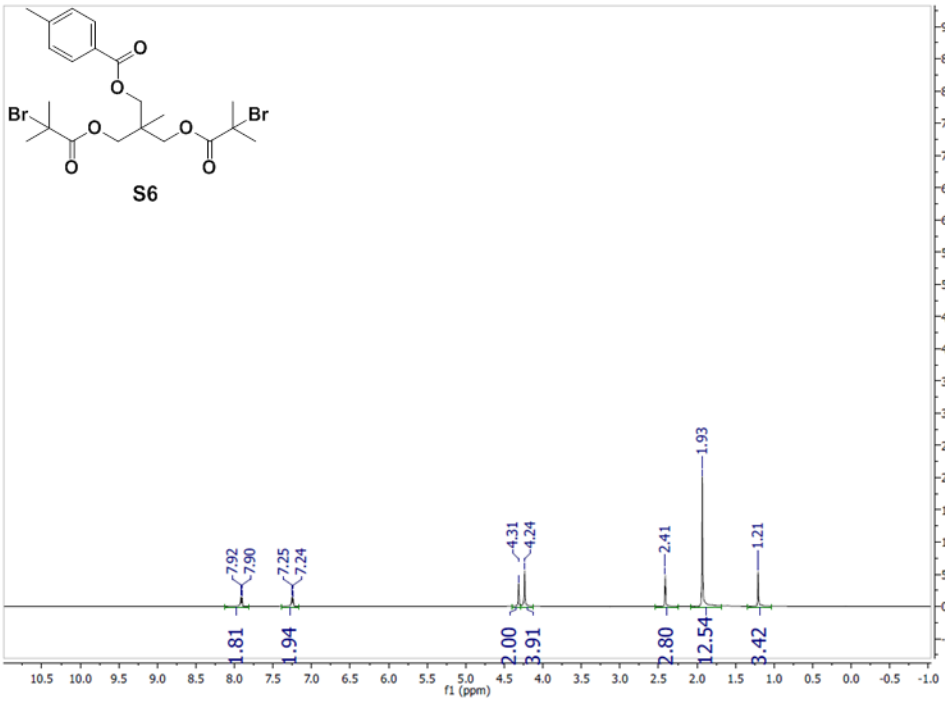
Br
Br
O
O
O
O
O
O
S6
7.92
7.90
7.25
7.24
4.31
4.24
2.41
1.93
1.21
1.81
1.94
2.00
3.91
2.80
12.54
3.42
f1 (ppm)

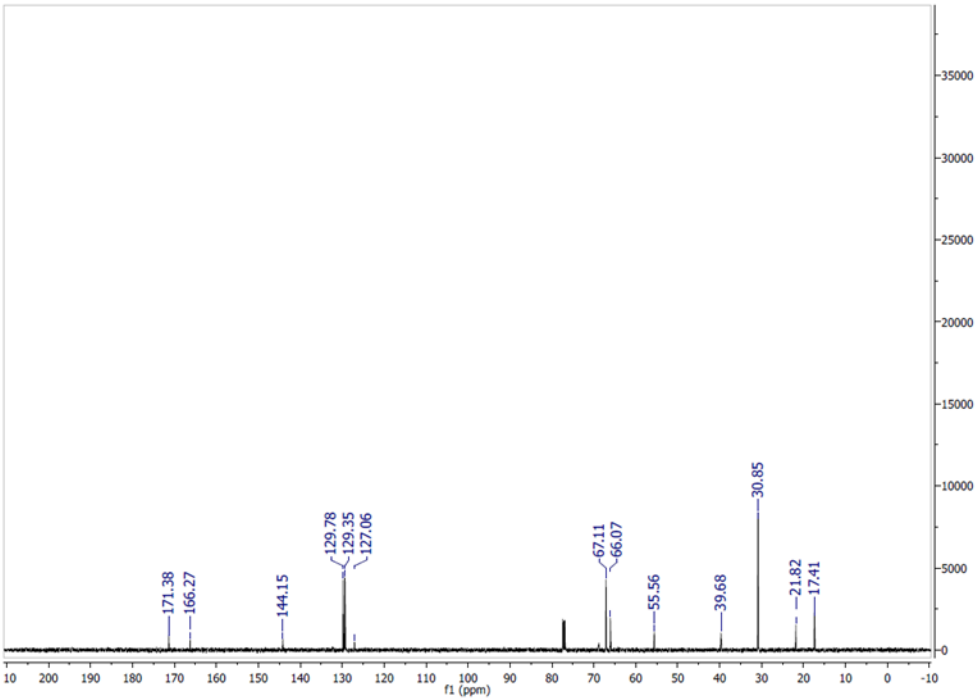
171.38
166.27
144.15
129.78
129.35
127.06
67.11
66.07
55.56
39.68
30.85
21.82
17.41
f1 (ppm)

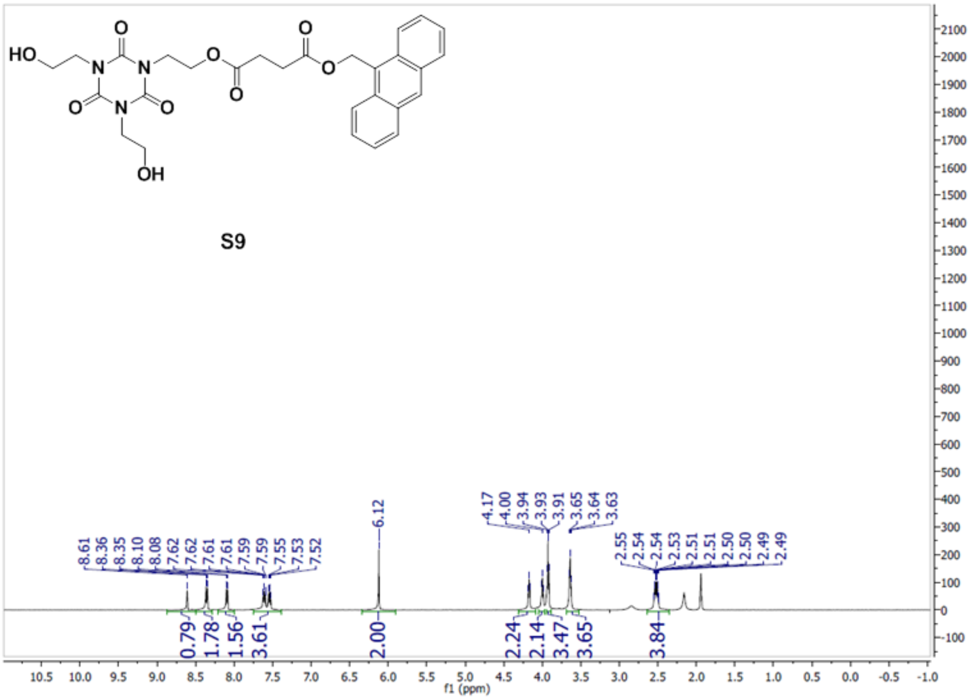
HO
OH
S9
8.61
8.36
8.35
8.10
8.08
7.62
7.61
7.61
7.59
7.59
7.55
7.53
7.52
6.12
4.17
4.00
3.94
3.93
3.91
3.65
3.64
3.63
2.55
2.54
2.54
2.53
2.51
2.51
2.50
2.50
2.49
2.49
0.79
1.78
1.56
3.61
2.00
2.24
2.14
3.47
3.65
3.84
f1 (ppm)

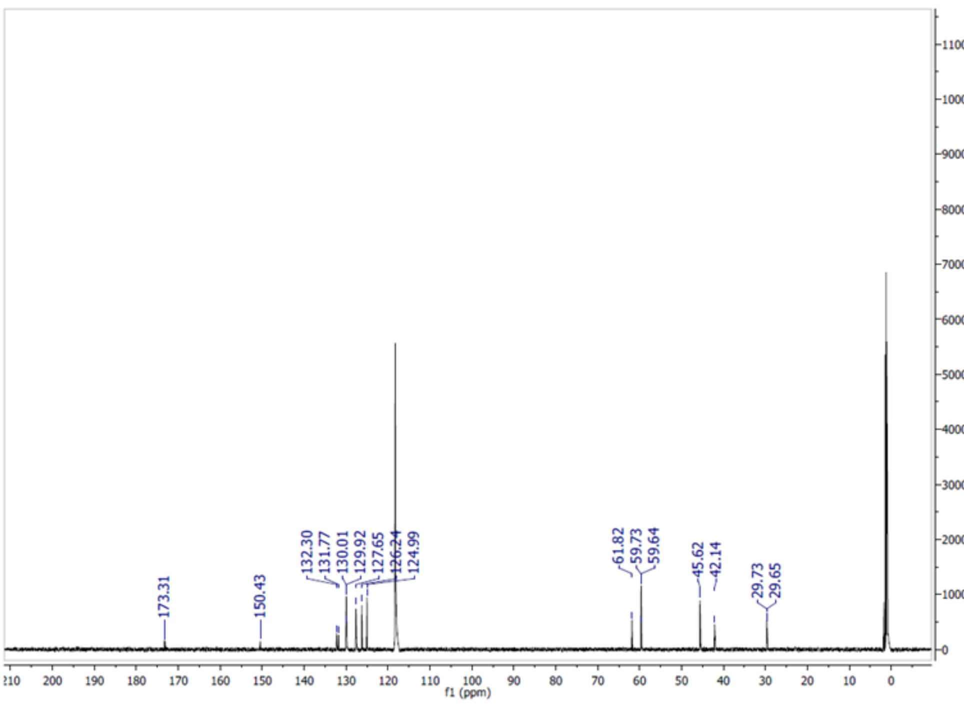
173.31
150.43
132.30
131.77
130.01
129.92
127.65
126.24
124.99
61.82
59.73
59.64
45.62
42.14
29.73
29.65
f1 (ppm)

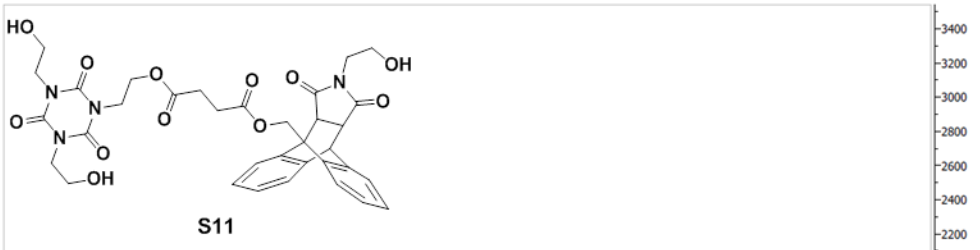
HO
OH
OH
O
N
O

S11

7.46
7.45
7.45
7.44
7.39
7.39
7.38
7.37
7.28
7.28
7.21
7.21
7.21
7.20
7.20
7.19
7.18
7.18
7.17
5.41
4.77
4.76
4.24
4.24
4.23
4.22
4.22
4.07
4.06
4.05
3.95
3.93
3.92
3.66
3.64
3.63
3.30
3.29
3.27
3.11
3.10
3.08
2.85
2.84
2.83
2.69
2.67
2.66
2.59
2.58
2.57
0.96
1.01
0.99
4.93
1.99
1.01
2.10
2.12
3.97
3.96
1.03
0.96
2.17
2.33
2.19
2.08
f1 (ppm)

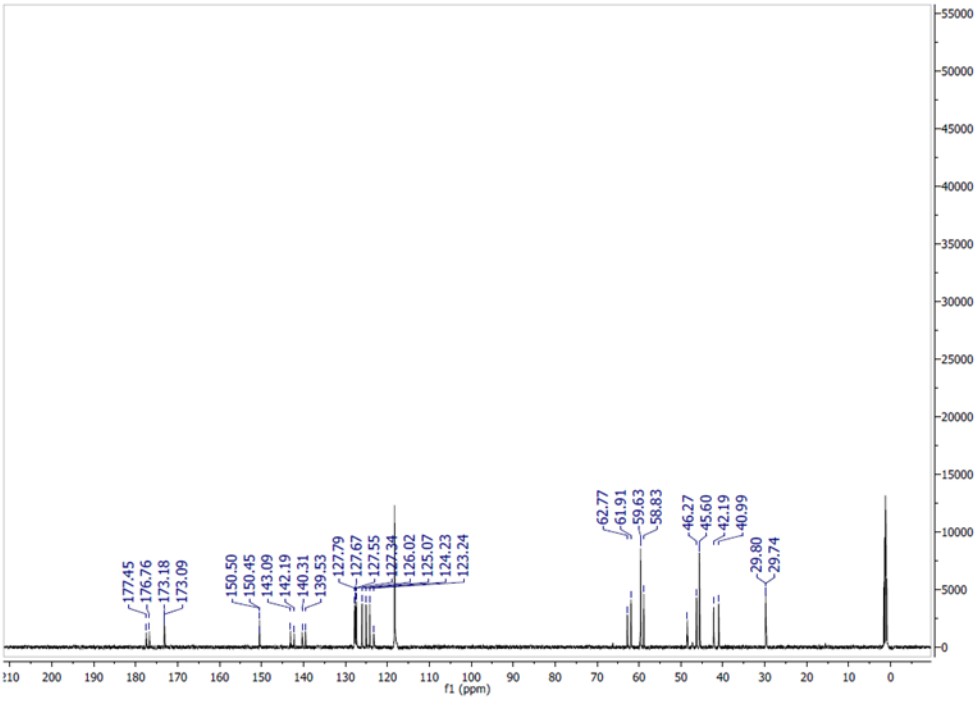
177.45
176.76
173.18
173.09
150.50
150.45
143.09
142.19
140.31
139.53
127.79
127.67
127.55
127.34
126.02
125.07
124.23
123.24
62.77
61.91
59.63
58.83
46.27
45.60
42.19
40.99
29.80
29.74
f1 (ppm)

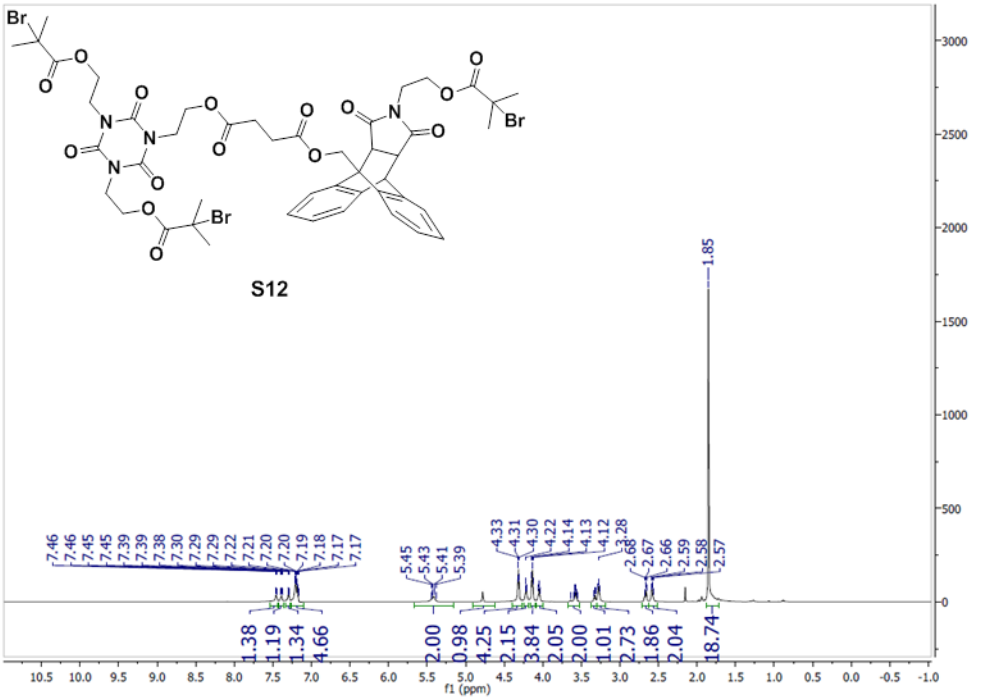
Br
Br
Br
S12
1.85
7.46
7.46
7.45
7.45
7.39
7.39
7.38
7.30
7.29
7.29
7.22
7.21
7.20
7.20
7.19
7.18
7.17
7.17
5.45
5.43
5.41
5.39
4.33
4.31
4.30
4.22
4.14
4.13
4.12
3.28
2.68
2.67
2.66
2.59
2.58
2.57
1.38
1.19
1.34
4.66
2.00
0.98
4.25
2.15
3.84
2.05
2.00
1.01
2.73
1.86
2.04
18.74
f1 (ppm)

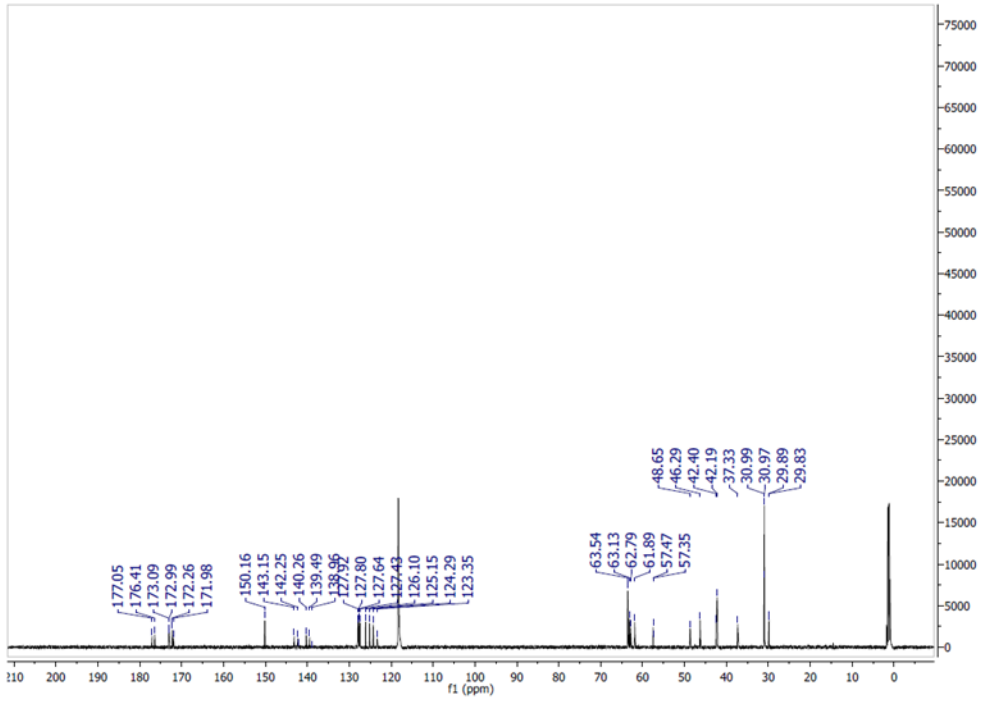
177.05
176.41
173.09
172.99
172.26
171.98
150.16
143.15
142.25
140.26
139.49
138.96
127.92
127.80
127.64
127.43
126.10
125.15
124.29
123.35
63.54
63.13
62.79
61.89
57.47
57.35
48.65
46.29
42.40
42.19
37.33
30.99
30.97
29.89
29.83
f1 (ppm)

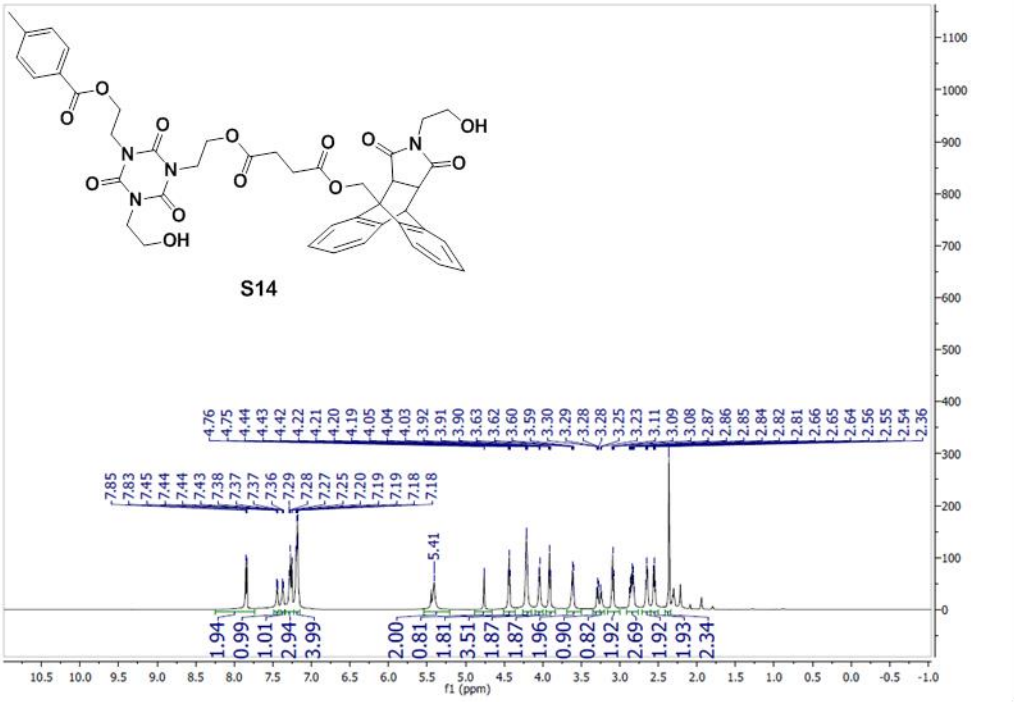
S14
4.76 4.75 4.44 4.43 4.42 4.22 4.21 4.20 4.19 4.05 4.04 4.03 3.92 3.91 3.90 3.63 3.62 3.60 3.59 3.30 3.29 3.28 3.25 3.23 3.11 3.09 3.08 2.87 2.86 2.85 2.84 2.82 2.81 2.66 2.65 2.64 2.56 2.55 2.54 2.36
7.85 7.83 7.45 7.44 7.44 7.43 7.38 7.37 7.37 7.36 7.29 7.28 7.27 7.25 7.20 7.19 7.19 7.18 7.18
5.41
1.94 0.99 1.01 2.94 3.99 2.00 0.81 1.81 3.51 1.87 1.87 1.96 0.90 0.82 1.92 2.69 1.92 1.93 2.34
f1 (ppm)

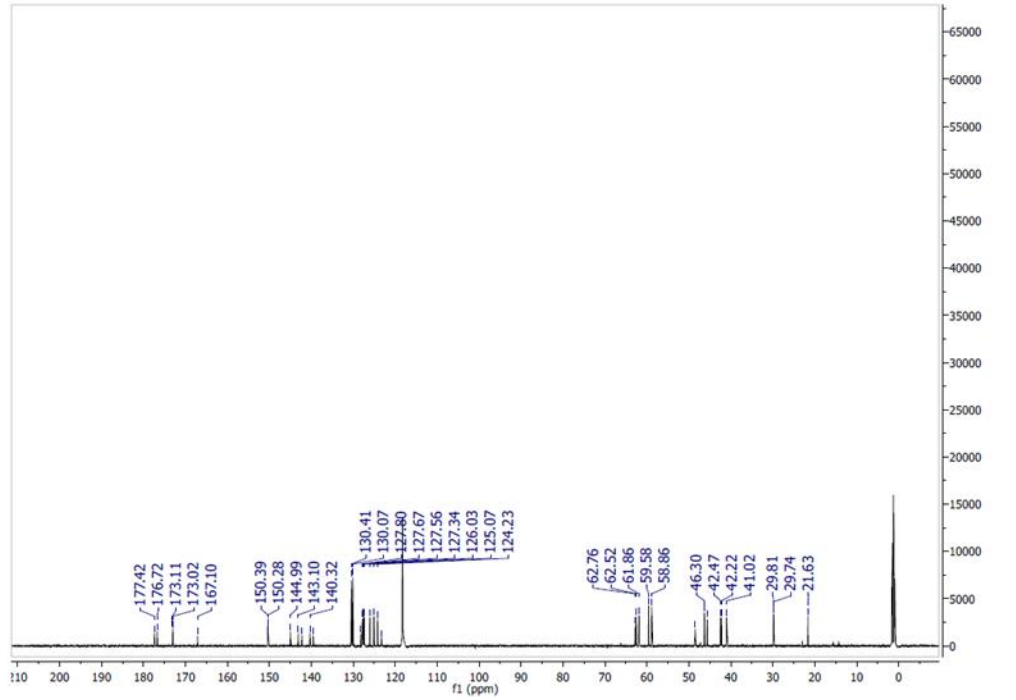
177.42 176.72 173.11 173.02 167.10
150.39 150.28 144.99 143.10 140.32
130.41 130.07 127.80 127.67 127.56 127.34 126.03 125.07 124.23
62.76 62.52 61.86 59.58 58.86
46.30 42.47 42.22 41.02
29.81 29.74 21.63
f1 (ppm)

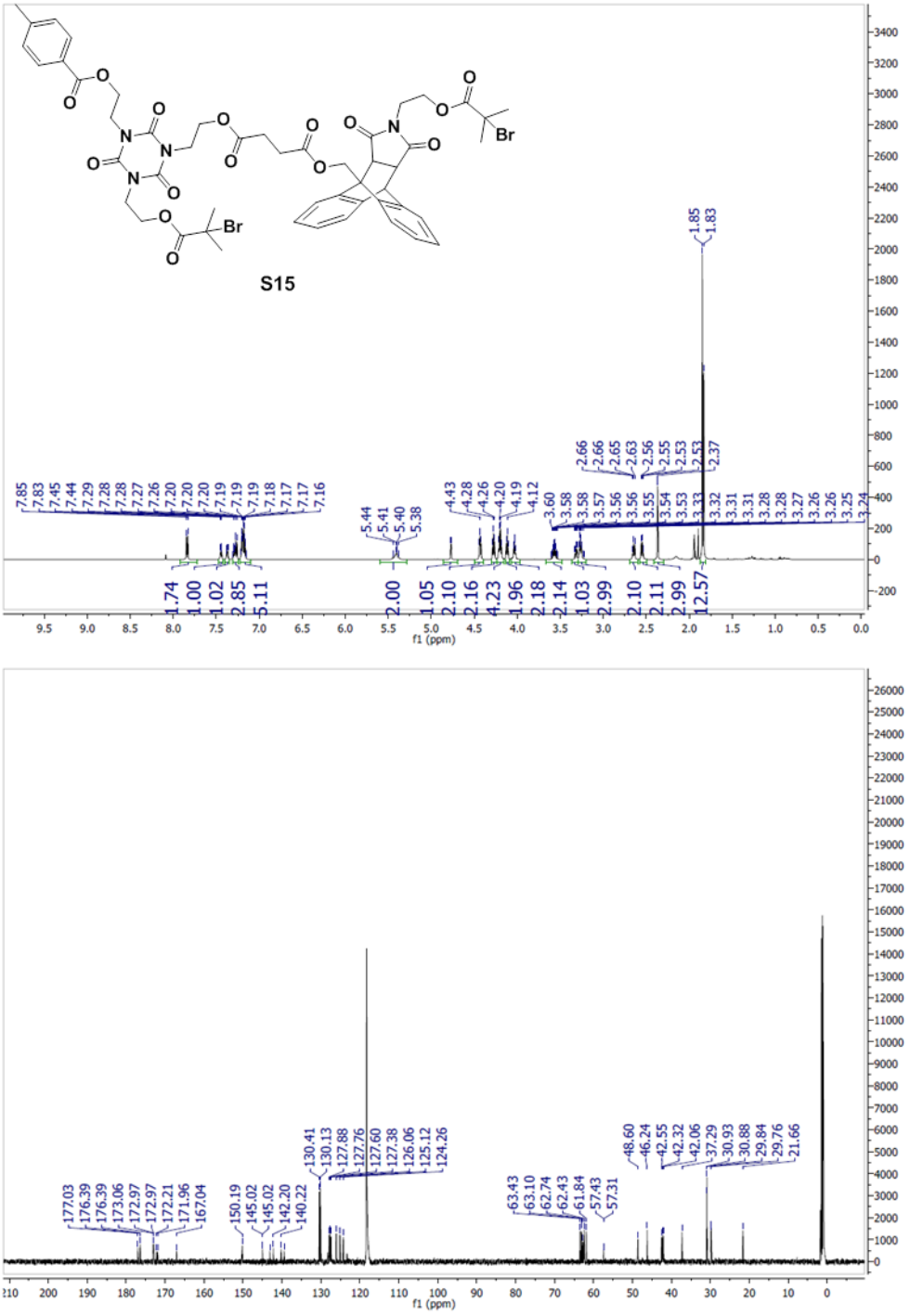

6.5.22 *Experimental References*

1) Potisek, S. L.; Davis, D. A.; Sottos, N. R.; White, S. R.; Moore, J. S. *J. Am. Chem. Soc.* **2007**, *129*, 13808.

2) Lei, X.; Porco, Jr., J. A.; *Org. Lett.* **2004**, 6, 795.

3) Heath, W. H.; Palmieri, F.; Adams, J. R.; Long, B. K.; Chute, J.; Holcombe, T. W.; Zieren, S.; Truitt, M. J.; White, J. L.; Willson, C. G. *Macromolecules* **2008**, *3*, 719.

4) Nikitas, P.; Pappa-Louisi, A.; Papageorgiou, A. *J. Chrom. A* **2001**, *912*, 13.

Chapter 7. MECHANOCHEMICAL REACTIVITY OF 1,2-OXAZINES AND POTENTIAL APPLICATIONS

7.1 INTRODUCTION

Polymer mechanochemistry has become an established field in recent years with the overarching goal of obtaining new mechanoresponsive polymeric materials.[1] Self-healing materials, mechanoresponsive drug delivery platforms, and strain-sensing materials are just some of the purported applications that could arise from continued development in this area. The crux on which these potential applications rely upon is the utility of mechanically-sensitive moieties termed "mechanophores".[2] These mechanophores can undergo various strain-induced transformations such as homolytic scission,[3] ring-opening[4] and cycloreversion[5] reactions. To ensure the continued growth of this field, new mechanosensitive moieties capable of triggering unique responses must be developed.

Recently, our research has focused on the study of 1,2-oxazines for thermally responsive materials.[6] These moieties can undergo a thermally induced [4 + 2] cycloreversion at relatively moderate temperatures to release a diene and nitroso dienophile (Scheme 7.1).[7] By tuning the diene and nitroso moiety, the thermal barrier for the retro Diels–Alder reaction can be attenuated and affords high modularity to this system. These moieties have already been demonstrated to have interesting capabilities in the context of polymer chemistry. For example, we have harnessed the unique breakdown pathway of N-carbonyl functionalized 1,2-oxazines to thermally trigger depolymerization of a polycarbamate at physiological conditions (Scheme 7.2A).[6c] Read de Alaniz has demonstrated that these moieties can be used towards polymer conjugation via a diene exchange at mild temperatures (Scheme 7.2B).[8]

Scheme 7.1. Reversibility of 1,2-oxazines.

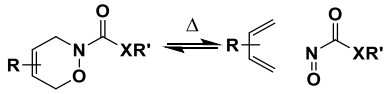

Inspired by the thermal activation of 1,2-oxazines at relatively moderate temperatures as well as the precedent for Diels–Alder adducts to undergo mechanochemically-induced [4 + 2] cycloreversion reactions,[5f] we decided to examine the potential of 1,2-oxazines as a mechanophore. We find these Diels–Alder adducts particularly interesting due to the asymmetry of the moiety compared to previously examined [4 + 2] adducts, such as the furan-maleimide adducts studied by Bielawski and coworkers. We suspect that the reactivity resulting from elongation of the *distal* isomer should differ from that of the *proximal* isomer (Scheme 7.2C). The mechanochemical consequences of polymer attachment and elongation across a mechanophore has been previously explored, both experimentally and computationally, in a variety of different systems.[4a,4h,9] Our findings will further compliment the growing understanding of the structure-mechanochemical activity relationships that affect the mechanical activation of mechanophores. Furthermore, these 1,2-oxazine adducts are unique with respect to other mechanophores in their potential to trigger further downfield processes such as self-immolative polymer depolymerizations.[6c]

Scheme 7.2. Precedence and current work on stimuli-responsive 1,2-oxazine-containing polymers.

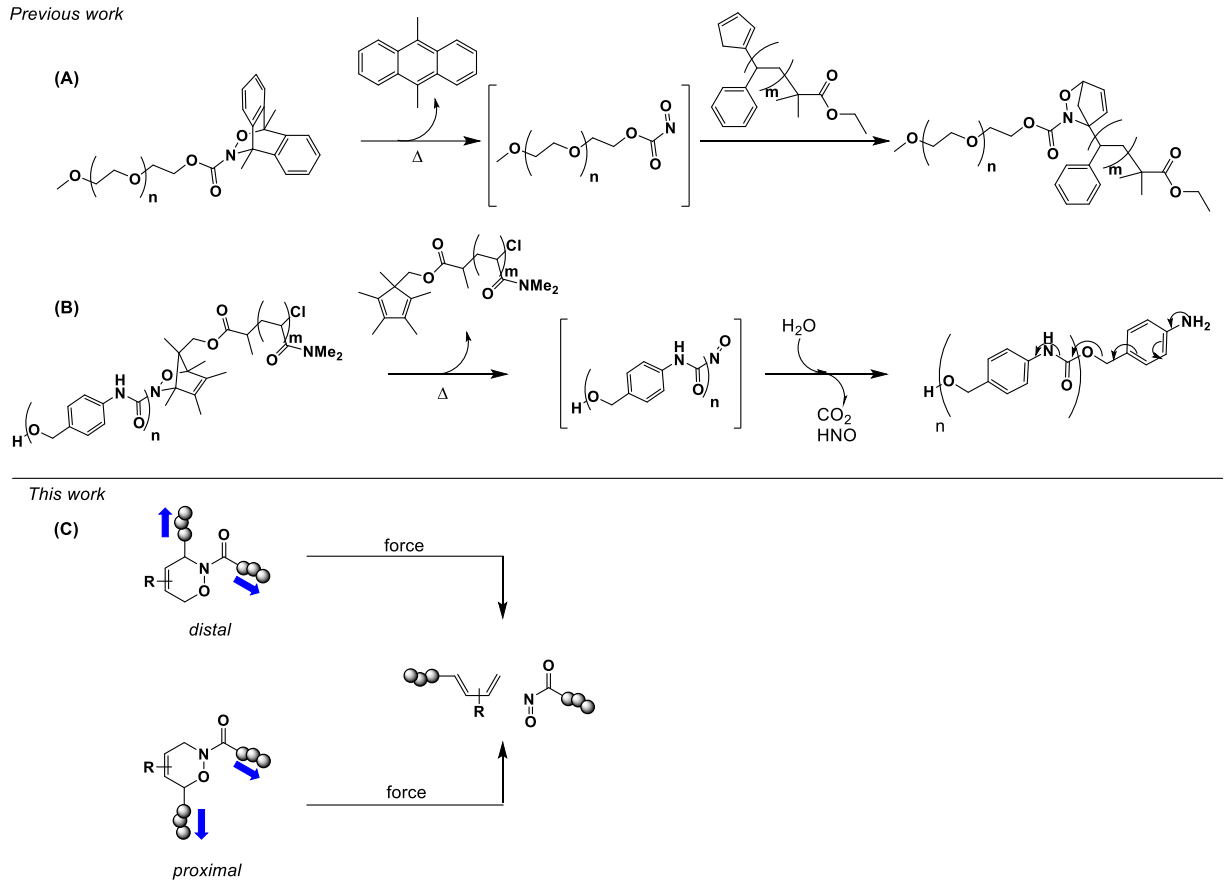

7.2 Mechanochemical Reactivty of 1,2-Oxazines

We initially examined the mechanochemical reactivity of the *distal* and *proximal* isomers of both mono- and disubstituted oxazine adducts computationally via the constrained geometries simulate external force (CoGEF) computational technique.[10] In this method the distance between two anchor nuclei on the molecule of study is increased in a step-by-step manner, mimicking mechanochemical elongation. The barrier to bond scission can thus be estimated as the potential energy of the molecule just prior to bond cleavage.

By increasing the distance between the terminal oxygens of the 1,2-oxazine consistent with the *distal* isomer, **Ox1**-*distal* (Figure 7.1), we observed that the activation barrier to [4 + 2] cycloreversion was ~55 kcal/mol. By comparison, elongation of the **Ox1**-*proximal* adduct revealed that the barrier to cycloreversion was ~60 kcal/mol higher than the *distal* isomer. This trend holds true when we apply it to disubstituted oxazines, **Ox2**-*distal* and **Ox2**-*proximal*, which collectively are slightly more susceptible to cycloreversion than their monosubstituted counterparts by ~5 kcal/mol (Table 7.1).

It must also be noted that there is currently no method to accurately model elongation from three points across a given mechanophore such as in a star polymer containing **Ox3** at its center. Therefore, conclusions regarding its susceptibility to cycloreversion cannot at this time be determined computationally, but was an intriguing consideration experimentally. Our previous work demonstrated that there is no apparent additive effect on scission rates when a mechanophore is placed within a star polymer versus in a linear polymer topology when both polymers have identical $M_{n,arm}$.[11] Based on these previous results, one would expect polymers containg **Ox2** or **Ox3** should have identical scission rate constants as long as both polymers have identical $M_{n,arm}$.

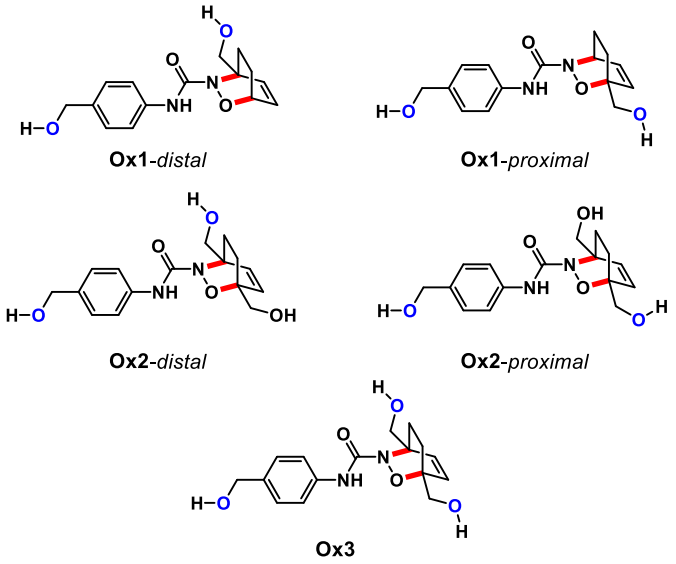

Figure 7.1. Model compounds for CoGEF calculations. Blue oxygen atom indicates points for elongation *in silico.*

Table 7.1. CoGEF determined force-induced activation of **Ox1** and **Ox2** isomers.

Oxazine	E_A (kcal/mol)
Ox1-distal	54.6
Ox1-proximal	113.0
Ox2-distal	50.2
Ox2-proximal	100.4

Ox1, **Ox2**, **Ox3**, and **Ox4** were synthesized by the in situ oxidation of the hydroxyurea component in the presence of the corresponding diene to form the Diels–Alder adduct (Scheme 7.3). In the case of **Ox1**, the *distal* and *proximal* isomers were separated by straightforward column chromatography. For **Ox2**, a mono-protected 1,3-cyclohexadiene-1,4-diol using the bulky trityl protecting group was used for the Diels–Alder reaction, which gave exclusively a single isomer. **Ox2-***distal* and **Ox2-***proximal* could then be obtained by alternating the order in which the polymerization initiator and pivaloyl chloride-capping moieties were installed.

Scheme 7.3. Synthesis of **Ox1**, **Ox2** and **Ox3**.

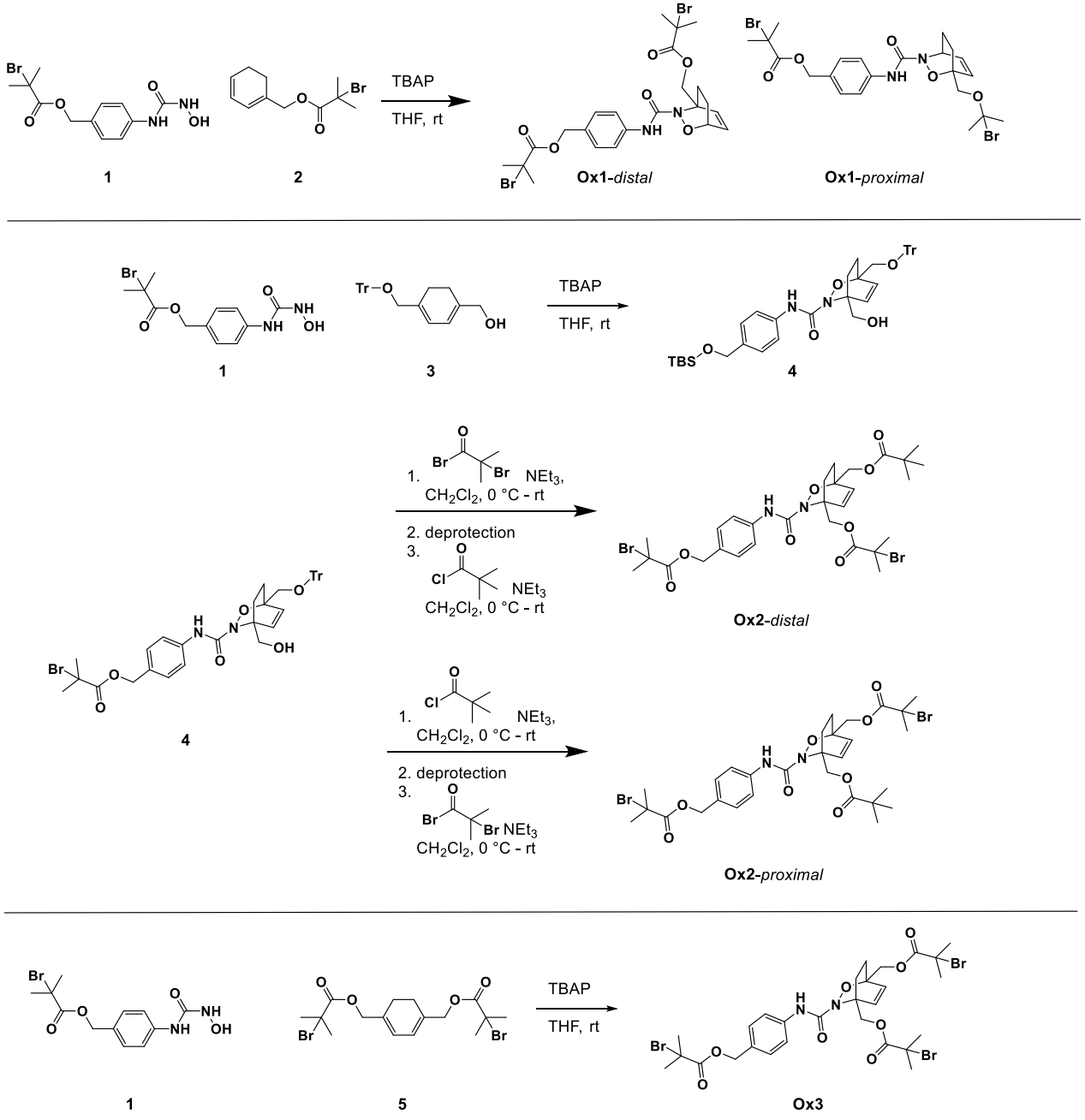

PolyOx1-*distal*, **polyOx1**-*proximal*, **polyOx2**-*distal* and **polyOx2**-*proximal* were synthesized via atom transfer radical polymerization (ATRP) from their respective initiators (See Supporting Information), producing polymers of ~60 kDa and narrow dispersity. P**olyOx3** was similarly synthesized by ATRP, however, with a molecular weight of ~90 kDa. Previously we

demonstrated that kinetic degradation comparisons of polymers with star and linear topologies must examine polymers with identical $M_{n,arm}$ as opposed to total molecular weight.[11] Control polymers **polyOx4** and **poly5** were also synthesized. In **polyOx4**, the oxazine should undergo no activation due to its terminal location on the polymer chain end and therefore should have a slower degradation kinetic profile than a oxazine-centered polymer. For **poly5** we wanted to verify that the carbamate-like linkage of the oxazine was not susceptible to preferential chain scission. Figure 7.2 summarizes the structure of polymers studied.

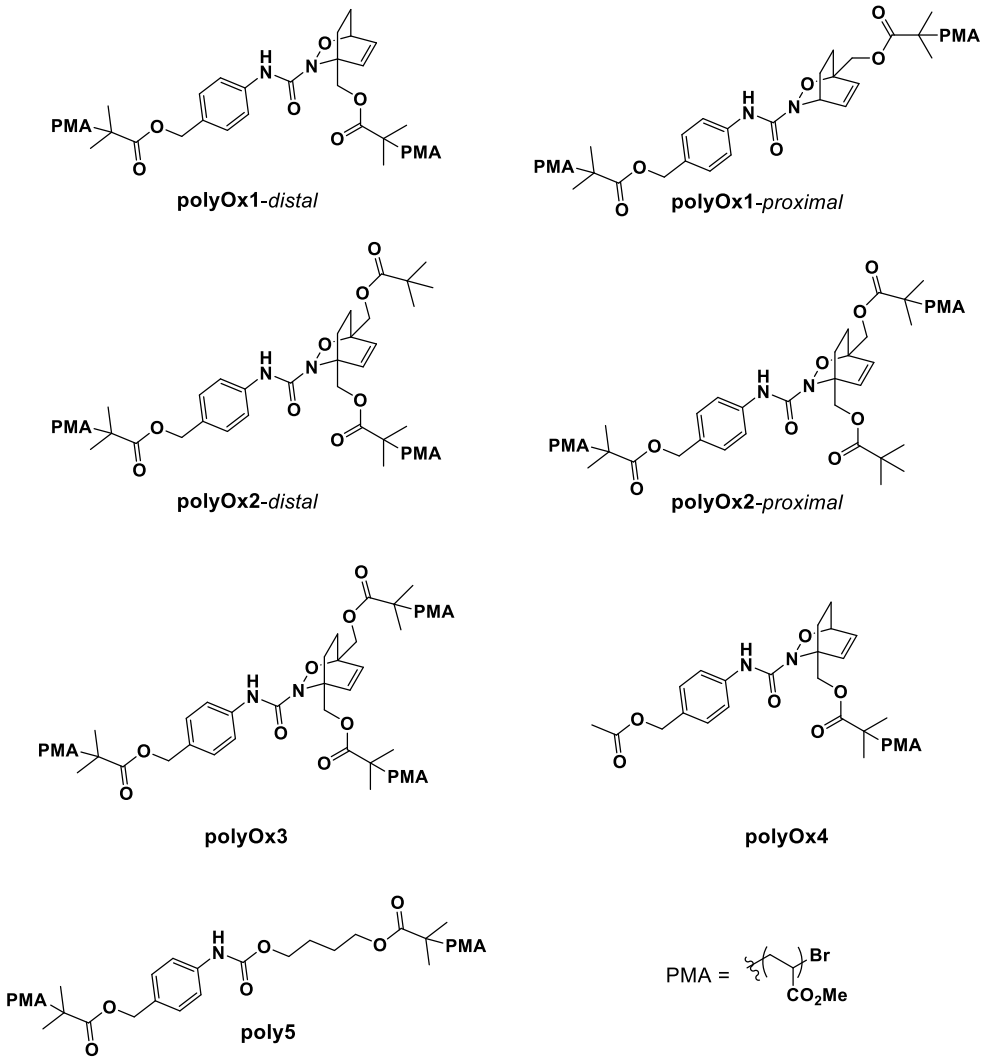

Figure 7.2. Structures of 1,2-oxazine containing polymers and control polymers.

Each polymer was sonicated in dry, N_2-purged THF at 13.8 W/cm^2 and its degradation was monitored by size exclusion chromatography (SEC) with in-line multi-angle light scattering (MALS) and refractive index (RI) detector. The first-order rate constant for polymer degradation was determined by monitoring the depletion of the RI intensity corresponding to the P_{max} retention time of the parent polymer chromatogram as a function of sonication time.[12] The results obtained thus far are summarized in Table 7.2.

Table 7.2. Summary of k_{RI} for mechanochemical chain scission of control and oxazine-containing polymers.

Polymer	$M_{n,total}$ (kDa)	$M_{n,arm}$ (kDa)	k_{RI} ($\times 10^{-2}$ min^{-1})
polyOx1-proximal	59.2	29.6	0.99 ± 0.09
polyOx1-*distal*	59.3	29.6	1.06 ± 0.06
polyOx3	90.7	30.2	1.35 ± 0.08
polyOx4	59.4	29.7	0.83 ± 0.06
poly5	57.8	28.9	0.83 ± 0.02

M_{total} (M_n values) determined by GPC analysis using multi-angle laser light scattering (MALS) to give M_w values from which M_n values were calculated. Rate constants were calculated from linear regression of the RI signal intensity at the M_p retention time of the virgin sample versus ultrasonication "on time" and are an average of three runs ± one standard deviation.

PolyOx4 in which the oxazine mechanophore is placed at the non-mechanochemically active polymer chain end and **poly5** in which no mechanophore is present at all, expectedly have identical chain scission rate constants of 0.83 × 10^{-2} min^{-1}. In the case of **poly5**, it is important to note that the presence of the centrally located carbamate linkage provides no preferential rate enhancement to chain scission.

Both **polyOx1** isomers displayed faster chain scission rate constants than the control polymers. Specifically, **polyOx1**-*proximal* had a rate constant of polymer breakdown of 0.99 × 10^{-2} min^{-1} while **polyOx1**-*distal* isomer had a slightly faster rate constant of 1.06 × 10^{-2} min^{-1}, in line with the relative cycloreversion activation barriers derived by CoGEF. The rate enhancement (~1.3 fold) of the latter relative to control polymers **polyOx4** and **poly5** is consistent with previous reports comparing polymer chain scission with and without a single chain-centered mechanophores under sonication conditions.[5h,11a] The similarities in rate constants of the **polyOx1** isomers, despite the large differences in activation energies to cycloreversion derived *in silico*, may be due to shortcomings of the CoGEF computational method.

PolyOx3 had an increased rate constant for polymer breakdown of 1.35 × 10^{-2} min^{-1}, a ~1.3 fold rate enhancement over **polyOx1** and ~1.6 fold enhancement over the control polymers. Analysis of polymer breakdown for **polyOx2** is necessary before any meaningful conclusions can be made about this result.

To confirm that the enhanced scission rate is due to oxazine cycloreversion, trapping studies were conducted via the in situ oxidation of **Pyr-HU** in the presence of sonicated solutions of **polyOx1**-*distal* and **polyOx4 (**Figure 7.3A). After subsequent purification of excess small molecule (see Supplementary Information), photoluminescent measurements of the resulting polymer solutions clearly display a signal consistent with the pyrene fluorescent tag for the sonicated solution of **polyOx1**-*distal* while **polyOx4** displayed a complete absence of this signal (Figure 7.3B). This further corroborates the mechanochemically-induced cycloreversion of 1,2-oxazines as activation occurs only when the adduct is placed centrally within a polymer chain where the forces are greatest.

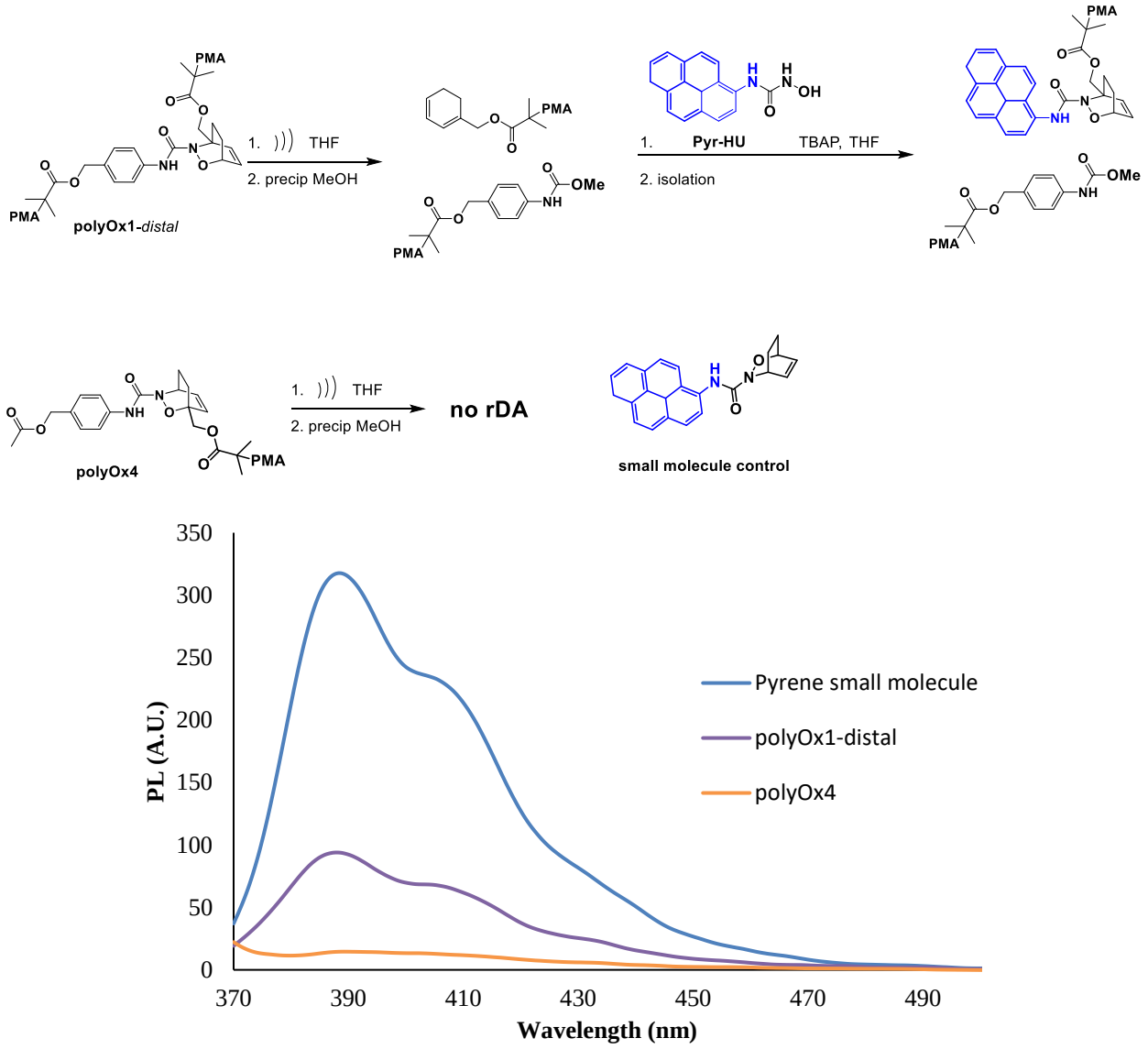

Figure 7.3. A) Reaction scheme for in situ oxidation and tagging of liberated diene with **Pyr-HU**. B) Photoluminescent spectra of sonicated solutions of **polyOx1** and **polyOx4** in THF.

7.3 Mechanochemical Oxazine Activation for SIP Depolymerization

Thus far we have demonstrated that the 1,2-oxazine moiety appears to be a tunable, mechanoresponsive moiety analogous to previously explored [4 + 2] cycloreversion adducts such as those developed by Bielawski and coworkers. However, the mechanochemical activation of

1,2-oxazines offers additional functionality compared to previously explored mechanoresponsive Diels–Alder adducts.

We have previously demonstrated that cyclopentadiene-based 1,2-oxazine adducts can be used as thermal triggers for self-immolative polymers (SIPs). Upon thermal cycloreversion of these adducts and uncovering of the nitrosocarbonyl intermediate, subsequent hydrolysis and decarboxylation to release a free aniline can be utilized to trigger a series of 1,6-eliminations to depolymerize the polymer chain (Scheme 7.4). Initial evidence suggests that 1,2-oxazine adducts are mechanochemically active and therefore it is conceivable that mechanical stimuli could also be used to trigger a head-to-tail SIP depolymerization process.

Scheme 7.4. Mechanochemical activation of SIPs for head-to-tail depolymerization.

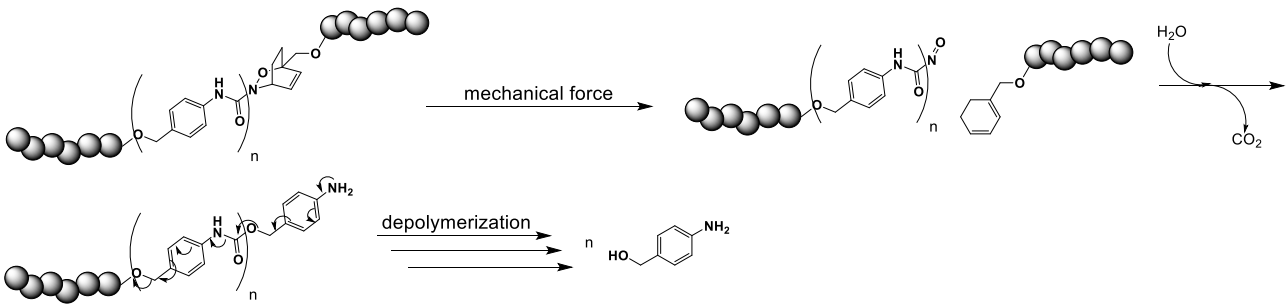

7.4 Conclusions for Mechanochemical Activation of 1,2-Oxazines

Preliminary evidence has been obtained that suggests the 1,2-oxazine moiety is mechanochemically active. Polymers that contain a chain-centered 1,2-oxazine degrade more rapidly under ultrasonic conditions than polymers in which this moiety is absent or at the chain end. Furthermore, trapping studies suggest that these enhancements in the rate of chain scission is due to cycloreversion of the 1,2-oxazine DA adduct. Full understanding of the structural

properties that affect the mechanochemical activation of 1,2-oxazines will be vital for future applications of this mechanophore.

These adducts could make valuable contributions to the field of self-healing materials. Mechanical deformation of the material would mediate the cycloreversion process while spontaneous self-healing could occur under mild conditions once the mechanical load is removed. Comparatively, the formation of the widely utilized furan-maleimide DA adduct requires temperatures near 70 °C for rapid adduct formation and material self-healing. Another unique characteristic of 1,2-oxazines is its ability to trigger SIP depolymerization upon cycloreversion and release of the nitrosocarbonyl dienophile. This property could be harnessed for a unique new class of mechanically degradable materials.

7.5 References

1) For recent reviews, see: (a) Larsen, M. B.; Boydston, A. J. *Macromol. Chem. Phys.* **2016**, *217*, 354. (b) Sottos, N. R. *Nat. Chem.* **2014**, *6*, 381. (c) Brantley, J. N.; Bailey, C. B.; Wiggins, K. M.; Keatinge-Clay, A. T.; Bielawski, C. W. *Polym Chem.* **2013**, *4*, 3916. (d) May, P. A.; Moore, J. S. *Chem. Soc. Rev.* **2013**, *42*, 7497. (e) Wiggins, K. M.; Brantley, J. N.; Bielawski, C. W. *Chem. Soc. Rev.* **2013**, *42*, 7130. (f) Groote, R.; Jakobs, R. T. M.; Sijbesma, R. P. *Polym. Chem.* **2013**, *4*, 4846. (g) Brantley, J. N.; Wiggins, K. M.; Bielawski, C. W. *Polym. Int.* **2013**, *62*, 2 (h) Ariga, K.; Mori, T.; Hill, J. P. *Adv. Mater.* **2012**, *24*, 158. (i) Boulatov, R. *Pure Appl. Chem.* **2011**, *83*, 25. (j) Caruso, M. M.; Davis, D. A.; Shen, Q.; Odom, S. A.; Sottos, N. R.; White, S. R.; Moore, J. S. *Chem. Rev.* **2009**, *109*, 5755. (k) Beyer, M. K.; Clausen-Schaumann, H. *Chem. Rev.* **2005**, *105*, 2921.

2) Li, J.; Ngamani, C.; Moore, J. *Acc. Chem. Res.* **2015**, *48*, 2818.

3) (a) Verstraeten, F.; Göstl, R.; Sijbesma, R. P. *Chem. Commun.* **2016**, *52*, 8608. (b) Imato, K.; Irie, A.; Kosuge, T.; Ohishi, T.; Nishihara, M.; Takahara, A.; Otsuka, H. *Angew. Chem. Int. Ed.* **2015**, *54*, 6168. (c) Imato, K.; Kanehara, T.; Ohishi, T.; Nishihara, M.; Yajima, H.; Ito, M.; Takahara, A.; Otsuka, H. *ACS Macro Lett.* **2015**, *4*, 1307. (d) Li, Y.; Nese, A.; Lebedeva, N. V.; Davis, T.; Matyjaszewski, K.; Sheiko, S. S. *J. Am. Chem. Soc.* **2011**, *133*, 17479. (e) Sheiko, S. S.; Sun, F. C.; Randall, A.; Shirvanyants, D.; Rubinstein, M.; Lee, H-i.; Matyjaszewski, K. *Nature* **2006**, *440*, 191. (f) Berkowski, K. L. Potisek, S. L.; Hickenboth, C. R; Moore, J. S. *Macromolecules* **2005**, *38*, 8975. (g) Encina, M. V.; Lissi, E.; Sarasua, M.; Gargallo, L.; Radic, D. J. *Polym. Sci., Polym. Lett. Ed.* **1980**, *18*, 757.

4) (a) Robb, M. J.; Kim, T. A.; Halmes, A. J.; White, S. R.; Sottos, N. R.; Moore, J. S. *J. Am. Chem. Soc.* **2016**, DOI: 10.1021/jacs.6b07610. (b) Zhang, H.; Gao, F.; Cao, X.; Li, Y.; Xu, Y.; Weng, W.; Boulatov, R. *Angew. Chem. Int. Ed.* **2016**, *55*, 3040. (c) Wang, Z.; Ma, Z.; Wang, Y.; Xu, Z.; Luo, Y.; Wei, Y.; Jia, X. *Adv. Mater.* **2015**, *27*, 6469. (d) Diesendruck, C. E.; Steinberg, B. D.; Sugai, N.; Silberstein, M. N.; Sottos, N. R.; White, S. R.; Braun, P. V.; Moore, J. S. *J. Am. Chem. Soc.* **2012**, *134*, 12446. (e) Klukovich, H. M.; Kean, Z. S.; Ramirez, A. L. B.; Lenhardt, J. M.; Lin, J. X.; Hu, X. Q.; Craig, S. L. *J. Am. Chem. Soc.* **2012**, *134*, 9577. (f) Lenhardt, J. M.; Black, A. L.; Craig, S. L. *J. Am. Chem. Soc.* **2009**, *131*, 10818. (g) Davis, D.A.; Hamilton, A.; Yang, J.; Cremar, L.D.; Gough, D.V.; Potisek, S. L.; Ong, M. T.; Braun, P. V.; Martínez, T. J.; White, S. R.; Moore, J. S.; Sottos, N. R. *Nature* **2009**, *459*, 68. (h) Hickenboth, C. R.; Moore, J. S.; White, S. R.; Sottos, N. R.; Baudry, J.; Wilson, S. R. *Nature* **2007**, *446*, 423.

5) (a) Robb, M. J.; Moore, J. S. *J. Am. Chem. Soc.* **2015**, *137*, 4558. (b) Gossweiler, G. R.; Hewage, G. B.; Soriano, G.; Wang, Q. M.; Welshofer, G.W.; Zhao, X.H.; Craig, S.L. *ACS*

Macro Lett. **2014**, *3*, 216. (c) Larsen, M. B.; Boydston, A. J. *J. Am. Chem. Soc.* **2013**, *135*, 8189. (d) Chen, Y. L.; Spiering, A. J. H.; Karthikeyan, S.; Peters, G. W. M.; Meijer, E. W.; Sijbesma, R. P. *Nat. Chem.* **2012**, *4*, 559. (e) Kean, Z. S.; Ramirez, B.; Yan, Y. F.; Craig, S. L. *J. Am. Chem. Soc.* **2012**, *134*, 12939. (f) Wiggins, K. M.; Syrett, J. A.; Haddleton, D. M.; Bielawski, C. W. *J. Am. Chem. Soc.* **2011**, *133*, 7180. (g) Klukovich, H. M.; Kean, Z. S.; Lacono, S. T.; Craig, S. L. *J. Am. Chem. Soc.* **2011**, *133*, 17882. (h) Kryger, M.J.; Ong, M.T.; Odom, S.A.; Sottos, N.R.; White, S.R.; Martinez, T. J.; Moore, J. S. *J. Am. Chem. Soc.* **2010**, *132*, 4558.

6) (a) Church, D. C.; Nourian, S.; Lee, C.; Yakelis, N.; Toscano, J.; Boydston, A. J. *ACS Macro Lett.* **2017**, *6*, 46; (b) Kensy, V. K.; Peterson, G. I.; Church, D. C.; Yakelis, N. A.; Boydston, A. J. *Org. Biomol. Chem.* **2016**, 14, 5617. (c) Peterson, G. I.; Church, D. C.; Yakelis, N. A.; Boydston, A. J. *Polymer* **2014**, 55, 5980.

7) (a) Kirby, G.; Sweeny, J. *J. Chem. Soc., Perkins Trans 1* **1981**, 12, 3250. (b) Christie, C.; Kirby, G.; McGuigan, H.; Mackinnon, J. *J. Chem. Soc., Perkins Trans. 1* **1985**, 11, 2469. (c) Kirby, G.; McGuigan, H.; Mackinnon, J.; McLean, D.; Sharma, R. P. *J. Chem. Soc., Perkins Trans. 1* **1985**, 7, 1437. (d) Atkinson, R. N.; Storey, B. M.; King, S. B. *Tet. Lett.*, **1996**, 37, 9287. (e) Xu, Y.; Alavanja, M.; Johnson, V. L.; Yasaki, G.; Kings, S. B. *Tet. Lett.*, **2000**, 41, 4265

8) Samoshin, A. V.; Hawker, C. J.; Read de Alaniz, J. ACS Macro Lett. 2014, 3, 753.

9) (a) Kryger, M. J.; Munaretto, A. M.; Moore, J. S. *J. Am. Chem. Soc.* **2011**, *133*, 18992. (b) Kean, Z. S.; Niu, Z.; Hewage, G. B.; Rheingold, A. L.; Craig, S. L. *J. Am. Chem. Soc.* **2013**, *135*, 13598. (c) Wang, J.; Kouznetsova, T. B.; Niu, Z.; Ong, M. T.; Klukovich, H. M.; Rheingold, A. L.; Martinez, T. J.; Craig, S. L. *Nat. Chem.* **2015**, *7*, 323. (d) Dopieralski, P.;

Ribas-Arino, J.; Marx, D. *Angew. Chem., Int. Ed.* **2011**, *50*, 7105. (e) Gossweiler, G. R.; Kouznetsova, T. B.; Craig, S. L. *J. Am. Chem. Soc*. **2015**, *137*, 6148. (f) Smalø, H. S.; Uggerud, E. *Chem. Commun.* **2012**, *48*, 10443. (g) Jacobs, M. J.; Schneider, G.; Blank, K. G. *Angew. Chem., Int. Ed.* **2016**, *55*, 2899. (h) Konda, S. S. M.; Brantley, J. N.; Varghese, B. T.; Wiggins, K. M.; Bielawski, C. W.; Makarov, D. E. *J. Am. Chem. Soc.* **2013**, *135*, 12722. (i) Groote, R.; Szyja, B. M.; Leibfarth, F. A.; Hawker, C. J.; Doltsinis, N. L.; Sijbesma, R. P. *Macromolecules* **2014**, *47*, 1187.

10) Beyer, M. K. J. *Chem. Phys.* **2000**, *112*, 7307.

11) (a) Church, D. C.; Peterson, G. I.; Boydston, A. J. *ACS Macro Lett.* **2014**, *3*, 648. (b) Striegel, A. M. *J. Biochem. Biophys. Methods* **2003**, *56*, 117.

12) Florea, M. *J. Appl. Polym. Sci.* **1993**, *50*, 2039.

13) Li, H.; Göstl, R.; Delgove, M.; Sweeck, J.; Zhang, Q.; Sijbesma, R. P.; Heuts, J. P. A. *ACS Macro Lett.* **2016**, *5*, 995.

14) Wang, L. J.; Zhou, X. J.; Zhang, X. H.; Du, B. Y. *Macromolecules* **2016**, *49*, 98.

15) Liu, G.; Wang, X.; Hu, J.; Zhang, G.; Liu, S. *J. Am. Chem. Soc.* **2014**, *136*, 7492.

7.6 EXPERIMENTAL

7.6.1 *General Considerations*

Dry toluene, pyridine, and CH_2Cl_2 were obtained from a Glass Contour solvent purification system. Et_3N and methyl acrylate were distilled under N_2 after drying over CaH_2 overnight. All other reagents and solvents were used as obtained from commercial sources. Compound **S1**,[1] **S3**,[2] **S5**,[3] **S14**,[4] and **S15**[5] was prepared according to literature procedure. ^1H and ^{13}C NMR spectra were recorded on a Bruker AVance 300 or 500 MHz spectrometer. Chemical shifts are

reported in delta (δ) units, expressed in parts per million (ppm) downfield from tetramethylsilane using the residual protio-solvent as an internal standard ($CDCl_3$, ^1H: 7.26 ppm and ^{13}C: 77.2 ppm; CD_3CN, ^1H: 1.94 ppm and ^{13}C: 118.3 ppm). LRMS was performed on a Bruker Esquire equipped with either an electrospray ionization (ESI) or IonSense SVP100 DART source. GPC setup consists of: an Agilent 1260 Infinity II HPLC pump, three in-line MZ-Gel 10 μm size-exclusion columns (pore sizes = 10^3, 10^3, and 10^5 Å), miniDAWN-TREOS 3-angle multi-angle laser light scatter and OptiLab T-rEx refractive index detectors (each from Wyatt Technologies Corporation). The mobile phase consisted of HPLC grade THF. No calibration standards were used, and dn/dc values were obtained for each injection assuming 100% mass elution from the columns. Sonication experiments were done using a 20 kHz Sonics VSX series sonication probe (1.2 cm tip diameter) calibrated according to literature procedures.[1] Fluorescence spectroscopy was conducted using a Perkin Elmer Luminescence Spectrometer LS 50 B.

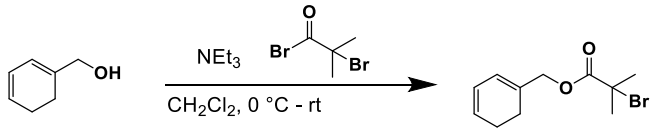

S1 **2**

7.6.2 *Synthesis of **2***

Into a flame-dried round bottom flask, **S1** (60 mg, 0.55 mmol, 1.0 equiv.), dry CH_2Cl_2 (1 mL) and a magnetic stir bar were added. The reaction mixture was placed in an ice bath. NEt_3 (85 μL, 0.61 mmol, 1.1 equiv.) was then added to the solution. A solution of α-bromoisobutyryl bromide (75 μL, 0.61 mmol, 1.1 equiv.) in dry CH_2Cl_2 (1 mL) was then added dropwise. The reaction mixture was stirred for 18 h, during which time the ice bath expired. The solvent was removed under reduced pressure. The crude residue was taken up in ether and washed successively with DI H_2O (2 × 10 mL), sat. $NaHCO_3$ (2 × 10 mL) and brine (1 × 10 mL). The

organic layer was dried over Na_2SO_4, filtered through a thin pad of Celite, and concentrated under reduced pressure. The product was isolated via flash column chromatography (10% EtOAc/hexanes) to obtain a colorless transparent oil in 65% yield. ^{1}H NMR (500 MHz, $CDCl_3$) δ 6.09 – 5.72 (m, 2H), 4.66 (s, 2H), 2.20 (s, 4H), 1.95 (s, 6H).

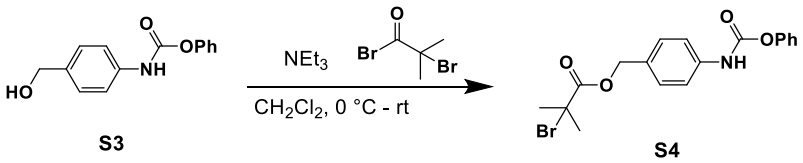

7.6.3 *Synthesis of **S4***

Into a flame-dried round bottom flask, **S3** (1.0 g, 4.11 mmol, 1.0 equiv.), dry CH_2Cl_2 (14 mL) and a magnetic stir bar were added. The reaction mixture was placed in an ice bath. NEt_3 (0.64 mL, 4.52 mmol, 1.1 equiv.) was then added to the solution. A solution of α-bromoisobutyryl bromide (0.56 mL, 4.52 mmol, 1.1 equiv.) in dry CH_2Cl_2 (4 mL) was then added dropwise. The reaction mixture was stirred for 18 h, during which time the ice bath expired. The solvent was removed under reduced pressure. The crude residue was taken up in diethyl ether and washed successively with DI H_2O (2 × 10 mL), sat. $NaHCO_3$ (2 × 10 mL) and brine (1 × 10 mL). The organic layer was dried over Na_2SO_4, filtered through a thin pad of Celite, and concentrated under reduced pressure. The product was isolated via flash column chromatography (20% EtOAc/hexanes) to obtain a yellow crystalline solid in 68% yield. ^{1}H NMR (500 MHz, $CDCl_3$) δ 7.66 – 7.04 (m, 9H), 5.20 (s, 2H), 1.98 (s, 6H).

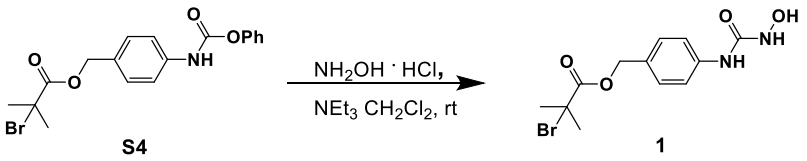

7.6.4 *Synthesis **1***

Into a flame-dried round bottom flask, **S4** (2.37 g, 6.04 mmol, 1.0 equiv.), hydroxylamine hydrochloride (629 mg, 9.06 mmol, 1.5 eq.), dry CH_2Cl_2 (12 mL) and a magnetic stir bar were added. NEt_3 (2.55 mL, 18.12 mmol, 3 equiv.) was then added to the solution. The reaction mixture was stirred for 18 h at room temperature. The solvent was removed under reduced pressure. The crude residue was taken up in ethyl acetate and washed with brine (3 × 50 mL). The organic layer was dried over Na_2SO_4, filtered through a thin pad of Celite, and concentrated under reduced pressure. The residual solids were suspended in diethyl ether, filtered and washed with diethyl ether. The product was obtained as a off white solid in 44% yield. ^{1}H NMR (500 MHz, DMSO) δ 9.00 (s, 1H), 8.89 (d, J = 3.3 Hz, 2H), 7.64 (d, J = 8.3 Hz, 2H), 7.28 (d, J = 8.3 Hz, 2H), 5.12 (s, 2H), 1.90 (s, 6H). ^{13}C NMR (126 MHz, $CDCl_3$) δ 170.7, 158.6, 139.5, 129.0, 128.5, 119.1, 67.0, 57.3, 30.3.

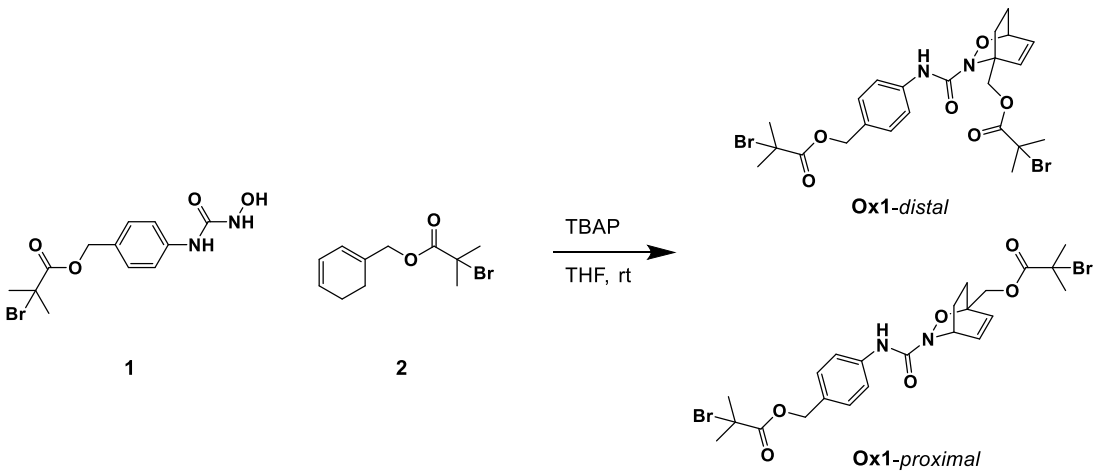

7.6.5 *Synthesis of **Ox1***

Into a round bottom flask, **1** (128 mg, 0.39, 1.1 eq.), **2** (95 mg, 0.36 mmol, 1.0 eq.), THF (2 mL) and a magnetic stir bar were added. Tetrabutylammonium periodate (169 mg, 0.39 mmol, 1.1 eq.) was then added. The reaction was allowed to stir at room temperature for 3 hours. Ethyl acetate (10 mL) was added and the reaction mixture was washed with sat. sodium bisulfite (2 × 10 mL), sat. $NaHCO_3$ (1 × 10 mL0, 1 M HCl (1 × 10 mL) and diH_2O (1 × 10 mL). The organic layer was dried over Na_2SO_4, filtered through a thin pad of Celite, and concentrated under reduced pressure. Each isomer was isolated via flash column chromatography (gradient 20 - 40% EtOAc/hexanes) to obtain the proximal isomer (54% yield) and *distal* (6% yield) as yellow oils. *Proximal Isomer:* ^{1}H NMR (500 MHz, $CDCl_3$) δ 7.77 (s, 1H), 7.49 (d, J = 7.7 Hz, 2H), 7.30 (d, J = 7.9 Hz, 2H), 6.67 (t, J = 6.9 Hz, 1H), 6.44 (d, J = 8.4 Hz, 1H), 5.14 (s, 2H), 5.03 (s, 1H), 4.56 (d, J = 12.5 Hz, 1H), 4.42 (d, J = 12.5 Hz, 1H), 2.23 (t, J = 11.1 Hz, 1H), 2.06 (d, J = 14.9 Hz, 2H), 1.94 (d, J = 6.3 Hz, 6H), 1.92 (s, 6H), 1.67 (t, J = 12.3 Hz, 1H), 1.37 (t, J = 10.3 Hz, 1H). ^{13}C NMR (126 MHz, $CDCl_3$) δ 171.5, 171.4, 159.3, 137.8, 133.6, 130.5, 129.6, 129.0, 119.5, 78.0, 67.3, 66.5, 55.8, 55.2, 50.4, 30.8, 30.7, 30.7, 26.3, 20.5. LRMS (ESI): $[M+Na]^+$ calcd for $NaC_{23}H_{28}Br_2N_2O_6$, 611.02, found 611.1.

Distal Isomer: ^{1}H NMR (500 MHz, $CDCl_3$) δ 7.83 (s, 1H), 7.41 (d, J = 7.8 Hz, 2H), 7.30 (d, J = 8.0 Hz, 2H), 6.60 – 6.50 (m, 2H), 5.24 (d, J = 11.3 Hz, 1H), 5.13 (s, 2H), 5.01 – 4.81 (m, 2H), 2.29 (dd, J = 14.5, 7.0 Hz, 1H), 2.14 (t, J = 13.4 Hz, 1H), 1.95 (d, J = 4.4 Hz, 7H), 1.91 (s, 7H), 1.70 (t, J = 12.2 Hz, 1H), 1.44 (dt, J = 16.3, 8.2 Hz, 1H). LRMS (ESI): $[M+Na]^+$ calcd for $NaC_{23}H_{28}Br_2N_2O_6$, 611.02, found 611.2.

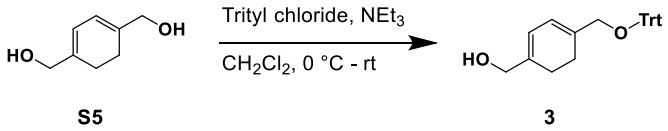

S5 3

7.6.6 *Synthesis of **3***

Into a flame-dried round bottom flask, **S5** (422 mg, 3.01 mmol, 1.0 equiv.), NEt_3 (0.63 mL, 4.51 mmol, 1.5 equiv.), dry THF (2 mL) and a magnetic stir bar were added. The reaction mixture was then cooled in an ice bath. Trityl chloride (839 mg, 9.06 mmol, 1.5 eq.) in dry THF (20 mL) was then added to the reaction mixture dropwise. The reaction mixture was stirred for 18 h, during which time the ice bath expired. The solvent was removed under reduced pressure. The crude residue was taken up in diethyl ether and washed successively with DI H_2O (2 × 10 mL), sat. $NaHCO_3$ (2 × 10 mL) and brine (1 × 10 mL). The organic layer was dried over Na_2SO_4, filtered through a thin pad of Celite, and concentrated under reduced pressure. The product was isolated via flash column chromatography (40% EtOAc/hexanes) to obtain a colorless oil in 22% yield. ^1H NMR (500 MHz, $CDCl_3$) δ 7.61 – 7.18 (m, 15H), 6.03 (m, 2H), 4.13 (s, 2H), 3.59 (s, 2H), 2.18 (m, 4H).

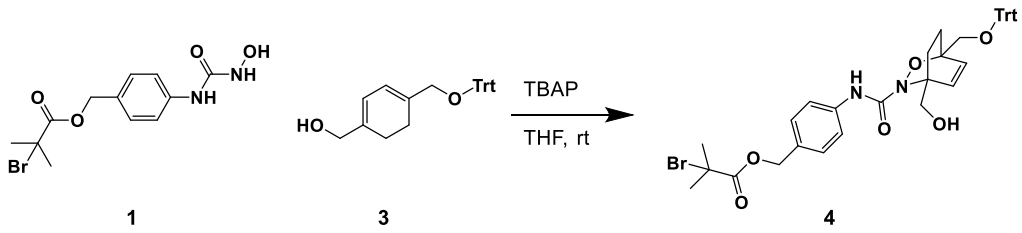

1 3 4

7.6.7 *Synthesis of **4***

Into a round bottom flask, **1** (235 mg, 0.71, 1.1 eq.), **3** (250 mg, 0.65 mmol, 1.0 eq.), and THF (3 mL) were added. Tetrabutylammonium periodate (308 mg, 0.71 mmol, 1.3 eq.) was then added. The reaction was allowed to stir at room temperature for 3 hours. Ethyl acetate (10 mL)

was added and the reaction mixture was washed with sat. sodium bisulfite (2 × 10 mL), sat. $NaHCO_3$ (1 × 10 mL0, 1 M HCl (1 × 10 mL) and diH_2O (1 × 10 mL). The organic layer was dried over Na_2SO_4, filtered through a thin pad of Celite, and concentrated under reduced pressure. The product was isolated via flash column chromatography (gradient 20 - 30% EtOAc/hexanes) to obtain a yellow oil in 31% yield. ^{1}H NMR (500 MHz, $CDCl_3$) δ 8.23 (s, 1H), 7.43 (d, J = 6.9 Hz, 6H), 7.25 (s, 9H), 7.14 (m, 4H), 6.83 (d, J = 8.4 Hz, 1H), 6.61 (d, J = 8.4 Hz, 1H), 5.09 (s, 3H), 4.18 (d, J = 12.6 Hz, 1H), 3.93 (t, J = 11.1 Hz, 1H), 3.53 (d, J = 10.7 Hz, 1H), 3.44 (d, J = 8.8 Hz, 2H), 2.10 (t, J = 8.9 Hz, 1H), 1.90 (d, J = 9.1 Hz, 6H), 1.86 (t, J = 10.9 Hz, 1H), 1.31 (t, J = 12.0 Hz, 1H).

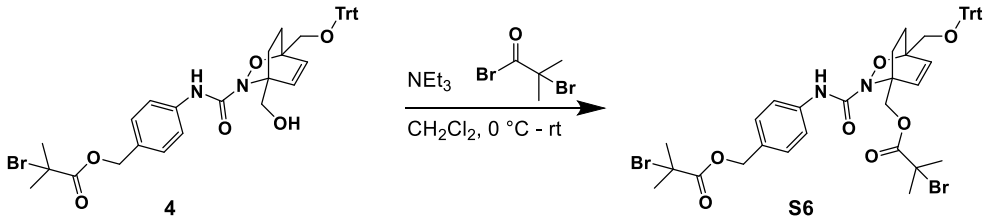

7.6.8 *Synthesis of **S6***

Into a flame-dried round bottom flask, **4** (144 mg, 0.2 mmol, 1.0 equiv.), dry CH_2Cl_2 (2 mL) and a magnetic stir bar were added. The reaction mixture was placed in an ice bath. NEt_3 (34 µL, 0.24 mmol, 1.2 equiv.) was then added to the solution. A solution of α-bromoisobutyryl bromide (29 µL, 024 mmol, 1.2 equiv.) in dry CH_2Cl_2 (4 mL) was then added dropwise. The reaction mixture was stirred for 18 h, during which time the ice bath expired. The solvent was removed under reduced pressure. The crude residue was taken up in diethyl ether and washed successively with DI H_2O (2 × 10 mL), sat. $NaHCO_3$ (2 × 10 mL) and brine (1 × 10 mL). The organic layer was dried over Na_2SO_4, filtered through a thin pad of Celite, and concentrated

under reduced pressure. The product was isolated via flash column chromatography (20% EtOAc/hexanes) to obtain a yellow crystalline solid in 50% yield. ^{1}H NMR (500 MHz, $CDCl_3$) δ 8.15 (s, 1H), 7.46 – 7.28 (m, 6H), 7.18 (s, 9H), 7.07 (m, 4H), 6.62 – 6.45 (m, 2H), 5.02 (s, 2H), 5.02 (s, 2H), 4.90 (d, J = 11.4 Hz, 1H), 3.42 (d, 10.8 Hz, 2H), 2.12 (d, J = 18.2 Hz, 1H), 1.88 (d, J = 2.8 Hz, 6H), 1.85 (s, 6H), 1.63 (t, J = 12.9 Hz, 1H), 1.32 – 1.06 (m, 3H).

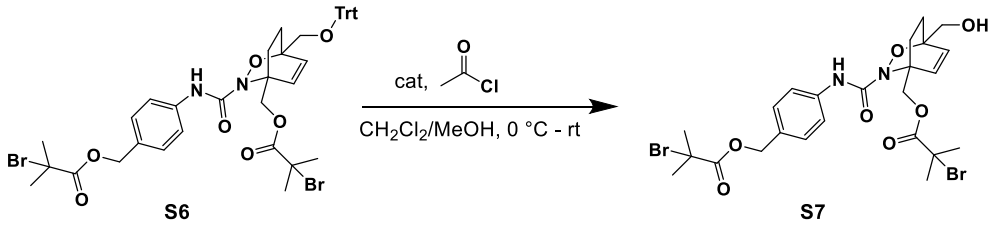

7.6.9 *Synthesis of **S7***

Into a round bottom flask, **S6** (90 mg, 0.1 mmol, 1.0 eq.), MeOH (1 mL), CH_2Cl_2 (1 mL) and a magnetic stir bar were added. The reaction mixture was placed in an ice bath. Acetyl chloride (2.8 µL, 0.04 mmol, 0.4 eq.) was then added. After 5 hours, the reaction mixture was concentrated under reduced pressure. The product was isolated via column chromatography (gradient 20% - 40% EtOac/Hex) to obtain a colorless oil in 57% yield. ^{1}H NMR (500 MHz, $CDCl_3$) δ 8.45 (s, 1H), 7.39 (d, J = 7.9 Hz, 2H), 7.26 (d, J = 7.0 Hz, 2H), 6.54 (s, 2H), 5.28 (d, J = 11.4 Hz, 1H), 5.12 (s, 2H), 4.89 (d, J = 11.3 Hz, 1H), 4.05 (d, J = 11.7 Hz, 1H), 3.91 (d, J = 11.7 Hz, 1H), 2.34 (s, 1H), 2.18 (dd, J = 15.7, 11.9 Hz, 1H), 1.96 (d, J = 7.5 Hz, 7H), 1.91 (s, 6H), 1.74 (t, J = 12.2 Hz, 1H), 1.31 (dd, J = 21.9, 10.4 Hz, 2H).

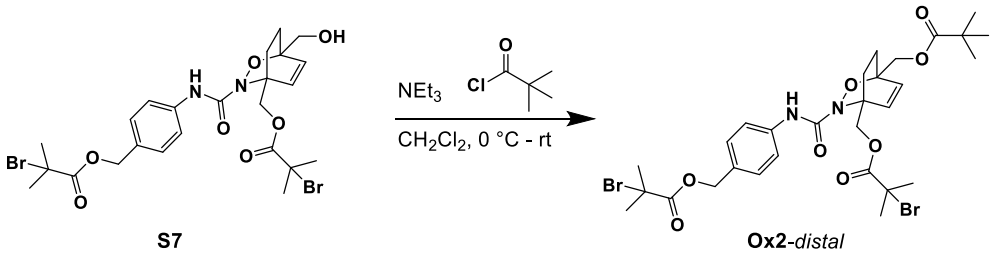

S7 **Ox2**-*distal*

7.6.10 *Synthesis of **Ox2**-distal*

Into a flame-dried round bottom flask, **S7** (35 mg, 0.057 mmol, 1.0 equiv.), dry CH_2Cl_2 (0.5 mL) and a magnetic stir bar were added. The reaction mixture was placed in an ice bath. NEt_3 (9 µL, 0.063 mmol, 1.1 equiv.) was then added to the solution. A solution of pivaloyl chloride (7.6 µL, 0.063 mmol, 1.1 equiv.) in dry CH_2Cl_2 (0.5 mL) was then added dropwise. The reaction mixture was stirred for 18 h, during which time the ice bath expired. The solvent was removed under reduced pressure. The crude residue was taken up in diethyl ether and washed successively with DI H_2O (2 × 10 mL), sat. $NaHCO_3$ (2 × 10 mL) and brine (1 × 10 mL). The organic layer was dried over Na_2SO_4, filtered through a thin pad of Celite, and concentrated under reduced pressure. The product was isolated via flash column chromatography (20% EtOAc/hexanes) to obtain a yellow oil in 53% yield.^{1}H NMR (300 MHz, $CDCl_3$) 7.96 (s, 1H), 7.37 (dd, J = 50.6, 8.6 Hz, 4H), 6.52 (dd, J = 81.8, 8.5 Hz, 2H), 5.31 (d, J = 11.3 Hz, 1H), 5.13 (s, 2H), 4.89 (d, J = 11.4 Hz, 1H), 4.57 (d, J = 12.7 Hz, 1H), 4.32 (d, J = 12.7 Hz, 1H), 2.22 (dd, J = 10.5, 5.9 Hz, 1H), 1.94 (d, J = 1.8 Hz, 6H), 1.91 (s, 6H), 1.83 – 1.70 (m, 2H), 1.16 (s, 9H).

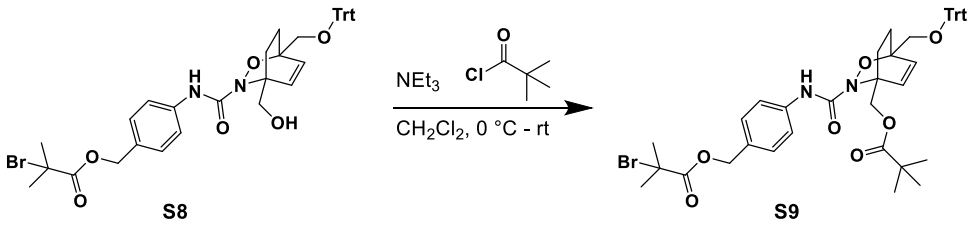

S8 **S9**

7.6.11 *Synthesis of **S9***

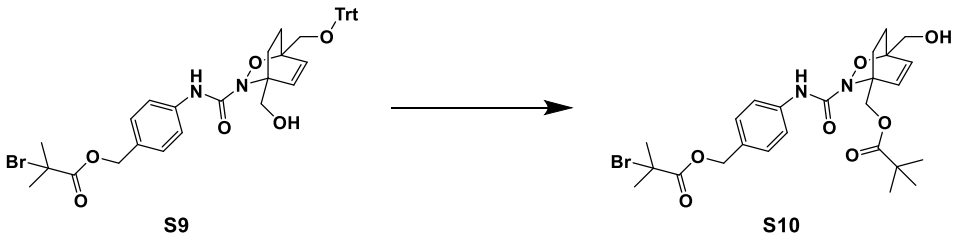

7.6.12 *Synthesis of **S10***

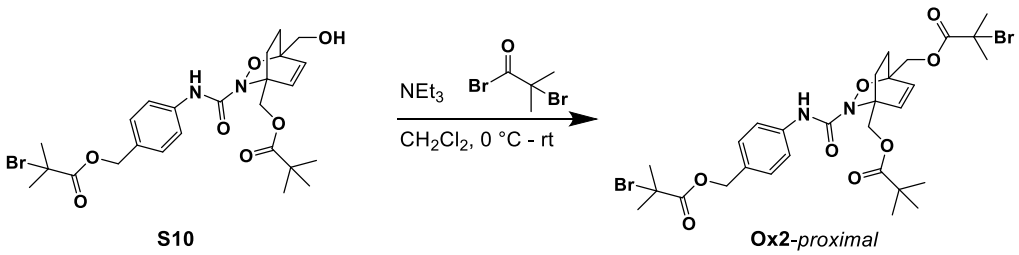

7.6.13 *Synthesis of **Ox2**-proximal*

LRMS (ESI): $[M+Na]^+$ calcd for $NaC_{29}H_{38}Br_2N_2O_8$, 725.09, found 725.3.

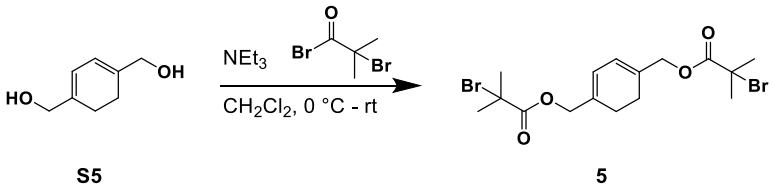

7.6.14 *Synthesis of **5***

Into a flame-dried round bottom flask, **S5** (60 mg, 0.55 mmol, 1.0 equiv.), dry CH_2Cl_2 (1 mL) and a magnetic stir bar were added. The reaction mixture was placed in an ice bath. NEt_3 (85 µL, 0.61 mmol, 1.1 equiv.) was then added to the solution. A solution of α-bromoisobutyryl bromide (75 µL, 0.61 mmol, 1.1 equiv.) in dry CH_2Cl_2 (1 mL) was then added dropwise. The reaction mixture was stirred for 18 h, during which time the ice bath expired. The solvent was

removed under reduced pressure. The crude residue was taken up in ether and washed successively with DI H_2O (2 × 10 mL), sat. $NaHCO_3$ (2 × 10 mL) and brine (1 × 10 mL). The organic layer was dried over Na_2SO_4, filtered through a thin pad of Celite, and concentrated under reduced pressure. The product was isolated via flash column chromatography (10% EtOAc/hexanes) to obtain a colorless transparent oil in 65% yield. ^{1}H NMR (500 MHz, $CDCl_3$) δ 5.98 (s, 2H), 4.67 (s, 4H), 2.26 (s, 4H), 1.95 (s, 12H).

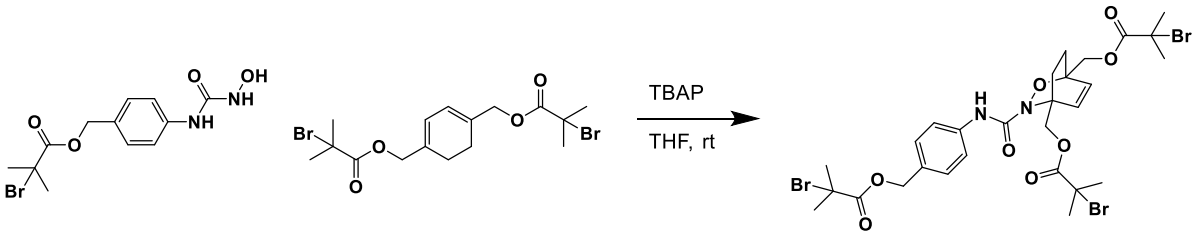

1 **5** **Ox3**

Synthesis of **Ox3**

Into a round bottom flask, **1** (149 mg, 0.45, 1.3 eq.), **5** (152 mg, 0.35 mmol, 1.0 eq.), THF (3 mL) and a magnetic stir bar were added. Tetrabutylammonium periodate (195 mg, 0.45 mmol, 1.3 eq.) was then added. The reaction was allowed to stir at room temperature for 3 hours. Ethyl acetate (10 mL) was added and the reaction mixture was washed with sat. sodium bisulfite (2 × 10 mL), sat. $NaHCO_3$ (1 × 10 mL0, 1 M HCl (1 × 10 mL) and diH_2O (1 × 10 mL). The organic layer was dried over Na_2SO_4, filtered through a thin pad of Celite, and concentrated under reduced pressure. The product was isolated via flash column chromatography (gradient 20 - 30% EtOAc/hexanes) to obtain a yellow oil in 38% yield. ^{1}H NMR (500 MHz, $CDCl_3$) δ 7.92 (s, 1H), 7.46 (d, J = 7.9 Hz, 2H), 7.29 (d, J = 7.9 Hz, 2H), 6.68 (d, J = 8.4 Hz, 1H), 6.45 (d, J = 8.4 Hz, 1H), 5.29 (d, J = 24.8 Hz, 1H), 5.13 (s, 2H), 4.90 (d, J = 11.3 Hz, 1H), 4.66 (d, J = 12.6 Hz, 1H), 4.41 (d, J = 12.7 Hz, 1H), 2.38 – 2.10 (m, 2H), 1.90 (dd, J = 26.5, 12.1 Hz, 18H), 1.79 (t, J = 12.0 Hz, 1H), 1.42 (t, J = 13.3 Hz, 1H). ^{13}C NMR (126 MHz, $CDCl_3$) δ 171.8, 171.5, 171.1,

159.7, 137.7, 135.8, 131.0, 129.1, 129.0, 120.2, 78.6, 67.9, 67.4, 66.2, 61.5, 55.9, 55.0, 30.9, 30.9, 30.8, 30.7, 28.5, 24.6. LRMS (ESI): $[M+Na]^+$ calcd for $NaC_{28}H_{35}Br_3N_2O_8$, 788.98, found 789.3

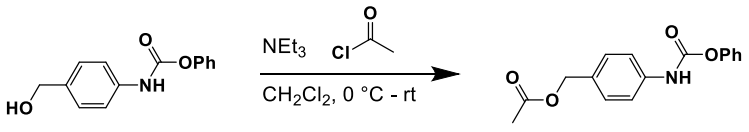

S3 **S11**

7.6.15 *Synthesis of **S11***

Into a flame-dried round bottom flask, **S3** (2.56g, 10.52 mmol, 1.0 equiv.), dry CH_2Cl_2 (50 mL) and a magnetic stir bar were added. The reaction mixture was placed in an ice bath. NEt_3 (1.62 mL, 11.57 mmol, 1.1 equiv.) was then added to the solution. A solution of acetyl chloride (0.83 mL, 11.57 mmol, 1.1 equiv.) in dry CH_2Cl_2 (12 mL) was then added dropwise. The reaction mixture was stirred for 18 h, during which time the ice bath expired. The solvent was removed under reduced pressure. The crude residue was taken up in diethyl ether and washed successively with DI H_2O (2 × 10 mL), sat. $NaHCO_3$ (2 × 10 mL) and brine (1 × 10 mL). The organic layer was dried over Na_2SO_4, filtered through a thin pad of Celite, and concentrated under reduced pressure. Clean product obtained as a off-white crystalline solid in 93% yield. ^1H NMR (500 MHz, $CDCl_3$) δ 7.57 – 7.12 (m, 9H), 5.10 (s, 2H), 2.14 (s, 3H). ^{13}C NMR (126 MHz, $CDCl_3$) δ 171.1, 150.5, 137.6, 131.3, 129.5, 129.4, 125.8, 121.7, 118.8, 100.0, 66.0, 21.1. LRMS (ESI): $[M+Na]^+$ calcd for $NaC_{16}H_{15}NO_4$, 308.09, found 308.1.

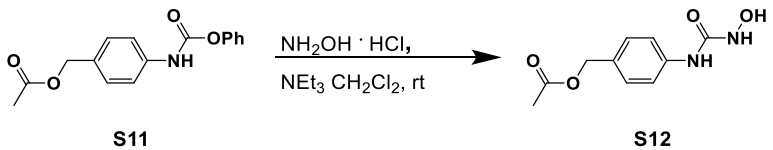

S11 **S12**

7.6.16 *Synthesis of **S12***

Into a flame-dried round bottom flask, **S7** (2.57 g, 9.01 mmol, 1.0 equiv.), hydroxylamine hydrochloride (939 mg, 13.52 mmol, 1.5 eq.), dry CH_2Cl_2 (18 mL) and a magnetic stir bar were added. NEt_3 (3.80 mL, 27.03 mmol, 3 equiv.) was then added to the solution. The reaction mixture was stirred for 18 h at room temperature. The solvent was removed under reduced pressure. The crude residue was taken up in ethyl acetate and washed with brine (3 × 50 mL). The organic layer was dried over Na_2SO_4, filtered through a thin pad of Celite, and concentrated under reduced pressure. The residual solids were suspended in diethyl ether, filtered and washed with diethyl ether. The product was obtained as a off white solid in 75% yield. ^{1}H NMR (500 MHz, DMSO) δ 9.00 (s, 1H), 8.87 (d, J = 9.0 Hz, 2H), 7.63 (d, J = 7.8 Hz, 2H), 7.25 (d, J = 7.9 Hz, 2H), 4.98 (s, 2H), 2.03 (s, 3H). ^{13}C NMR (126 MHz, DMSO) δ 170.4, 158.6, 139.4, 129.7, 128.8, 119.1, 65.5, 20.8.

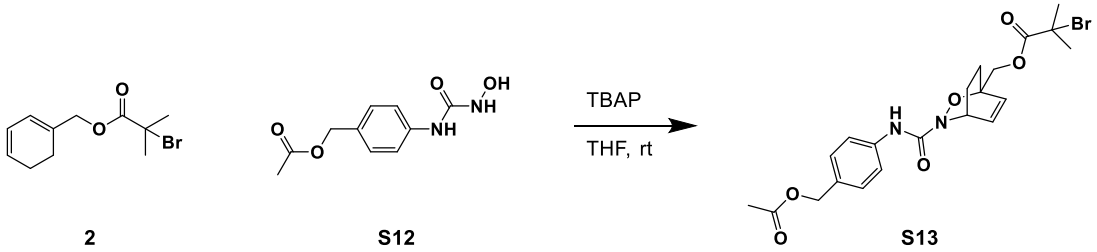

2 **S12** **S13**

7.6.17 *Synthesis of **S13***

Into a round bottom flask, **2** (138 mg, 0.53 mmol, 1.0 eq.), **S12** (130 mg, 0.58, 1.1 eq.), THF (3 mL) and a magnetic stir bar were added. Tetrabutylammonium periodate (251 mg, 0.58 mmol, 1.1 eq.) was then added. The reaction was allowed to stir at room temperature for 3 hours. Ethyl acetate (10 mL) was added and the reaction mixture was washed with sat. sodium bisulfite (2 × 10 mL), sat. $NaHCO_3$ (1 × 10 mL0, 1 M HCl (1 × 10 mL) and diH_2O (1 × 10 mL). The organic layer was dried over Na_2SO_4, filtered through a thin pad of Celite, and concentrated

under reduced pressure. The *distal* isomer was isolated via flash column chromatography (30% EtOAc/hexanes) to obtain a yellow oil in 23% yield. ^{1}H NMR (500 MHz, $CDCl_3$) δ 7.73 (s, 1H), 7.48 (d, J = 8.5 Hz, 2H), 7.29 (d, J = 8.1 Hz, 2H), 6.76 – 6.61 (m, 1H), 6.44 (d, J = 8.4 Hz, 1H), 5.04 (s, 3H), 4.57 (d, J = 12.5 Hz, 1H), 4.41 (d, J = 12.5 Hz, 1H), 2.25 (t, J = 6.6 Hz, 1H), 2.07 (q, J = 4.6 Hz, 4H), 1.95 (d, J = 3.4 Hz, 6H), 1.73 – 1.61 (m, 1H), 1.38 (td, J = 11.8, 4.0 Hz, 1H). ^{13}C NMR (126 MHz, $CDCl_3$) 171.7, 171.1, 159.4, 137.8, 133.7, 131.2, 129.6, 129.3, 119.6, 78.0, 66.6, 66.1, 55.2, 50.4, 30.8, 26.4, 21.2, 20.6.

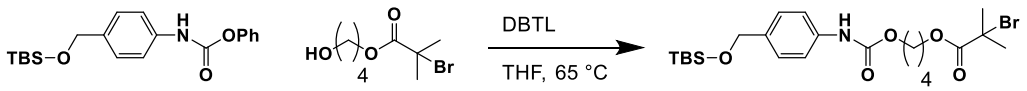

S14 **S15** **S16**

7.6.18 *Synthesis of **S16***

Into a flame-dried, N_2-purged round bottom flask, **S14** (213 mg, 0.62 mmol, 1.0 eq.), **S15** (223 mg, 0.65, 1.05 eq.), dry THF (1 mL) and a magnetic stir bar were added. Dibtuyltin dilaurate (18 µL, 0.031 mmol, 0.05 eq.) was added and the reaction mixture was placed in a pre-heated oil bath. After 24 hours, ether was added and the organic layer was washed with 1 M NaOH (2 × 5 mL) and brine (1 × 5 mL). The organic layer was dried over Na_2SO_4, filtered through a thin pad of Celite, and concentrated under reduced pressure. The product was isolated via flash column chromatography (20% EtOAc/hexanes) to obtain a colorless oil in 60% yield. ^{1}H NMR (500 MHz, $CDCl_3$) δ 7.34 (d, J = 8.3 Hz, 2H), 7.25 (d, J = 8.3 Hz, 2H) 6.59 (s, 1H), 4.69 (s, 2H), 4.28 – 4.16 (m, 4H), 1.94 (s, 6H), 1.81 (d, J = 6.0 Hz, 4H), 0.93 (s, 9H), 0.08 (s, 6H).

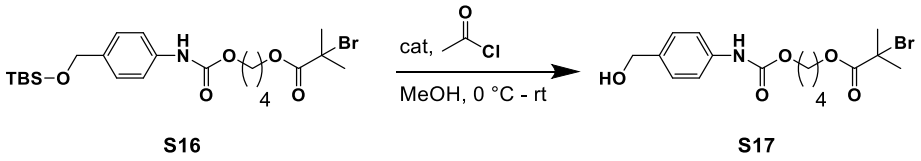

7.6.19 *Synthesis of **S17***

Into a round bottom flask, **S23** (187 mg, 0.37 mmol, 1.0 eq.), MeOH (2 mL) and a magnetic stir bar were added. The reaction mixture was placed in an ice bath. Acetyl chloride (4.3 µL, 0.06 mmol, 0.15 eq.) was then added. After 2.5 hours, the reaction mixture was concentrated under reduced pressure. The product was isolated via column chromatography (gradient 30% - 50% EtOac/Hex) to obtain a colorless oil in 71% yield. ^{1}H NMR (500 MHz, $CDCl_3$) δ 7.38 (d, J = 8.5 Hz, 2H), 7.31 (d, J = 8.5 Hz, 2H), 6.64 (s, 1H), 4.65 (s, 2H), 4.35 – 4.17 (m, 4H), 1.94 (s, 6H), 1.88 – 1.75 (m, 4H).

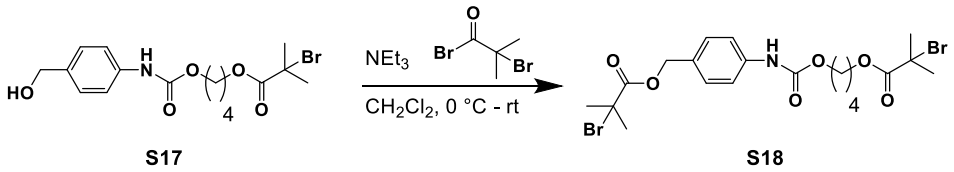

7.6.20 *Synthesis of **S18***

Into a flame-dried round bottom flask, **S24** (102 mg, 0.26 mmol, 1.0 equiv.), dry CH_2Cl_2 (1 mL) and a magnetic stir bar were added. The reaction mixture was placed in an ice bath. NEt_3 (42 µL, 0.30 mmol, 1.1 equiv.) was then added to the solution. A solution of α-bromoisobutyryl bromide (37 µL, 0.30 mmol, 1.1 equiv.) in dry CH_2Cl_2 (0.5 mL) was then added dropwise. The reaction mixture was stirred for 18 h, during which time the ice bath expired. The solvent was removed under reduced pressure. The crude residue was taken up in ether and washed successively with DI H_2O (2 × 10 mL), sat. $NaHCO_3$ (2 × 10 mL) and brine (1 × 10 mL). The

organic layer was dried over Na_2SO_4, filtered through a thin pad of Celite, and concentrated under reduced pressure. The product was isolated via flash column chromatography (10% EtOAc/hexanes) to obtain a colorless transparent oil in 55% yield. ^{1}H NMR (500 MHz, $CDCl_3$) δ 7.39 (d, 2H), 7.32 (d, J = 8.1 Hz, 2H), 6.80 (s, 1H), 4.23 (s, 4H), 1.93 (s, 12H), 1.80 (s, 4H). ^{13}C NMR (126 MHz, $CDCl_3$) δ 171.9, 171.6, 129.3, 118.7, 67.4, 65.5, 64.9, 56.0, 55.9, 30.8, 25.5, 25.3. LRMS (ESI): $[M+Na]^+$ calcd for $NaC_{20}H_{27}Br_2NO_6$, 560.01, found 560.2.

7.6.21 *Representative Example Polymerization Procedure*

In a nitrogen-filled drybox, initiator **Ox1**-*distal* (20.7 mg, 0.035 mmol, 1.0 equiv.), methyl acrylate (3.17 mL, 35 mmol, 1000 equiv.), dry DMF (5.6 mL) and a magnetic stir bar were added into a scintillation vial. A solution of CuBr (5.0 mg, 0.035 mmol, 1.0 equiv.) and PMDETA (7.3 μL, 0.035 mmol, 1.0 equiv.) in DMF (0.6 mL) was then added to reaction mixture. The vial was sealed with a Teflon-lined screw cap and the reaction solution was stirred at room temperature for 18 h. The viscous solution was then added dropwise into an excess of MeOH causing the polymer to precipitate from solution. The solvent was decanted and the resulting polymer residue was rinsed with MeOH (3 × 20 mL). The polymer was dissolved in CH_2Cl_2 (10 mL) and filtered through a plug of alumina to remove residual copper. The solvent was removed under reduced pressure and the resulting polymeric residue was dried under reduced pressure. General structures are shown in Figure 7.4, and data from GPC analysis is given in Table 7.3.

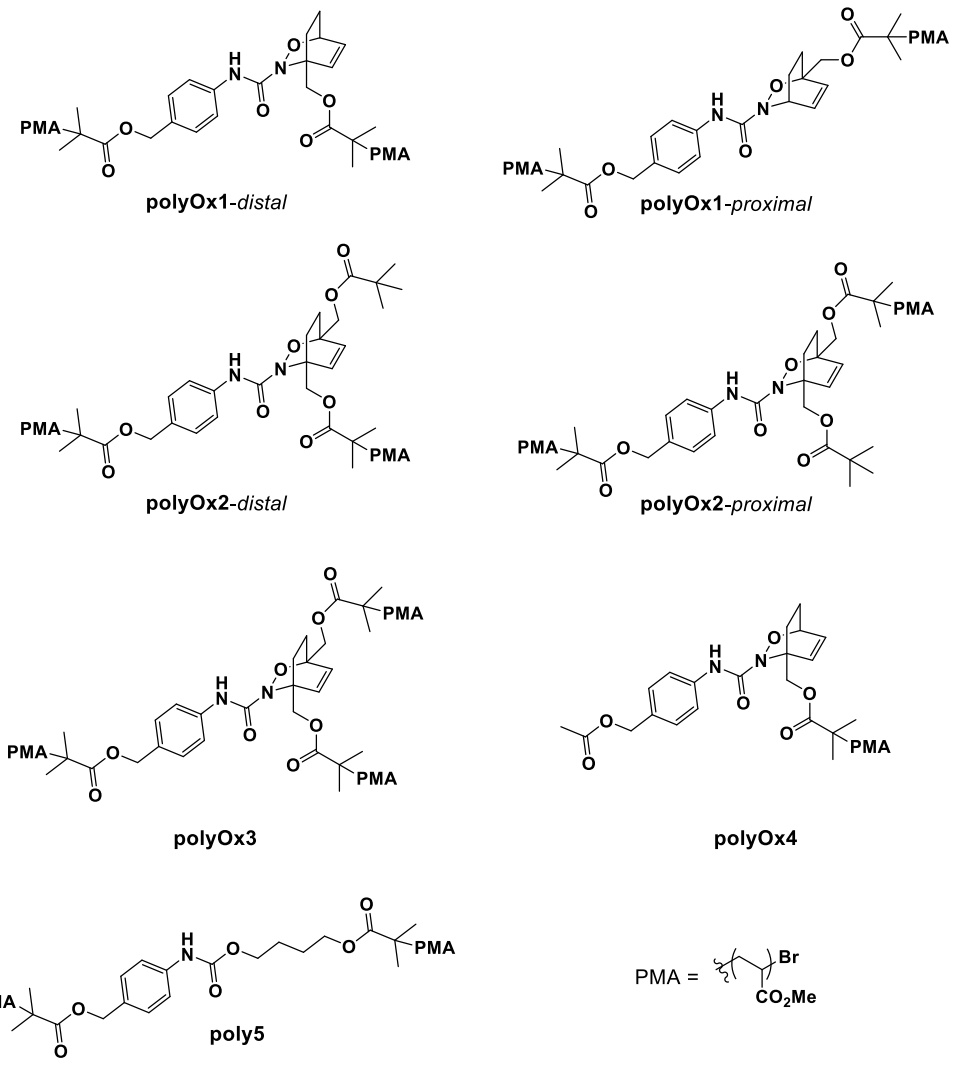

Figure 7.4. Structure of polymers investigated in this study.

Table 7.3. Polymer molecular weights and dispersity.

Polymer	M_n (kDa)	Đ
polyOx1-proximal	59.2	1.07
polyOx1-*distal*	59.3	1.05
polyOx3	90.7	1.04
polyOx4	59.4	1.06
Poly5	57.8	1.08

7.6.22 *Sonication Procedure*

Sonication experiments were done in a flame-dried, N_2-purged Suslick flask, with the sonication horn (1 cm diameter) already attached to Suslick flask. Each arm of the Suslick flask was fitted with a rubber septum. In a separate flame-dried round bottom flask, the polymer sample was dissolved in dry THF at a concentration of 5 mg/ml. The polymer solution was then transferred to the Suslick flask under dry N_2 via syringe. The entire apparatus (sonication horn + Suslick flask) was then transferred to a cold room (4 °C) for the duration of sonication experiment. Polymer solutions were sonicated at 13.8 W/cm^2 for a pulse of 1s on, 9s off. Aliquots of 0.5 mL were withdrawn from the reaction periodically and analyzed by GPC.

7.6.23 *Procedure for Tagging and Isolation of Mechanochemically Liberated Diene*

A **polyOx1**-*distal* solution in dry THF (5 mg/mL, 12 mL) was sonicated for 220 minutes of total on time consisting of the following time points: 20, 40, 60, 80, 100, 120, 140, 180, and 220 minutes. The sonicated solution was carefully poured into a round bottom flask and MeOH (12 mL) was then added to the solution mixture to quench any residual acyl nitroso end groups. The solution was then concentrated (~100 mg/mL) under reduced pressure and precipitated into MeOH (10 mL). The supernatant was removed and the residual polymer was washed with diethyl ether and dried, providing 50 mg of polymer. The polymer was dissolved in 3 mL of THF. **PyrHU** (13 mg, 0.05 mmol) and tetrabutylammonium periodate (20.4 mg, 0.05 mmol) were then added and the reaction mixture was allowed to stir for 5 hours at room temperature. The tagged polymer was then isolated from the small molecule reaction mixture via size exclusion chromatography (see GPC setup under *General Considerations*) and collection of the waste stream corresponding to the polymer retention times (17 – 27 minutes). The

photoluminescence emission spectrum of the resulting polymer solution was collected from 370 to 600 nm using an excitation wavelength of 360 nm.

7.6.24 *NMR Spectra*

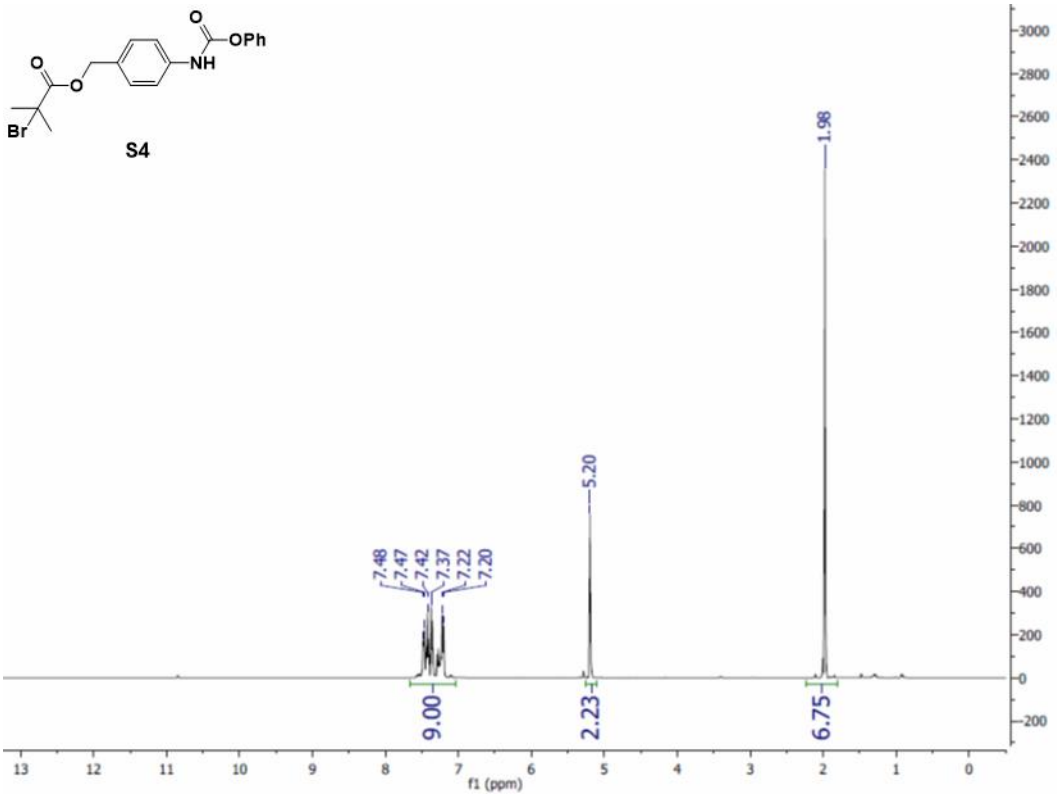

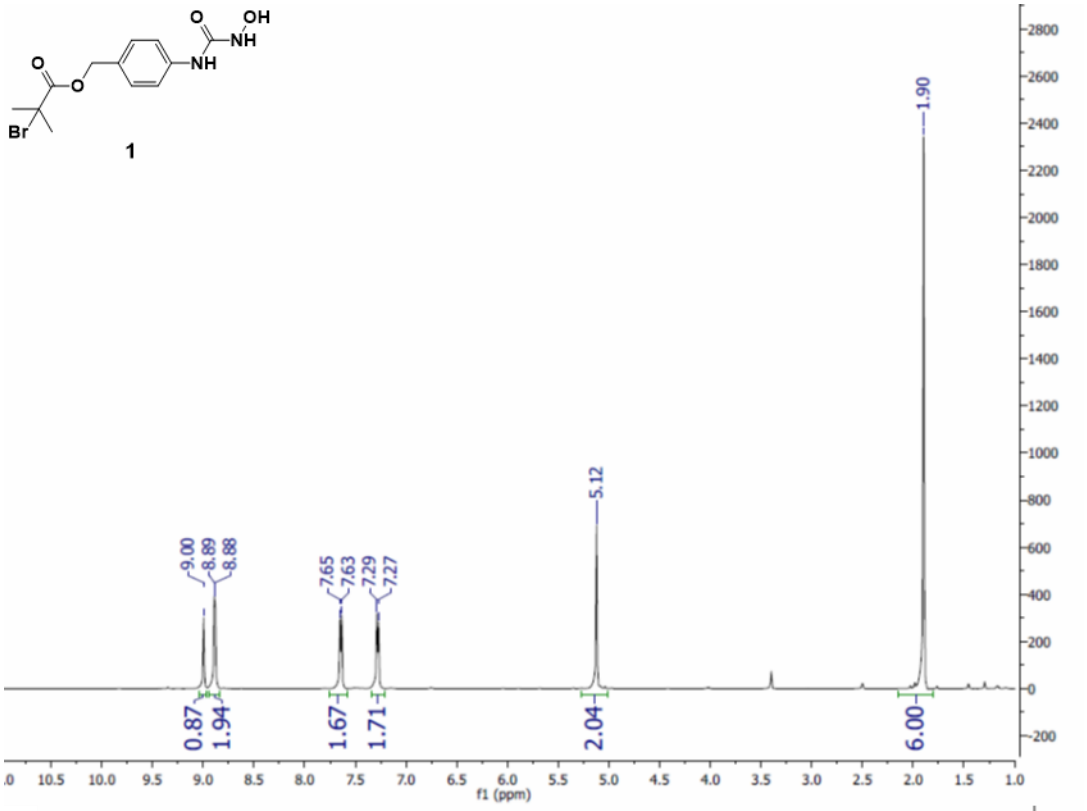
O
OH
NH
NH
O
O
Br
1
9.00
8.89
8.88
7.65
7.63
7.29
7.27
5.12
1.90
0.87
1.94
1.67
1.71
2.04
6.00
f1 (ppm)

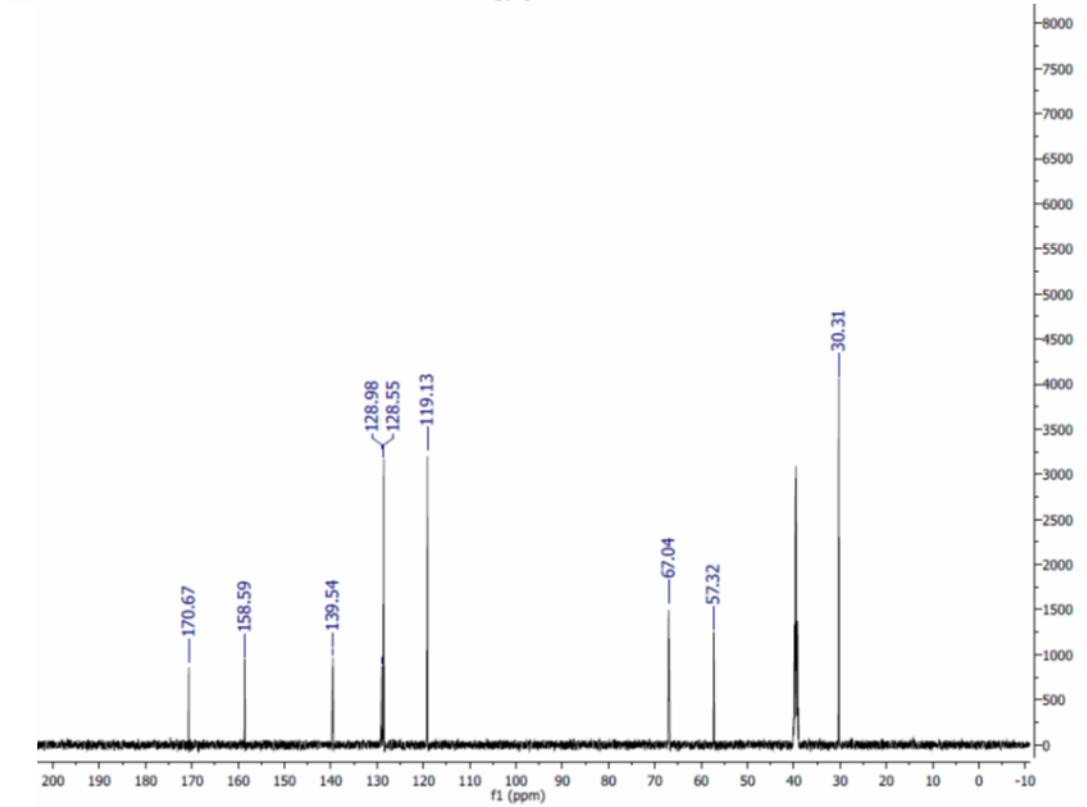
170.67
158.59
139.54
128.98
128.55
119.13
67.04
57.32
30.31
f1 (ppm)

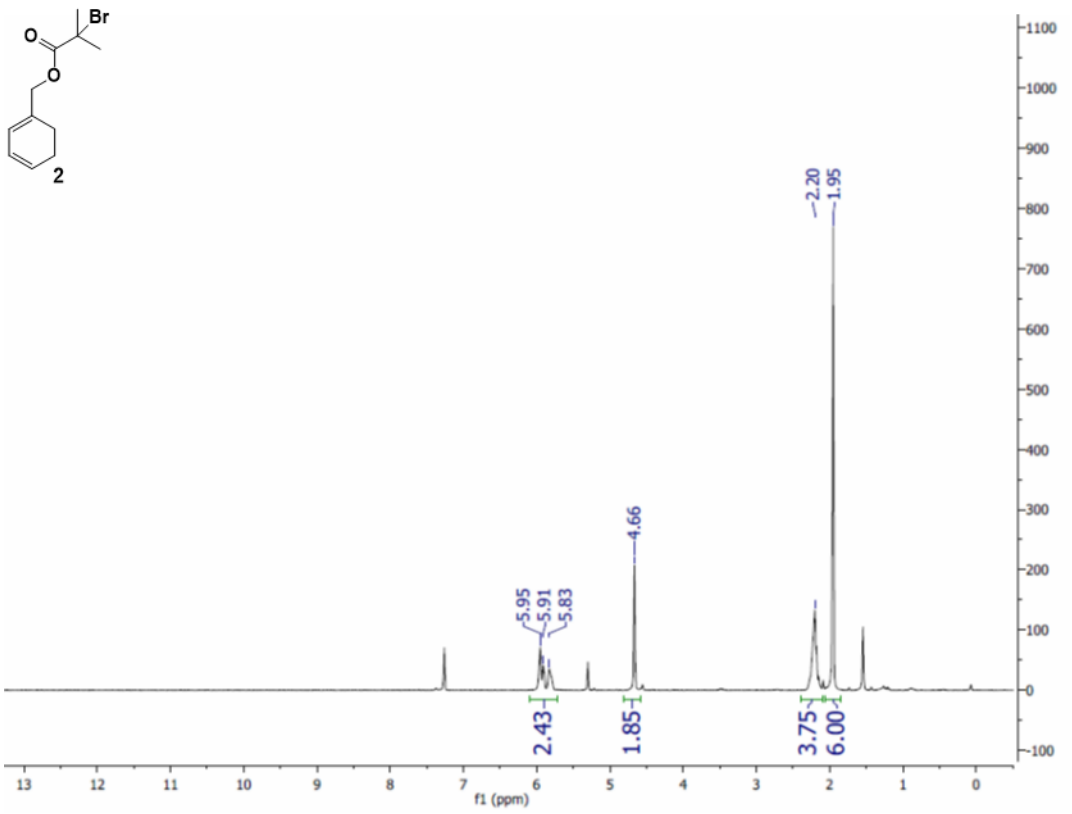
Br
O
O
2
5.95
5.91
5.83
4.66
2.20
1.95
2.43
1.85
3.75
6.00
f1 (ppm)

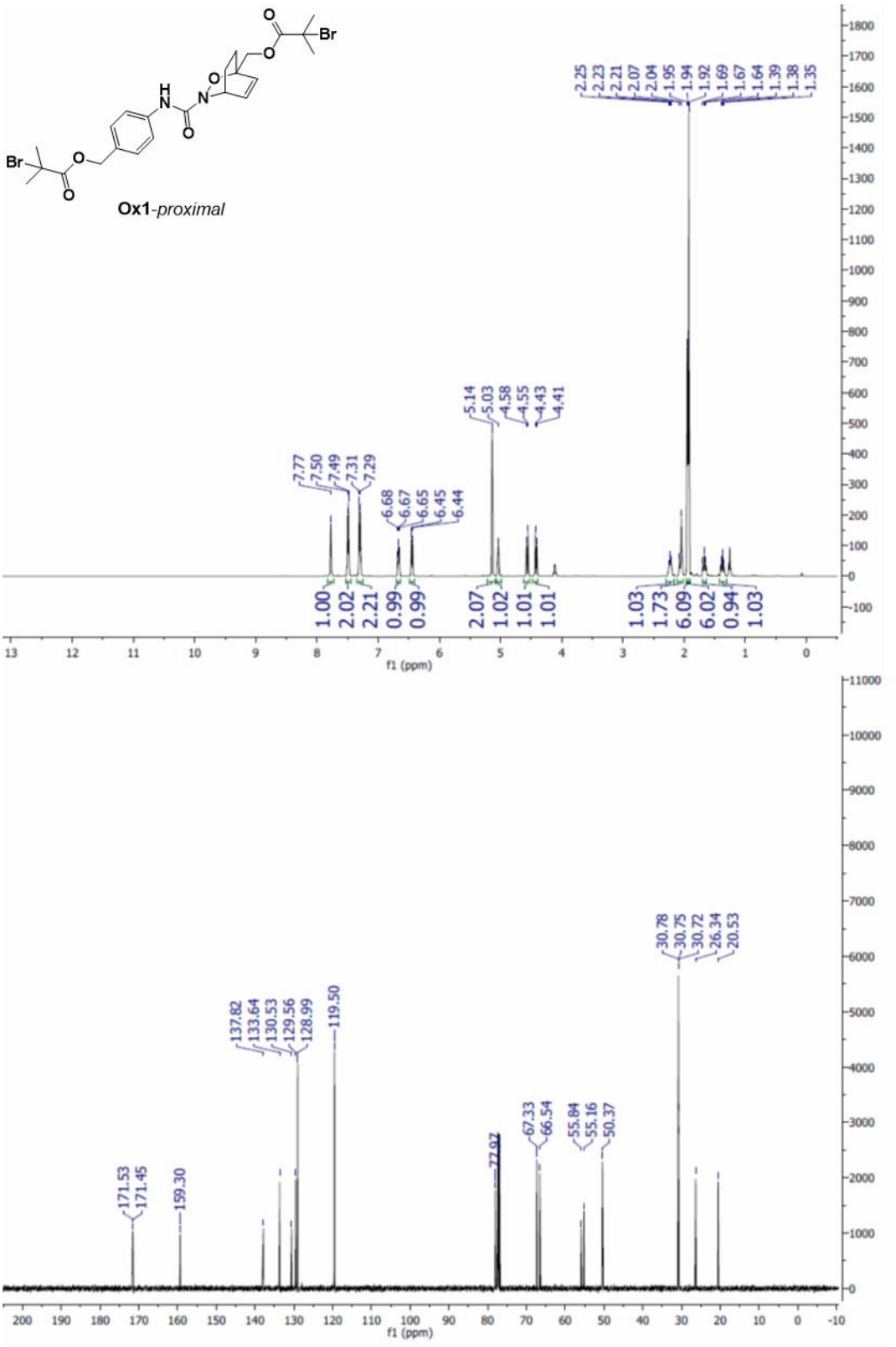
Ox1-proximal
f1 (ppm)
f1 (ppm)

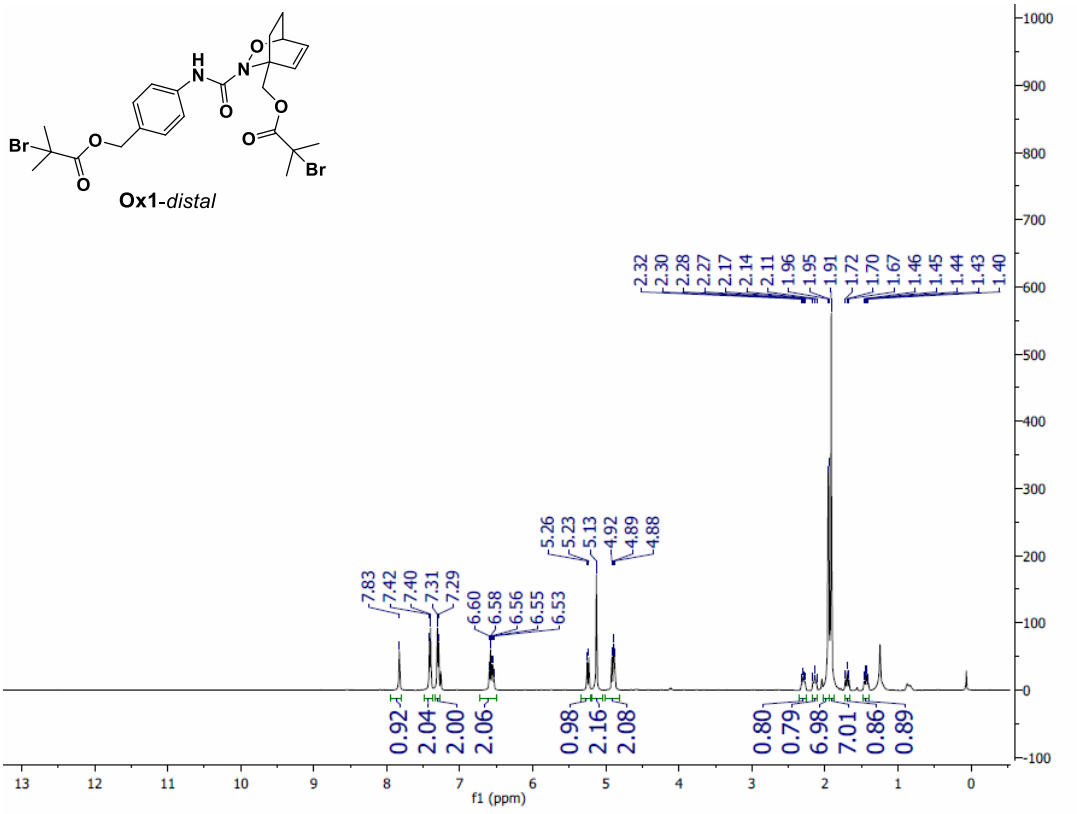
Ox1-distal
7.83
7.42
7.40
7.31
7.29
6.60
6.58
6.56
6.55
6.53
5.26
5.23
5.13
4.92
4.89
4.88
2.32
2.30
2.28
2.27
2.17
2.14
2.11
1.96
1.95
1.91
1.72
1.70
1.67
1.46
1.45
1.44
1.43
1.40
0.92
2.04
2.00
2.06
0.98
2.16
2.08
0.80
0.79
6.98
7.01
0.86
0.89
f1 (ppm)

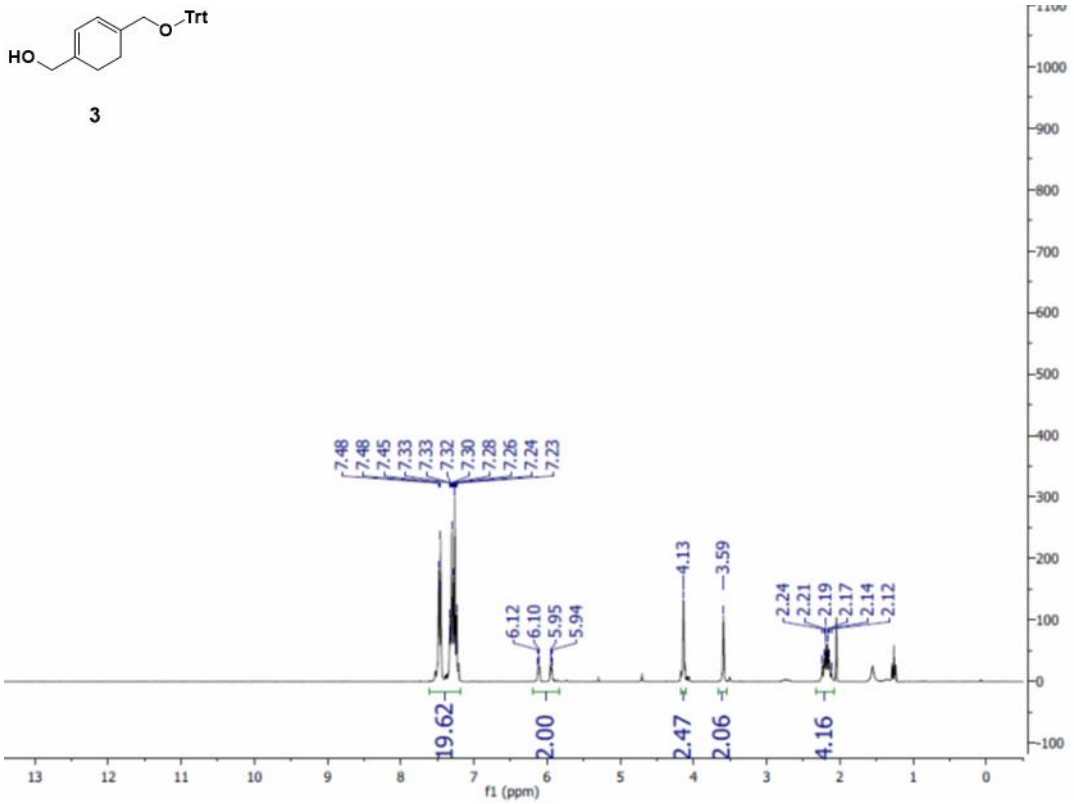
HO
O
Trt
3
7.48
7.48
7.45
7.33
7.33
7.32
7.30
7.28
7.26
7.24
7.23
6.12
6.10
5.95
5.94
4.13
3.59
2.24
2.21
2.19
2.17
2.14
2.12
19.62
2.00
2.47
2.06
4.16
f1 (ppm)

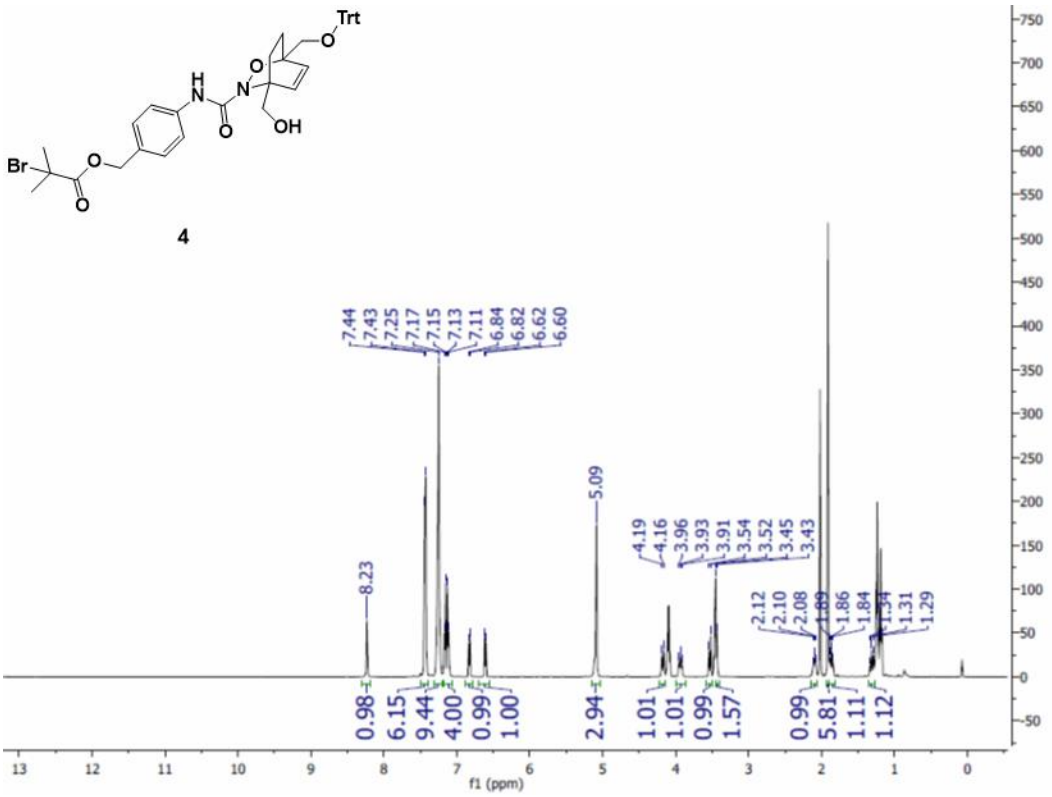
Trt
O
H
N
O
N
O
OH
Br
O
O
4
7.44
7.43
7.25
7.17
7.15
7.13
7.11
6.84
6.82
6.62
6.60
8.23
5.09
4.19
4.16
3.96
3.93
3.91
3.54
3.52
3.45
3.43
2.12
2.10
2.08
1.89
1.86
1.84
1.34
1.31
1.29
0.98
6.15
9.44
4.00
0.99
1.00
2.94
1.01
1.01
0.99
1.57
0.99
5.81
1.11
1.12
f1 (ppm)

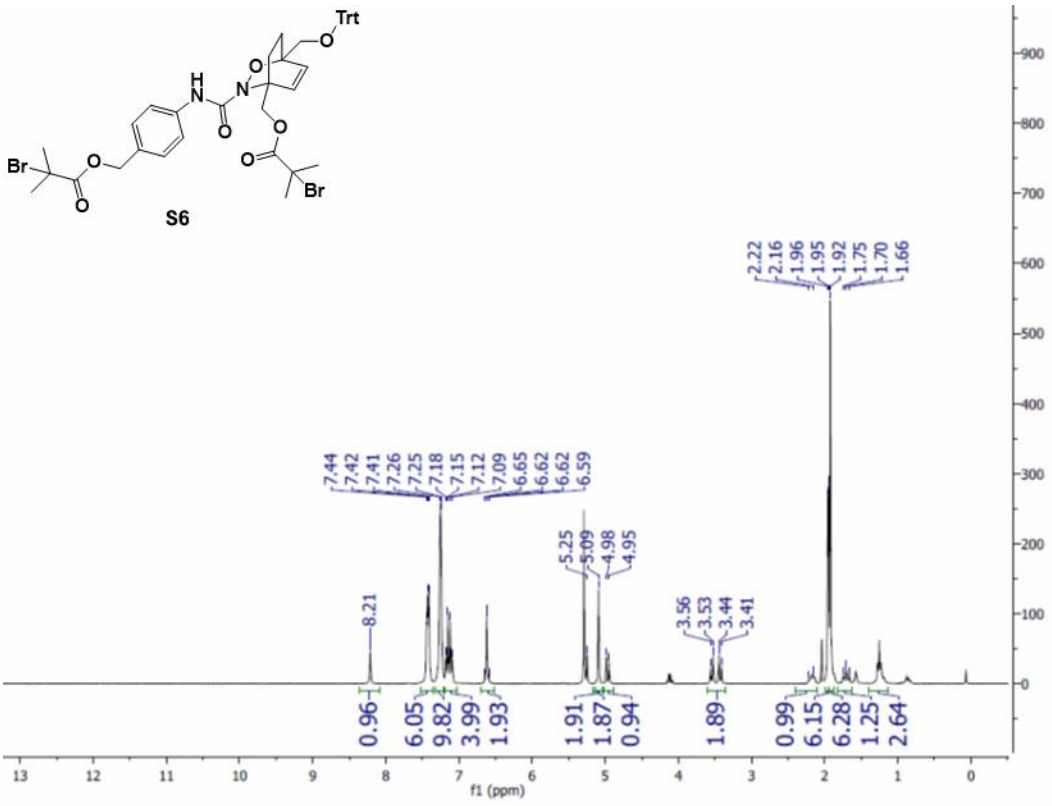
Trt
Br
Br
S6
7.44
7.42
7.41
7.26
7.25
7.18
7.15
7.12
7.09
6.65
6.62
6.62
6.59
8.21
5.25
5.09
4.98
4.95
3.56
3.53
3.44
3.41
2.22
2.16
1.96
1.95
1.92
1.75
1.70
1.66
0.96
6.05
9.82
3.99
1.93
1.91
1.87
0.94
1.89
0.99
6.15
6.28
1.25
2.64
f1 (ppm)

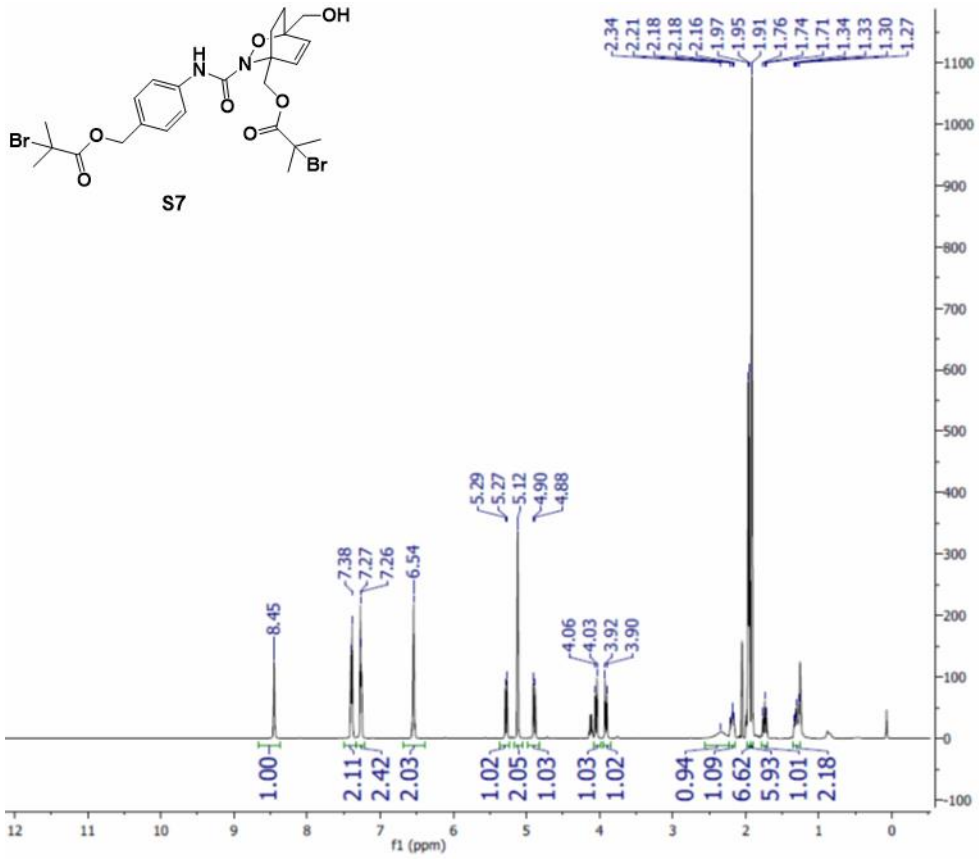
OH
H
N
O
N
O
O
O
Br
O
O
Br
S7
2.34
2.21
2.18
2.18
2.16
1.97
1.95
1.91
1.76
1.74
1.71
1.34
1.33
1.30
1.27
5.29
5.27
5.12
4.90
4.88
7.38
7.27
7.26
6.54
8.45
4.06
4.03
3.92
3.90
1.00
2.11
2.42
2.03
1.02
2.05
1.03
1.03
1.02
0.94
1.09
6.62
5.93
1.01
2.18
f1 (ppm)

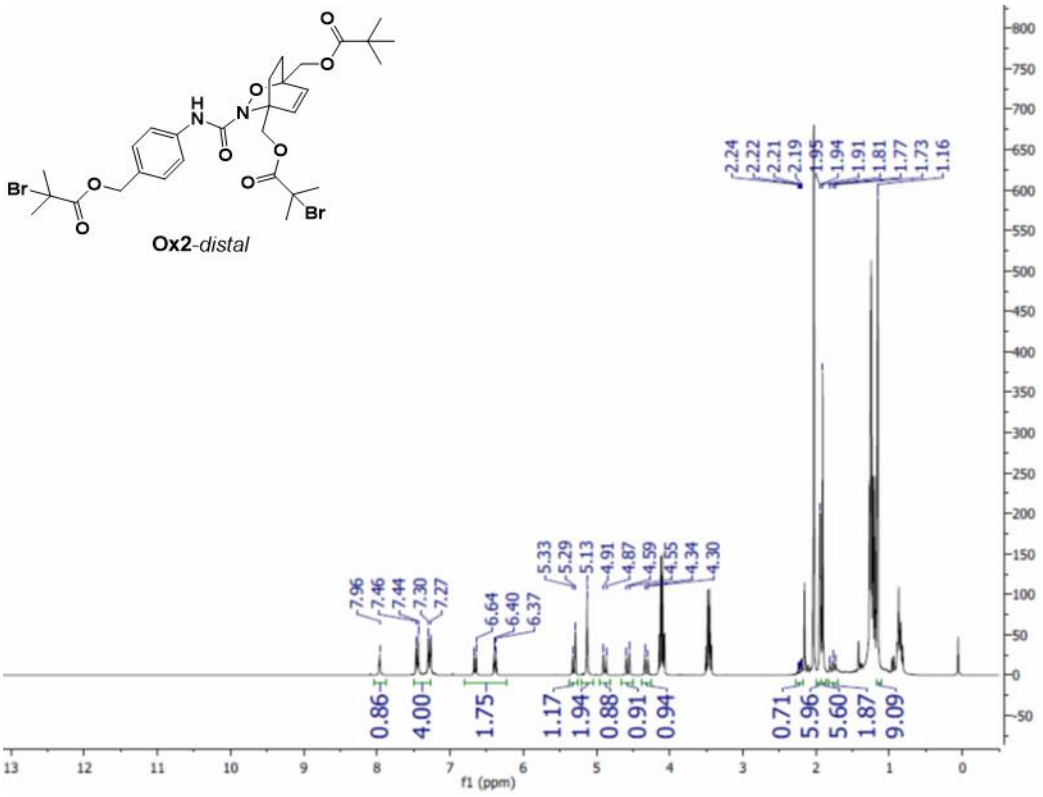
Ox2-distal
7.96
7.46
7.44
7.30
7.27
6.64
6.40
6.37
5.33
5.29
5.13
4.91
4.87
4.59
4.55
4.34
4.30
2.24
2.22
2.21
2.19
1.95
1.94
1.91
1.81
1.77
1.73
1.16
0.86
4.00
1.75
1.17
1.94
0.88
0.91
0.94
0.71
5.96
5.60
1.87
9.09
f1 (ppm)

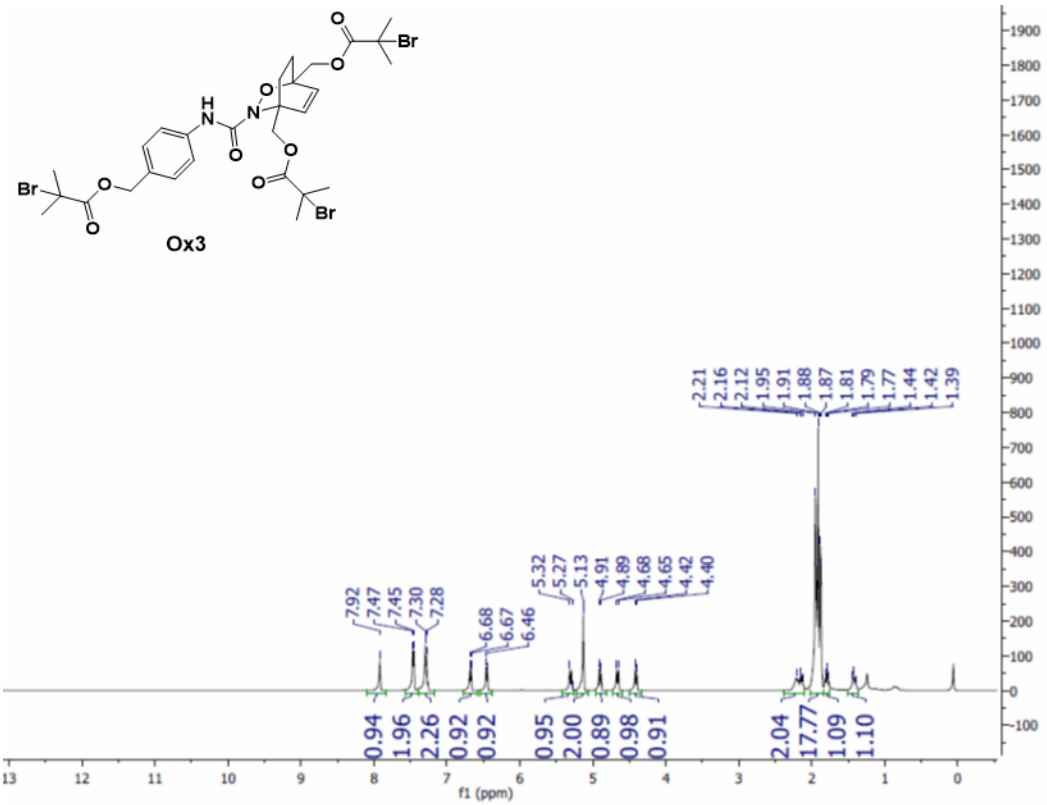
Br
O
O
H
N
O
N
O
O
O
Br
Br
O
O
Ox3
7.92
7.47
7.45
7.30
7.28
6.68
6.67
6.46
5.32
5.27
5.13
4.91
4.89
4.68
4.65
4.42
4.40
2.21
2.16
2.12
1.95
1.91
1.88
1.87
1.81
1.79
1.77
1.44
1.42
1.39
0.94
1.96
2.26
0.92
0.92
0.95
2.00
0.89
0.98
0.91
2.04
17.77
1.09
1.10
f1 (ppm)

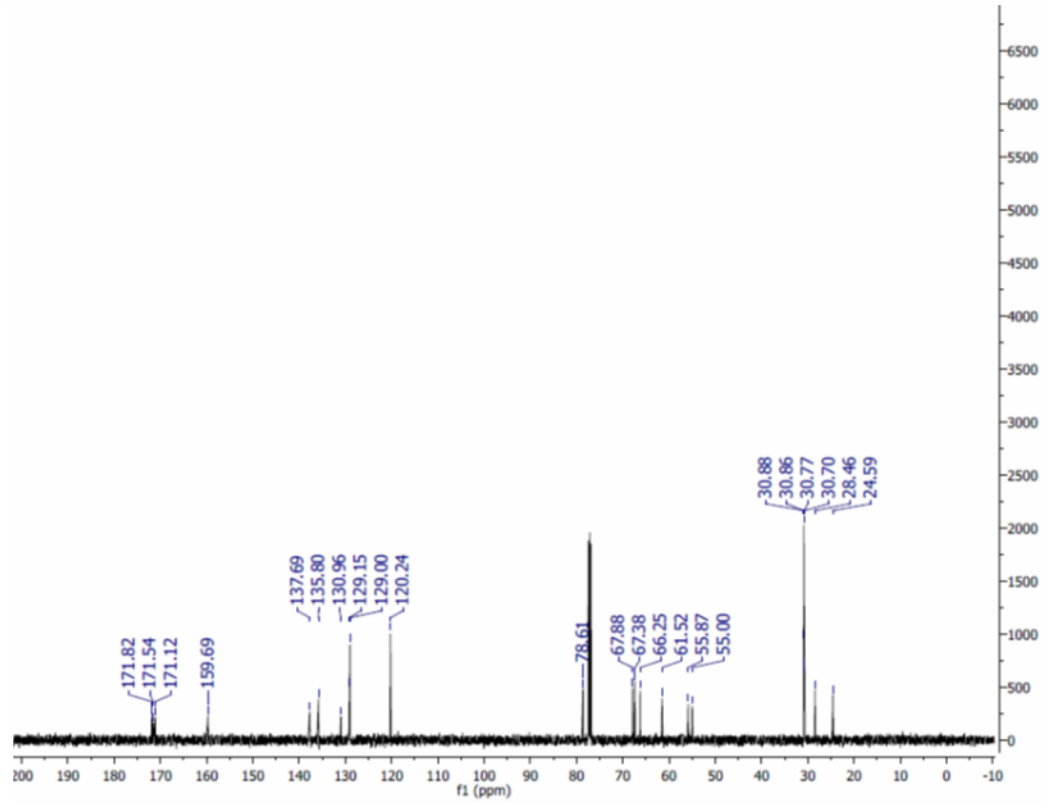
171.82
171.54
171.12
159.69
137.69
135.80
130.96
129.15
129.00
120.24
78.61
67.88
67.38
66.25
61.52
55.87
55.00
30.88
30.86
30.77
30.70
28.46
24.59
f1 (ppm)

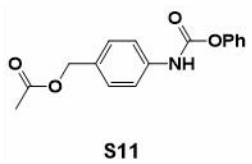
O
OPh
NH
O
O

S11

7.48
7.47
7.44
7.42
7.41
7.39
7.35
7.33
7.29
7.28
7.26
7.22
7.21
5.10
2.14
9.00
2.25
2.60
f1 (ppm)

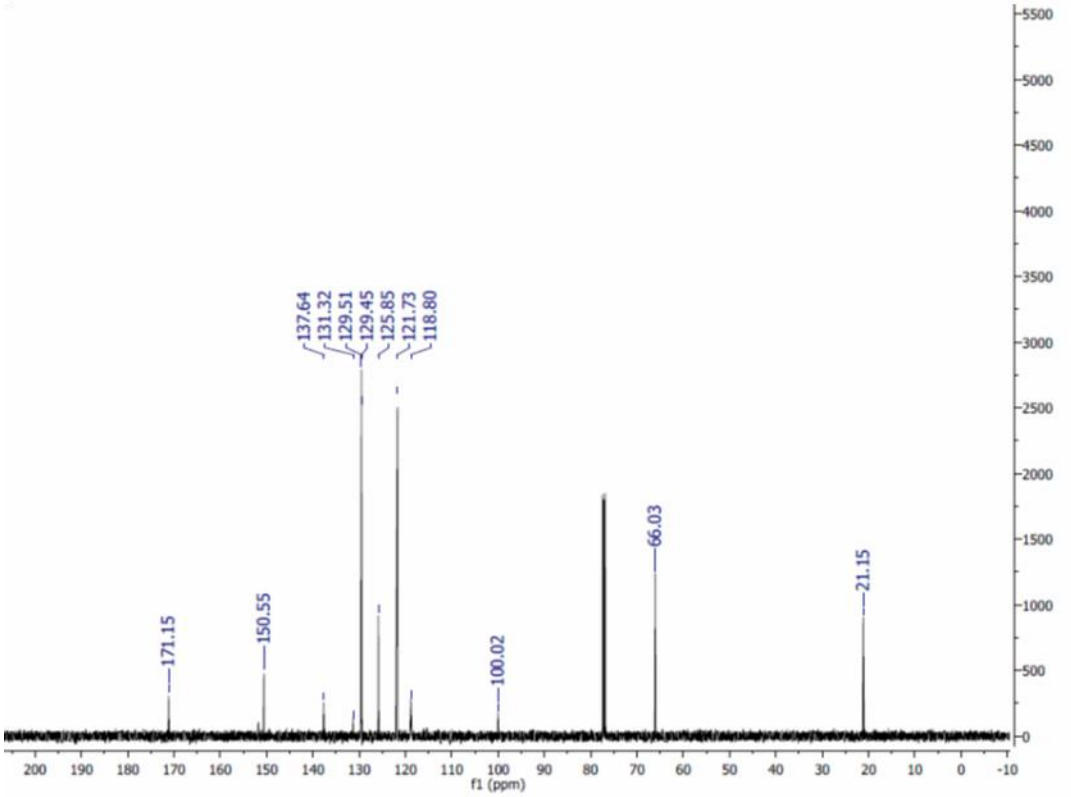
137.64
131.32
129.51
129.45
125.85
121.73
118.80
171.15
150.55
100.02
66.03
21.15
f1 (ppm)

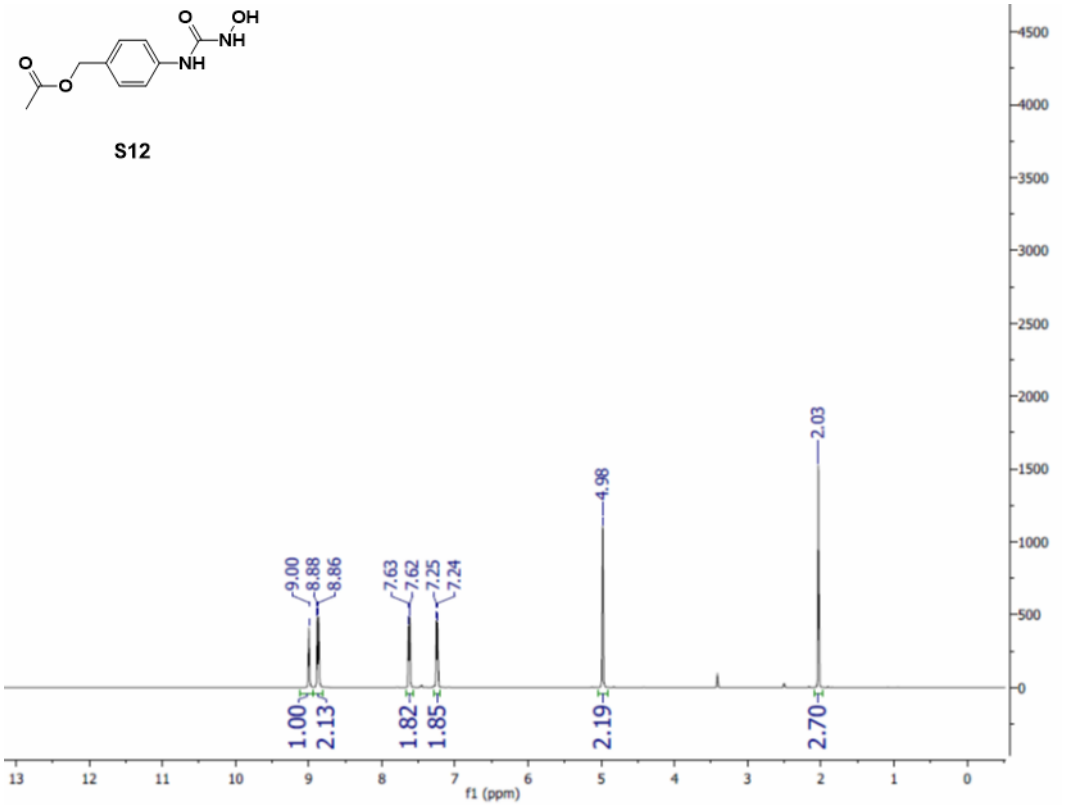
9.00
8.88
8.86
7.63
7.62
7.25
7.24
4.98
2.03
1.00
2.13
1.82
1.85
2.19
2.70
f1 (ppm)

S12

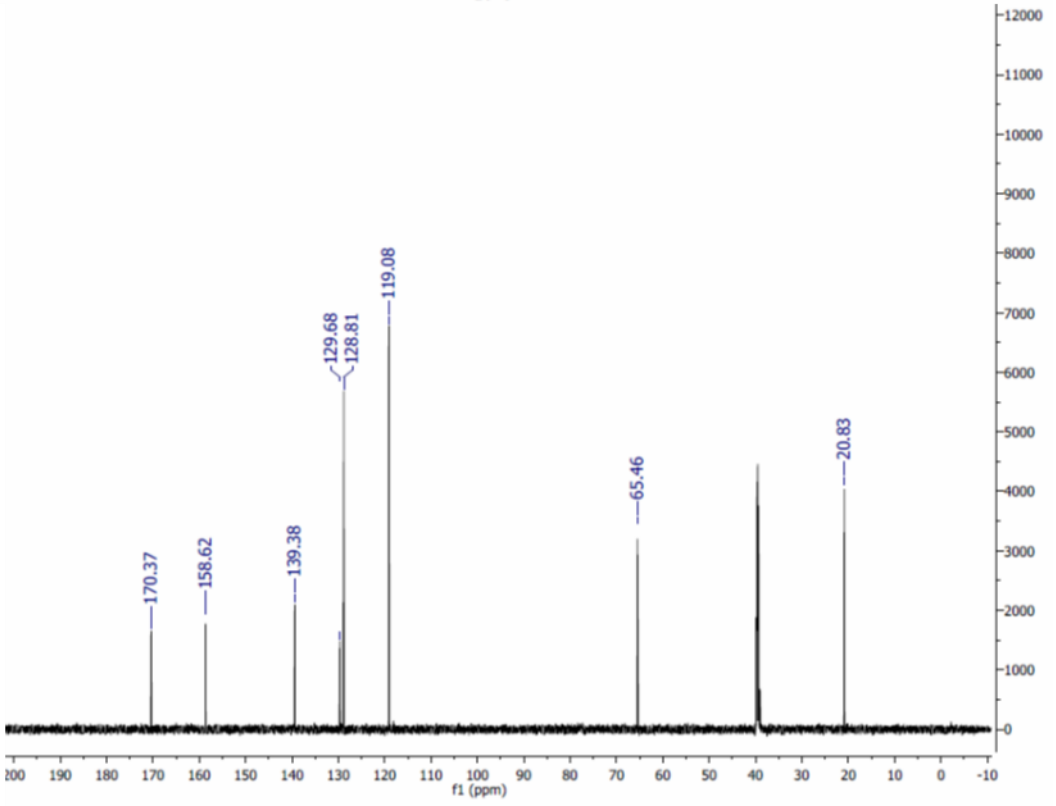
170.37
158.62
139.38
129.68
128.81
119.08
65.46
20.83
f1 (ppm)

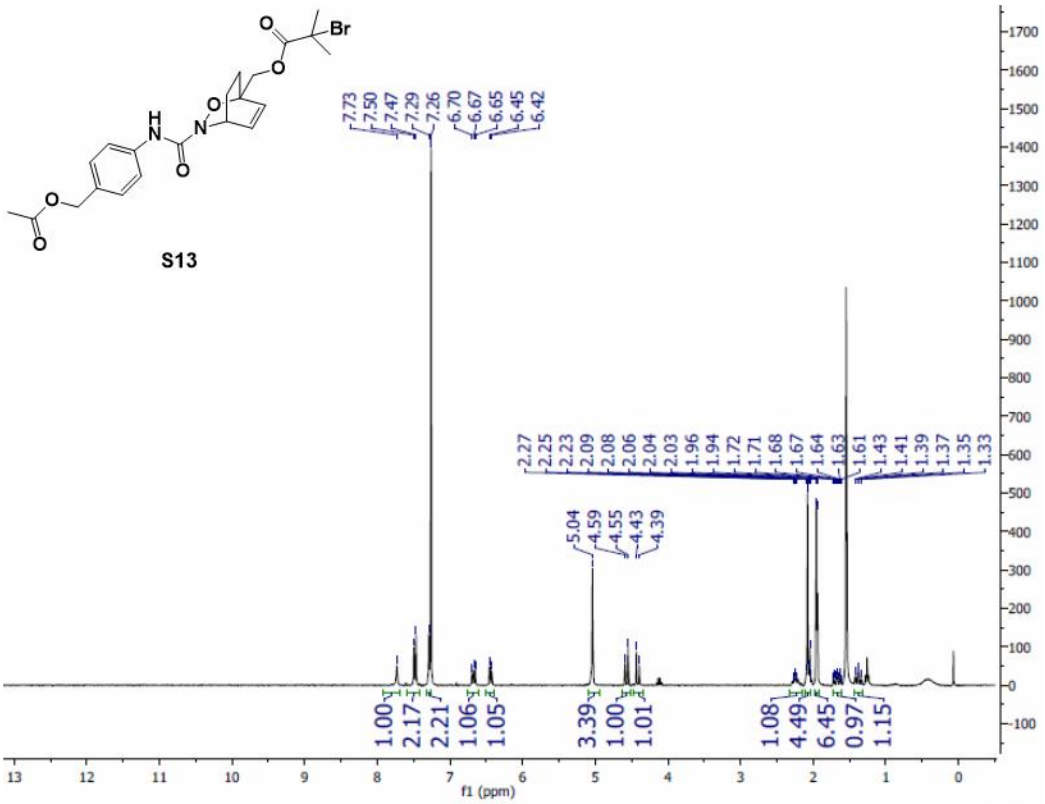
S13
7.73
7.50
7.47
7.29
7.26
6.70
6.67
6.65
6.45
6.42
5.04
4.59
4.55
4.43
4.39
2.27
2.25
2.23
2.09
2.08
2.06
2.04
2.03
1.96
1.94
1.72
1.71
1.68
1.67
1.64
1.63
1.61
1.43
1.41
1.39
1.37
1.35
1.33
1.00
2.17
2.21
1.06
1.05
3.39
1.00
1.01
1.08
4.49
6.45
0.97
1.15
f1 (ppm)

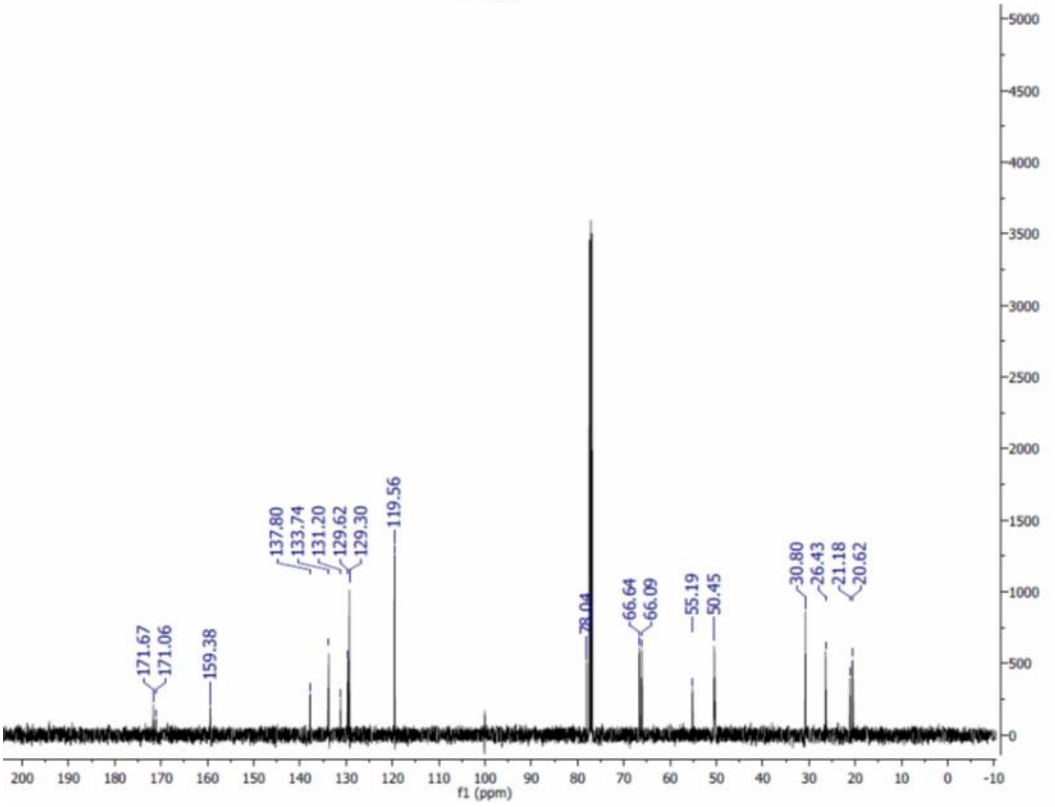
171.67
171.06
159.38
137.80
133.74
131.20
129.62
129.30
119.56
78.04
66.64
66.09
55.19
50.45
30.80
26.43
21.18
20.62
f1 (ppm)

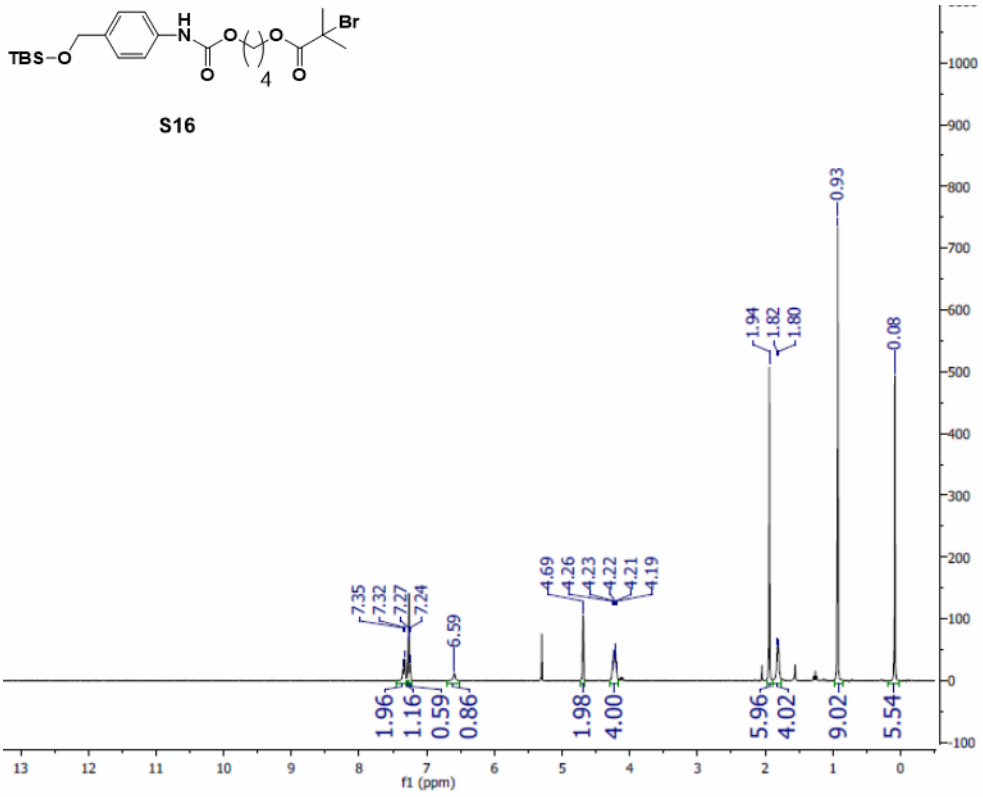
TBS
O
H
N
O
O
4
O
O
Br
S16
7.35
7.32
7.27
7.24
6.59
4.69
4.26
4.23
4.22
4.21
4.19
1.94
1.82
1.80
0.93
0.08
1.96
1.16
0.59
0.86
1.98
4.00
5.96
4.02
9.02
5.54
f1 (ppm)

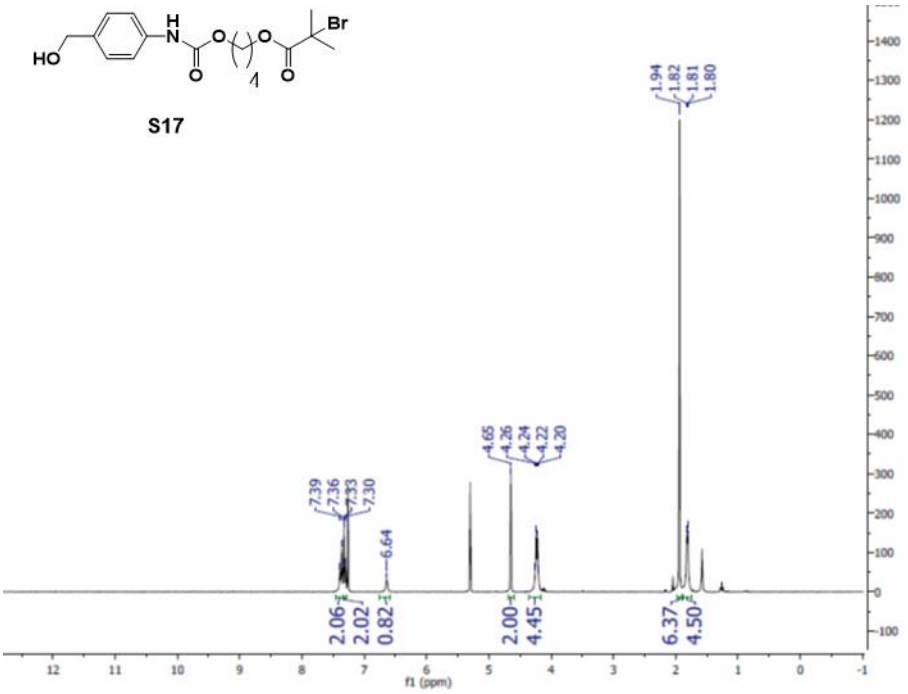
HO
H
N
O
O
4
O
O
Br
S17
7.39
7.36
7.33
7.30
6.64
4.65
4.26
4.24
4.22
4.20
1.94
1.82
1.81
1.80
2.06
2.02
0.82
2.00
4.45
6.37
4.50
f1 (ppm)

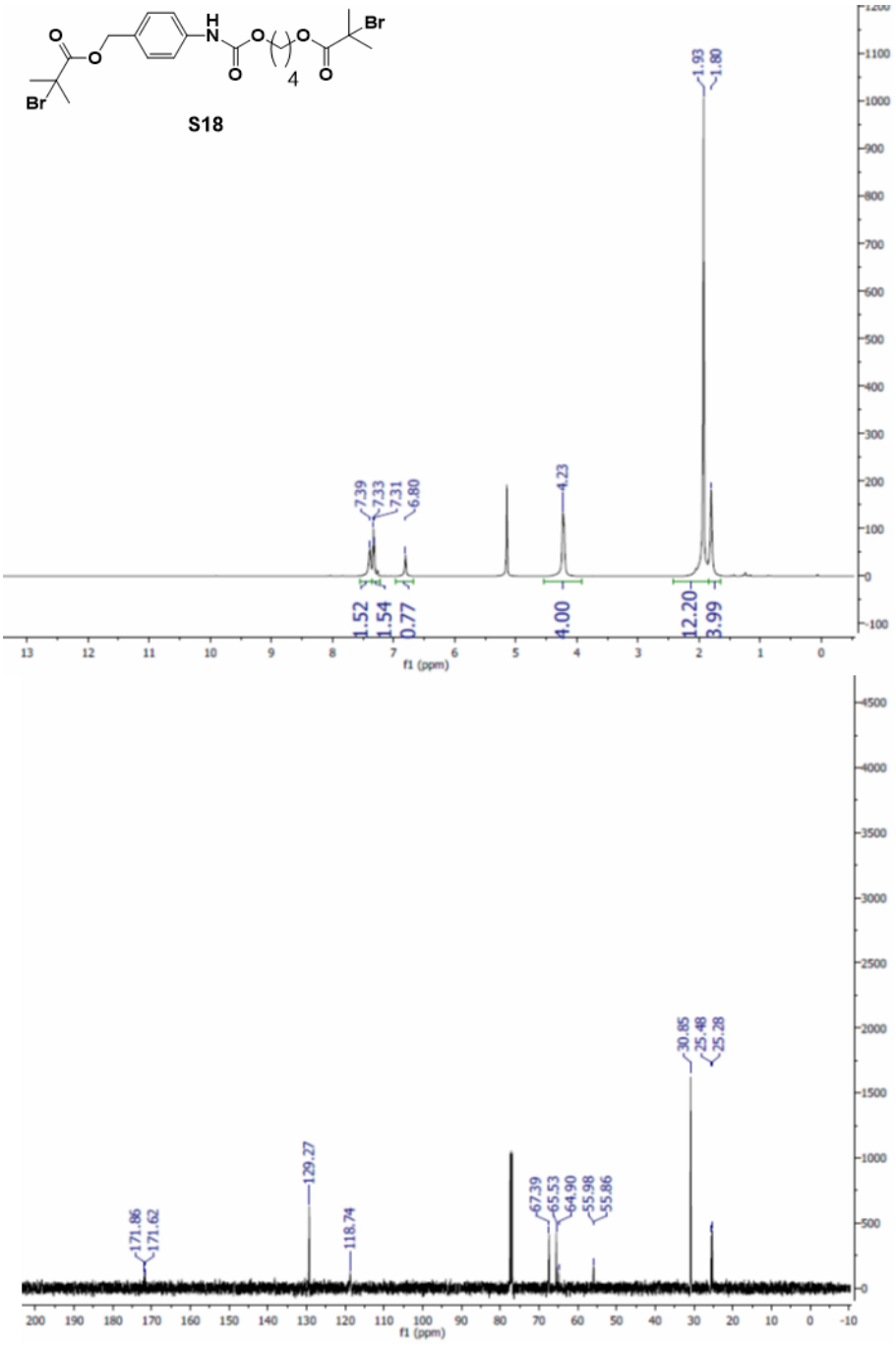
S18
7.39
7.33
7.31
6.80
4.23
1.93
1.80
1.52
1.54
0.77
4.00
12.20
3.99
f1 (ppm)
171.86
171.62
129.27
118.74
67.39
65.53
64.90
55.98
55.86
30.85
25.48
25.28
f1 (ppm)

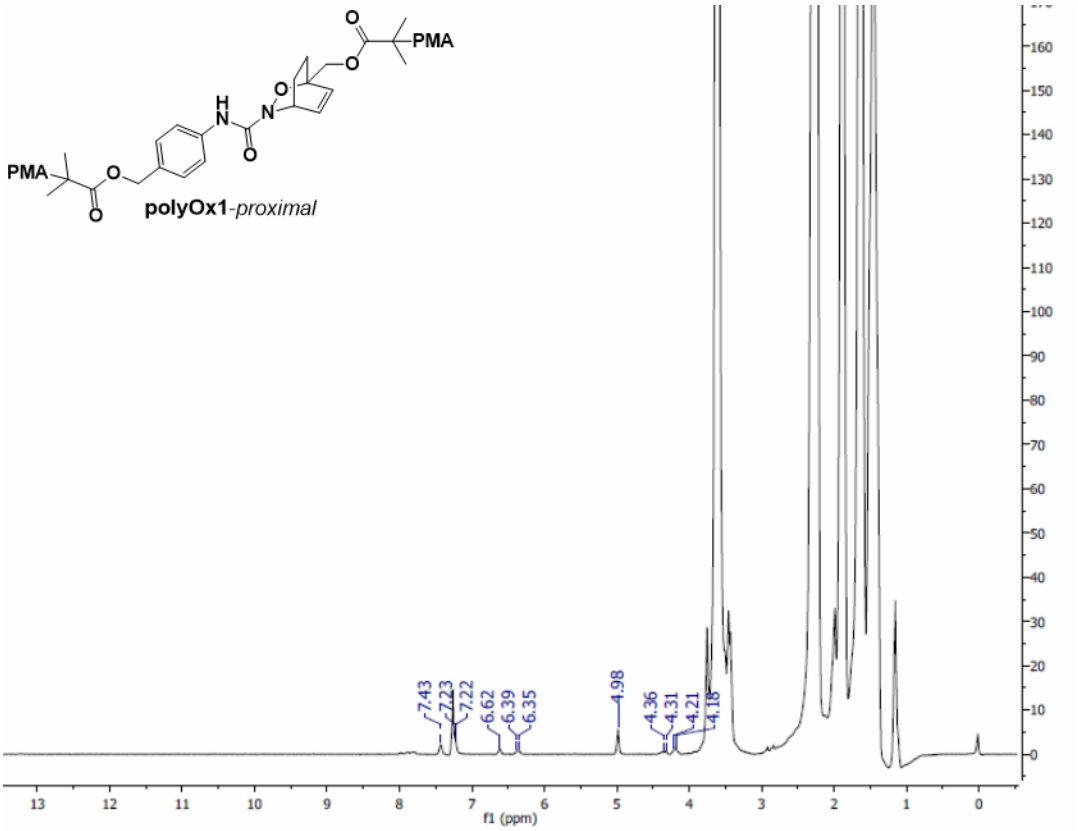
PMA
PMA
polyOx1-proximal
7.43
7.23
7.22
6.62
6.39
6.35
4.98
4.36
4.31
4.21
4.18
f1 (ppm)

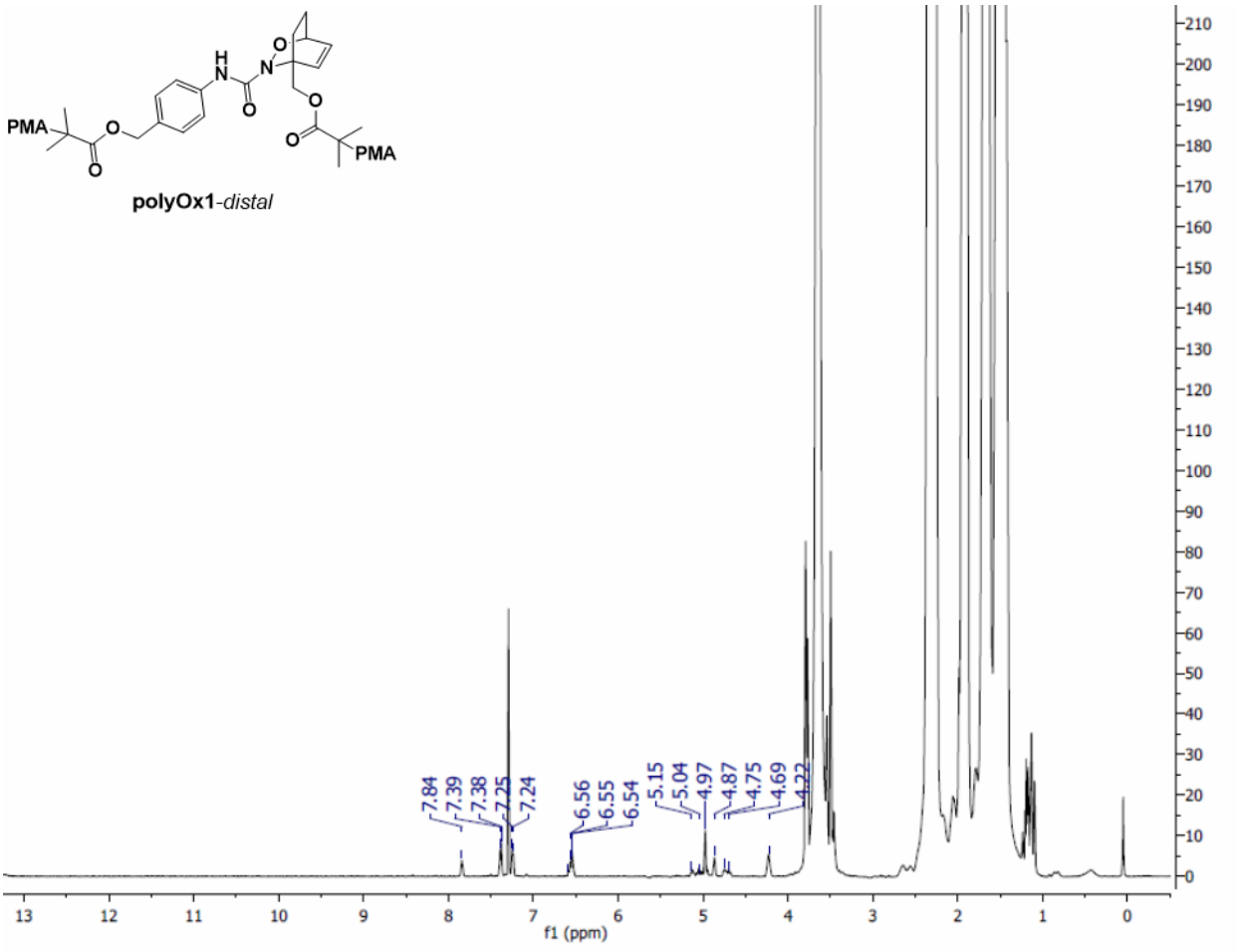
PMA
PMA
polyOx1-distal
7.84
7.39
7.38
7.25
7.24
6.56
6.55
6.54
5.15
5.04
4.97
4.87
4.75
4.69
4.22
f1 (ppm)

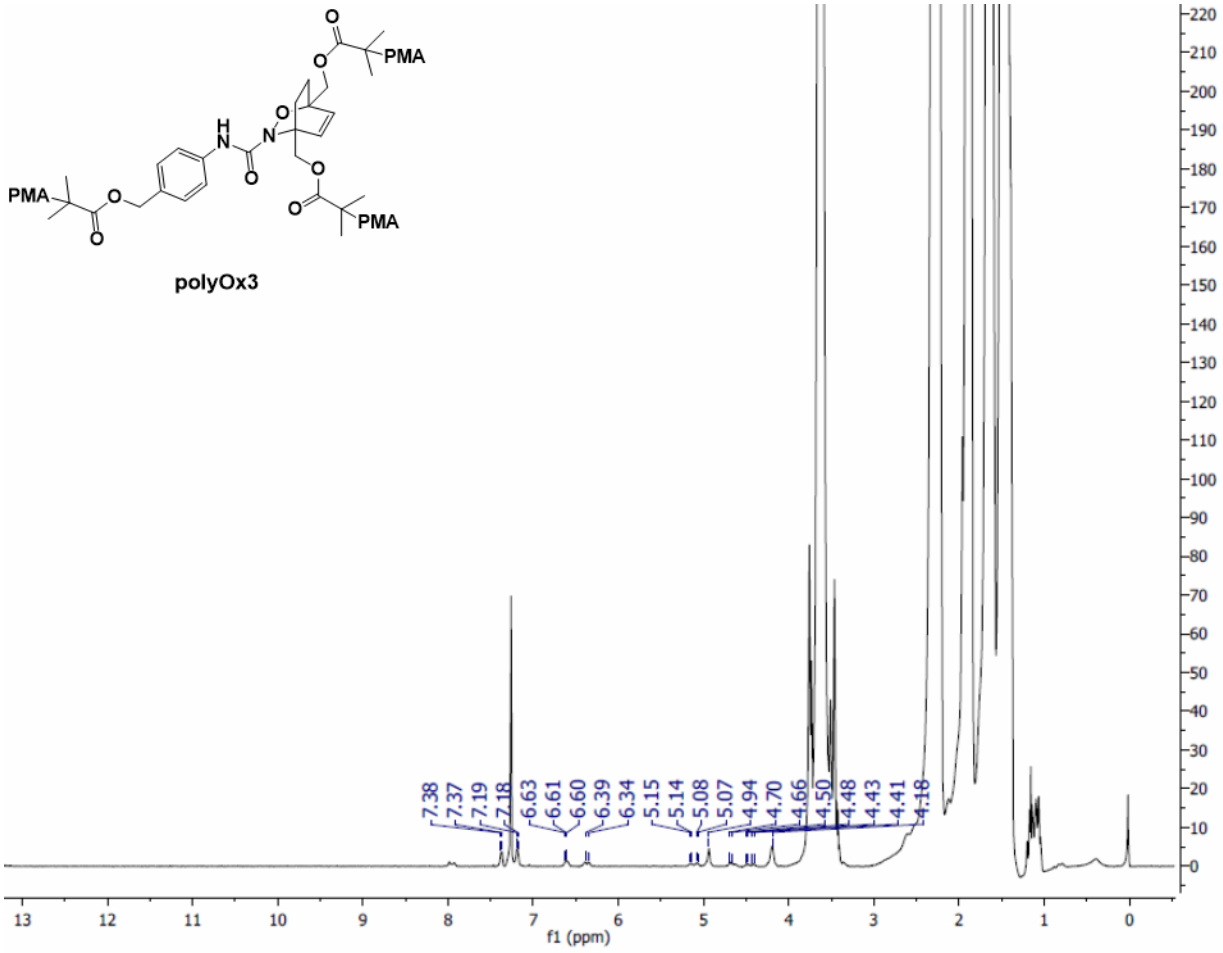
PMA
PMA
PMA
polyOx3
7.38
7.37
7.19
7.18
6.63
6.61
6.60
6.39
6.34
5.15
5.14
5.08
5.07
4.94
4.70
4.66
4.50
4.48
4.43
4.41
4.18
f1 (ppm)

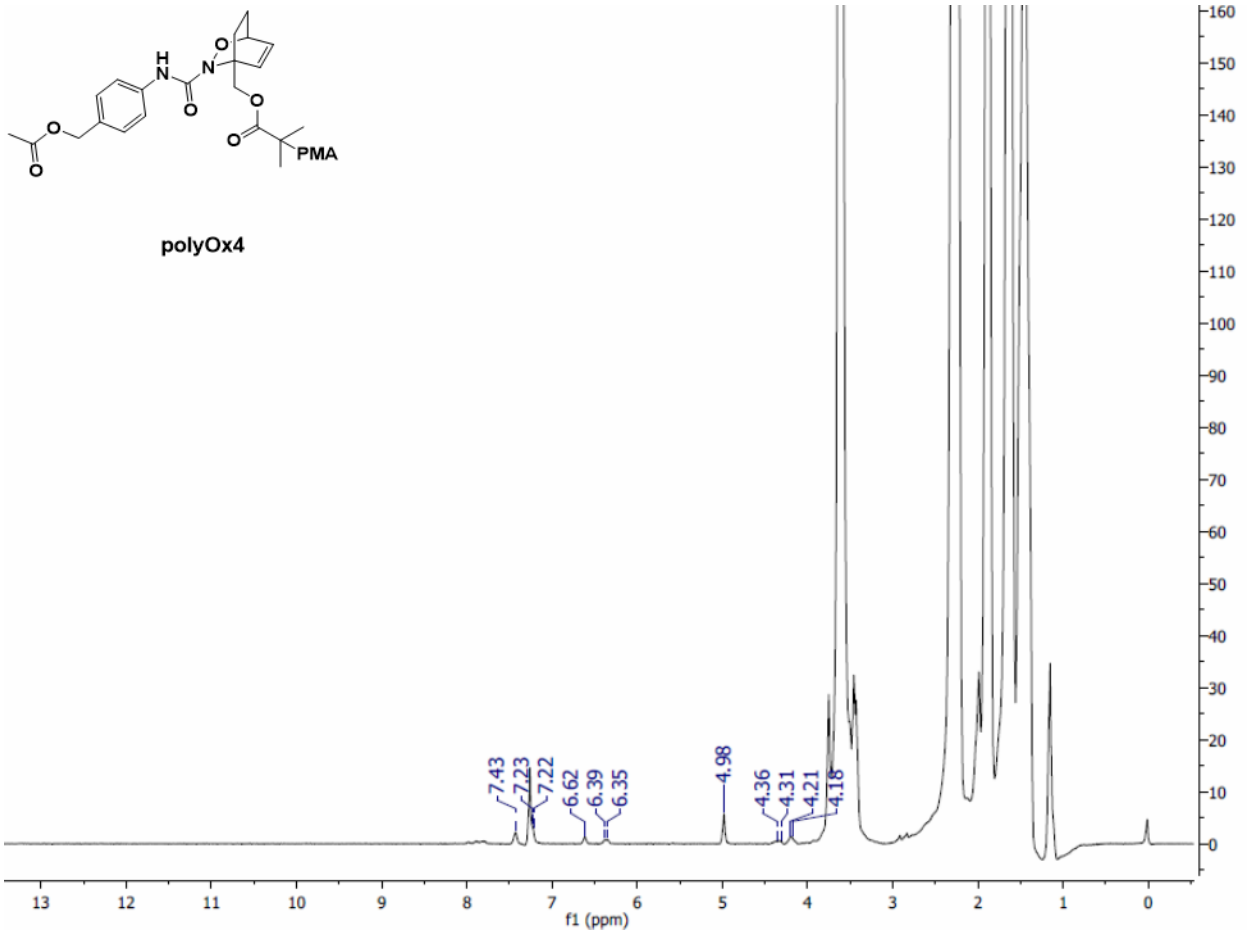
PMA
polyOx4
7.43
7.23
7.22
6.62
6.39
6.35
4.98
4.36
4.31
4.21
4.18
f1 (ppm)

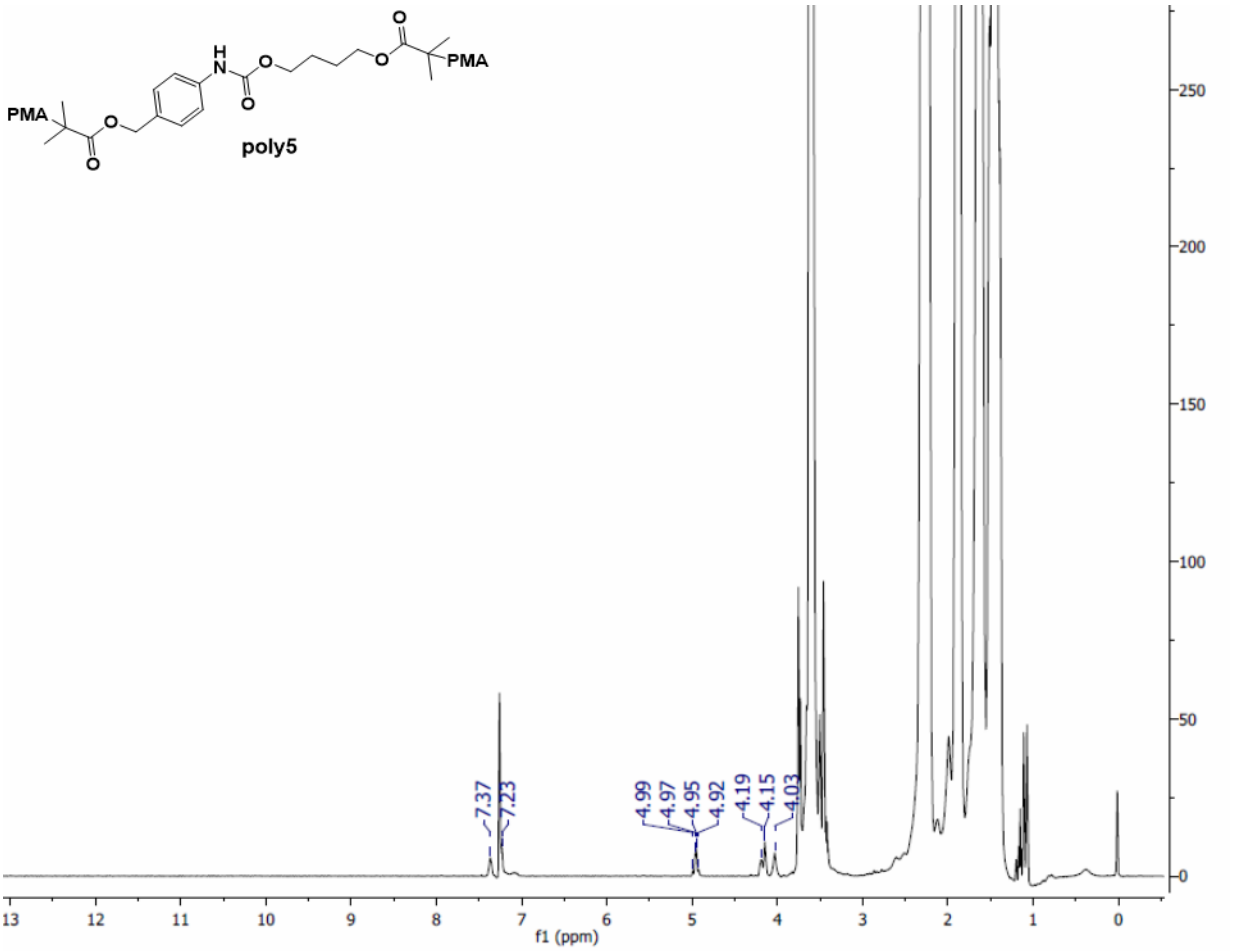

7.6.25 *Experimental References*

1) Holtz, H. D.; Stock L. M. *J. Am. Chem. Soc.* **1964**, *86*, 5183.

2) Sagi, A.; Weinstain, R.; Karton, N.; Shabat, D. *J. Am. Chem. Soc.* **2008**, *130*, 5434.

3) (a) Chapman, N. B.; Sotheeswaran, S.; Toyne, K. J. *J. Org. Chem.* **1969**, *36*, 917; (b) Chu, Y.; Lynch, V.; Iverson, B. L. *Tetrahedron* **2006**, *62*, 5536.

4) El Alaoui, A.; Schmidt, F.; Monneret, C.; Florent, J.-C. *J. Org. Chem.* **2006**, *71*, 9628.

5) Bernaerts, K. V; Schacht, E. H.; Goethals, E. J.; Prez, F. E. D. U. *J. Polym. Sci.: Part A: Polym. Chem.* **2003**, *281*, 3206.

APPENDIX A

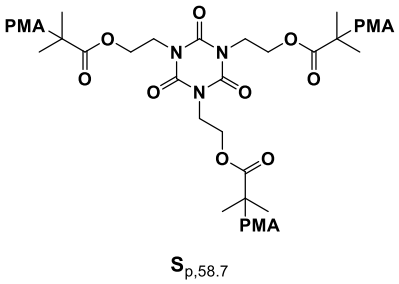

$S_{p,58.7}$

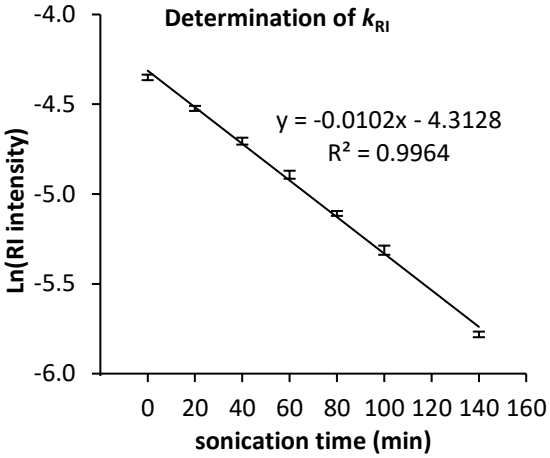

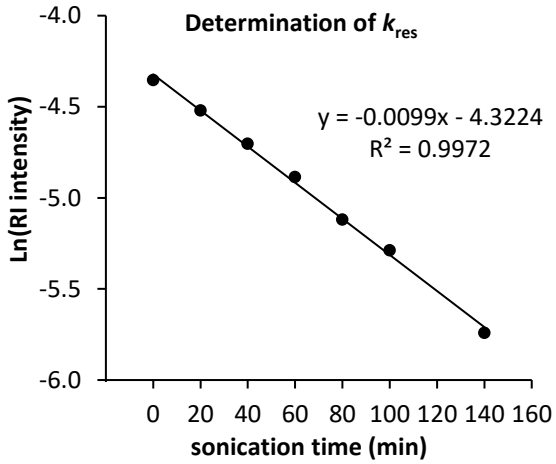

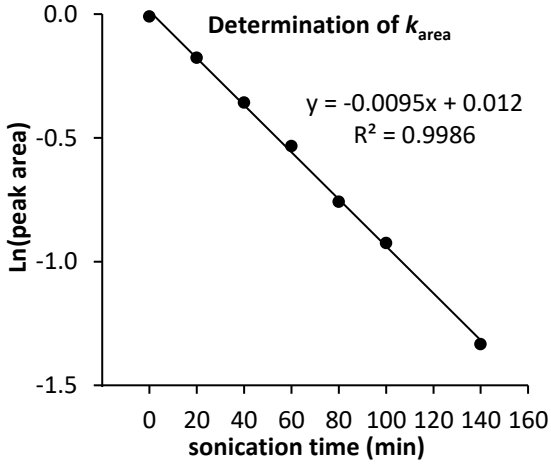

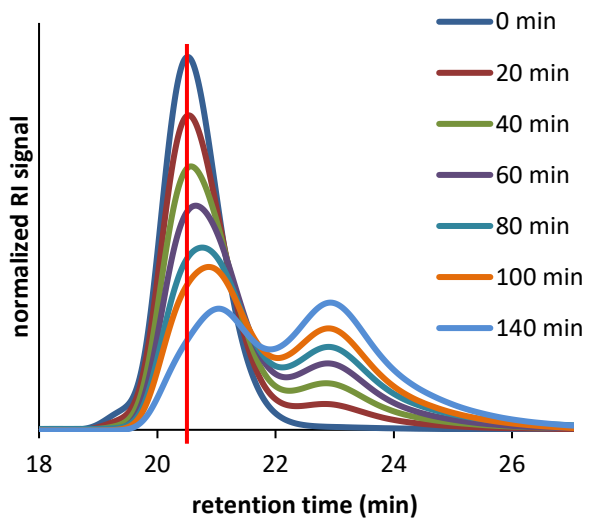

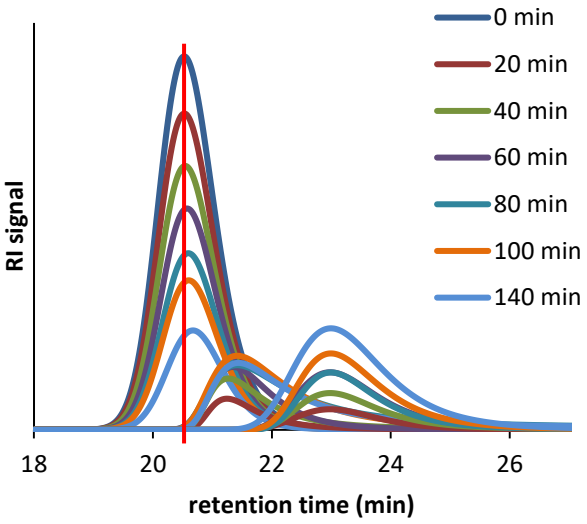

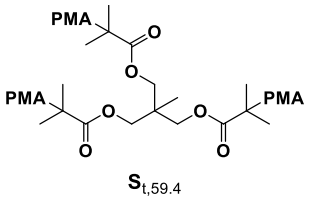
PMA
PMA
PMA
O
O
O
O
O
O
$S_{t,59.4}$

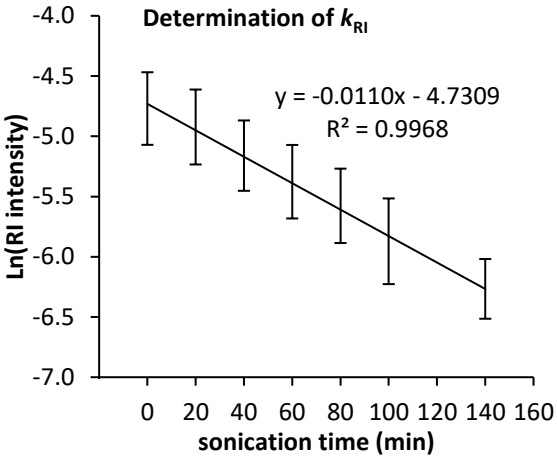
Determination of k_{RI}
y = -0.0110x - 4.7309
R² = 0.9968
Ln(RI intensity)
-4.0
-4.5
-5.0
-5.5
-6.0
-6.5
-7.0
0 20 40 60 80 100 120 140 160
sonication time (min)

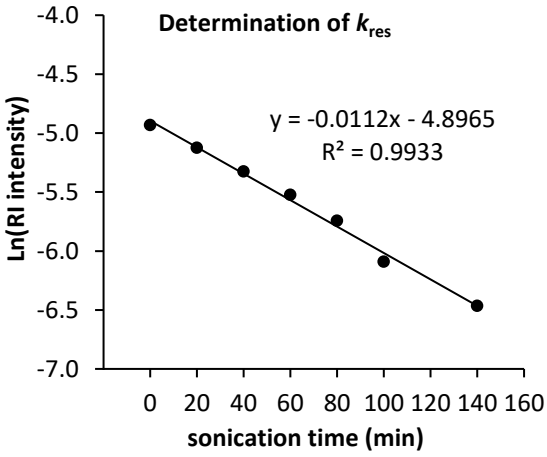
Determination of k_{res}
y = -0.0112x - 4.8965
R² = 0.9933
Ln(RI intensity)
-4.0
-4.5
-5.0
-5.5
-6.0
-6.5
-7.0
0 20 40 60 80 100 120 140 160
sonication time (min)

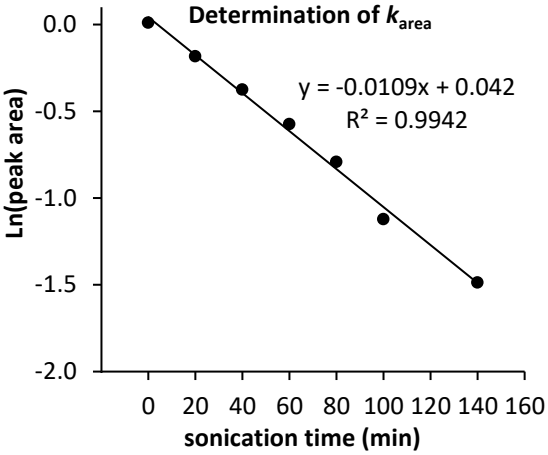
Determination of k_{area}
y = -0.0109x + 0.042
R² = 0.9942
Ln(peak area)
0.0
-0.5
-1.0
-1.5
-2.0
0 20 40 60 80 100 120 140 160
sonication time (min)

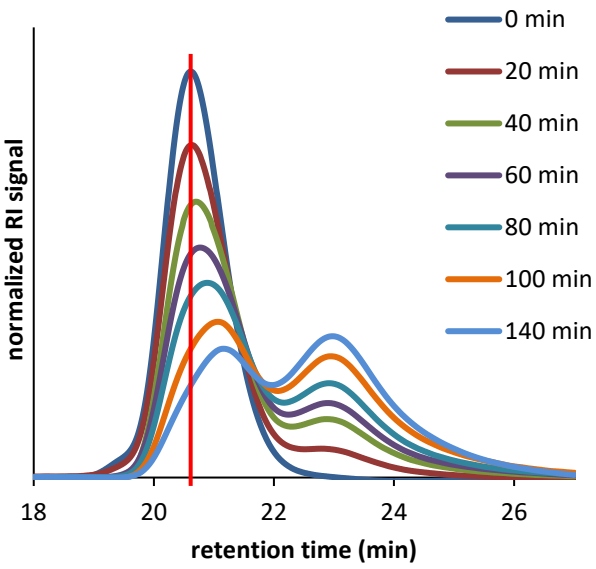
normalized RI signal
0 min
20 min
40 min
60 min
80 min
100 min
140 min
18 20 22 24 26
retention time (min)

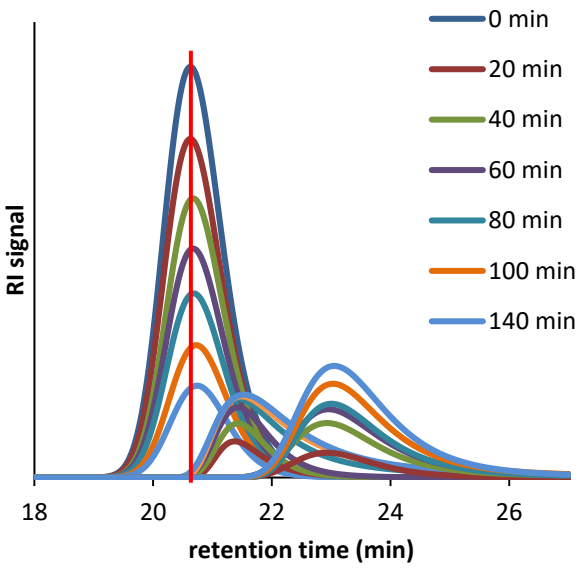
RI signal
0 min
20 min
40 min
60 min
80 min
100 min
140 min
18 20 22 24 26
retention time (min)

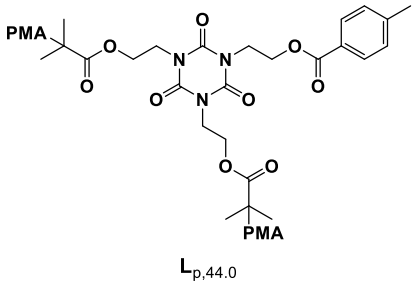
PMA
PMA
$L_{p,44.0}$

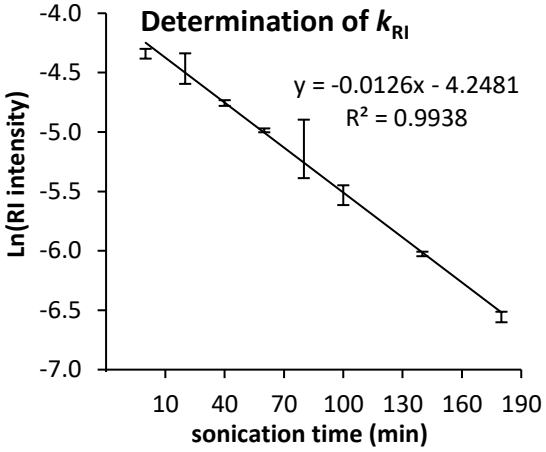
Determination of k_{RI}
y = -0.0126x - 4.2481
R² = 0.9938
Ln(RI intensity)
sonication time (min)

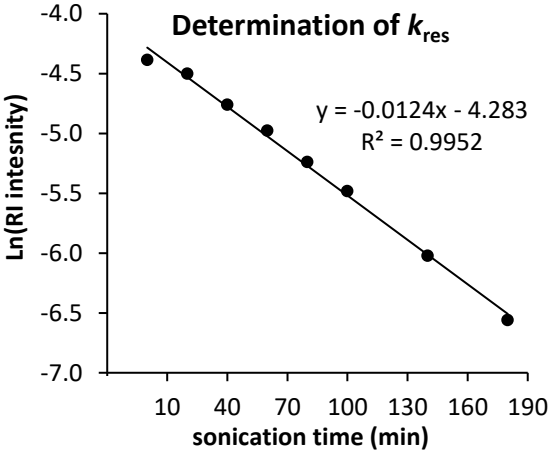
Determination of k_{res}
y = -0.0124x - 4.283
R² = 0.9952
Ln(RI intesnity)
sonication time (min)

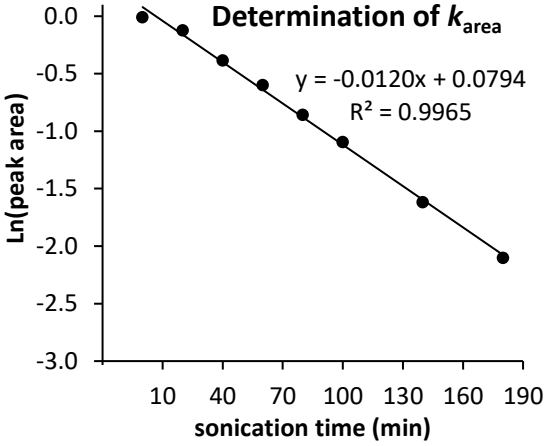
Determination of k_{area}
y = -0.0120x + 0.0794
R² = 0.9965
Ln(peak area)
sonication time (min)

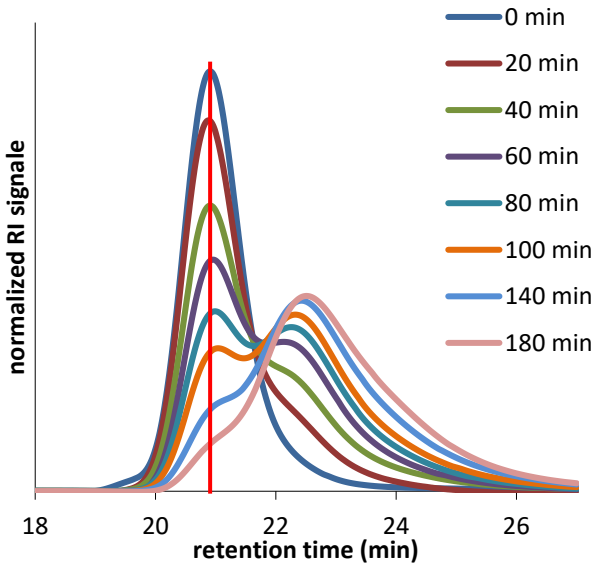
0 min
20 min
40 min
60 min
80 min
100 min
140 min
180 min
normalized RI signale
retention time (min)

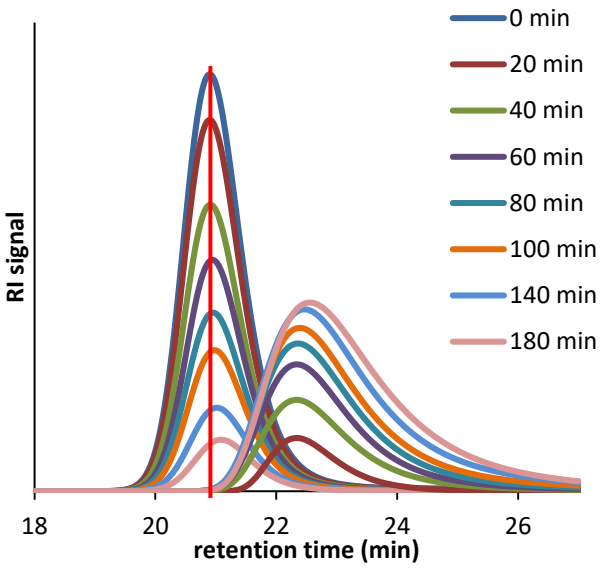
0 min
20 min
40 min
60 min
80 min
100 min
140 min
180 min
RI signal
retention time (min)

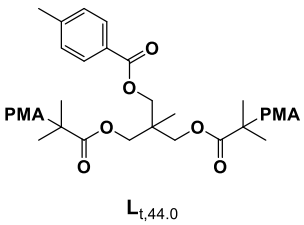
PMA
PMA
O
O
O
O
O
O
$L_{t,44.0}$

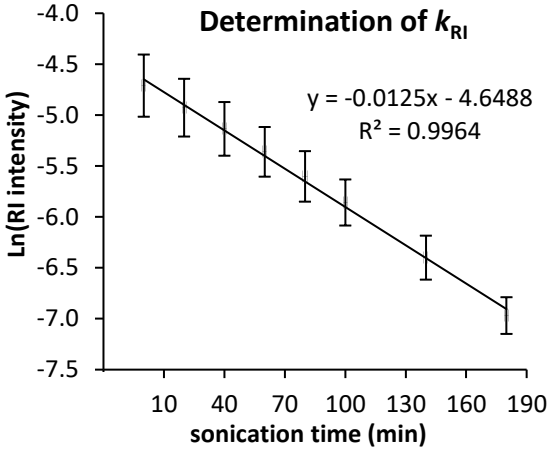
Determination of k_{RI}
y = -0.0125x - 4.6488
R² = 0.9964
Ln(RI intensity)
-4.0
-4.5
-5.0
-5.5
-6.0
-6.5
-7.0
-7.5
10 40 70 100 130 160 190
sonication time (min)

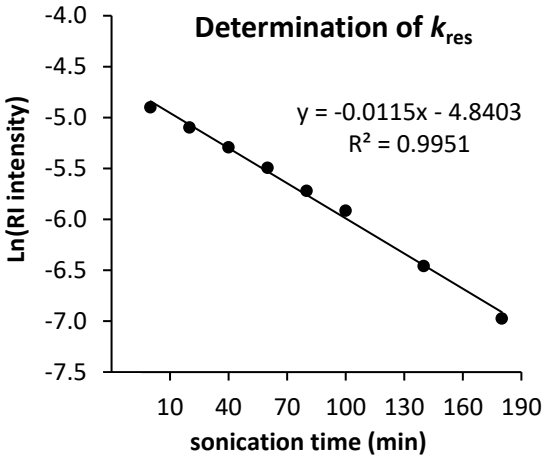
Determination of k_{res}
y = -0.0115x - 4.8403
R² = 0.9951
Ln(RI intensity)
-4.0
-4.5
-5.0
-5.5
-6.0
-6.5
-7.0
-7.5
10 40 70 100 130 160 190
sonication time (min)

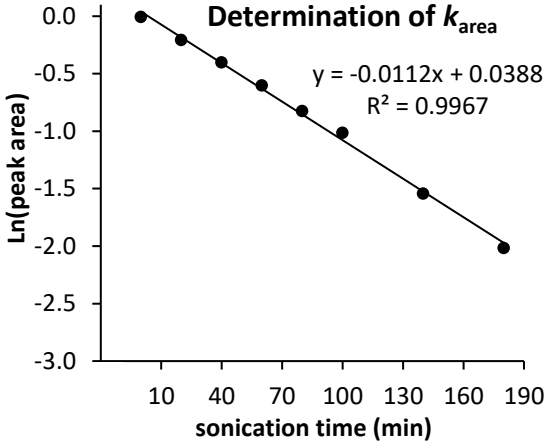
Determination of k_{area}
y = -0.0112x + 0.0388
R² = 0.9967
Ln(peak area)
0.0
-0.5
-1.0
-1.5
-2.0
-2.5
-3.0
10 40 70 100 130 160 190
sonication time (min)

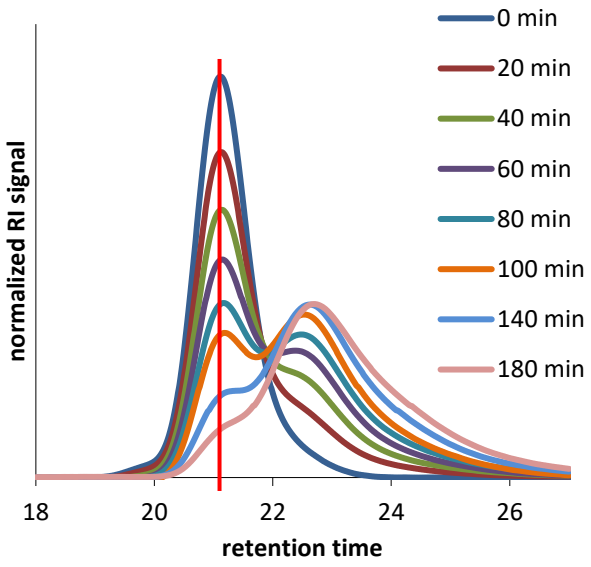
normalized RI signal
0 min
20 min
40 min
60 min
80 min
100 min
140 min
180 min
18 20 22 24 26
retention time

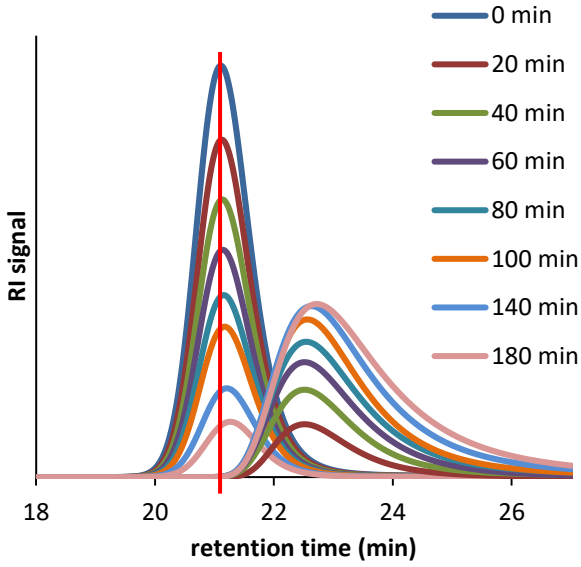
RI signal
0 min
20 min
40 min
60 min
80 min
100 min
140 min
180 min
18 20 22 24 26
retention time (min)

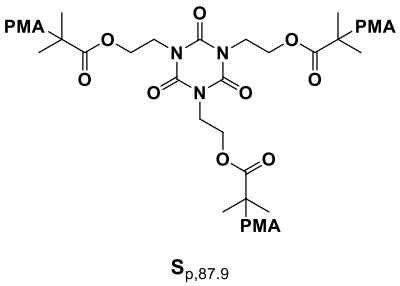
PMA
PMA
PMA

$S_{p,87.9}$

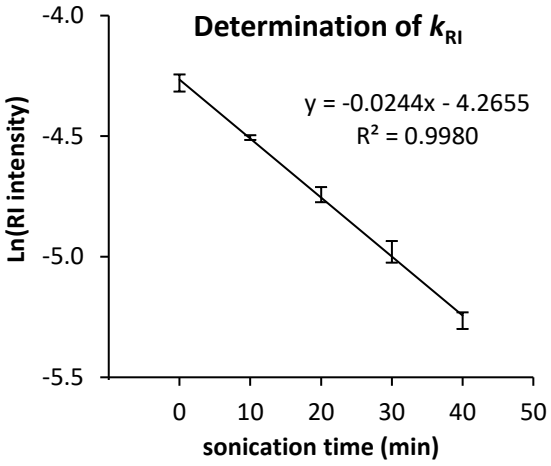
Determination of k_{RI}
y = -0.0244x - 4.2655
R² = 0.9980
Ln(RI intensity)
-4.0
-4.5
-5.0
-5.5
0
10
20
30
40
50
sonication time (min)

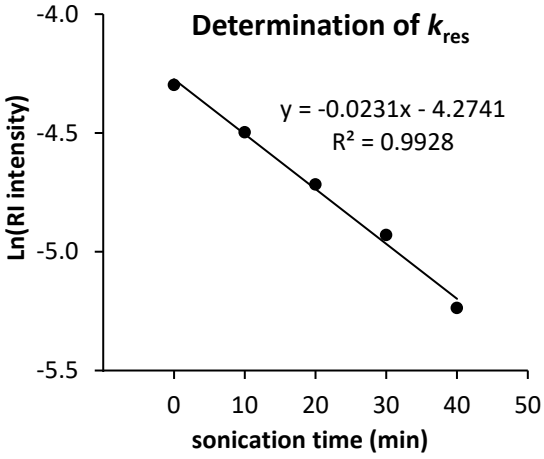
Determination of k_{res}
y = -0.0231x - 4.2741
R² = 0.9928
Ln(RI intensity)
-4.0
-4.5
-5.0
-5.5
0
10
20
30
40
50
sonication time (min)

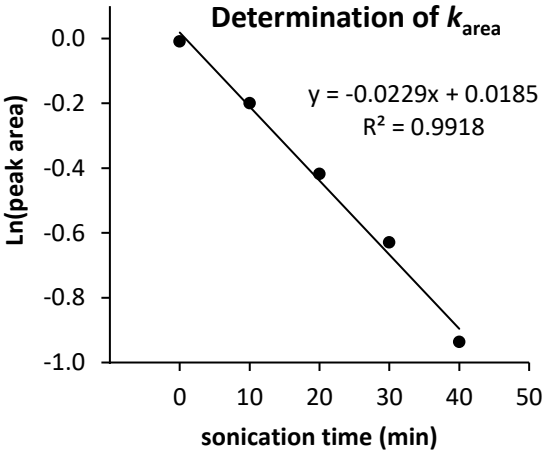
Determination of k_{area}
y = -0.0229x + 0.0185
R² = 0.9918
Ln(peak area)
0.0
-0.2
-0.4
-0.6
-0.8
-1.0
0
10
20
30
40
50
sonication time (min)

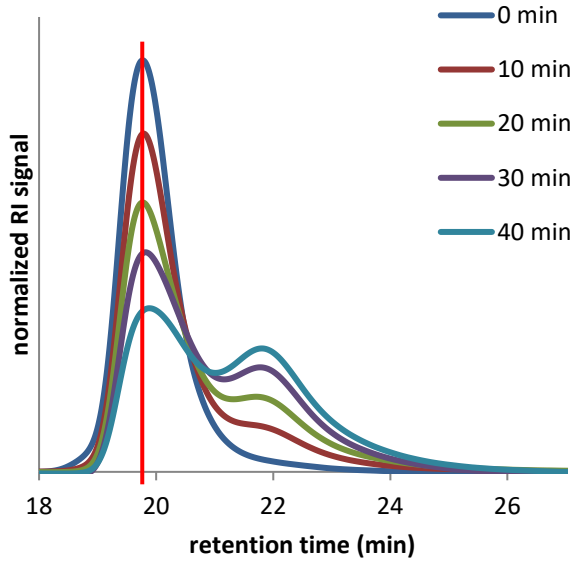
0 min
10 min
20 min
30 min
40 min
normalized RI signal
18
20
22
24
26
retention time (min)

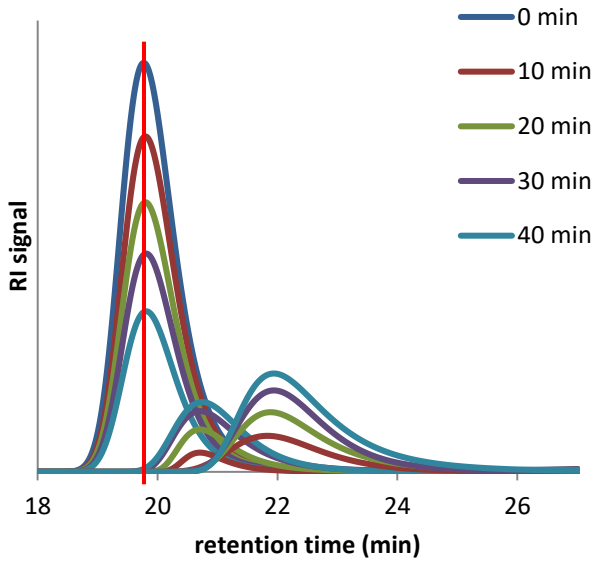
0 min
10 min
20 min
30 min
40 min
RI signal
18
20
22
24
26
retention time (min)

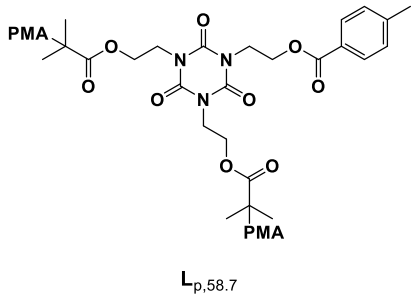
PMA
PMA

$L_{p,58.7}$

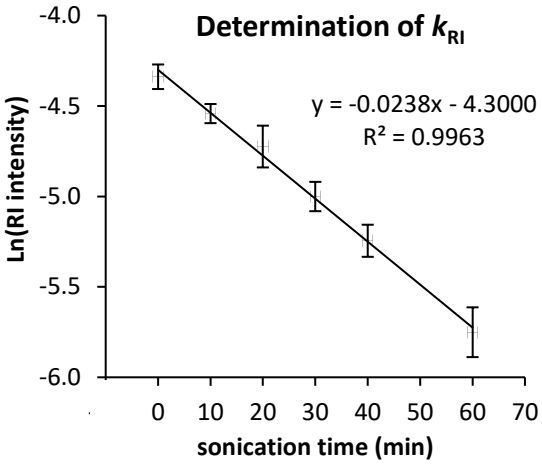
Determination of k_{RI}
y = -0.0238x - 4.3000
R² = 0.9963
Ln(RI intensity)
sonication time (min)

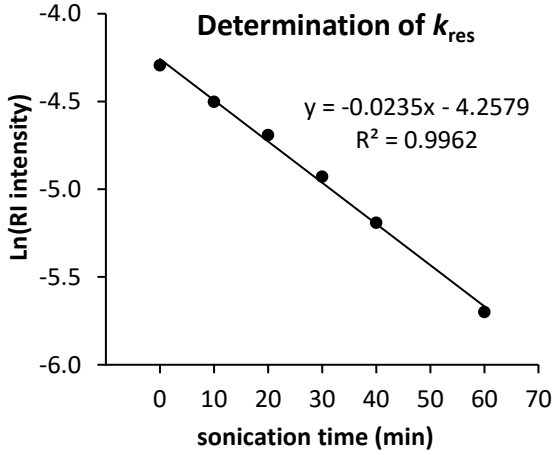
Determination of k_{res}
y = -0.0235x - 4.2579
R² = 0.9962
Ln(RI intensity)
sonication time (min)

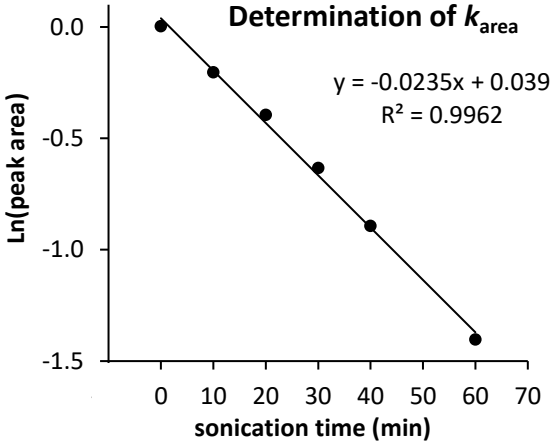
Determination of k_{area}
y = -0.0235x + 0.039
R² = 0.9962
Ln(peak area)
sonication time (min)

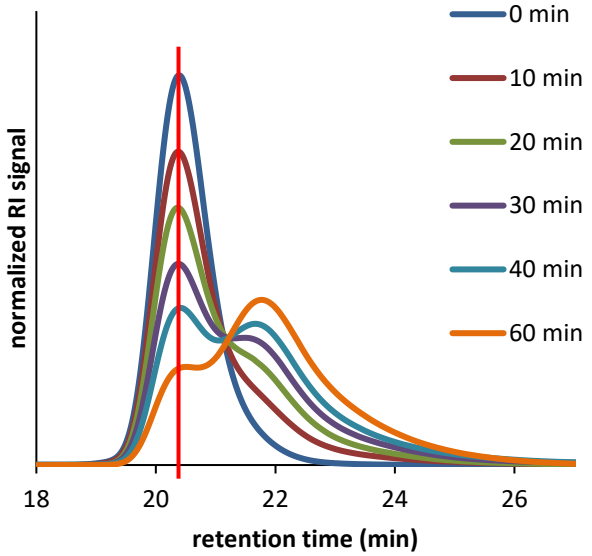
0 min
10 min
20 min
30 min
40 min
60 min
normalized RI signal
retention time (min)

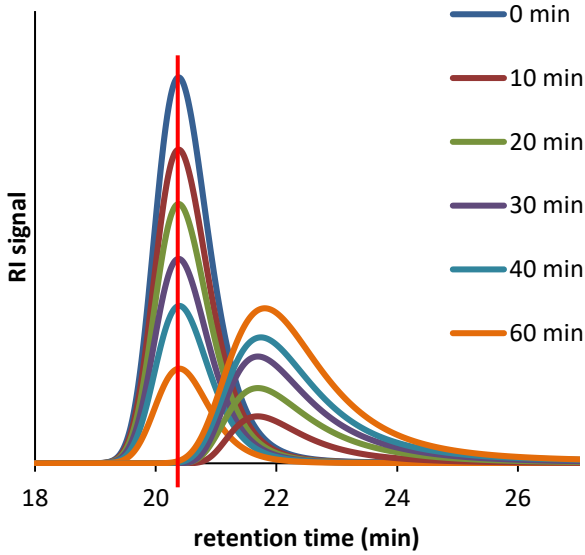
0 min
10 min
20 min
30 min
40 min
60 min
RI signal
retention time (min)

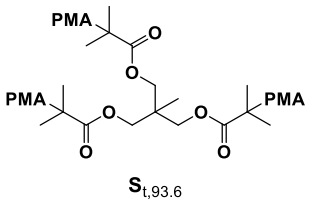
PMA
PMA
PMA
O
O
O
O
O
O
$S_{t,93.6}$

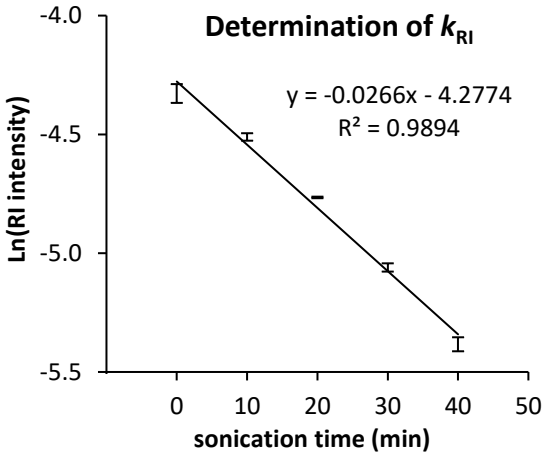
Determination of k_{RI}
y = -0.0266x - 4.2774
R² = 0.9894
Ln(RI intensity)
-4.0
-4.5
-5.0
-5.5
0
10
20
30
40
50
sonication time (min)

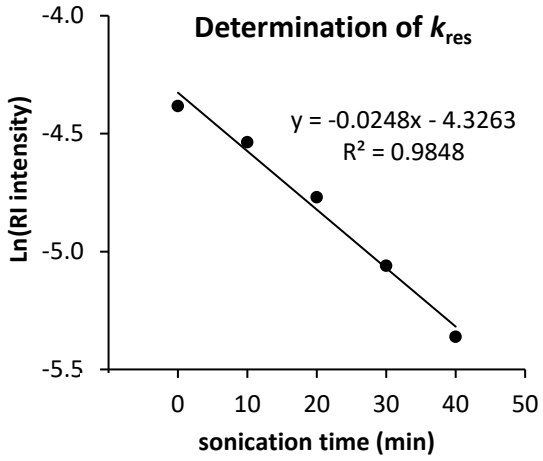
Determination of k_{res}
y = -0.0248x - 4.3263
R² = 0.9848
Ln(RI intensity)
-4.0
-4.5
-5.0
-5.5
0
10
20
30
40
50
sonication time (min)

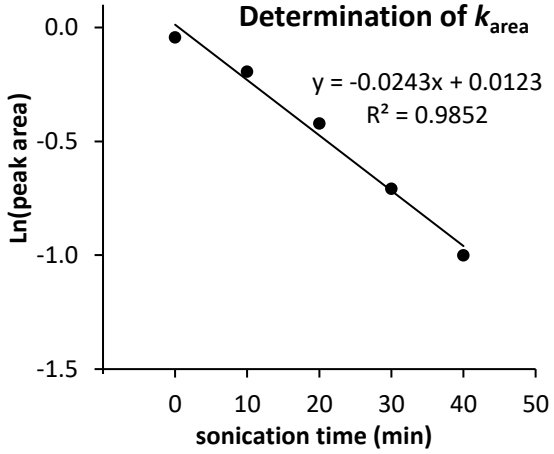
Determination of k_{area}
y = -0.0243x + 0.0123
R² = 0.9852
Ln(peak area)
0.0
-0.5
-1.0
-1.5
0
10
20
30
40
50
sonication time (min)

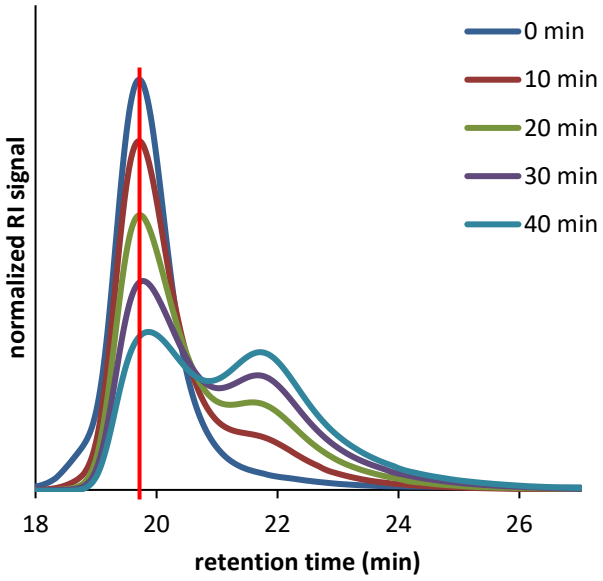
normalized RI signal
0 min
10 min
20 min
30 min
40 min
18
20
22
24
26
retention time (min)

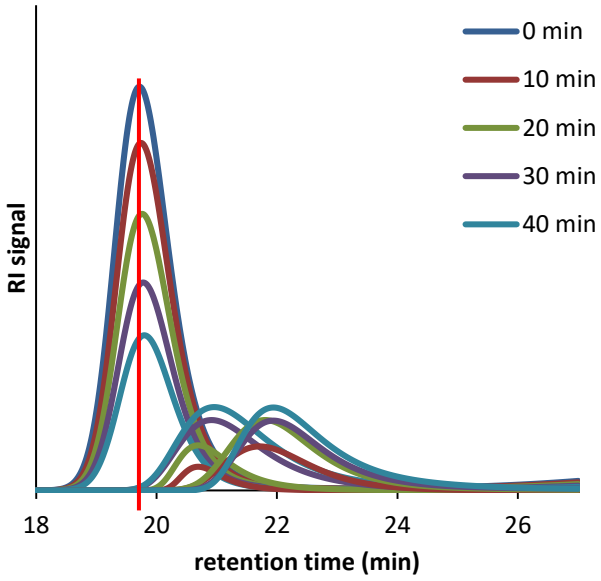
RI signal
0 min
10 min
20 min
30 min
40 min
18
20
22
24
26
retention time (min)

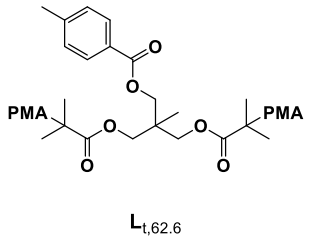
PMA
PMA
O
O
O
O
O
O

$L_{t,62.6}$

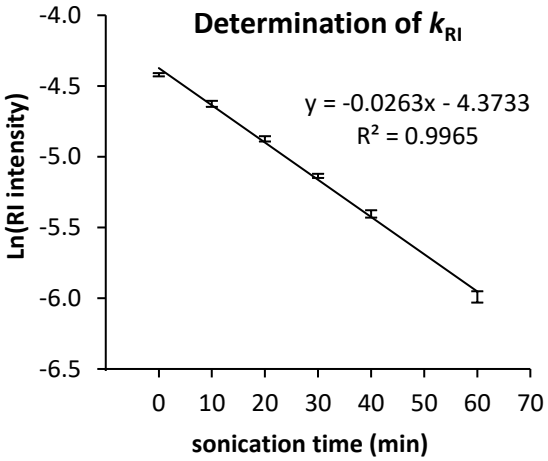
Determination of k_{RI}
y = -0.0263x - 4.3733
R² = 0.9965
Ln(RI intensity)
-4.0
-4.5
-5.0
-5.5
-6.0
-6.5
0
10
20
30
40
50
60
70
sonication time (min)

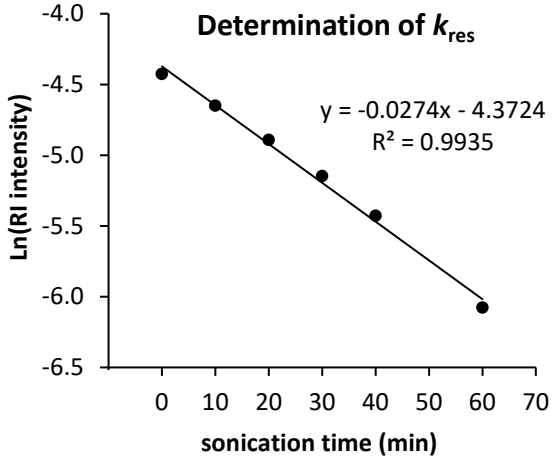
Determination of k_{res}
y = -0.0274x - 4.3724
R² = 0.9935
Ln(RI intensity)
-4.0
-4.5
-5.0
-5.5
-6.0
-6.5
0
10
20
30
40
50
60
70
sonication time (min)

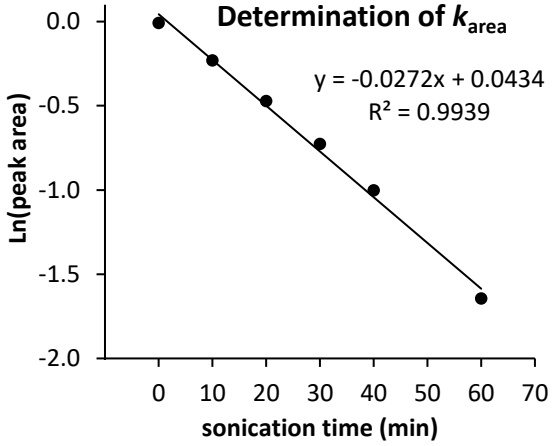
Determination of k_{area}
y = -0.0272x + 0.0434
R² = 0.9939
Ln(peak area)
0.0
-0.5
-1.0
-1.5
-2.0
0
10
20
30
40
50
60
70
sonication time (min)

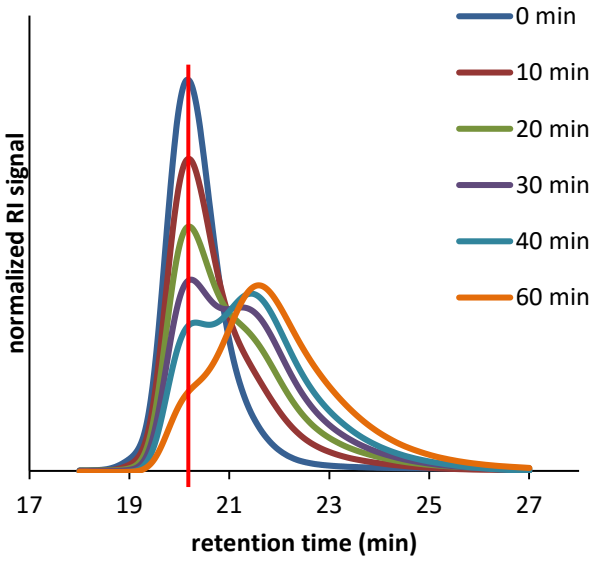
normalized RI signal
0 min
10 min
20 min
30 min
40 min
60 min
17
19
21
23
25
27
retention time (min)

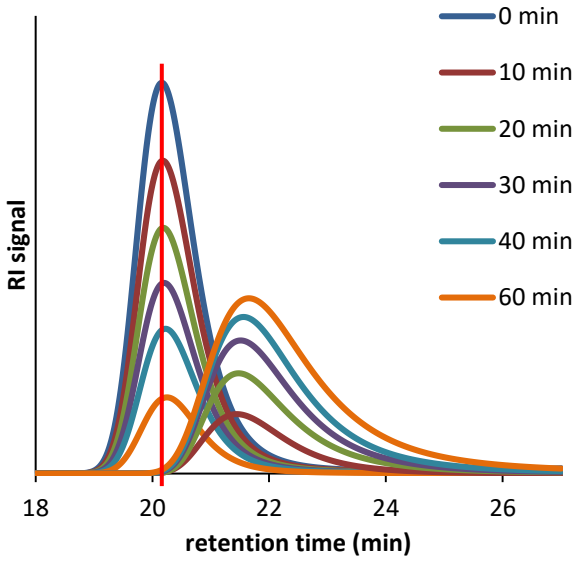
RI signal
0 min
10 min
20 min
30 min
40 min
60 min
18
20
22
24
26
retention time (min)

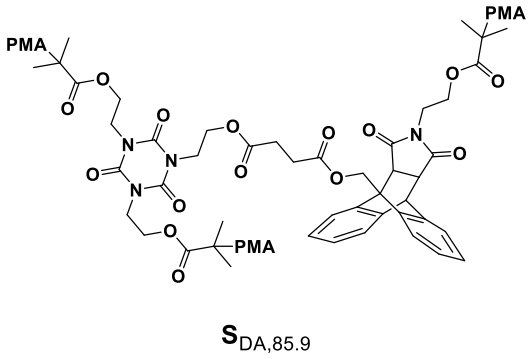
PMA
PMA
PMA

$S_{DA,85.9}$

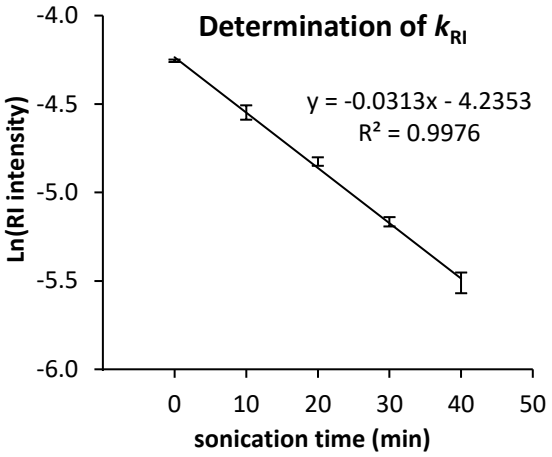
Determination of k_{RI}
y = -0.0313x - 4.2353
R² = 0.9976
Ln(RI intensity)
sonication time (min)

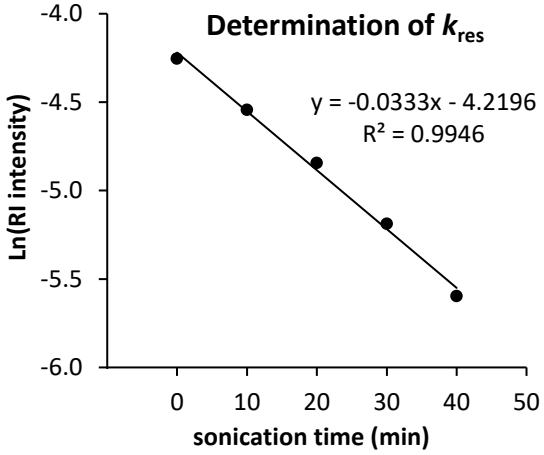
Determination of k_{res}
y = -0.0333x - 4.2196
R² = 0.9946
Ln(RI intensity)
sonication time (min)

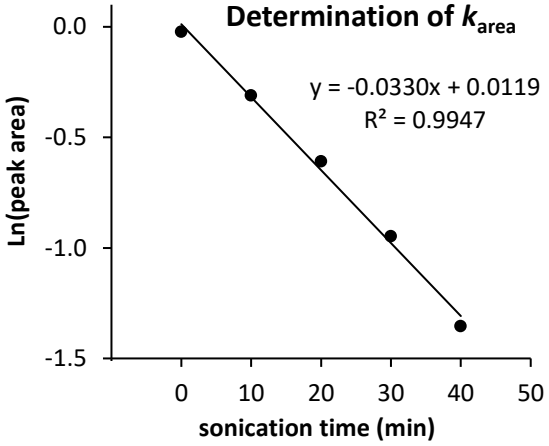
Determination of k_{area}
y = -0.0330x + 0.0119
R² = 0.9947
Ln(peak area)
sonication time (min)

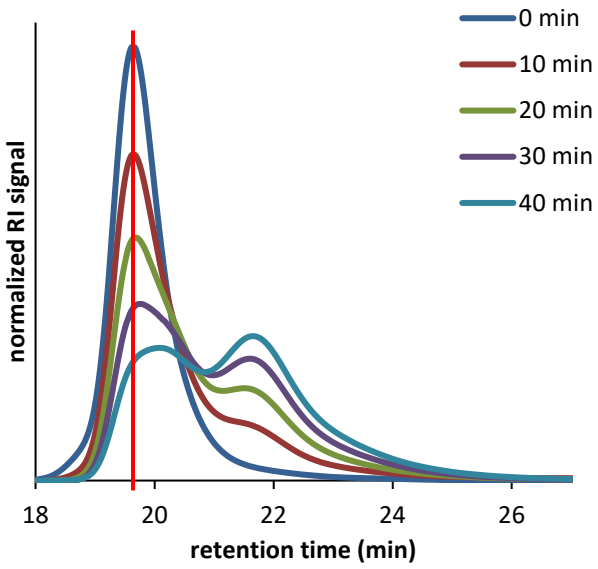
0 min
10 min
20 min
30 min
40 min
normalized RI signal
retention time (min)

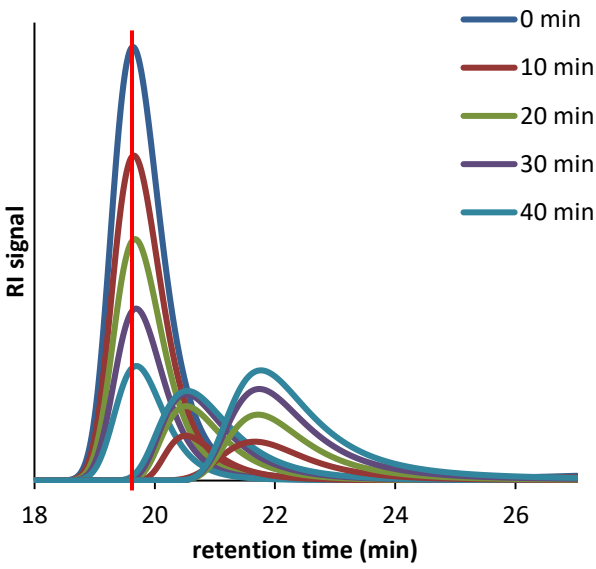
0 min
10 min
20 min
30 min
40 min
RI signal
retention time (min)

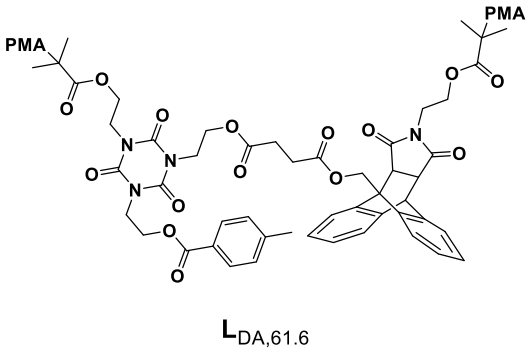
PMA
PMA

$L_{DA,61.6}$

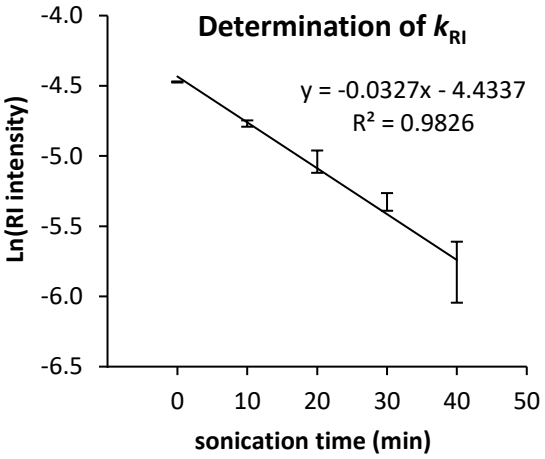
Determination of k_{RI}
y = -0.0327x - 4.4337
R² = 0.9826
Ln(RI intensity)
sonication time (min)

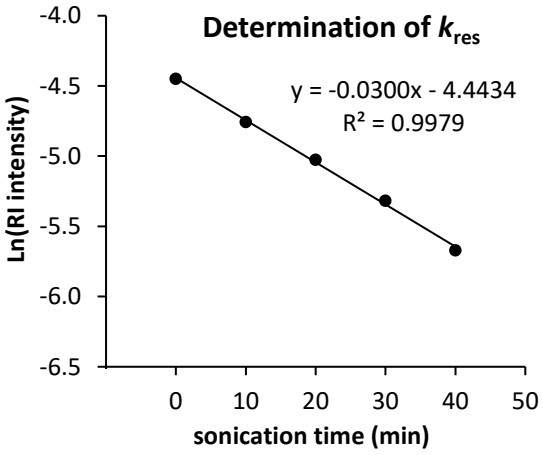
Determination of k_{res}
y = -0.0300x - 4.4434
R² = 0.9979
Ln(RI intensity)
sonication time (min)

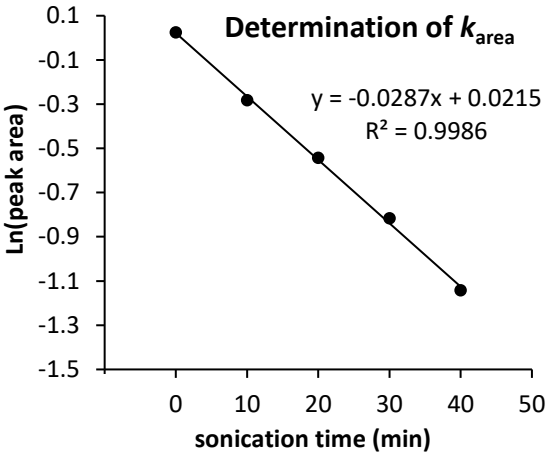
Determination of k_{area}
y = -0.0287x + 0.0215
R² = 0.9986
Ln(peak area)
sonication time (min)

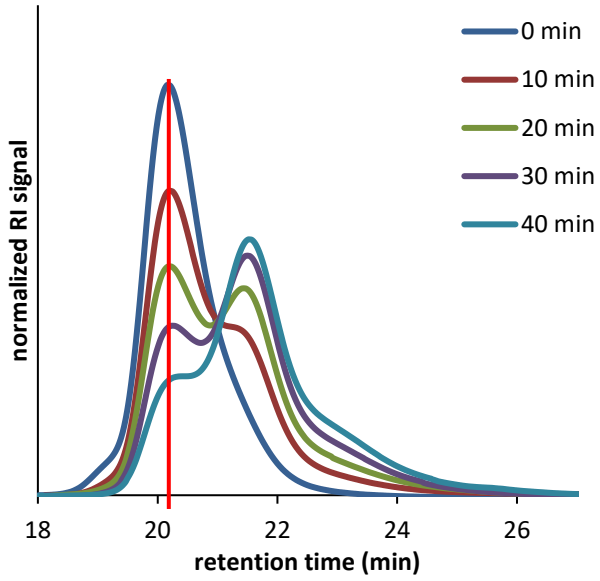
0 min
10 min
20 min
30 min
40 min
normalized RI signal
retention time (min)

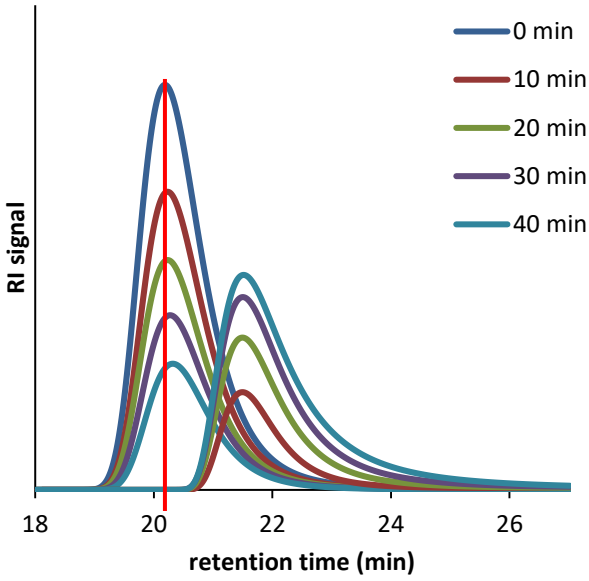
0 min
10 min
20 min
30 min
40 min
RI signal
retention time (min)

VITA

[A short bio of the author is required for a Ph.D. dissertation at the University of Washington. The vita section does not go into the Table of Contents. The formatting style follows the text of the dissertation.]

---

[i] Uesato, S.; Hashimoto, Y.; Nishino, M.; Nagaoka, Y.; Kuwajima, H. *Chem. Pharm. Bull.* **2002**, *50*, 1280-1282.